Partial Discharge Identification by using Signal Processing Techniques

CHIA TZE KEONG

School of Electrical & Electronic Engineering

A thesis submitted to the Nanyang Technological University
in fulfillment of the requirement for the degree of
Master of Engineering

2005

Statement of Originality

I hereby certify that the content of this thesis is the result of work done by me and has not been submitted for a higher degree to any other University or Institution.

30 September 2005

Date

Chia Tze Keong

Acknowledgement

I like to express my sincere appreciation and gratitude to my supervisor, Associate Professor S. Birlasekaran, for his invaluable advice and guidance throughout the project and to Professor Choi San Sing, Head of my division for his continued support and encouragement.

I also thank Mr. Lim Kim Peow, Mr. Benny Chia, Mrs. Jennifer Tan and Mr. Tsay Chi-Huang of System Protection Laboratory for their kind assistance and necessary support.

I appreciate the School of EEE, Nanyang Technological University for giving me the opportunity to pursue higher degree on part-time basis and for providing the necessary facilities to carry out my research work.

I thank Mr. Leong Weng Hoe, Managing Director of Hoestar Inspection International Pte Ltd, Singapore for providing one set of industrial data for this thesis work.

Last but not least, I acknowledge the loving moral and financial support and encouragement given by my parents to complete this research work in three years.

Partial Discharge Identification by Using Signal Processing Techniques

Abstract

Partial Discharge (PD) detection after denoising, characterization and identification are the three main signal processing requirements of PD analysis. Voluminous digital PD data are nowadays readily available with constant improvements in PD measurement techniques. Power Engineers may be able to detect prominent PDs using oscilloscope and existing couplers. But identification of the types of developing and random occurring PD is a real challenge to any practicing engineer. In this thesis, details on using wavelet transform in the form of either continuous wavelet transform or discrete wavelet transform with two methods to denoise, identify the location of PD and retrieve PD wave shape without magnitude distortion are presented. To identify the type of PD, some experimental studies and about six existing and developed signal processing methods are carried out. Laboratory experimental study provided reproducible data with enough number of sampled points on three types of pure PD and one multisources PD. The signal processing is done on PD random occurrence in 20 ms with multicycles, and is known as group PD analysis. In single PD analysis, the individual shape of PD is extracted and analysed. Group analysis includes the study of following distributions of PD: Φ-q, Φ-n and q-n, and the corresponding statistical operators Sk, Ku and CC, weibull parameters using q-cumulative n and Φ-cumulative n distributions, cluster analysis using (Δt-ΔV), (ΔV_n-ΔV_{n-1}), (Δt_n-Δt_{n-1}) and ($\Delta(\Delta V)$-$\Delta(\Delta t)$) distributions and Wavelet Transform

coefficients by varying scale. In single PD analysis, time and frequency domains features of the signal are analysed. With the above developed signal processing methods, laboratory recorded pure PD data are analysed for type identification. It is found that the statistical operators are sensitive to sampling windows. Then five of the signal processing methods are picked up for industrial application like identifying the types of PD in multisources signal and tested successfully with a laboratory generated multisources data and PD signal from an operating industrial transformer.

Contents

List of Symbols and Abbreviations

a	Scale factor of a wavelet
AC	Alternating cycle
Alpha, α	Weibull scale parameter
Beta, β	Weibull shape parameter
Bior6.8	Biorthogonal family of wavelet
C	Capacitor
CC	Cross-correlation factor
Coif5	Coiflet family of wavelet
CWT	Continuous Wavelet Transform
D1,d2…..	Detail coefficients at decomposition level 1, 2, …..
Db1,…DbN	Different orders of the daubechies family of wavelets
DFT	Discrete Fourier Transform
DSP	Digital Signal Processing
DWT	Discrete Wavelet Transform
EEE	Electrical and Electronic Engineering
f	frequency in Hertz
FFT	Fast Fourier Transform
Gnd	Electrical Ground
Gs/s	GigaSamples per second
HV	High Voltage
Hz	Hertz
IEE	Institution of Electrical Engineers, UK
IEEE	Institute of Electrical & Electronics Engineers, USA

Ku	Kurtosis
Ku(+)	Kurtosis of distribution during positive half cycle
Ku(-)	Kurtosis of distribution during negative half cycle
KV	Kilo-volts (= 1000 volts)
LHS	Left Hand Side
LV	Low Voltage
MΩ	Mega ohms
mm	millimeter
Ms/s	Mega-Samples per second
ms	Milliseconds
MVA	Mega Volt-amperes
n	Number of PDs
ns	Nano-seconds
NTU	Nanyang Technological University
PCB	Printed Circuit Board
PD	Partial Discharge
pF	Pico-farad of a capacitor
PILC	Paper insulated medium voltage cable
ps	Pico-seconds
PSD	Power Spectral Density
q	PD magnitude in volts
q_{mean}	Mean magnitude of PD in a distribution
$q_{\max}$	Maximum magnitude of PD in a distribution

RMS	Root Mean Square
R	Resistor
RHS	Right Hand Side
s	Scale parameter
Sk	Skewness
Sk(+)	Skewness of distribution during positive half cycle
Sk(-)	Skewness of distribution during negative half cycle
STFT	Short Time Fourier Transform
Sym4..SymN	Different orders of the Symlet family of wavelets
t	time in seconds
thr	threshold value
μs	Microseconds
VDE	German VDE uniform field voltage electrode
w	Radian frequency
WT	Wavelet Transform
Y	detail coefficients of signal after performing DWT
Φ	Phase angles (0 to 360 degrees)
α	Weibull scale parameter
β	Weibull shape parameter
F_a	Pseudo-frequency corresponding to scale a
F_c	Center frequency of a wavelet
ψ	Mother wavelet function
τ	Shift parameter of the Continuous Wavelet Transform

Δ	Sampling period of original signal
Δt, dt	time separation between consecutive PD pulses
ΔV, dV	amplitude separation between consecutive PD pulses
Δw	frequency bandwidth of a wavelet
Φ-q	Plot of magnitude (q) in volts against phase angle (Φ) in degrees
q-n	Plot of number of PDs (n) against magnitude (q) in volts
Δt-ΔV, dt-dV	Plot of amplitude separation between consecutive PD pulses (ΔV) against time separation between consecutive PD pulses (Δt)
$\Delta V_{n-1} - \Delta V_n$, $dV_{n-1} - dV_n$	Plot of amplitude separation between current consecutive PD pulses against amplitude separation between previous consecutive PD pulses
$\Delta t_{n-1} - \Delta t_n$, $dt_{n-1} - dt_n$	Plot of time separation between current consecutive PD pulses against time separation between previous consecutive PD pulses
Δ(Δt)-Δ(ΔV), d(dt)-d(dV)	Plot of the resultant change in amplitude separation between derived consecutive amplitude separation against the resultant change in time separation between derived consecutive time separation

List of Figures

List of Tables

Chapter 1

Introduction

1.1 Motivation

On-line partial discharge (PD) site measurement is one of the reliable condition monitoring techniques used in power industry [1,2,3]. Power utilities employ different measuring, recording and analyzing methods to detect and access PDs in their power network [4,5]. If one analyses the identical set of recorded data with statistical PD magnitude distribution and the corresponding phase angle of its occurrence in elliptical display, the types of developing PD can be identified using the reported signatures in IEEE and IEE standards [6,7,8]. On-line PD measurement on apparatus connected to HV network gets complicated as the simultaneously measured results at different measured nodes differ and the interpretation of results is more difficult [9,10,11]. The role of several other factors like noisy measuring environment, distortion of PD pulses from PD sites to the measuring nodes, lack of suitable node for sensitive PD measurement, the frequency response of sensors, amplifiers and recording devices and lack of database on types of PD make the identification of PDs more difficult [12,13,14]. The main intention for this research work is to apply digital signal processing techniques to detect, identify, and classify the types of PDs that will occur frequently in high voltage (HV) operating power systems so that an automated PD identification system may be developed. With that motivation in mind, identification characteristics of commonly occurring *corona, surface and cavity PD*

discharges are evaluated**.** PD experiments and new signal processing techniques are planned. Recently, there have been many references [15,16,17,18] on applying Wavelet Transform to denoise and identify PDs. New automated wavelet techniques have to be developed for processing the random occurring on-line PD data. It is found that many challenges exist on the detection of PDs buried in noise, identification of the types of developing PD, evaluation of the severity of PD, classification of different types of PD and location of PD in different individual and connected power apparatus. As a part-time research student with interest in signal processing, this research project on analyzing random occurring high frequency signals buried in noises is found to be interesting. After making a good literature survey, research study is planned. To get reliable data, controlled experiments in laboratory are carefully carried out. The application of Wavelet Transform (Continuous and Discrete) is studied for PD denoising and identification. It is found that the wavelet transforms and other processing techniques can identify unknown PDs emitted from single or multi-locations.

1.2 Objectives

The detailed objectives of my research are listed below:

a) Since controlled PD data are readily available in EEE,NTU through laboratory measurements and industrial field testing, it is aimed to develop new digital signal processing techniques to denoise, extract PDs from noisy data, characterize, classify and identify the types of PD. Wavelet Transform coefficients are used as a tool for

PD identification and is getting more popular because of its capability in identifying abnormality in time plane. However, so far, the publications on PD [19,20,21] described mainly on use of discrete type of Wavelet Transform. Continuous Wavelet Transform (CWT) has not really been investigated. Furthermore, the effect of many different settings of Discrete Wavelet Transform (DWT) on PD identification has also not been investigated. In this work, the effects of various settings of the DWT and the usefulness of CWT for PD analysis will be investigated.

b) It is accepted and reported that the phase (Φ) and magnitude (q) distribution profiles of PD data can be qualitatively used to identify the types of PD. Few researchers [22] report that the statistical operators like skewness (Sk), kurtosis (Ku) and cross-correlation (CC) between PD distribution in negative and positive half cycles may be used for identification of the types of PD in the laboratory. The polarity of skewness and kurtosis, and the closeness of these quantities as compared to a normal distribution for each type of PD are not reported and the usefulness of these factors in identifying known PDs by using a common phase window size of 1 degree of a 360 degree AC power cycle will be investigated.

c) Distribution of the sequential change in amplitude and the corresponding change in time separation between consecutive PD pulses over a substantial number of voltage cycles may be

indicators of range of random occurrence. The range and shape of cluster pattern of each type of PD are to be studied for PD identification.

d) The types of PD in mixed PD sources may be identified by determining the slope and shape parameters of the weibull-fitting on q and Φ with cumulative number of its occurrence distribution profiles.

e) Single PD characteristics like PD pulse shape and duration in time domain and dominant frequencies and its magnitude in frequency domain may be able to diagnose the different types of PD.

f) It is planned to group few reliable PD identification tests in identifying the types of PDs embedded in multi-source signals. One of multisource signal is recorded in the HV laboratory using the developed known pure PD models, and the other unknown is recorded at an industrial site. The results obtained with different methods are compared for reliable identification.

1.3 Major Contributions

1) For PD identification and characterization, three separate PD samples are designed, fabricated and tested to generate pure corona, surface, and cavity PDs. The developed corona and surface samples are connected in parallel to generate multi-sources PD signal with two known PDs occurring simultaneously in the measured period as per the respective mechanism.

2) Two digital wavelet CWT and DWT techniques with the developed correlation and energy methods to extract PDs from noisy data samples are reported. Newly developed denoising technique by optimizing the low scale detail coefficients of DWT is found to result in better denoised signal with minimum distortion. For optimal denoising in sampled discrete data, two methods of estimating the threshold value in wavelet technique are proposed and tested. The main advantages and disadvantages of CWT and DWT for PD analysis, and the various critical parameters to tune for PD detection are researched.
3) PD identification using PD random distribution in 20 ms is made using the statistical, cluster patterns and weibull parameters. Using the laboratory measurements on the developed samples, Φ and q distribution in 20 ms period is analysed with the characteristic and quantitative PD distribution features like skewness, kurtosis, cross-correlation factors, $\Delta\Phi$-Δq range distribution, and weibull shape and scale parameters. In that classical method, it is found that window size plays a critical role.
4) New detailed single PD analysis is introduced. Using CWT, the time location of individual PD is identified. The time and frequency domain characteristics of extracted single pure PD pulse are classified for respective PD identification. Using correlation, these features are used to identify the types of PD embedded in multi-source signal.
5) Signal from known multi-PD sources with corona and surface PDs is collected in the laboratory using developed PD models. In addition,

substantial PD data in 20ms and 2ms time durations using adequate sampling rate are also collected from an industrial operating transformer of 2MVA for analysis. It is shown that the five PD identification tests can be used sequentially to identify the types of PD in those collected multi-source signals.

1.4 Organization of thesis

Chapter 1 : presents the motivation, objectives of the research work, the major contributions of this research work and the organization of this thesis.

Chapter 2 : details the literature survey on types of PD, stochastic character of PD, PD measuring methods, PD identification methods, denoising techniques, various used transforms for PD analysis, theory of wavelet transform, CWT and DWT for PD identification, identification of the type of PD using statistical operators, cluster analysis, weibull parameters, individual PD pulse analysis and identification of PDs buried in multi-source signals. Finally, it presents the planned research work.

Chapter 3 : discusses the details on the measurement setup, digital resolution of recorded PD data for group and individual pulse analysis, voltage phase referencing, test objects to generate pure source and mixed-sources PD and the details on the developed software modules.

Chapter 4 : explains in detail the use of the CWT and DWT to detect and identify PDs. It presents the typical recorded pure PD distribution,

PD detection using CWT, selection of the best fit wavelet of CWT for PD detection using correlation and energy methods, selection of wavelet scale in CWT, PD detection using DWT, DWT coefficients, effect of sampling rate on detail coefficients, steps involved in obtaining denoised signal, best fit wavelet based on correlation and energy methods in DWT, role of levels of decomposition, threshold value for denoising and thresholding methods, and reconstructed detail coefficients to get the best denoised signal. It concludes with the procedure to follow on the selection of CWT and DWT for denoising.

Chapter 5 : describes the results obtained from group and single PD analysis. The 20 ms PD group distribution analysis is based on q-Φ-n distribution of each type of PD, statistical parameter calculation, weibull parameter determination and cluster analysis based on Δt-ΔV and $\Delta(\Delta t)$- $\Delta(\Delta V)$ of consecutive PD pulses. With corona, cavity and surface PDs, the characteristic features are brought out. Then it presents the individual pulse analysis in time and frequency domains. A summary of the characteristic features with each type of PD is presented.

Chapter 6 : explains the five selected tests used for identification of the types of PD buried in a mixed-source signal recorded in the laboratory and operating transformer. It presents the PD distribution of mixed-source signal before and after denoising in one AC cycle,

correlation factors distribution in 20ms, FFT content of single PD, variation of CWT coefficients with scale, and analysis by mixed-weibull techniques. It summarises the identification procedure for mixed-source signal to get reliable prediction.

Chapter 7 : summarises the findings. It discusses the main advantages and disadvantages of the reported new techniques and presents the new recommendations for future research work.

Chapter 2

Literature Survey

2.1 Introduction

This chapter presents the literature survey on PD and signal processing connected with PD analysis. Existence of PD activity is an indicator of insulation degradation. For this reason, the detection and diagnosis of PD activity is adopted for condition monitoring purposes to analyze the insulation integrity and remaining life of HV equipment. PD analysis involves the capturing, processing and characterization of PD signals to determine the severity, type of developing PD and the location of it. PD data is normally acquired at accessible locations such as HV terminals of equipment using coupling devices and measuring transducers. The emphasis nowadays is on the processing of PD data digitally and to develop methods to characterize and classify them because PD digital data are readily transportable through different communication links. Fourier analysis can no longer be used as a single tool for processing the PD data. The potential application of Wavelet Transform to PD detection has been discussed in some publications [23,24,25,26]. However, the focus of these publications is on the use of DWT and not by the CWT. Furthermore, the effects of different settings of Wavelet Transform like threshold level and methods, types of wavelet, decomposition levels, noise removal, and limitation of Wavelet Transform for PD analysis are not discussed and reported. It is planned to investigate in this research the role of different settings on wavelet analysis. Statistical operators

like the Skewness, Kurtosis and Cross-correlation factors are utilized to quantify the shape of PD magnitude and phase distribution profiles [27]. Thereafter, the polarity of those quantities and closeness to the normal distribution show the characteristic patterns for each type of PD. In addition, the Weibull and mixed-Weibull fitting techniques [28,29] are investigated with focus on getting the appropriate ranges of scale and shape parameters unique to each type of PD upon variations in applied voltages. The statistical profiles and Weibull analysis coupled with the results of the individual pulse analysis may be the desirable inputs for the identification of the types of PDs in multi-sources signals [30,31].

2.2 Theory of PD

2.2.1 An overview

PD can be described as an electrical pulse or discharge in gas-filled void occurring very locally [32]. It may occur with increased electrical stress on a dielectric surface of a solid [33] or liquid insulation system [34] or in the environmental air if sharp electrode edges [35] are present. The duration of PD pulse is very short typically in nano-seconds range. In other words, these pulses have very steep rise and fall times representing high frequency pulse. The discharges are effectively small arcs occurring within the insulation system causing localized insulation damage known as localized degradation to the HV machines [36,37]. Occurrence of PDs can be observed in the form of light (i.e. red-bluish glow exhibited by corona), heat, sound, electrical current, and degraded surfaces with chemical changes. The complete failure may happen in 1 to 20 years period depending on the severity. PD is a

symptom of deterioration in a machine and early detection enable engineers to evaluate the progress of insulation degradation. Exponential rising trend of PD activity with time is of main concern to the maintenance engineers.

2.2.2 Types of PD

Corona, surface and cavity are the three common PDs which occur frequently in many power apparatus [38,39,40]. The causes of their occurrences and the damages they pose to the machines and environment [41,42,43] are important considerations.

2.2.2.1 Corona PD

Many high voltage power system layouts have the tendency to have sharp edges on their conductive parts or connectors [44] due to bad workmanship or wear and tear during operation. When the electrical stress is around 3 kV per mm, corona PD will occur from the sharpest edge. The emitted radiation is sensed by different sensors. Corona tends to be repetitive depending on the applied electrical stress and ambient environment.

Insulation in the close vicinity of corona occurrence gets degraded [45]. Corona in oil produces hydrogen and other gases which may cause fire [46]. In overhead power transmission lines, it causes power loss. It also causes radio interference voltage. Corona is quite commonly seen on dry-type power transformers and often practical symptoms include fading of color, white powder, bluish-green powder (if copper is involved), dark tracks on insulation near conductors, radio frequency noise, and smell of ozone.

2.2.2.2 Surface PD

Surface discharges are PDs which occur due to contamination on the insulation surface. The contamination can be foreign particles like moisture from the ambient air, or just dust particles collected on the insulation surfaces. Such contaminants chemically attack the insulation resulting in reduced surface insulation resistivity. It permits the flow of substantial current in the surface film leading to carbonization of the underlying insulation surface known as surface tracking. Figure 2-1 [47] below shows the scenario where surface discharges occurring on the surface of the dielectrics of a typical electric motor when they are subjected to high-impulse voltages [48].

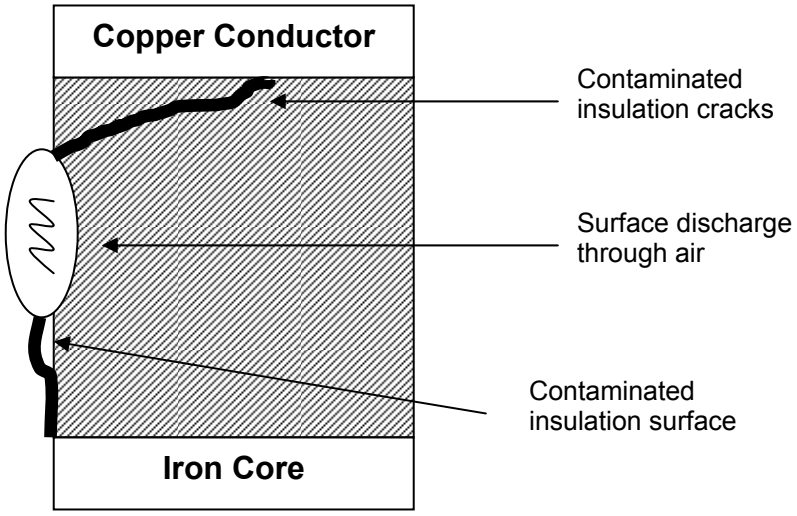

Figure 2-1: Surface PD in electric motor [47]

2.2.2.3 Cavity PD

Cavity PDs occur in cavities of solid or liquid dielectrics due to high voltages. It is well-known that the electric stress in cavity is increased by the relative dielectric constant of the surrounding dielectric. In addition, the magnitude of the field depends on the shape and location of the cavity. When the field becomes sufficiently high in the cavity, ionization will start and then the breakdown in void will occur. The field in the cavity will go to nearly zero as the charge tries to distribute in a very short time. This transient change in electric field distribution causes a change in voltage at the HV electrode which can be detected. Figure 2-2 [47] below shows a typical distribution of cavities in electric motor insulation. These voids are common in insulation of power equipment [49] and if partial discharges occur at these voids, it will cause treeing and damage the insulation locally after a prolonged period of operating time. Figure 2-3 shows the phenomenon of electrical treeing [50] caused initially by some internal cavities in the medium voltage cable. Failure of cable system may occur if internal discharges continue to cause the treeing in the cable.

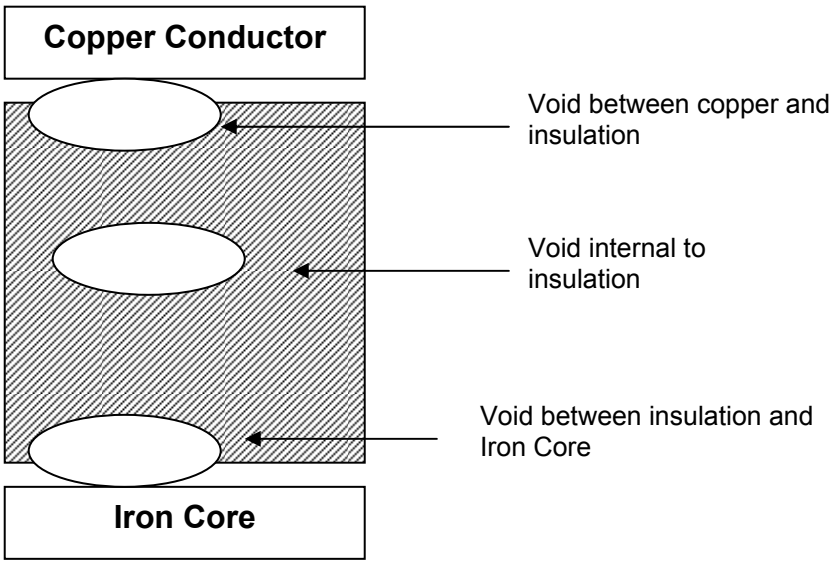

Figure 2.2 Possible cavity void distributions in motor insulation [47]

Figure 2-3: Electrical treeing in paper insulated medium voltage cable (PILC) [50]

2.3 PD Identification

PD tests are done on HV equipment rated more than 3.3 kV. A wide range of detection techniques like acoustic, ultrasonic, electrical, optical and chemical detection techniques are employed. Out of these techniques, the acoustic and electrical detection are the most commonly used.

Weak PD data is normally embedded in noise. Various hardware techniques [51,52] like differential mode of measurement, tuned frequency techniques, time domain and frequency domain analyses are used in the industry to

identify PD. With the availability of fast sampling digital techniques, large memory and fast communication links at reasonable cost, digital processing techniques are researched for PD identification and classification. For PD identification, embedded noise should be removed. Several methods like averaging, digital filtering, fourier analysis, and wavelet transform are proposed for denoising the PD data [53,54,55]. Out of these methods, Wavelet Transform is a more recent development in PD signal processing tools and a survey is made on the reported work to plan for the future research work on PD identification in sections 2.4, 2.5, 2.6 and 2.7.

2.4 Wavelet Transform

PDs are random pulses (i.e. non-stationary signals). They have finite duration (discrete) and occur only for a very short period of time. In most practical field environment, PD is embedded in the background electrical noise.

2.4.1 Various used transforms for PD analysis

Prior to actual PD type analysis, the acquired PD data must be denoised and the phase location of PDs must be extracted by digital detection technique. Fourier Transform cannot be applied for PD detection because it assumes that the signals to be transformed are stationary and infinite in time [56]. Stationary signals are signals whose frequency contents do not change with time. Fast Fourier Transform (FFT) [57] is an efficient way of calculating the Discrete Fourier Transform (DFT) [58] of discrete time domain signals. It is not good for continuous PD statistical analysis because it is unable to tell us at what time intervals are the spectral components of PD occurring. However, since individual

PD pulses are found to be well-defined in shape by a number of sampled points the FFT can be applied to find the frequency content of each type of PD pulse The Short Time Fourier Transform (STFT) [59] aims to provide a time-frequency representation of a discrete time signal. It may not be appropriate for PD analysis due to the fixed-width window that STFT uses throughout the analysis of the entire discrete signal and by the resolution dilemma introduced by the Heisenberg Uncertainty Principle [60]. The Heisenberg Uncertainty Principle states that good time and frequency representation of a signal cannot coexist. That means if the size of the window in STFT is narrow, then good time localization is obtained but looses frequency localization. The reverse happens for wide window size. In view of the mentioned limitations of the various types of FT, WT is introduced for PD analysis [61]. The WT helps to solve the problem of fixed-width window function and the resolution dilemma in STFT as it uses a mother wavelet of varying sizes to analyze the different frequency content of a signal and thus offers better signal processing. In addition, WT is found to be useful as a denoising tool as well as a PD extraction tool since it is capable of extracting the time/phase location of PDs buried in noise.

2.4.2 Theory of Wavelet Transform

Figure 2-4 below shows some typical popular wavelets [62,63] available in Matlab toolbox. They are Db1, Db2, Db4, Db8, Db9, Db15, Db20, Sym4, Sym8, Bior6.8 and Coif5. They are selected as they resemble many of the observed single PD waveshapes and are good in detecting abrupt changes in a signal. The horizontal width represents the finite time duration and the vertical amplitude is

the magnitude of the wavelet. All the wavelets decay to zero after a finite duration and they have zero average value. As seen from figure 2-4, a wavelet is an oscillatory signal but decays to zero in short time duration and has zero average value with a finite energy.

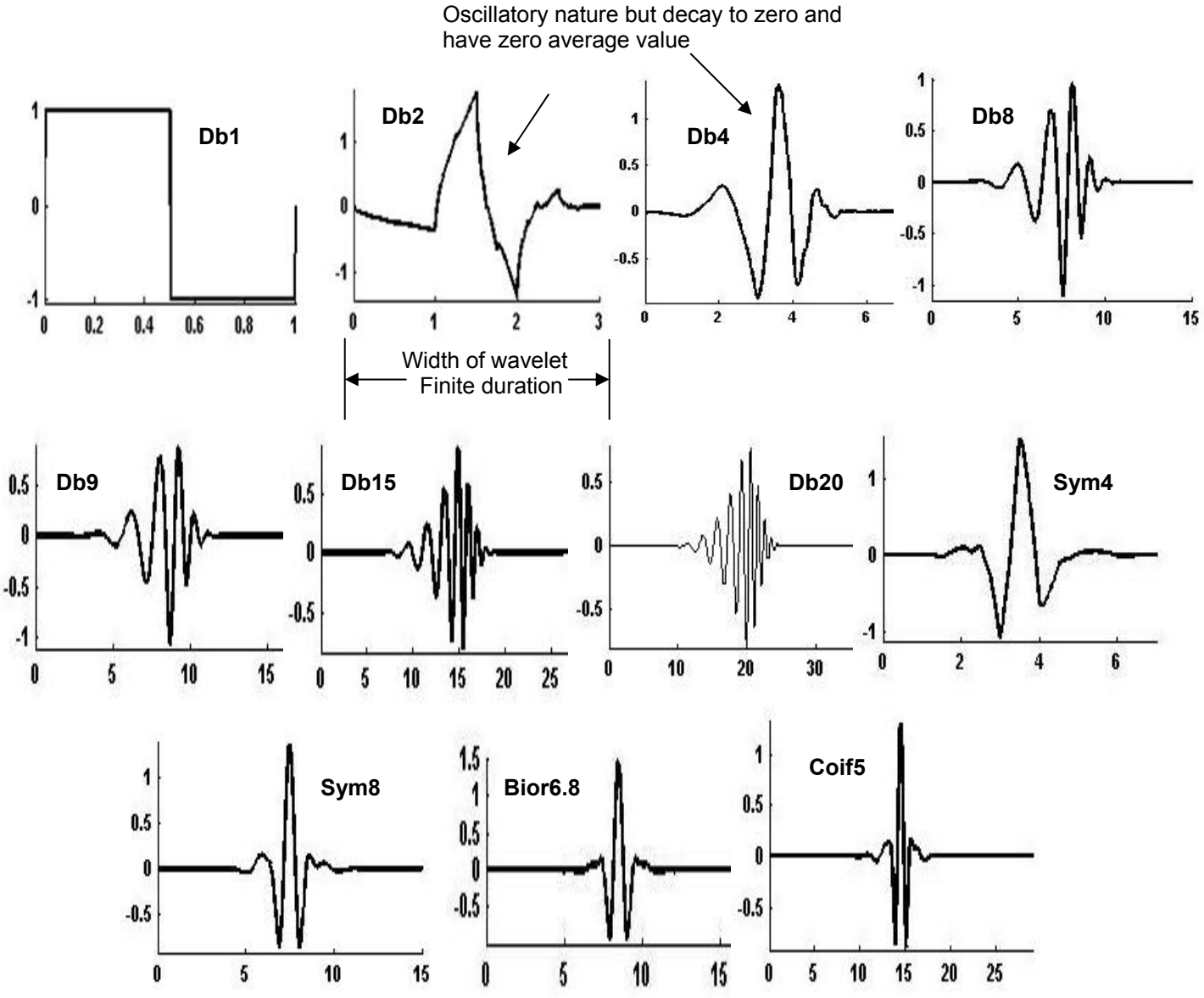

Figure 2-4: Shapes of 11 selected mother wavelets for PD analysis

Mathematically, a wavelet can be expressed as:

$$\psi_{\tau,s}(t) = \frac{1}{\sqrt{s}}\psi\left(\frac{t-\tau}{s}\right) \longrightarrow (2\text{-}1)$$

and FT of the mathematical expression of a wavelet can be derived as below:

$$F(\psi_{\tau,s}(t)) = \sqrt{s} * \psi(sw) \longrightarrow (2\text{-}2)$$

In (2-1), ψ is the mother wavelet, and τ and s refer to the shift and scale parameters respectively. These two parameters can be varied to analyze different frequency content at various time positions of a sampled signal. Wavelets are chosen to be localized in the time and frequency domains for use in PD analysis. In time-domain, it is a localized window centered at time zero. In frequency domain, it is also well localized with a center frequency close to zero and can be regarded as a bandpass filter. One can quantify the time and frequency localization of a wavelet by defining its time duration as Δt and its frequency bandwidth as Δw. Changes in the scale of a wavelet changes its behaviour in time duration and frequency bandwidth as shown by (2-3) and (2-4).

$$\Delta_t\left(\psi\left(\frac{t}{s}\right)\right) = s.\Delta_t(\psi(t)) \longrightarrow (2\text{-}3)$$

$$\Delta_w(\psi(sw)) = \frac{\Delta_w(\psi(w))}{s} \longrightarrow (2\text{-}4)$$

From the results [64] shown in (2-3) and (2-4) together with the FT of a wavelet (2-2), one can see that increasing the scale parameter **s** increases the time duration while decreases the frequency bandwidth of the wavelet. Figure 2-5

illustrates the scenario. This implies that wavelet provides poorer time resolution but better frequency resolution at lower frequencies and vice-versa.

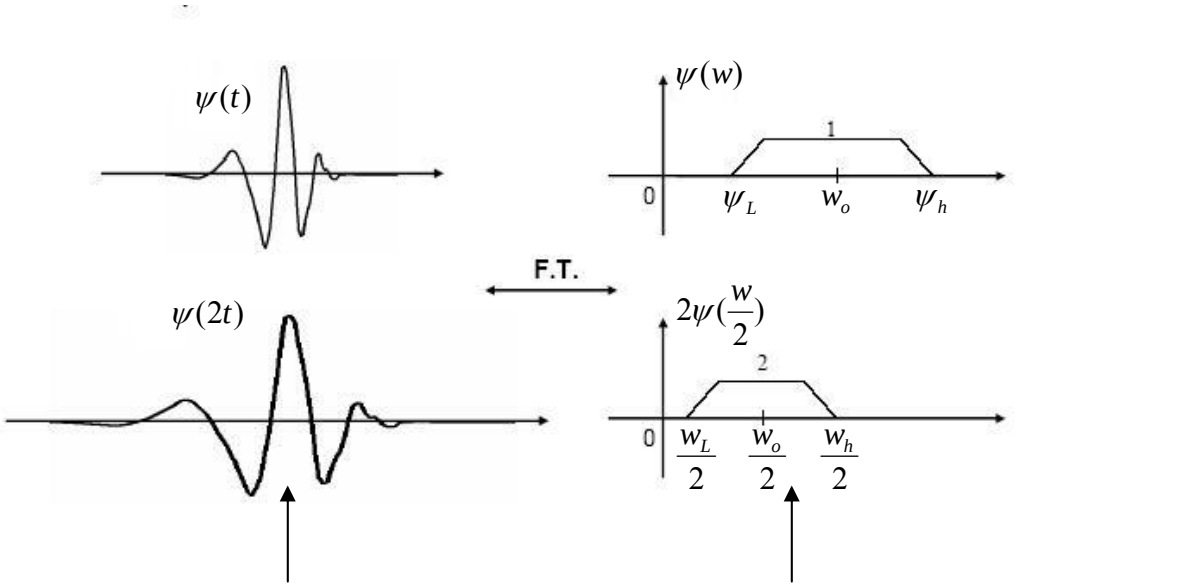

Figure 2-5: Effect of changing the scale of a wavelet

Two types of Wavelet Transform which utilize the understanding of the properties of wavelet are being investigated for PD analysis [65,66,67]. They are the **Continuous Wavelet Transform (CWT)** and the **Discrete Wavelet Transform (DWT).**

2.4.2.1 Continuous Wavelet Transform

In CWT, a selected wavelet is used as a window function similar to STFT. CWT can be mathematically expressed as (2-5).

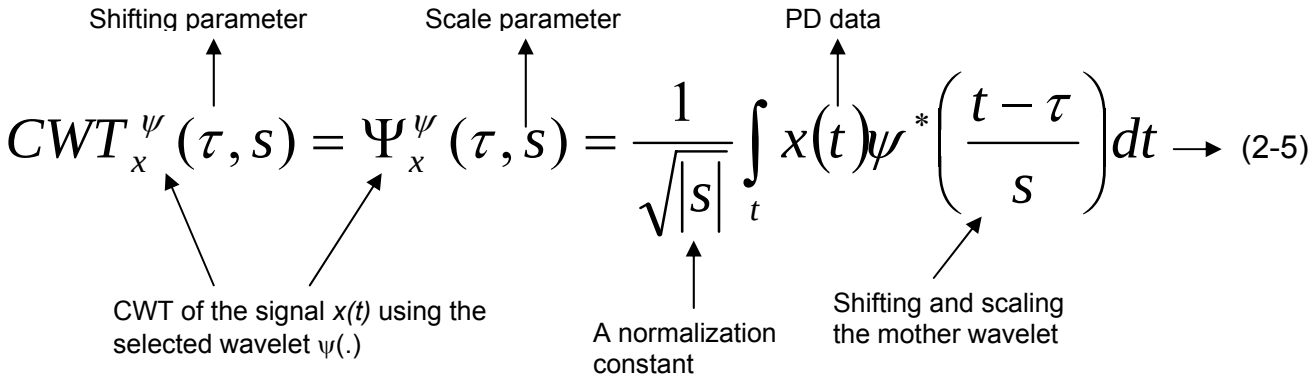

From (2-5), it can be seen that the CWT is defined as the sum over all time of the sampled signal multiplied by scaled and shifted versions of the time-localized wavelet function Ψ. Unlike STFT which uses a fixed-width window, the advantage of using CWT for PD analysis is that the width of the wavelet can be varied by varying the parameters of (2-5) to analyze different frequencies in a signal. High value of s (highly scaled wavelet) is equivalent to a stretched wavelet having long time duration (poor time resolution but better frequency resolution) and the purpose is to analyze low frequencies. On the other hand, a low scale wavelet corresponds to a compressed wavelet having short time duration (better time resolution but poorer frequency resolution) and is useful for analyzing rapidly changing details (i.e. high frequencies) like PDs. Thus, the scale of wavelet is inversely proportional to the frequency. In addition, even at scale 1 (lowest scale) of the selected wavelet, the frequency bandwidth of the wavelet is still localized. Thus, CWT is well-suited for PD analysis [68].

2.4.2.2 Relationship of scale in CWT to frequency

In CWT, the common syntax used is the scale factor and many CWT analysis rely on the time-scale plots and not on time-frequency plots. In many technical papers, the relationship of the scale of the mother wavelet to frequency was not explicitly explained [69, 70, 71]. They state that the scale is inversely related to the frequency. For example, high scale means low frequency analysis while low scale means high frequency analysis of a signal. In the Matlab reference guide, the frequency corresponding to a particular scale can be calculated by equation 2-6 below:

$$F_a = \frac{F_c}{a * \Delta} \quad \text{---------- (2-6)}$$

Where

F_a is the pseudo-frequency corresponding to scale a

F_c is the center frequency of the particular wavelet

Δ is the sampling period of the original signal.

The idea is to associate with a given wavelet a purely periodic signal of frequency Fc as shown in figure 2-6. In figure 2-6, the time axis runs up to 14 seconds. It can be seen that the center frequency-based approximation captures the main wavelet oscillations. The center frequency is a simple characterization of the dominant frequency of a wavelet. The sinusoidal wave fitting the wavelet db7 has a period of 1.4444 second. Thus, the center frequency is 0.692 Hz. In a similar manner, the center frequencies of other types of wavelet can be found.

When the wavelet is dilated by a factor a, the center frequency becomes $\frac{F_c}{a}$ and if the underlying sampling period of the original signal is Δ, then (2-6) can be used to calculate frequency relating to the selected scale.

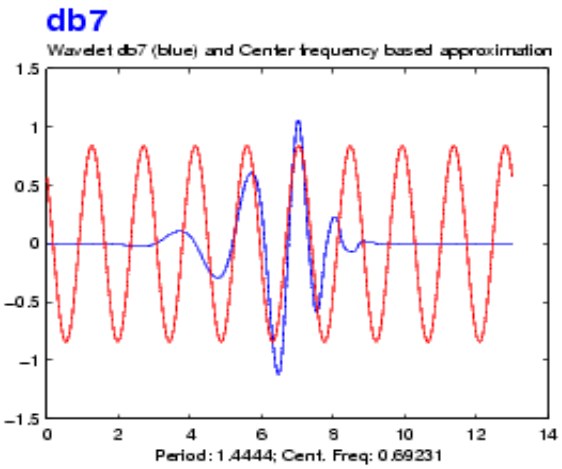

Figure 2-6: Associating a db7 wavelet with a pure sinusoidal signal

2.4.2.3 CWT to identify PDs embedded in signal

To capture the rapidly changing details of embedded PD in a time domain signal by using CWT, a desired wavelet (i.e. db8, db9, or sym8) is first selected. Then by using scaling and shifting of the selected wavelet, the sampled signal x(t) containing PDs is analysed using (2-5). The analysis is done by determining the correlation coefficient between the wavelet and windowed sections (determined by width of the selected wavelet and parameter τ) of the signal until the entire measured time domain signal is covered. Figure 2-7 shows a brief description of how CWT picks up abnormalities like PD in signals.

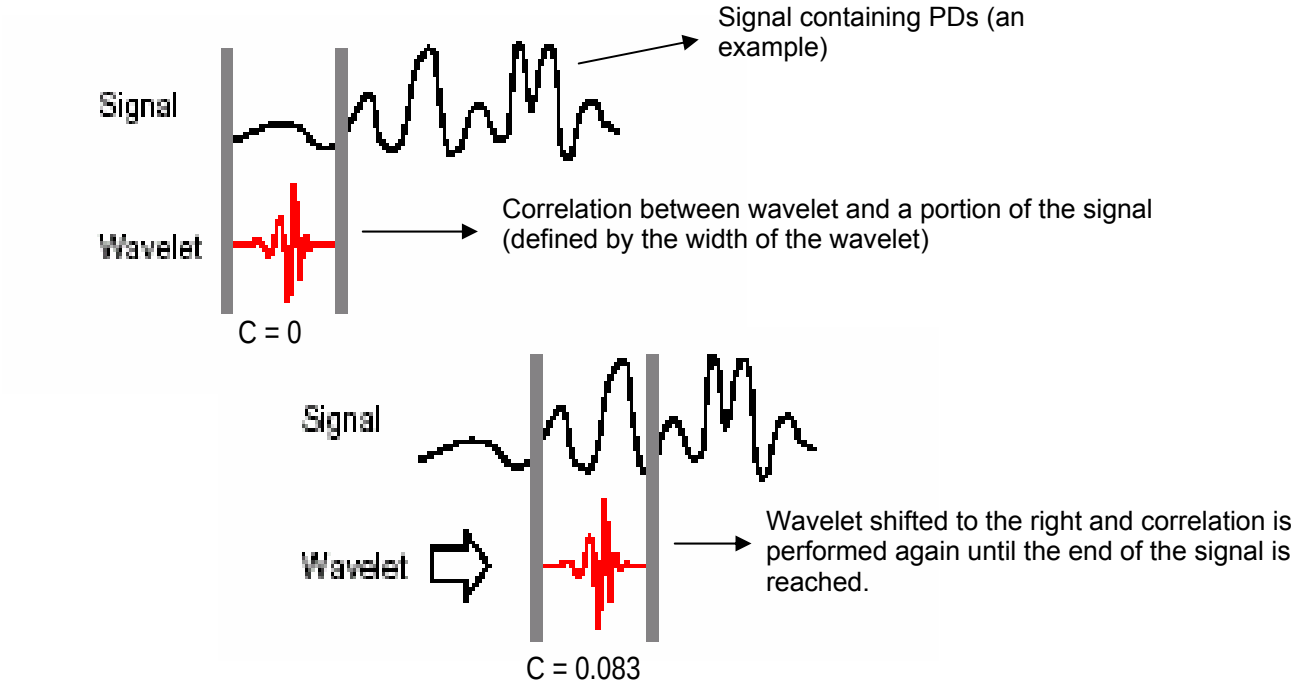

Figure 2-7: Determination of correlation coefficients by shifting in CWT

CWT starts the correlation analysis by using the lowest scale of 1 (most compressed) of the chosen wavelet and places it at the beginning of the signal. The result of the correlation between the wavelet and the portion of the signal (defined by the width of the wavelet) is recorded and then the wavelet is shifted to the right determined by position parameter τ. Again, the correlation result is recorded. Similar procedure is followed until the end of the signal. A number of correlation results are obtained by varying τ. The correlation results are often referred to as CWT coefficients denoted by C. Next, the wavelet is now stretched to scale 2 (double the time duration of wavelet which means poorer time resolution but reduces frequency bandwidth of wavelet by half to have better frequency resolution). The same procedure is repeated again until the end of the signal is reached. There will be another set of wavelet coefficients for scale 2. A

lot of wavelet coefficients corresponding to continuous scales of 1,2,…to n of the selected wavelet will be obtained. High frequency bursts like PDs can be detected by looking at the correlation results of the lower scale wavelet. A high coefficient value will be recorded if the low scale wavelet is closely matched with the PD pulse that resides in the windowed section of the signal. The occurrence of high wavelet coefficients at lower scales (i.e. scale 1,2, and 3) reveals the time occurrences of PDs. The correlation results of CWT at each scale depend on the shape of selected wavelet. A time-scale representation of the coefficient values of the signal is obtained after performing CWT at a specified number of scales n. n is limited by the nyquist frequency and is selected by the user. The main disadvantage of CWT is that it generates a lot of coefficients which may use large computational resources and time. The DWT [72] aims to solve this computational problem. DWT uses a power of 2 for the scaling i.e. (1,2,4,8,….) and the end results are equally satisfactory with an added advantage of being more simplified.

2.4.2.4 Best fit wavelet for use by CWT to detect PDs

Since CWT performs the correlation analysis between the selected wavelet and sections of the sampled signal defined by the width of the wavelet, an appropriate wavelet most similar to PD is selected. Some wavelets are better than others in the sense that they correlate better with a particular type of PD and are able to get high CWT coefficient associated with PD while suppressing coefficients associated with background noises. Although the daubechies wavelets are localized in design and well-known in picking up abnormalities, but

within the family itself lies several different orders of daubechies wavelet like db2, db4, db8, db9,….and dbN. In addition, other popular wavelet families like the Symlet, Biorthogonal, and Coiflet may also be useful and thus are investigated together with daubechies wavelets for their usefulness in PD analysis. A best fit wavelet out of these popular wavelets is selected based on high coefficient value with PD and lowest coefficient value with noise on typical signal containing PD spikes and noise shown in figure 2-8.

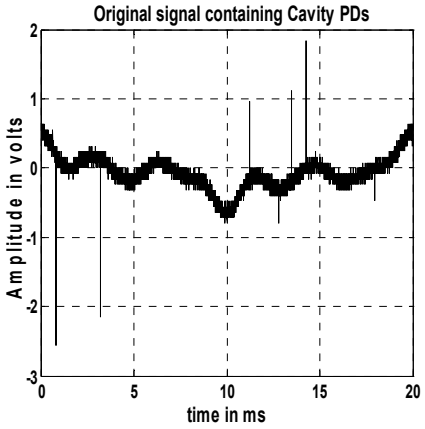

Figure 2-8 Spiky cavity PDs with 50 Hz harmonics noise

2.4.2.5 Discrete Wavelet Transform

DWT analyzes the original signal at different frequency bands with different resolutions by decomposing the signal into a *coarse approximation* and *detail* information. DWT uses two sets of functions called scaling functions, and wavelet functions which are associated with low pass and high pass filters.

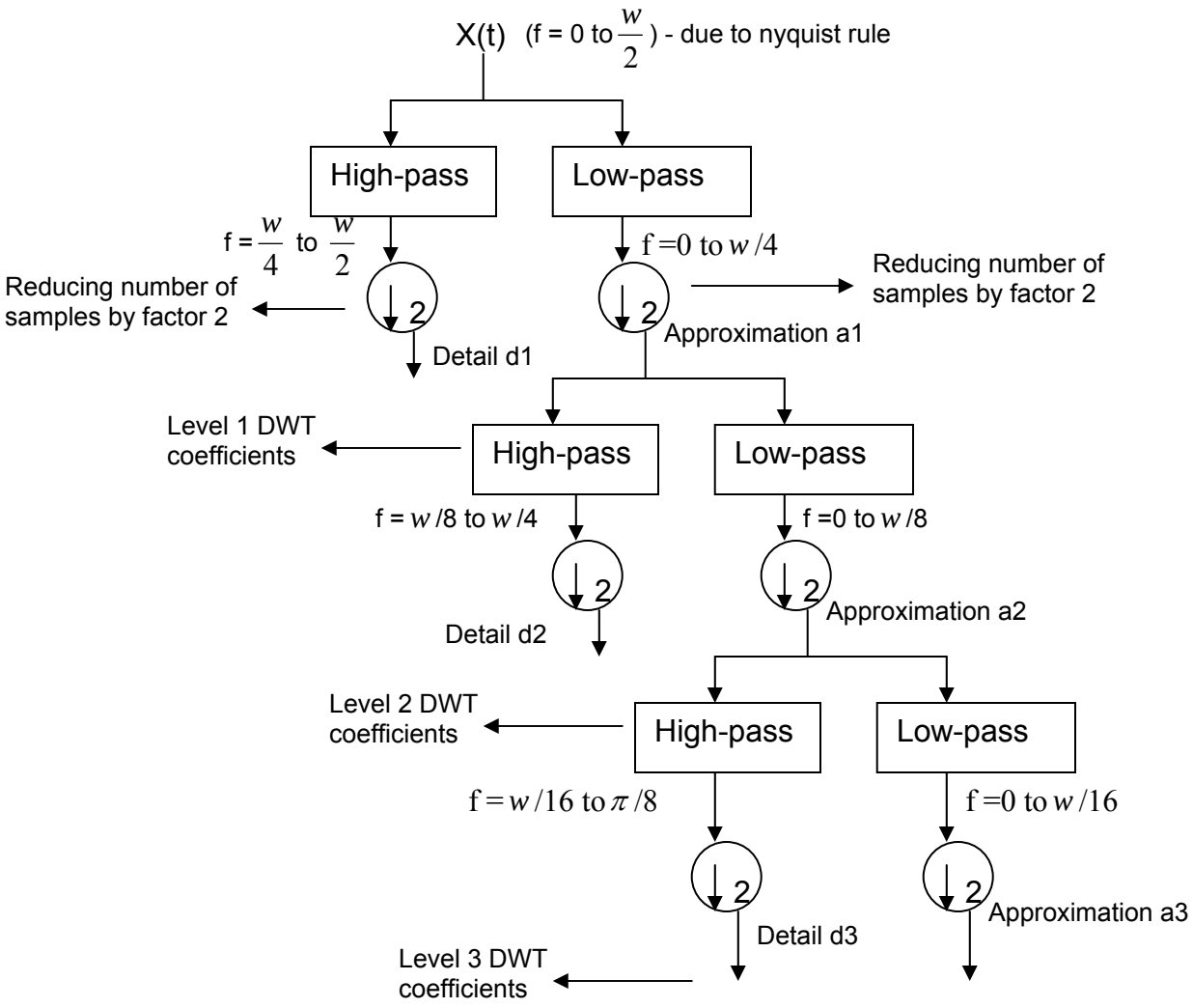

Figure 2-9: Multi-level decomposition by DWT

The decomposition of the original signal into different frequency bands is obtained by successive highpass and lowpass filtering of the time domain signal. In figure 2-9, the original signal x[t] with frequency contents up to $\frac{w}{2}$ radians is first passed through a highpass filter (wavelet function) and a lowpass filter (scaling function). After passing through the filters, detail d1 contains the upper half of the frequency band of the original signal (i.e. $\frac{w}{4}$ to $\frac{w}{2}$) while the approximation a1 takes the lower half band (0 to $\frac{w}{4}$). By removing half of the

spectral components from the original signal, half the number of samples is made redundant. Therefore half of the samples can be eliminated by down-sampling (reducing the number of sample points) according to the Nyquist's rule for the approximation and detail. The first stage decomposition halves the time resolution since the approximation which has only half the number of samples now characterizes the entire original signal and will be fed into stage 2. However, this operation doubles the frequency resolution as the uncertainty in frequency is reduced by half and the frequency band of the approximation now spans only half the previous frequency band. In short, the filtering process by the wavelet filters actually improves the frequency resolution (by 2 times) but the reduction of the number of samples (down-sampling) degrades the time resolution (by 2 times). At every level, the filtering and samples reduction by a factor of 2 will result in half the number of samples (i.e. half the time resolution) and half the frequency band spanned (i.e. double the frequency resolution). After the decomposition process is completed, the frequencies that are most prominent in the original signal will appear as high amplitudes in that region of the DWT signal that includes those particular frequencies. The difference of DWT from the Fourier Transform is that the time localization of these frequencies will not be lost. However, the time localization will have a resolution that depends on which level they appear. If the main information of the original signal lies in the high frequencies like PDs, then the time localization of these frequencies will be more precise, since they are characterized by more number of sample points in the lower scale level of the decomposition tree. If the main information lies only at very low frequencies, the time localization will not be very precise, since few sample points are used to express signal at these frequencies. This procedure in

effect offers a good time resolution at high frequencies, and good frequency resolution at low frequencies. PDs are high frequency pulses, and it is desirable to have good time resolution at high frequencies. Hence DWT at lower decomposition level (i.e. d1, & d2) is a good candidate for PD analysis since the filtering processes at lower levels improve frequency resolutions while still providing decent time resolutions.

2.4.2.6 Frequency range of detected PD in DWT

An important limitation of DWT (or CWT) is that it is unable to determine at what time intervals are the exact frequency components of the original PD signal are occurring. DWT can only tell at what time intervals are a band of frequencies occurring for a PD signal. For example, after high pass filtering at level 1, the frequency range for detail d1 is from $\frac{w}{4}$ to $\frac{w}{2}$. If PDs are captured at level 1 (which can be observed as high amplitudes in the detail signal d1), then those PDs are considered to reside in that frequency regions described by the time intervals of the high amplitudes in the detail signal. Such short-coming is common to other transforms. Exact frequency components of a signal can only be found by using the Fourier transform with large number of sampled points.

2.4.2.7 DWT to identify PDs embedded in signal

PD in DWT is identified in two steps.

1) DWT breaks down a signal's frequency band into several sub-bands determined by the number of levels in the decomposition tree. Since PD signals are high frequency pulses, presence of PDs can be identified by inspecting the detail coefficients at lower levels (i.e. levels 1 and 2).

2) Setting a threshold level, all coefficients of lower values are set to zero while all coefficients of higher values are retained. By picking high coefficients, inverse transform is done to get the denoised signal. The denoised signal reveals the time locations of PDs.

Figure 2-10 shows another typical recorded signal. It can be seen that there are several spikes (PDs) and the background noises that corrupt the entire signal. DWT reflects the intensity of the energies of the original signal in their detail coefficients [73]. For example, the background noises seen in figure 2-10 have energies much lower than the PD spikes because their energies are spread out in the sampled time period.

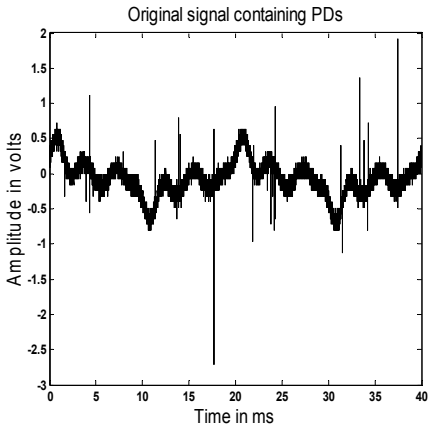

Figure 2-10 Original signal with PDs

Detail coefficients of higher amplitudes at low decomposition scale often denote high energy bursts like occurrence of PDs in the original signal. Detail

coefficients at higher decomposition contain information about the lower frequency components of the original signal and thus are not being used. The coefficients having lower values associated with background noises are chopped off by setting a threshold value (cut-off value). In this way, the original will be denoised. Figure 2-11 shows the steps involved in DWT for denoising the collected PD data.

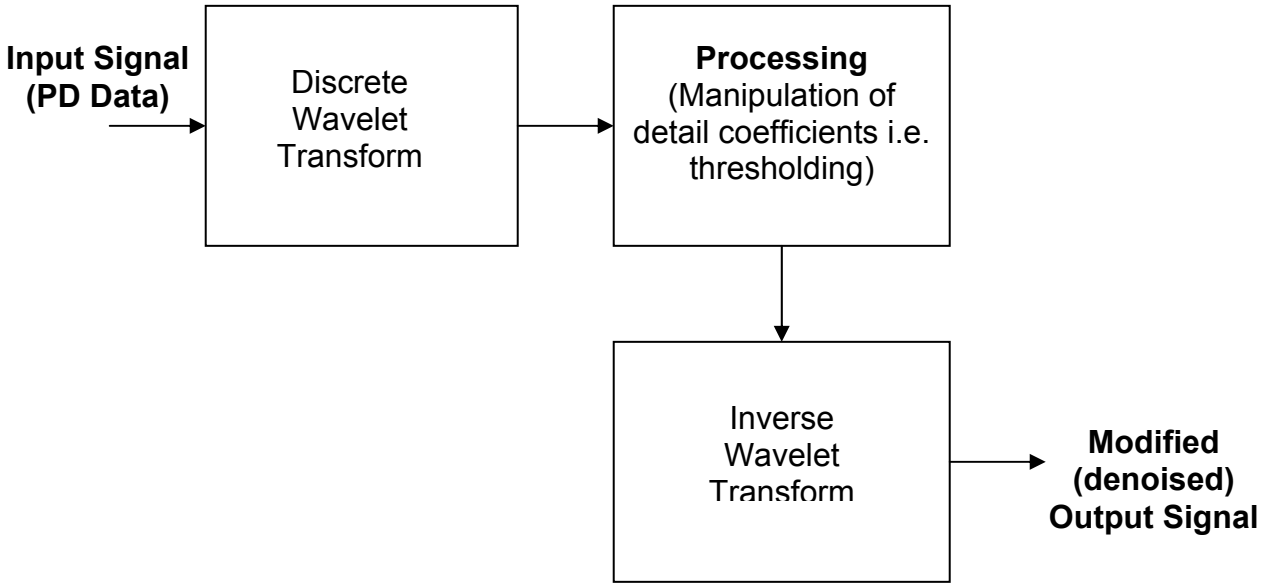

Figure 2-11 Steps used to denoise PD signal using DWT

2.5 Statistical operators used for the Identification of PD

The identification after denoising is done in two ways [74,75]. The first method is based on classical group analysis. The obtained single source PD data after employing DWT denoising appear in groups or packets of pulses relative to the cycle of the sine wave of an AC applied voltage. Based on the characteristics of its occurrence in Φ, the type of PD is identified [76,77]. The best example is that corona pulses appear in packets mainly in the negative half cycle. The above method is a qualitative method to identify the type of PD.

More quantitative methods are developed to analyze the distribution by determining the number, mean, maximum value in split windows. The q-Φ-n (magnitude-phase-number) plots are analysed by statistical operators like skewness, kurtosis and cross-correlation [78,79]. These statistical quantities numerically described the closeness of the shapes to a standard normal distribution and were used for identifying the distribution patterns of each type of PD. The definition of the various factors is presented below.

2.5.1 Skewness

The Skewness is mathematically defined as:

$$S_k = \frac{\sum_{i=1}^{N} (Y_i - \overline{Y})^3}{(N-1)s^3}, \qquad Y_i = Y_1, Y_2, ... Y_N$$

Where Y_i is the recorded data, $\overline{Y}$ is the mean of data, s is the standard deviation, and N is the total number of data points. The skewness for a normal distribution (or any perfectly symmetric distribution) is zero, and any symmetric data will have skewness value near zero. If skewness is negative, the data are spread out more to the left of the mean than to the right i.e. asymmetric to the right (skewed left). If skewness is positive, the data are spread out more to the right i.e. asymmetric to the left (skewed right).

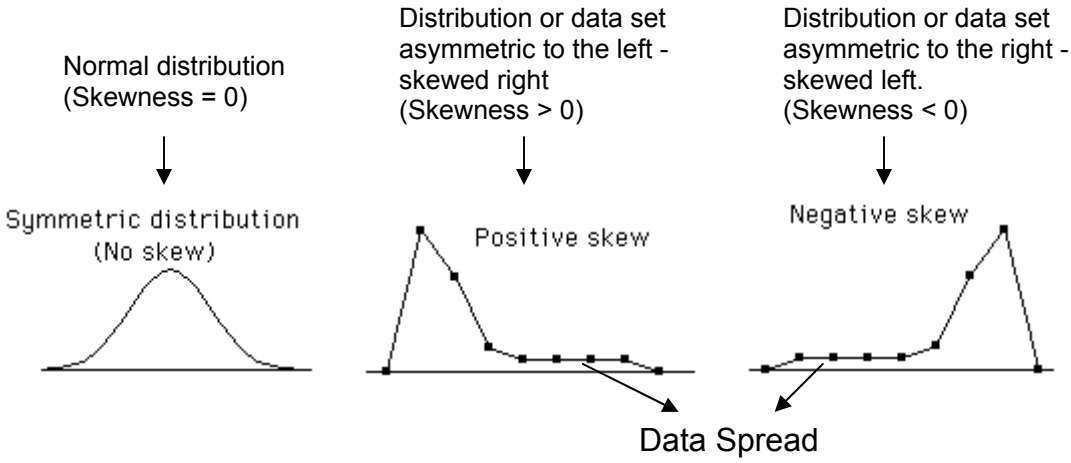

Figure 2-12 Graphical illustration of the Skewness used to describe data distribution

2.5.2 Kurtosis

Kurtosis is defined as:

$$Ku = \frac{\sum_{i=1}^{N}(Y_i - \overline{Y})^4}{(N-1)s^4}, \qquad Y_i = Y_1, Y_2, ...Y_N$$

Where Y_i is the recorded data value, $\overline{Y}$ is the mean of data, s is the standard deviation, and N is the total number of data points. The kurtosis for a standard normal distribution is three. For this reason, excess kurtosis is defined as:

$$Excess\ Ku = \frac{\sum_{i=1}^{N}(Y_i - \overline{Y})^4}{(N-1)s^4} - 3, \qquad Y_i = Y_1, Y_2, ...Y_N$$

Using the equation for excess Kurtosis will make the standard normal distribution to have a Kurtosis of zero. The Kurtosis indicates the sharpness or the amount of

concentration of the distribution around the mean value. It increases with the sharpness of the distribution. For an example, if the kurtosis of the distribution profile is greater than zero, it is said to be **leptokurtic** [80]. If its kurtosis is less than zero, it is said to be **platykurtic** [81]. Leptokurtosis is associated with distributions that are more "peaked" and have "fat or heavy tails" as compared to a normal distribution. Platykurtosis is associated with distributions that are less peaked and have thinner or lighter tails.

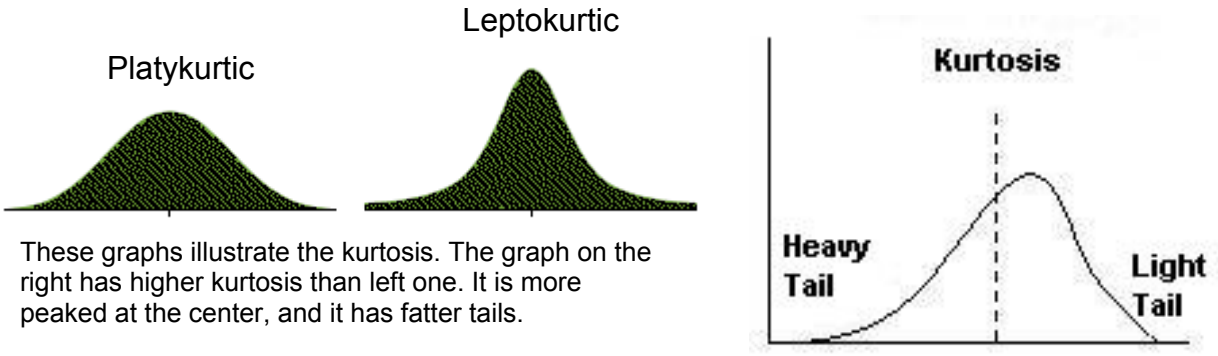

Figure 2-13 Graphical illustration of the Kurtosis used to describe data distribution

2.5.3 Cross-Correlation

The Cross-Correlation factor (CC) determines the degree of difference in shapes of the distributions in the positive and negative half cycles. If the shapes in the positive and negative cycles are similar, then the value of CC would be unity. If they differ entirely, CC would be zero. Generally, CC falls between 0 and 1. CC is described mathematically as:

$$CC = \frac{\sum x_i y_i \quad \sum x_i \ \sum y_i \ / n}{\sqrt{\left[\sum x_i^2 \quad \left(\sum x_i\right)^2 / n\right]\left[\sum y_i^2 \quad \left(\sum y_i\right)^2 / n\right]}} \qquad \text{--------- (2-7)}$$

Where x_i is the mean or maximum PD magnitude in window i of the positive half cycle and y_i is the mean or maximum PD magnitude in the corresponding window in the negative half cycle and n is equal to 180 i.e. the total number of phase windows per half cycle. Calculation of the values of CC reveals the difference in shapes of the phase distribution profiles for different types of PD.

In addition, the sequential time and amplitude change (ΔV & Δt) distribution between consecutive PD pulses [82,83] within a voltage cycle is also analysed to identify the type of PD. Each type of PD exhibit different types of cluster patterns. To identify the number of PD sources from unknown PD, Weibull and Mixed-Weibull fitting on q-n is used in the laboratory [84,85].

2.6 Individual PD pulse analysis

Beside analysing the phase distribution profiles of each type of PD for characteristic determination, the individual pulse of each type of PD also showed interesting characteristics which were harnessed for PD identification [86]. Not many publications discussed about such areas. It is planned in the research work to make use of the results of the individual pulse analysis like the FFT contents, time duration and pulse shape of each type of PD to be fed into the **Correlation Method** for identification of the types of PD embedded in multi-sources signal.

2.7 Identification of types of PD in multi-sources signal

Publications on identification method for multi-sources signal are also limited [87, 88]. One of the more prominent methods is the mixed-weibull technique which is applied to sets of PD populations residing in a multi-PD sources signal.

2.8 Summary

The literature study reveals that many signal processing techniques connected with denoising and type of PD identification are being developed based on more laboratory studies. This research is aimed in identifying and developing new techniques for practical field application. The study shows that there are characteristic changes in group and single PD responses with types of PD. It is planned to come up with some better signal processing techniques for denoising, type identification and determining the number of PD sources. The developed methods are reported in the subsequent chapters.

Chapter 3

Measurement Setup

This chapter describes the details on the PD measurement system used in my thesis. The HV measurement system consists of HV source, PD current recording system, sources to create the desired pure PD and software tools to process the recorded data.

3.1 Measurement Setup

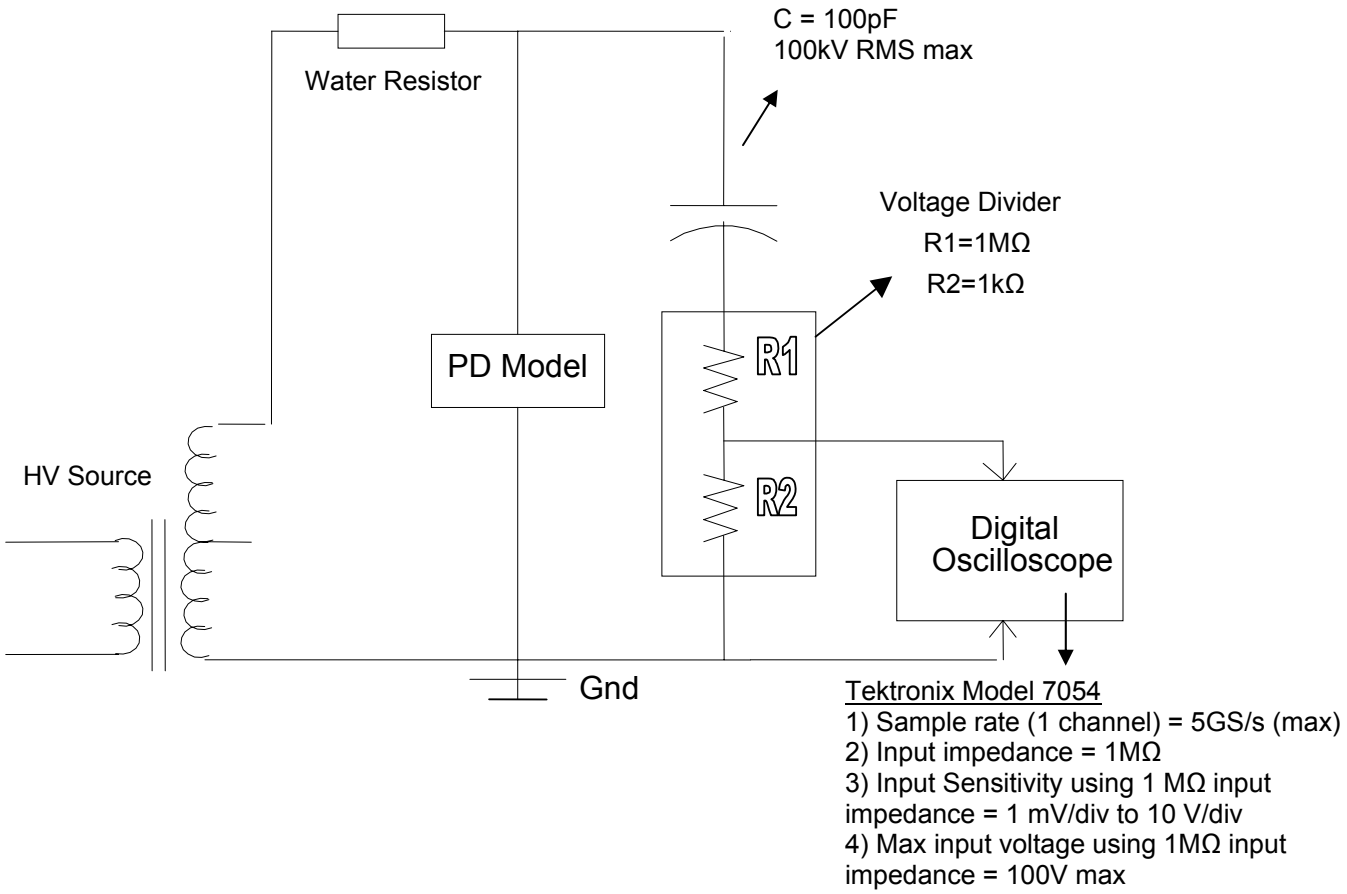

Figure 3-1: PD test arrangement in the laboratory

Figure 3-1 shows the PD test arrangement in the HV laboratory. LHS shows the AC HV test transformer of rating 230 V / 100 kV housed in a locked safe compartment during energized state. The LV is controlled by a variac provided with safety locks and tripping devices. A water resistor of 3 MΩ isolates PD signal from the transformer and limits the breakdown current. The developed PD sample is tested with the controlled HV source. Emitted PD signal is measured using a HV coupling capacitor, C of rating 100 pF/100 kV (rms) and a serially connected resistor chain of R1 and R2. A spark-gap is provided across R1 and ground for HV protection. At 50Hz, the impedance of the capacitor is very high (about 30MΩ) and therefore does not allow significant 50Hz HV signal to flow through. At high PD frequency like 10MHz, the impedance of the capacitor is almost negligible and C will allow PD signals to flow through with negligible PD voltage drop. A wide bandwidth digital oscilloscope of Tektronix model TDS7054 is used to record PD signal across R2. The scope input Impedance is set at 1 MΩ. The signal can be recorded from 1 mV to 100 V with a maximum sampling rate of 5 GS/s. The time duration can be from 2000 ps to 400 s. Simultaneously 4 channels can be recorded.

3.2 Resolution of PD data

Two types of computational analysis are planned to study the characteristics of PD. They are known as group pulse occurrence analysis in 20 ms duration and single pulse analysis from data in 1.6 ms duration as shown in figure 3-2.

a) **Group pulse analysis -** This is to observe and analyse the behaviour of the random occurrence of PDs in 20 ms cycles. The group analysis can also be referred as the statistical study of the PDs over a substantial number of voltage cycles. The setting of the digital oscilloscope used in recording for the group analysis is 40ms with 100 k sampling points resulting in 400 ns per sample point. The typical time duration of PD is in the range of 1 μs and the number of sampling points for the PD pulse would be 1 μs/ 400 ns = 2.5 points. Because FFT is performed on the individual PD pulse, more number of points like 128 sampling points or more may be needed for better analysis.

b) **Individual pulse analysis-** This is to study the time domain characteristics like time duration, pulse height and shape of each type of single PD pulse individually. Details of PD occurrence in 1.6 ms duration are recorded with 200k sampling points resulting in 8 ns per sample point. The number of sampled points in 1μs comes to be about 125.

3.3 Voltage reference for statistical PD analysis

The statistical occurrence of PD signals with Φ requires a common reference Φ of energizing voltage source for interpretation. Recorded random occurring PD current signals have phase shifts due to triggering. A phase-shifted reference sinusoidal low voltage source is phase synchronized with the energizing voltage source using a capacitor divider. That reference voltage source is also recorded simultaneously with the signal using another channel of scope.

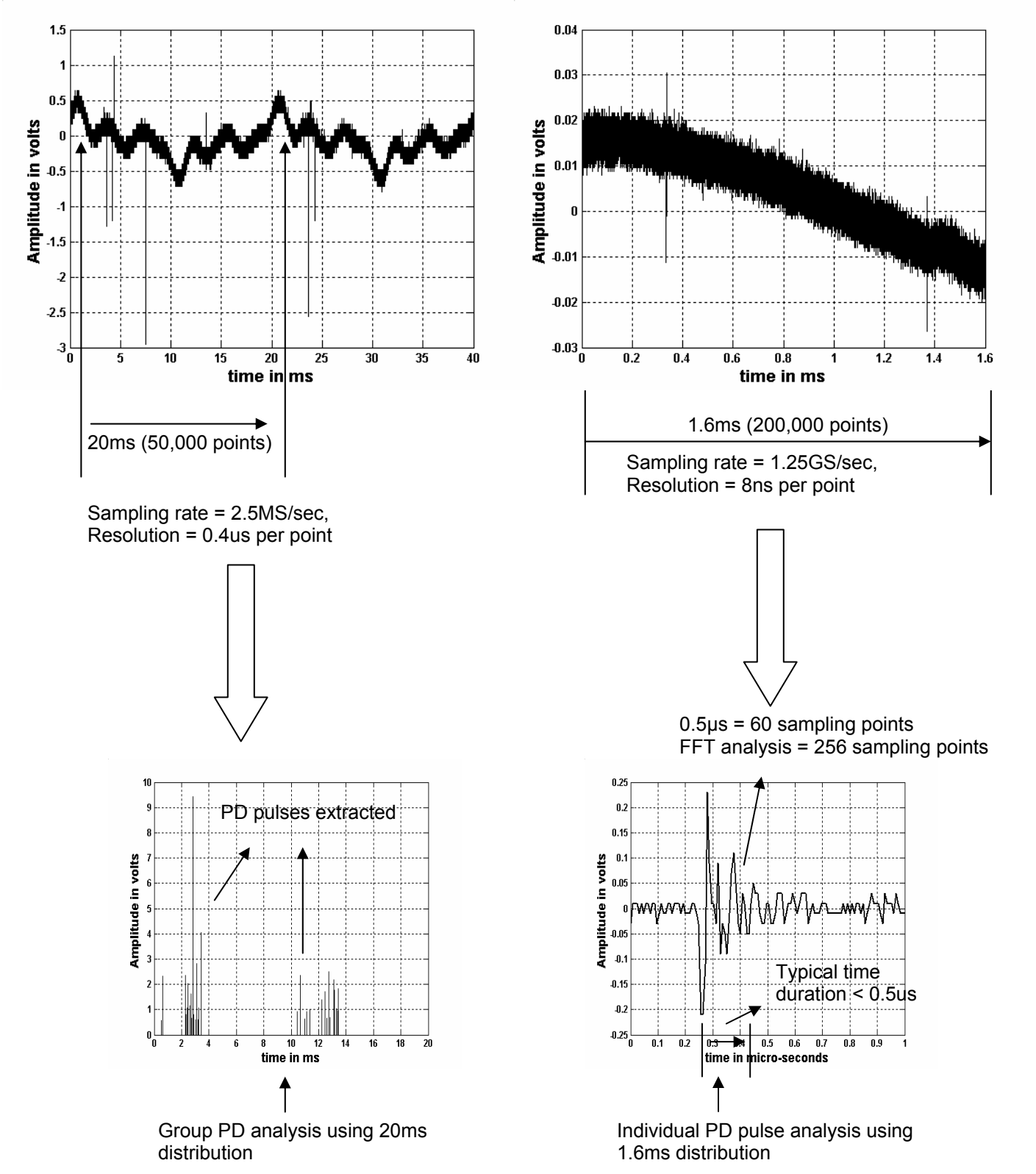

Figure 3-2: PD occurrence in 20 ms and 1.6 ms

In all the analysis, the PD data corresponding to zero ϕ of reference is taken as the starting of 20 ms PD signal. The PD data is Φ corrected for superposition of all the recorded 20 ms data. Since the voltage across the R2 resistor representing PD current waveform leads the source voltage by roughly 90 degrees, peak of 50 Hz current waveform should occur at zero degree as shown in figure 3-3.

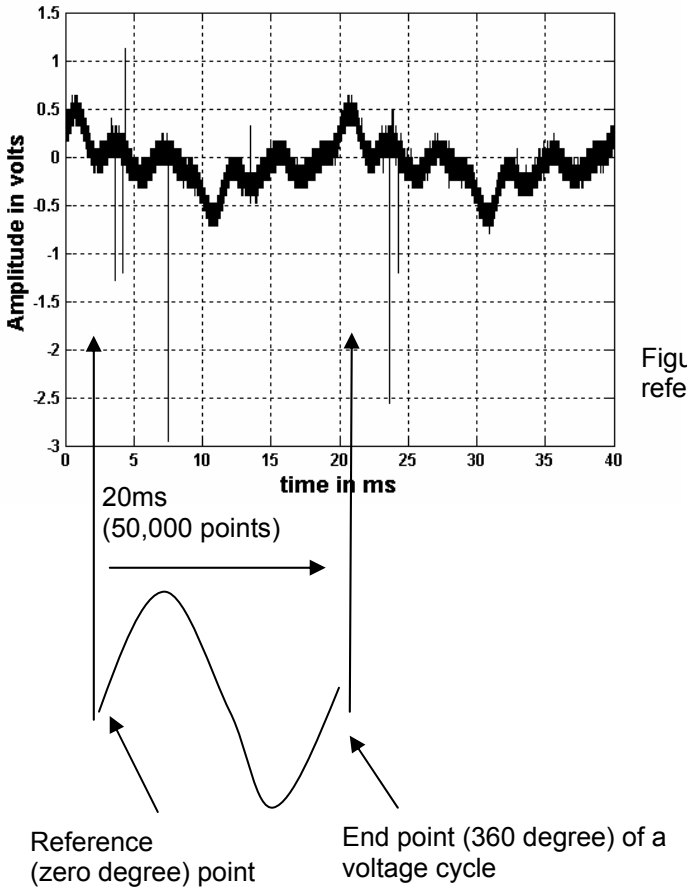

Figure 3-3: Phase referencing of 40 ms data

3.4 Test objects to generate pure PD signal

Pure or single source PD signal means that only one type of PD will be occurring at a time. Three test objects are fabricated to generate the three types of pure corona, surface, and cavity discharges.

3.4.1 Test object to generate corona PD

Corona PD occurs when there is sharp edge or point in power equipment. Therefore, to generate corona in the laboratory, a common household needle is used as a sharp point as shown in figure 3-4.

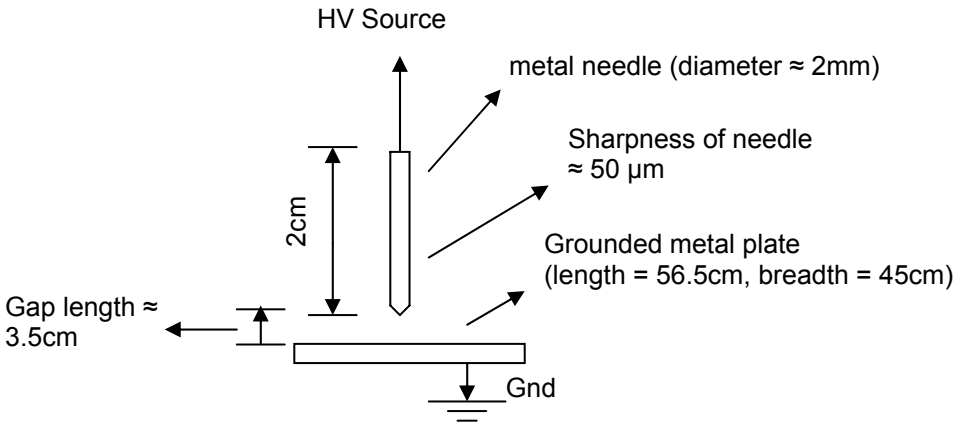

Figure 3-4: Test object to generate corona PD in the laboratory

The needle is polished to get rid of debris, dirt and dust and then connected to the HV source. A grounded metal plate is placed at a distance away from the needle to facilitate faster occurrence of corona discharge by increasing the voltage gradient. Physical dimension of the metal needle plays an important role in the generation of corona discharges. The sharper and thinner the metal needle, corona happens at a lower voltage stress. The applied HV level is gradually increased to observe corona discharges in the oscilloscope. Glowing bluish light can be seen and a hissing noise can be heard when corona happens.

3.4.2 Test object to generate surface PD

An oval shaped VDE metal electrode touching the epoxy surface is connected to the HV source to generate surface PDs. A PCB board with epoxy insulation on one side and the grounded metal surface on the other side is used as shown in

figure 3-5 to generate surface PD. High applied voltage in the range of 15kV creates “burn-marks” on the surface of the epoxy material due to surface PD tracking.

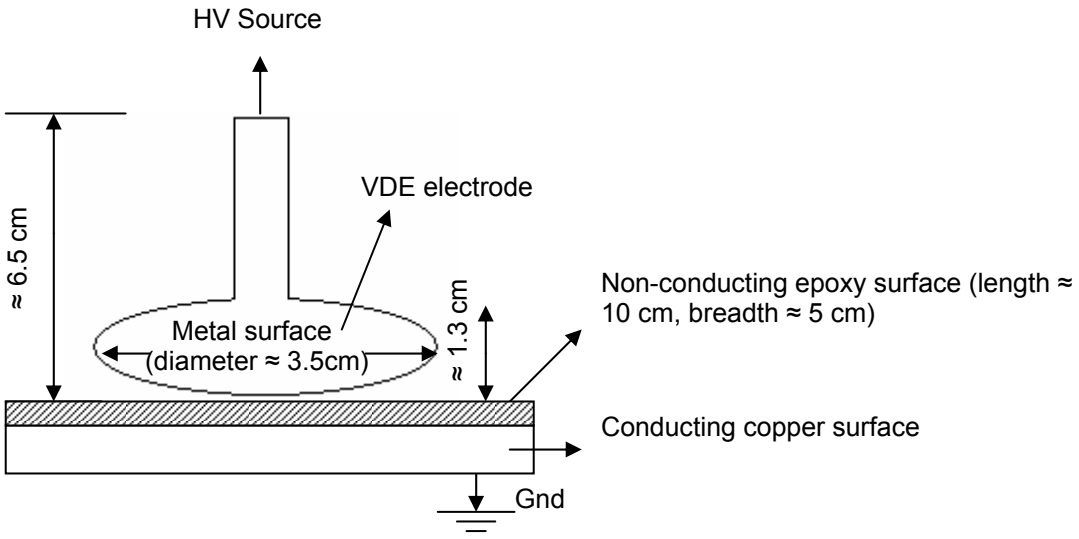

Figure 3-5: Test object to generate surface PD in the laboratory

3.4.3 Test object to generate cavity PD

To get cavity PD, epoxy material is used as an insulating material. A parallel plate capacitor filled with epoxy is fabricated. Before the thermal setting of epoxy, a hollow spherical plastic bead of 0.2 mm diameter is buried in epoxy kept in-between these two parallel metal plates to act as a small cavity. The two copper metal plates have leads connecting to HV source and the ground. The size of the cavity as well as the physical separation between the copper plates directly affects the voltage stress needed to initiate a cavity discharge. For example, larger the separation between copper plates and increased size of cavity increases the voltage needed to start a discharge. A few hollow plastic beads

can be placed between the plates to facilitate a better chance of PD occurrence from multi-sources.

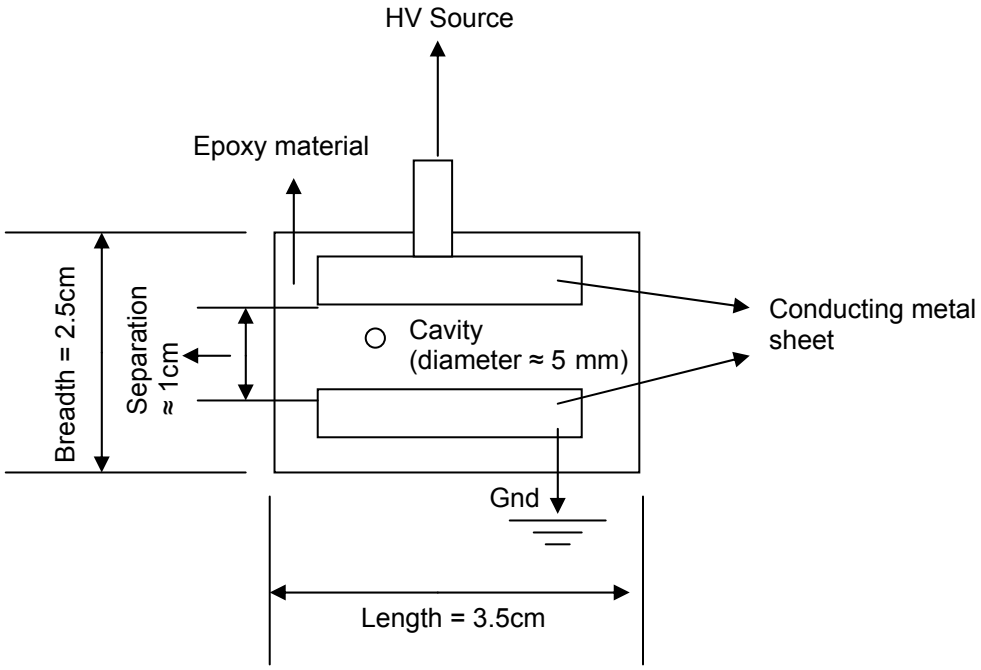

Figure 3-6: Test object to generate cavity PD in the laboratory

Extra care in terminal connection and edges is taken to ensure that the test object does not break down with low range of HV due to surface and corona discharges. Normally, the source voltage is increased gradually to observe and record PDs around 10 kV. High range HV can destroy or burn the test object and a new one is to be fabricated.

3.4.4 Test objects to generate mixed-sources PD

Mixed-sources PD signals mean the generation of two or more types of PDs simultaneously in 20 ms period. To generate corona and surface PDs simultaneously, both PD sources are connected in parallel as shown in figure 3-7. This set-up generates corona and surface PDs when an appropriate voltage is applied. Prior to connecting them in parallel, a check is made on HV level to

generate PD individually on each test object. At least 5 kV is required for corona to happen and at least 8 kV is needed to initiate surface PD with the developed test objects. Test is conducted with HV level in the range of 8 kV.

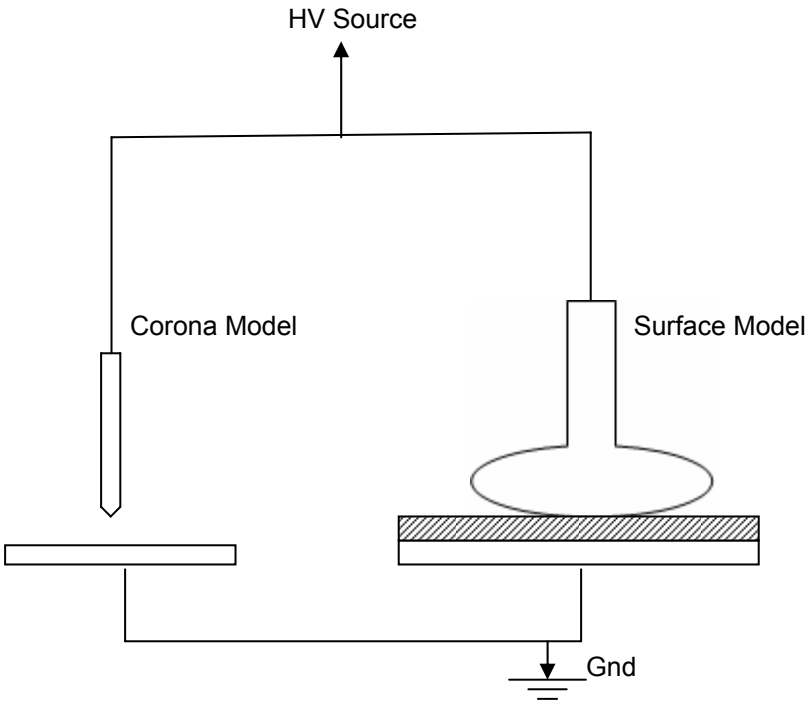

Figure 3-7: Test object to generate simultaneous corona and surface PDs in the laboratory

Extra care is also necessary not to increase the applied voltage too high such that one of the individual test objects may give rise to other types of PD or break down without the knowledge of the user thereby causing major error in data collection. Similar to the mixed corona and surface PDs, all the three PDs can be simultaneously generated by connecting test object on cavity in parallel to the arrangement shown in figure 3-7. It is found that the fabricated test object on cavity may not be able to withstand higher voltages like other two test objects on corona and surface PDs. Once the test object on cavity breaks down, it is not used anymore. Therefore, when all the three pure-PD sources are connected in

parallel, pre-determined safe HV levels are used to ensure all three types of pure PD occur without another new type of PD or damaging any test object. In this thesis, the typical result with two PD sources is presented.

3.5 Developed Software

PD data collection is done in the HV laboratory using the measurement setup and the developed PD test objects. PD data analysis is done using the Matlab software with utilization of the Matlab DSP and Wavelet toolboxes. The following software routines are developed for PD data analysis.

a) Prior to any group and individual pulse analysis, extraction of PDs from the collected noisy sampled signals is necessary. To extract PD pulses from the noisy data, the denoising techniques are developed. The objective of the denoising technique is to remove the background noises while retaining the shapes and amplitudes of PDs. In view of denoising and PD identification requirements, Matlab programs are written together with the use of Matlab Wavelet toolbox. The flexibility on it is described in chapter 4.

b) To achieve more creditable PD type analysis, Matlab programs are written to perform correlation analysis for the extracted pulses from the denoised signals. The developed correlation method is explained in detail in chapters 4 and 5.

c) For statistical group PD analysis in 20 ms period, Matlab programs are written to calculate the mean, maximum, and number of PDs against the phase angles and magnitude windows over several voltage cycles.

Statistical quantities like skewness, kurtosis, cross-correlation factor as well as weibull fitting parameters are also calculated for each type of PD to evaluate the inherent characteristics of pure PD.

d) For individual PD pulse analysis, Matlab programs are written to determine the shape, time duration, and amplitude of each type of PD in time domain, and the dominant FFT content of individual pulse in frequency domain.

e) Software programs are also written to identify the types of PD embedded in a mixed-sources signal using the developed CWT, correlation and mixed-weibull methods. Microsoft Excel is used to store the cumulative PD data and also to perform the mixed-Weibull fittings on the stored data in order to determine the mixed-Weibull parameters.

3.6 Summary

Using the measurement setup, developed PD test objects and software programs, desired type/ types of PD are generated, recorded and identified with noises using the developed wavelet and other techniques. Developed signal processing techniques on group and weibull parameters characterize pure PDs. Newly developed signal processing methods of single PD correlation using wavelet techniques and time and frequency domain analysis can identify the types of PD present simultaneously in mixed PD sources in terms of pure PDs. The details are reported in the subsequent chapters.

Chapter 4

PD Detection using Wavelet Transform

In this chapter, the applications of CWT and DWT for denoising and detection of the types of PD is presented. It is found that both wavelet transforms are able to detect PDs. After researching on both, DWT is chosen instead of CWT for PD data analysis because it offers better flexibility in processing the PD signals and uses less computational time and memory. In addition, the detail coefficients at lower levels of a DWT decomposition tree are extracted and reconstructed to obtain PD signals in time domain without noise. This chapter presents the following:

a) Typical recorded PD waveforms in the laboratory

b) PD identification using CWT

b) PD identification using DWT

Research is made to identify the type of mother wavelet, wavelet scale, and thresholding technique best suited for PD diagnosis. Wavelet processing on identifying the original Φ location of PD and in reconstruction of PD signal without noise is presented. The demerits of the techniques are also highlighted.

4.1 PDs generated in the laboratory

Figures 4-1a to 4-1c show the typical recorded signals in 20 ms period due to three types of PD respectively using the laboratory measurement setup described in chapter 3.

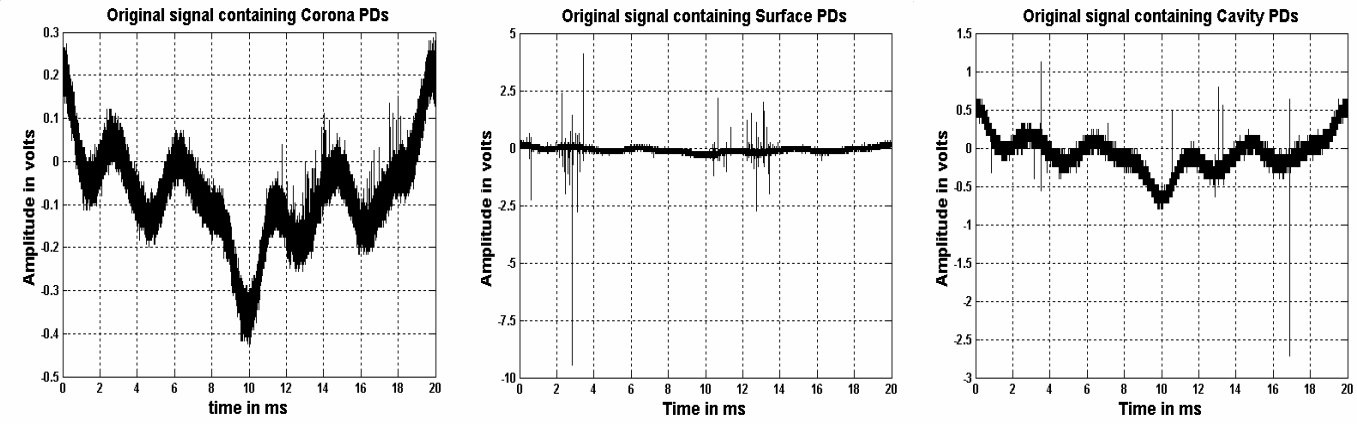

(a) corona PD at 5kV (b) surface PD at 5kV (c) cavity PD at 9kV

Figure 4-1: Recorded corona, surface and cavity PDs

Figure 4-1 shows the characteristics of recorded PD modulated with 50 Hz and other harmonics. PDs appear as “bursts” or “spikes”. Recorded corona PDs are seen to occur mainly in the negative half of a voltage cycle. Since the peak to peak 50 Hz and its harmonics magnitude is around 0.7 V, the 50 Hz and harmonics core also seen clearly in (a). Surface and cavity PDs occur in both positive and negative half cycles. Peak to peak magnitude varies up to 13 V for surface PD and about 4 V for cavity PD. Surface and corona PDs occur in limited phase angle period and the time interval between consecutive surface PDs is longer in comparison with corona PDs time interval. In the next two sections, the wavelet denoising methods to retrieve PD without distorting the time or Φ location, and shape are presented.

4.2 PD detection using CWT

4.2.1 PD detection by the determination of CWT coefficients

In CWT, a selected mother wavelet undergoes various scaling (stretching) to analyze different frequency components of a sampled signal. The derived results

are in the form of correlation coefficients and are dependent on the type of mother wavelet selected. Therefore, mother wavelets that are highly localized in time domain and resemble an abruptly changing signal like a PD is selected. After CWT, high CWT coefficients indicate a highly correlated result between the selected wavelet and the extracted portion of the data. Coefficients of lower values will be associated with background noises. Figure 4-2 shows the zoomed view of a PD pulse embedded in a signal and the determined CWT coefficients to illustrate the ability of CWT in capturing PD events and not the noise. The dashed line denotes the original signal while the bold line is the extracted CWT coefficients.

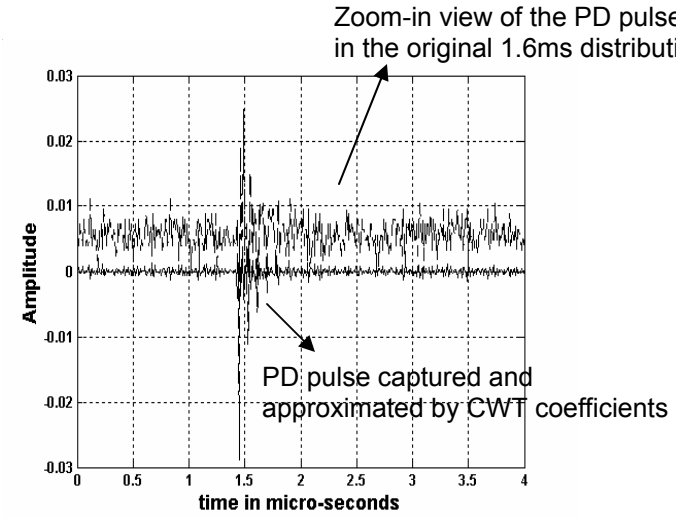

Figure 4-2: Variation of CWT coefficients using mother wavelet Coif5

The same determination is done on figure 4.1 data using wavelet coif5. The determined CWT coefficients with scale 1 and mother wavelet are shown in figure 4-3.

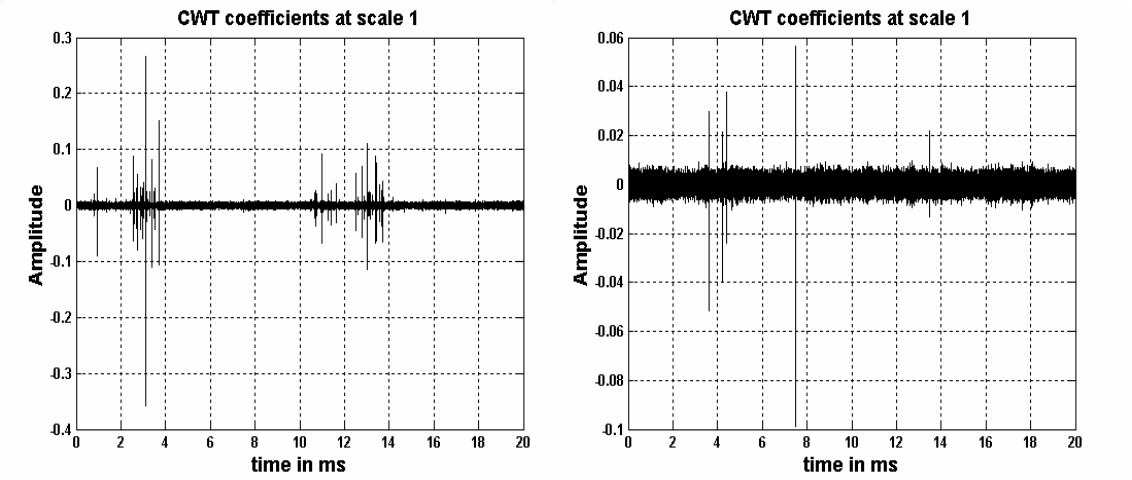

(a) surface PD (b) cavity PD

Figure 4-3: Variation of CWT coefficients for surface and cavity PDs

The locations of maximum CWT coefficient denote the occurrence of dominant PDs. The results depend on the selection of an appropriate wavelet to capture PD events. Simple comparison with original data confirms that the CWT coefficient distribution can be used to identify surface and cavity PD Φ locations. The evaluated peak magnitude of the coefficients does not vary linearly with PD peak magnitude but the coefficient distribution in time/Φ/sampled point plane is maintained.

4.2.2 Determination of the best fit wavelet of CWT for PD detection

In chapter 2, two methods of calculating the coefficient are introduced. In addition, appropriate wavelets for PD detection are also presented. The two methods are described below.

a) In the method 1, the correlation factor between the selected wavelet and extracted PD pulses is used as determined CWT coefficients. The best fit wavelet must capture correctly the exact Φ location of PD pulses and must be

able to show high coefficient values throughout the time duration of a PD pulse while suppressing the coefficients associated with noises to very low values.

b) In the method 2, the squared energy of the CWT coefficients is used to determine the best fit wavelet. The best fit wavelet presents the highest squared CWT coefficient values associated with PD and low squared coefficient values associated with noises.

4.2.2.1 Determination of an appropriate wavelet for PD detection using method 1

LHS of figure 4-4 shows a typical single PD with 4 sampled points. Wavelets db2, db4, db6, db8, db9, db15, db20, Sym4, Sym8, blor6.8 and Coif5 shown in figure 2-4 are used for PD detection [89]. The best fit wavelet is the one that can capture the location of PD occurrence while at the same time displaying high coefficient values at these 4 sampled locations.

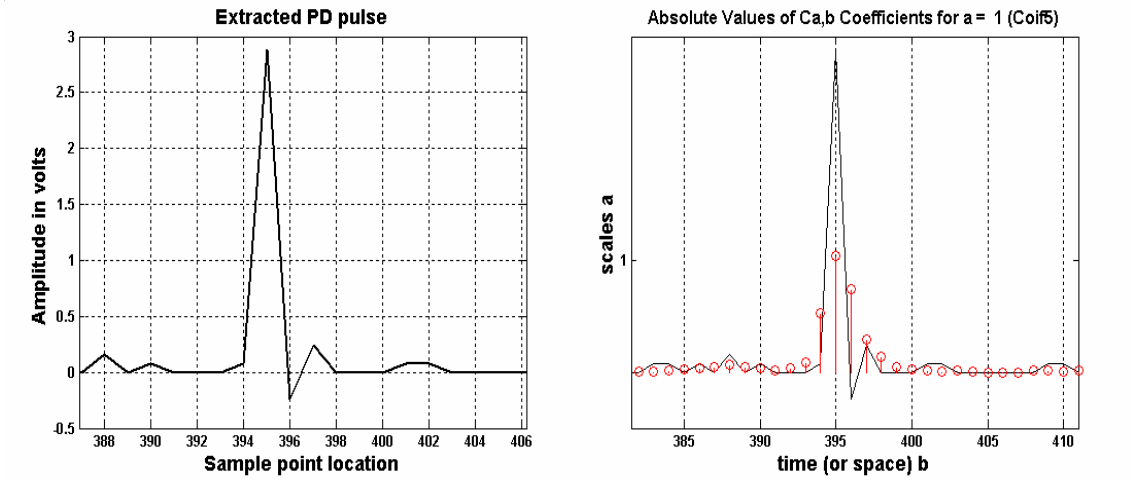

(a) Original single PD

(b) Variation of coefficients within the duration of PD pulse

Figure 4-4: Variation of CWT coefficients on single PD with Coif5

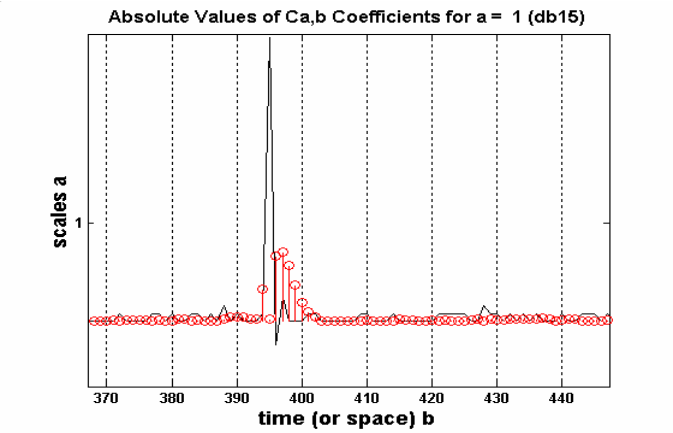

Figure 4-5: Variation of CWT coefficients on single PD with db15

Using other mother wavelets, distortion in location and magnitude is more. A typical example of using an inappropriate wavelet db15 is shown in figure 4-5. A satisfactory fitting is made in figure 4-4 by taking a scale factor, a =1 and mother wavelet, Coif5.

4.2.2.2 Determination of an appropriate wavelet for PD detection using method 2

The method 2 analyzes the PD distribution in 20 ms using coefficients to show the increase in sensitivity of identification while the method 1 deals with individual PD pulse to show the fitting. CWT is performed on the signal shown in LHS of figure 4-6. The square of the CWT coefficient aids the identification of the location of abnormalities as high CWT coefficient values are deemed to be associated with PD events. Wavelets Coif5, Sym4 and Sym8 are found to predict PD magnitude closely. Similar procedure is performed to obtain best fit wavelets for the detection of corona and cavity PDs. Analysing the results using the two methods, Coif5 is chosen because it captures the location of the PD pulses better than Sym4 and Sym8.

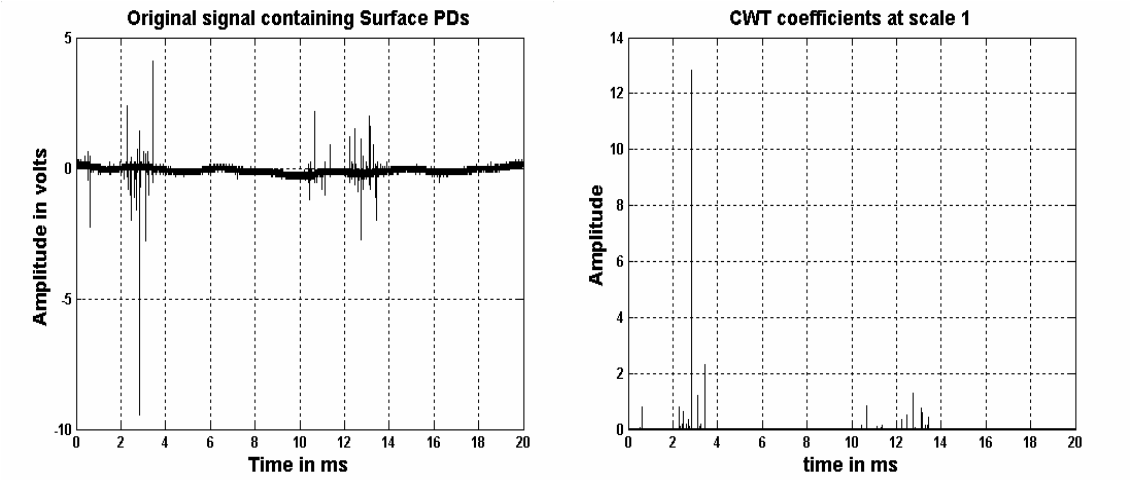

(a) Original PD distribution (b) Variation of coefficients with time

Figure 4-6: Variation of CWT coefficients in 20 ms with coif5 using method 2

4.2.3 Selection of Wavelet Scale

It is determined that surface and cavity PDs have higher frequency components than that of corona. The scale of a wavelet in CWT is inversely proportional to frequency i.e. low scale wavelet captures high frequency content in a signal and high scale picks the low frequency content. Therefore corona and surface PD pulses are found to exhibit different intensity of the CWT coefficients using different wavelet scales. This is tested with the following data shown in figure 4-7.

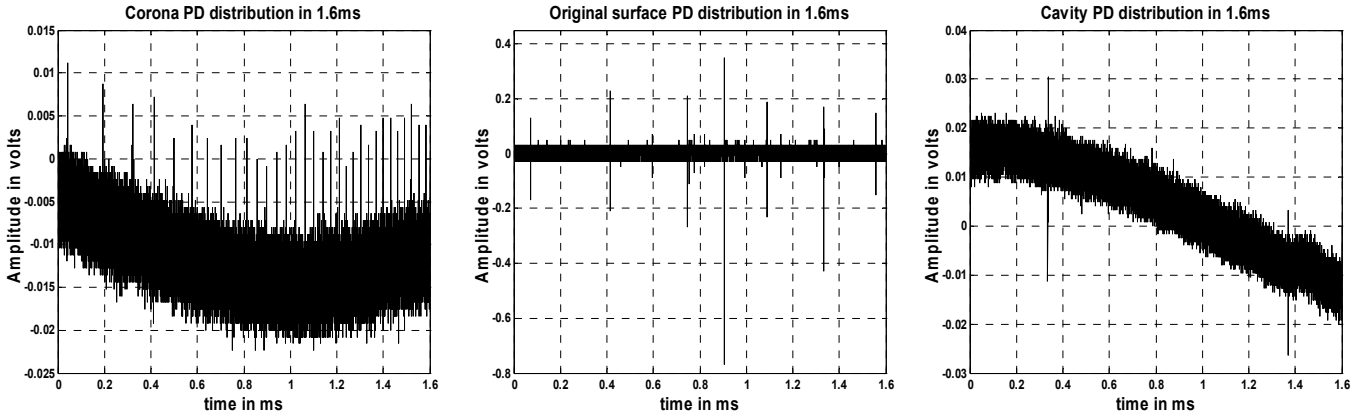

(a) corona (b) surface (c) cavity

Figure 4-7: Typical recorded single corona, surface and cavity PDs

CWT coefficients are calculated by varying the scales from 1 to 10 and by using wavelets db2, db4, db8, db15, db20, Sym4, Sym8, bior6.8 and Coif5. Typical results on corona, surface and cavity are shown in figures 4-8a, 4-8b, and 4-8c respectively. The used sampling rate is 125 Mega-samples per second with a nyquist frequency of 62.5 MHz. Using the relationship between scale of a wavelet and frequency as shown in equation 2.6 of section 2.4.2.2, it is found that using lower scale of a wavelet i.e. scale 1.5 (which corresponds to about 58 MHz), only surface and cavity PDs are detected independent of the types of used wavelet (see figures 4-8b and 4-8c). At higher scale levels (scales 5 and 10), high CWT coefficient amplitudes associated with corona bursts are observed (see figure 4-8a). Therefore, the wavelet scaling in CWT is another important consideration when analyzing different types of PDs. For the identification of the types of PD in an unknown multi-sources PD, this technique is found to be an effective tool (see section 6.2.4). One advantage of CWT over DWT is the flexibility in choosing different scales for signal frequency components analysis. Usually, the CWT uses continuous scales (i.e. 1, 2, 3….n) in order to observe for minute changes. The DWT (see chapter 2) aims to reduce computational requirement of CWT by breaking the original signal into frequency sub-bands (decomposition levels with dyadic scales) using wavelet filters.

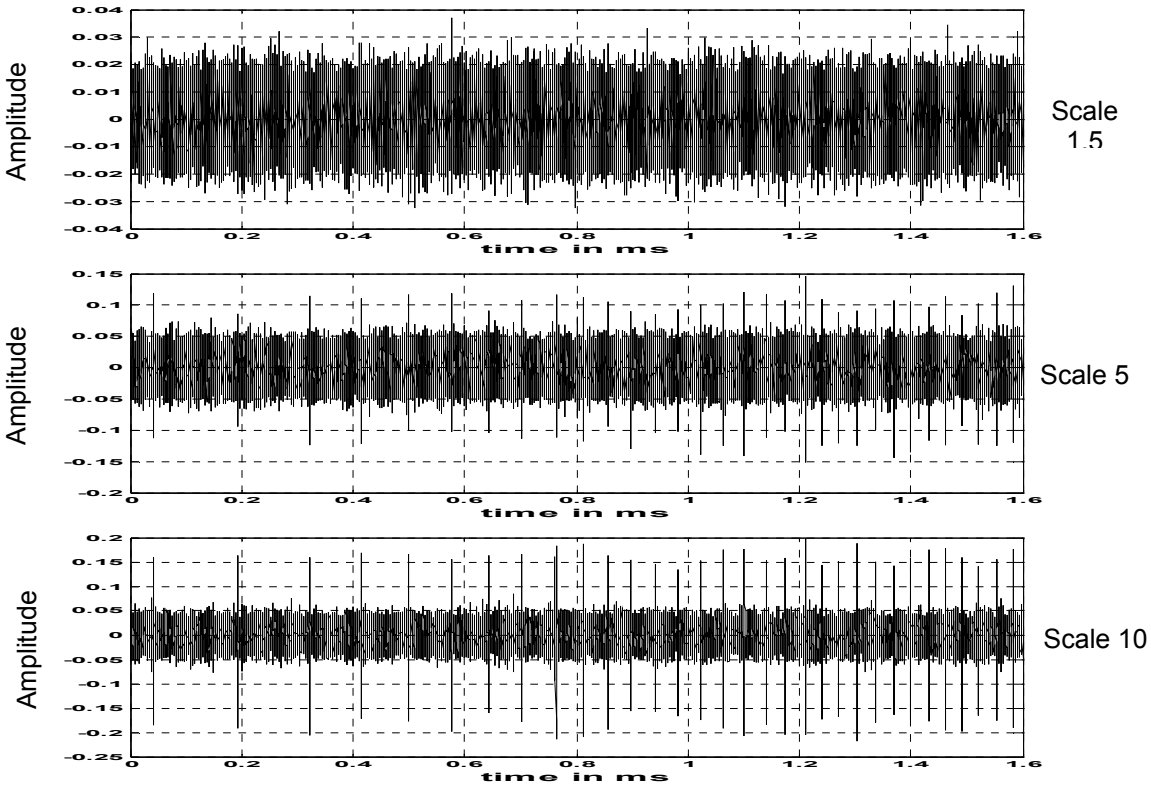

Figure 4-8a: Determined CWT coefficients by changing scale of db9 wavelet on corona PDs

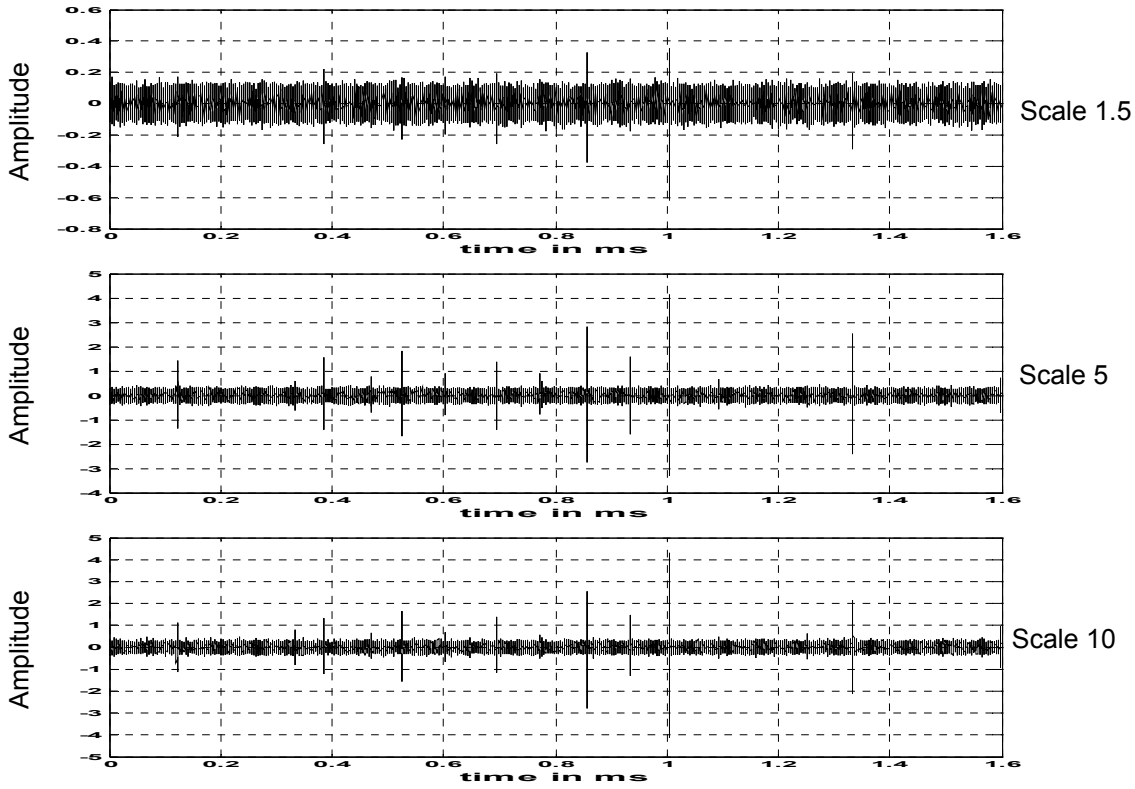

Figure 4-8b: Determined CWT coefficients by changing scale of db9 wavelet on surface PDs

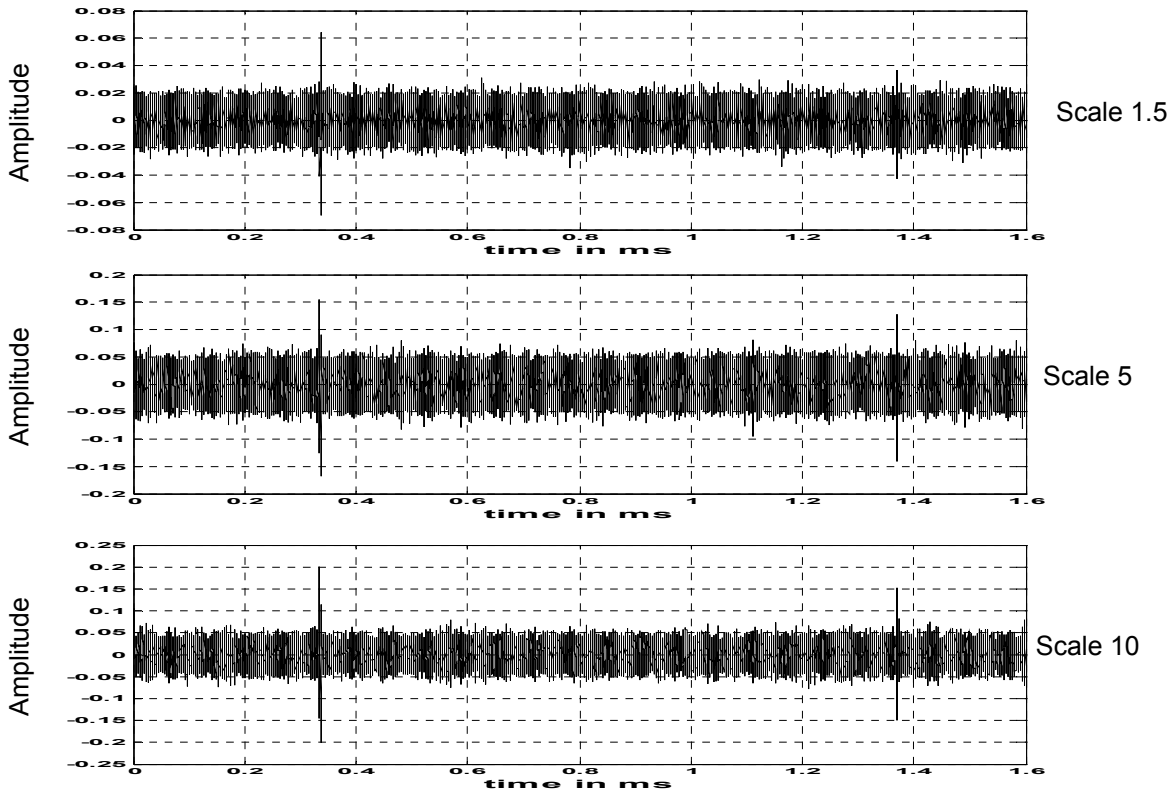

Figure 4-8c: Determined CWT coefficients by changing scale of db9 wavelet on cavity PDs

4.3 PD detection using DWT

PDs occur randomly in any measured signal. They are high-energy pulses concentrated in short time duration. As for the noises, it can be seen from figures 4-1(a) to 4-1(c) that they exist in the entire duration of sampled signal. Noise energy levels are lower than that of PDs. This energy difference between noises and PDs is also reflected in the extracted amplitudes of the DWT coefficients. In DWT, the coefficients are determined after filtering in various frequency ranges.

4.3.1 Determination of detail and approximate DWT coefficients

PD occurrences are detected by determining the DWT coefficients and locating the high DWT coefficients. In DWT, high-pass and low-pass filters are employed to determine the details and approximations of the measured signal. The details

at the lower scale levels (i.e. d1, d2, & d3) are associated with high-frequency components (i.e. d1 span in a frequency band of $0.25 * Sampling\ rate$ to $0.5 * Sampling\ rate$ due to Nyquist Frequency) of the measured signal. For PD analysis lower scale level coefficients are extracted while the details at higher scale levels are discarded. Figures 4-9 and 4-10 show the selected distribution of coefficients with cavity and surface discharges respectively. In figure 4-9, S represents the cavity PD distribution in 20 ms with 50 Hz harmonics sampled at 5 Megasamples per second. Using DWT, the signal is decomposed up to level 7. The evaluated approximate coefficients a7 and detail coefficients d1, d3, and d7 are indicated in the figure 4-9. Dominant high coefficient values associated with sampled locations of cavity PD are seen mainly at lower scale levels from d1 to d3. Low frequency ambient 50 Hz and harmonics noise are seen in DWT coefficient distribution shown in a7. This evaluation is also tested on surface PD distribution shown in figure 4-10. Dominant high coefficient values associated with sampled locations of surface PD are again seen at lower scale levels from d1 and d3. DWT is unable to give the exact frequency components of a signal but rather a band of frequencies that exists for a signal with time/sampled point. Therefore, FFT are performed on the PD signals using larger number of points to determine the frequency components in PDs.

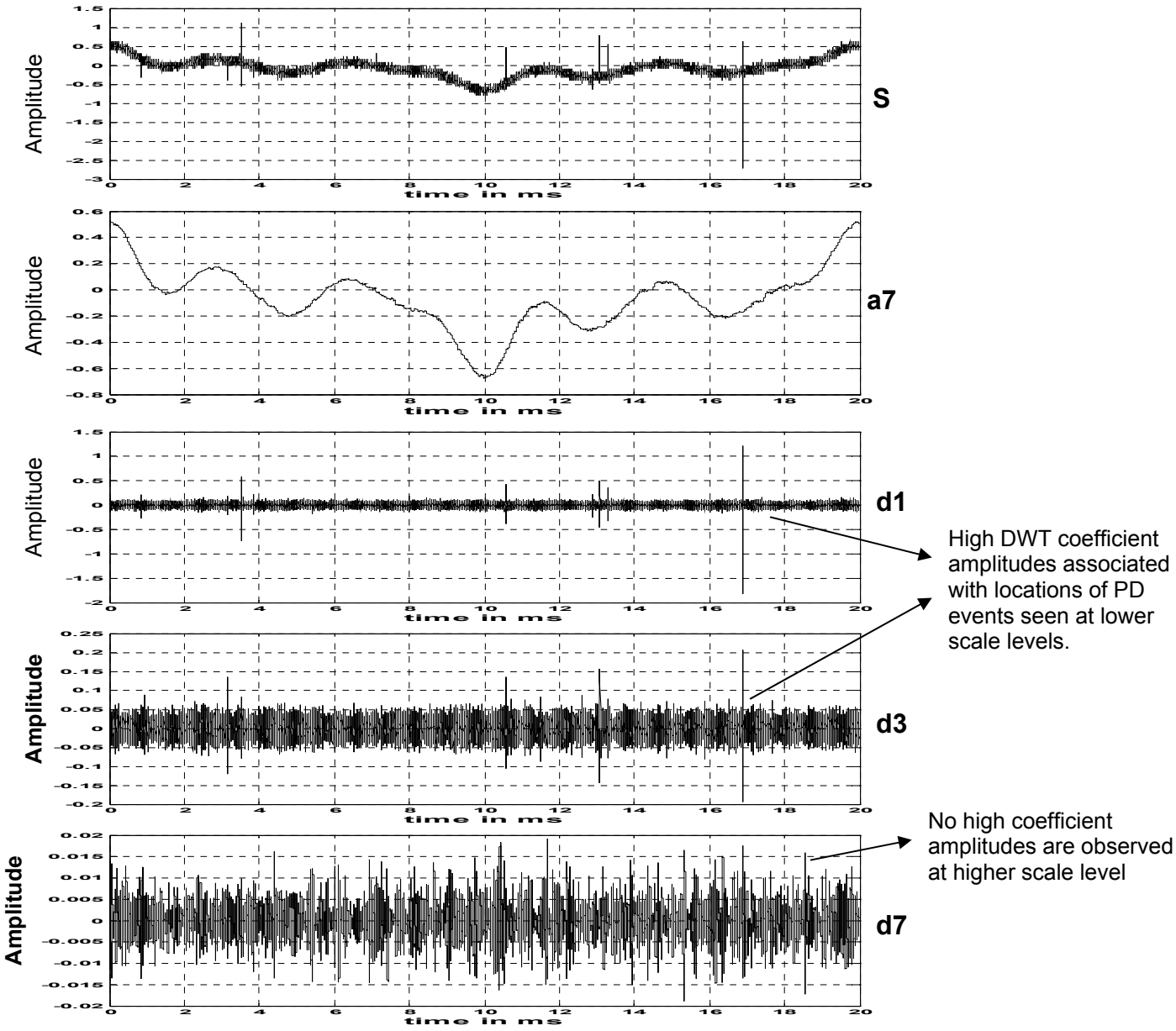

Figure 4-9: Evaluated DWT coefficients at levels 1, 3, and 7 on cavity PD

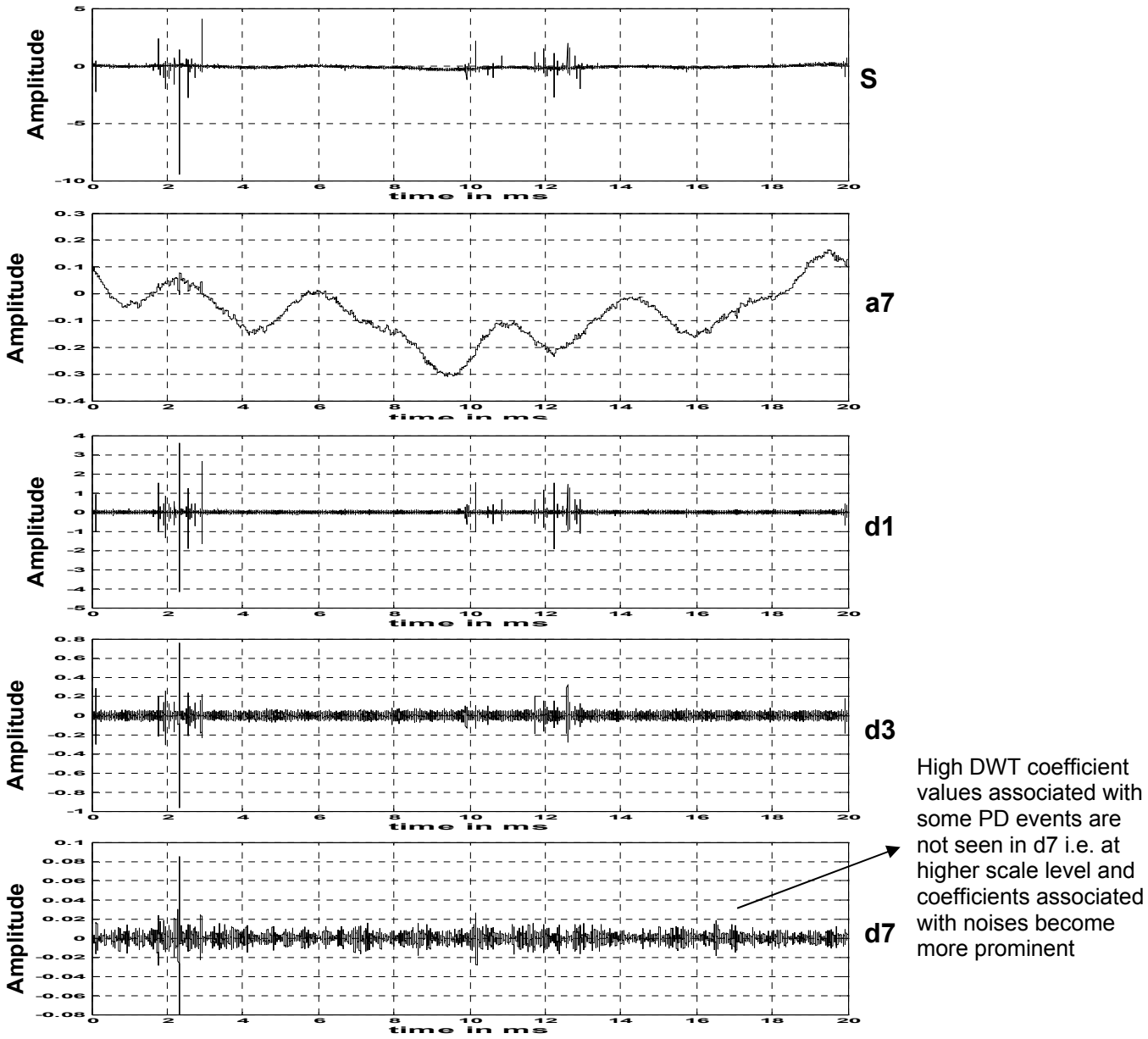

Figure 4-10: Evaluated DWT coefficients at levels 1, 3, and 7 on surface

4.3.2 Effect of sampling rate on detail coefficients associated with PDs

When high sampling rate is employed, the locations of high values of detail coefficients are seen to appear in higher detail levels i.e. d3, d5…etc instead of starting from d1. Such observations again show that the frequencies that exist in PD are reflected as high values of detail coefficients only at appropriate detail

levels that have frequency bands similar to that of PDs. Figure 4-11 show a signal containing a mixture of surface and corona PDs. It is sampled at a sampling rate of 250 Mega-samples per second and high amplitudes of detail coefficients connected with surface PD appear from d5 (frequency band ranging from 15 MHz to 31 MHz) and above instead of at level d1 which covers a frequency band from 62.5 MHz to 125 MHz. This is different from figures 4-9 and 4-10 which are sampled at 5 Mega-samples per second and corresponding surface PD occurs at d1.

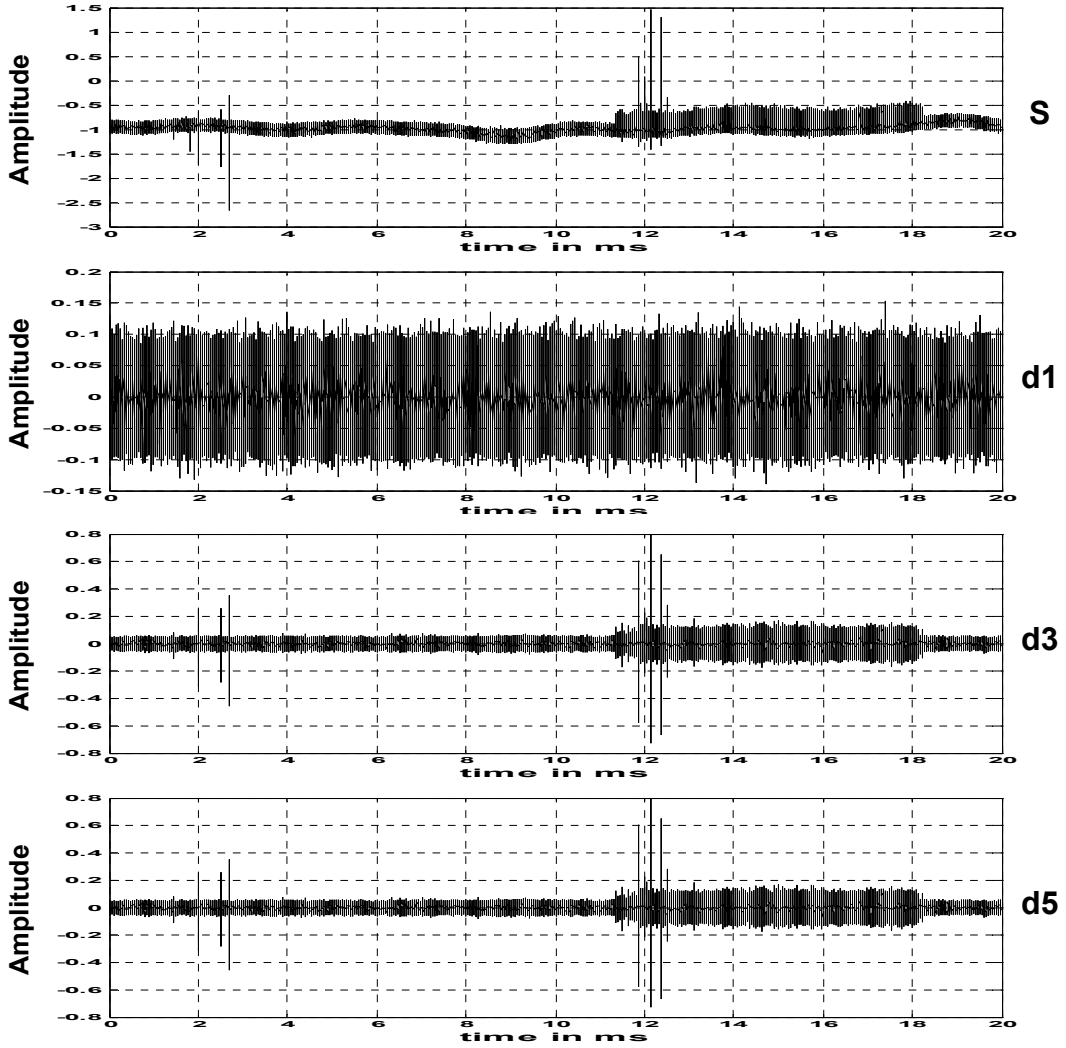

Figure 4-11: Evaluated DWT coefficients on surface and corona PDs sampled at 250 MS/s

4.3.3 Recovered signal after denoising using DWT

Using DWT, the location of PDs can be identified by high detail coefficient values at lower levels (i.e. d1, d2, etc). The usefulness of DWT lies on its ability to denoise the sampled signals by simply chopping off the lower detail coefficients which are associated with noises while retaining higher detail coefficients.

Signal (Y) = PD (S) + noise (e) …… (4.1)

Since WT is a linear transform [90], WT of (4.1) gives

WT(Y) = WT(S) + WT(e) ……(4.2)

It shows that there are coefficients associated with noises and the desired PD signals after transform. Using the energy difference between PD and noise, unwanted lower coefficients are discarded and higher ones are retained by setting appropriate threshold values on the detail coefficients. Regrouping the selected decomposed detail coefficients and then inverse transforming back to the time domain, PD signal can be denoised effectively. Figure 4-12 shows the denoised PD signal of the original signal shown in figures 4-1(a) to 4-1(c) by grouping the detail coefficients. With the background noises cleared, there are more “spikes” observed in the denoised signal than in the original signal. For all the processing, signals are processed to a level at which spikes of high DWT coefficients are obtained.

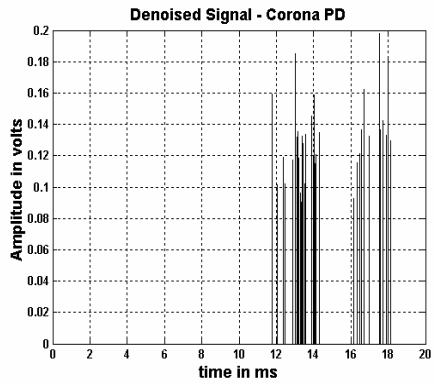

Figure 4-12(a): Denoised signal of figure 4-1a

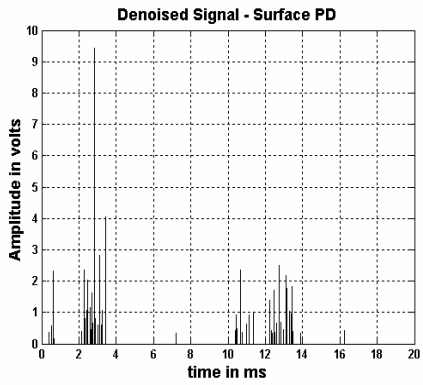

Figure 4-12(b): Denoised signal of figure 4-1b

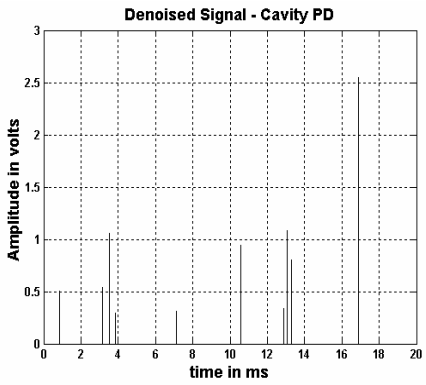

Figure 4-12(c): Denoised signal of figure 4-1c

Figure 4-12: Denoised signals by employing DWT for PD detection

4.3.3.1 Steps involved in DWT to denoise PD signals

Analysis using PD occurrence with Φ is made easier after denoising. A few essential steps in DWT are investigated during the denoising process.

a) The effect of selecting different mother wavelets for DWT analysis is done.

b) The effect of number of decomposition levels on the end denoised result is studied.

c) The appropriate threshold values for chopping off the unwanted background noises are determined. This step is found to be important as it affects the end result directly.

d) A threshold estimation method to estimate the threshold values for the detail coefficients may be selected. Four reported threshold estimation methods Heursure, Sqtwolog, Rigrsure, and Minimaxi [91,92] for PD analysis have to be investigated. This step is found to be necessary when threshold values are based on developed algorithms.

e) The effect of selecting hard and soft thresholding methods on the denoised PD result is investigated.

f) Verification of the credibility of using DWT in PD analysis is made by comparing magnitude, shape and location of the end result with the original.

4.3.4 Selecting a wavelet to use in DWT

Various authors [93,94,95] suggest to use of appropriate wavelets for different signal processing applications. The objective of selecting a particular type of wavelet from the pool of available wavelets is that using that wavelet, PD pulses are extracted from the noisy background without much distortion. The PD pulses in the denoised signal must be able to retain the shape, duration and amplitude of the original PD pulses. Among the wavelets, the daubechies wavelets are the most popular one because of their ability to detect abnormalities in signals. In this project, the effect of using different orders of the daubechies wavelets (i.e. db2, db4, db9, etc) and four other highly localized wavelets (sym4, sym8, bior6.8 and coif5) for PD analysis are investigated. The reasons for the selection of these wavelets are listed below.

1) Daubechies, symlets and biorthogonal family of wavelets meet the PD characteristics on localization in time domain.
2) There is a need on regularity or smoothness of the wavelet. To reconstruct the signal from wavelet coefficients the smoother the wavelet, the better will be the reconstructed properties [96]. Higher

order daubechies wavelets are found to be smoother than lower order ones.

3) For PD, value of coefficients in the wavelet filters (high-pass and low-pass) should be more. Higher order daubechies wavelets that have high coefficients in their wavelet filters are highly localized in time and frequency ranges [97].

A best fit wavelet in DWT can also be selected based on two methods used in CWT. Method 1 uses the correlation between the original PD pulse and the denoised PD pulse using DWT. Method 2 correlates the energy of the selected detail coefficients got after denoising with DWT.

4.3.4.1 Obtaining the best fit wavelet for DWT using Method 1

Since DWT approximates the original PD signal with the selected mother wavelet, the closeness of the shape of denoised PD pulse is compared to the shape of original PD pulse by correlation. Also in 20 ms period, the occurrence time location of PD is compared. The best fit wavelet is the one which retains the shape and amplitude of the original PD pulse and retains the number of PDs in 20 ms period. Typical results for surface, corona and cavity PDs are shown in figures 4-13, 4-14 and 4-15 respectively. Higher CC values mean better correlation results.

Surface PDs

The daubechies wavelet db9 exhibits the highest correlation coefficient (CC) i.e. it is able to retain the best approximation of the shape of the original PD pulse. In addition, using db9, the denoised PD pulse is able to retain the amplitude of the

original PD pulse. CC varies from 0.9044 to 0.9543 for different wavelets. The typical distributions using db9 and Coif5 are shown in figure 4-13. Coif5 is found to fit with CC of 0.9387. No difference in number of PD pulses extracted (35 in number) by using db9 and Coif5. Other wavelets are found to perform either the same or less optimum in number and shape of PD pulses extracted.

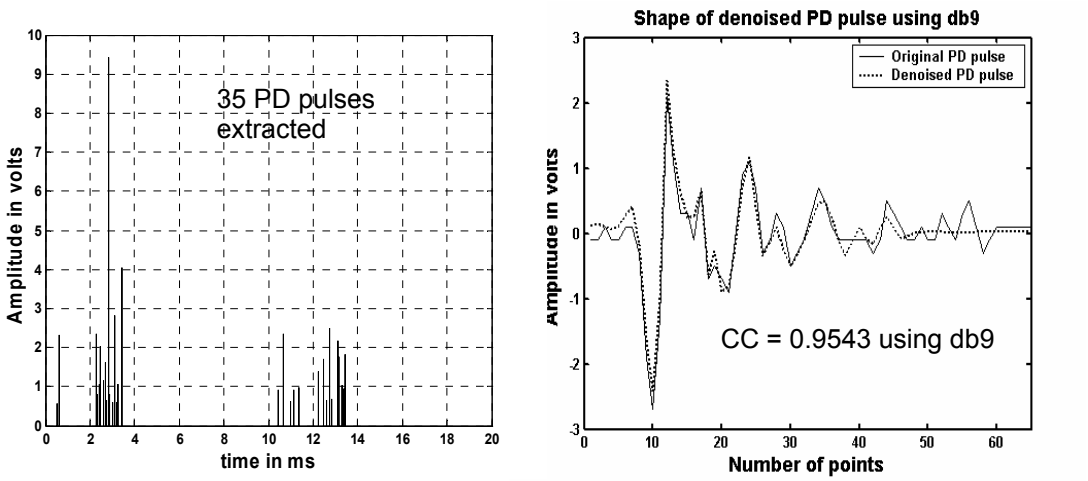

(a) Extracted group and single PDs using db9

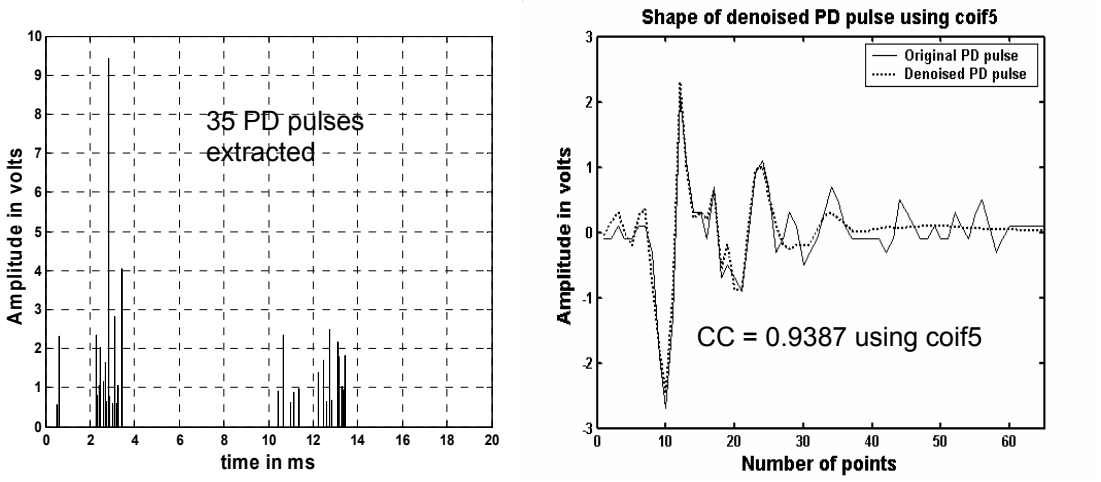

(b) Extracted group and single PDs using

Figure 4-13: Correlation between original and denoised surface PD

Corona PDs

No significant difference in CC is seen on the fitted approximation results. All wavelets exhibit almost the same value of correlation coefficients. For corona PD, CC varies from 0.9973 to 0.9975 for different wavelets. The typical distribution using db9 and Coif5 is shown in figure 4-14. Number of extracted PD pulses is around 31 for different wavelets.

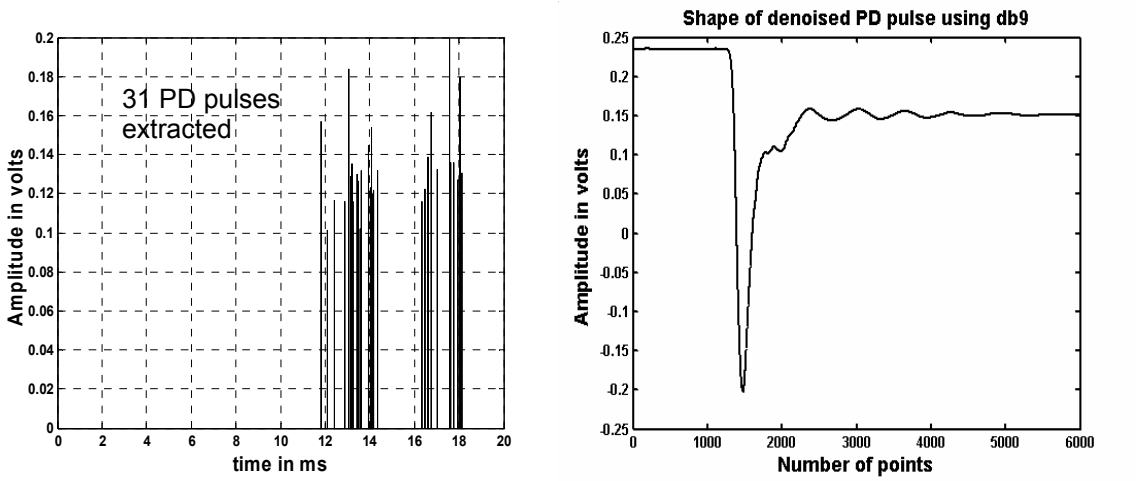

(a) Extracted group and single PD using db9

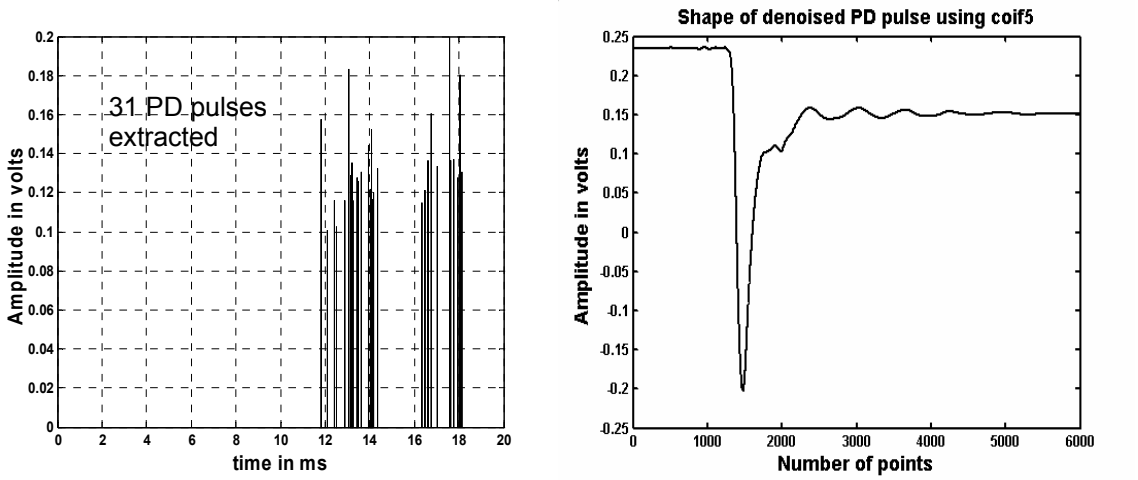

(b) Extracted group and single PD using Coif5

Figure 4-14: Correlation between original and denoised corona PD

Cavity PDs

The daubechies wavelet db4 is observed to exhibit the highest correlation coefficient value of 0.8828. It is only slightly better in shape approximation of the original PD pulse than db9 with CC of 0.8665. For cavity PD, CC varies from 0.8828 to 0.7422 for different wavelets. The typical distribution using db9 and coif5 is shown in figure 4-15. Coif5 is found to fit with CC of 0.8576. No significant difference in PD pulse extraction results is found for these wavelets and others.

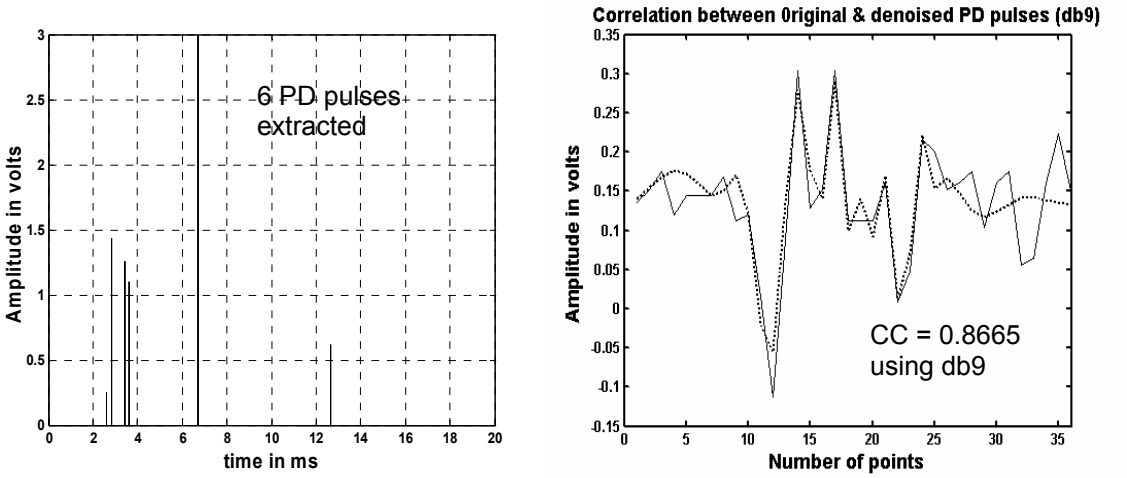

(a) Extracted group and single PD using db9

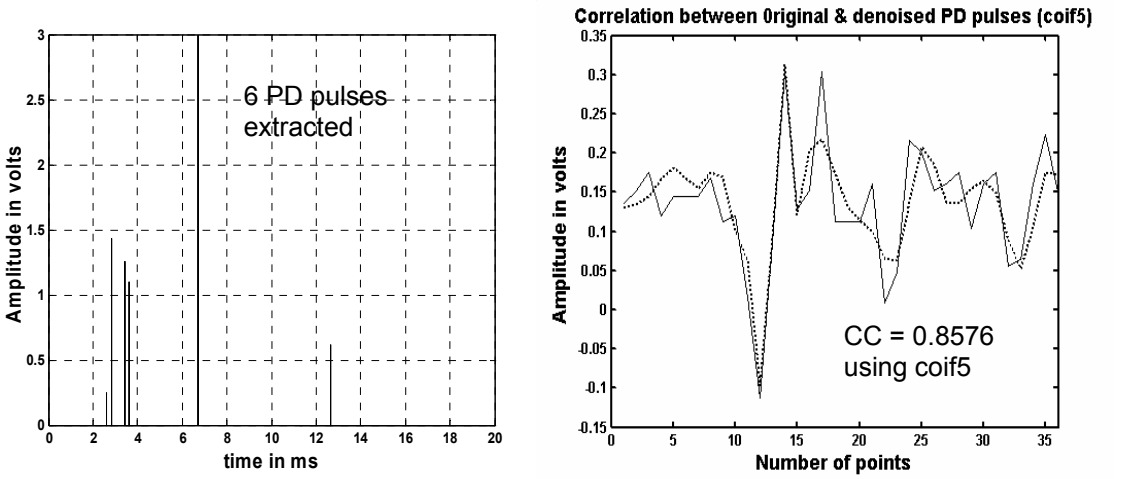

(b) Extracted group and single PD using coif5

Figure 4-15: Correlation between original and denoised cavity PD

Other observations

All the wavelets presented here is able to give reasonably good correlation results (i.e. cc > 0.7) and retain good shape approximation except that db9 performing slightly better than the rest. Appreciable results with predicted number of PDs in 20 ms period and better CC with single PD are obtained when Coif5 and db9 are used.

4.3.4.2 Obtaining the best fit wavelet for DWT using Method 2

Noises are well spread along the sampled signal and their energies are also spread out over the entire signal i.e not concentrated. Therefore after performing DWT, their energies are seen to be distributed over the wavelet coefficients in each decomposition level of DWT. PDs on the other hand exhibit high values of the detail coefficients because their energies are concentrated in short duration. Making use of such energy difference, the best fit wavelet is the one exhibiting highest detail coefficient values associated with PDs while suppressing noise coefficients at scale 1 (because scale 1 involves with the highest frequency range) based on a sampling rate of 5 mega-samples per second. In this way, the best fit wavelet makes the setting of the threshold value easier because of the maximum value of the detail coefficients associated with PDs by the best fit wavelet. Figure 4-16 shows the typical detail coefficient results at level 1 of an 8 levels decomposition tree using db9 and coif5 for surface PDs. The maximum peak value of detail coefficient is found to be around -6 with db9 and -4.2 with coif5.

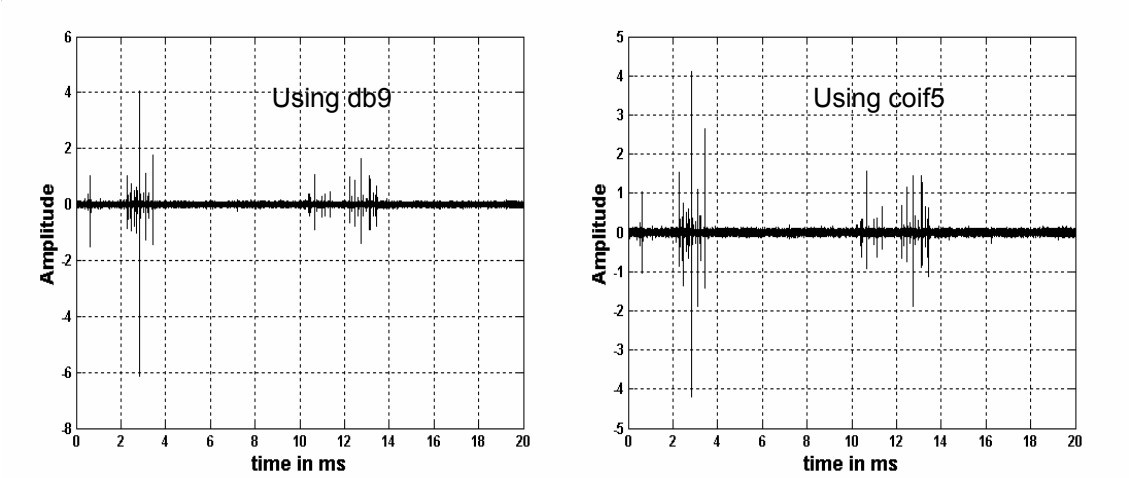

Figure 4-16: Method 2 – Detail coefficients at scale 1
for surface PD distribution using db9 and coif5

Figure 4-17 shows the typical detail coefficient results at scale level 1 of an 8 levels decomposition tree using db9 and Coif5 for corona PDs. The maximum peak value of detail coefficient is found to be around 0.085 with db9 and 0.12 with Coif5.

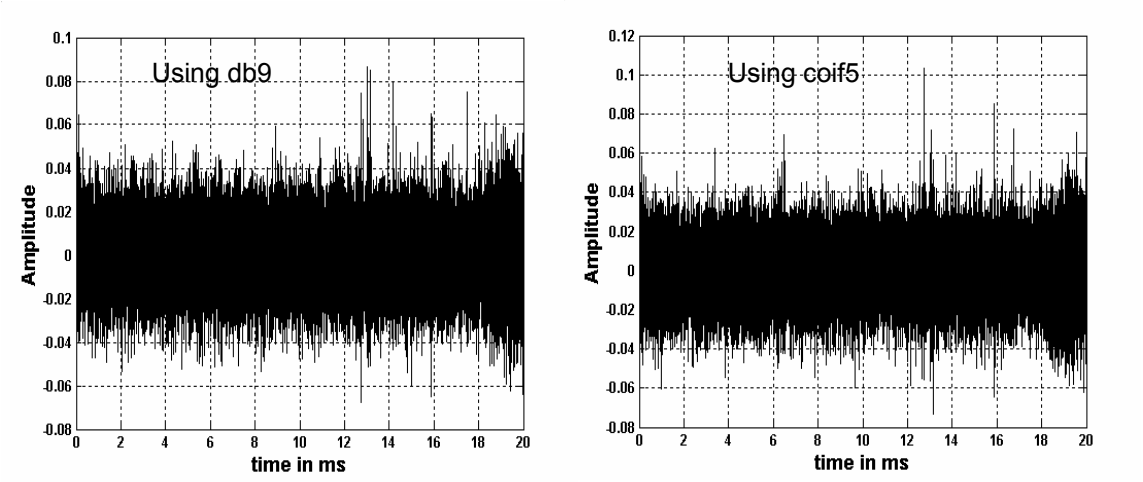

Figure 4-17: Method 2 – Detail coefficients at scale 1
for corona PD distribution using db9 and Coif5

Figure 4-18 shows the typical detail coefficient results at scale level 1 of an 8 levels decomposition tree using db9 and coif5 for cavity PDs. The maximum

peak value of detail coefficient is found to be around -1.65 with db9 and -1.1 with Coif5.

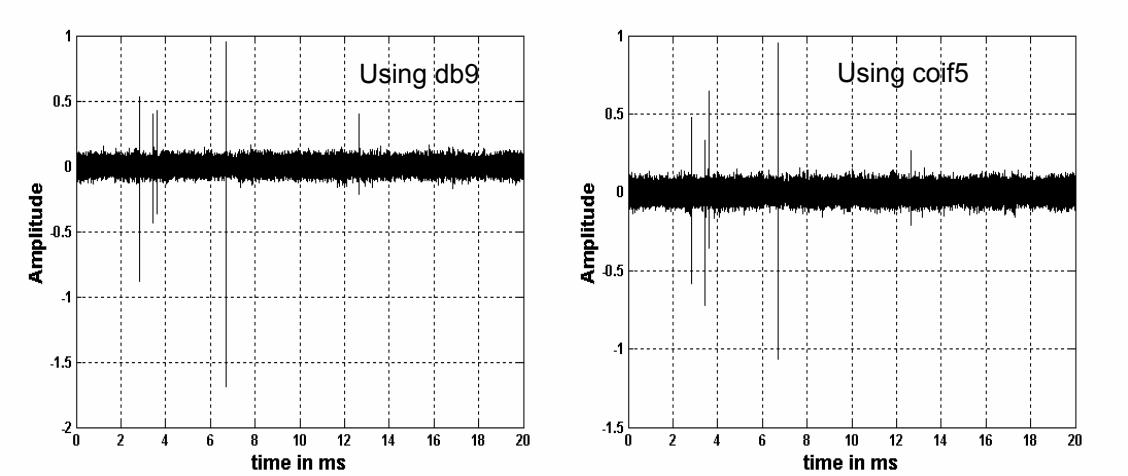

Figure 4-18: Method 2 –Detail coefficients at scale 1 for cavity PD distribution using db9 and Coif 5

It is found that the wavelets db9, sym8, bior6.8 and Coif5 are better in getting the maximum coefficients associated with PDs while suppressing coefficients associated with noises. However, no significant differences are seen between them. Therefore, based on method 2, one of these four wavelets can be chosen for DWT analysis. Other wavelets from the pool of selected wavelets (section 2.4.2 of chapter 2) also perform reasonably well but not optimum as compared to the indicated four wavelets.

4.3.4.3 Comparison of the methods 1 and 2 used in DWT

Method 1 shows that the db9 wavelet is slightly better PD extractor in terms of the shape and amplitude approximation of the individual PDs and number of PDs in the original signal than the rest of the highly localized wavelets. However, Coif5 wavelet is able to extract one more PD pulse from corona sampled data (figure 4-13b) as compared to db9. Correlation results using Coif5 is satisfactory

and comparable to that of db9 especially in terms of peak amplitude and PD duration. Based on other obtained results, the rest of the highly localized wavelets (indicated in section 2.4.2) besides db9 and Coif5 also perform reasonably well but not to the best fit. Method 2 reveals that db9, sym8, bior6.8 and Coif5 give maximum detail coefficients at scale 1 associated with PDs while suppressing detail coefficients associated with noises. Coif5 wavelet is *identified as the best fit wavelet by the two methods* because it predicts the maximum number of PDs and maintains the individual PD waveshape using method 1, and gets maximum detail coefficient values by method 2.

4.3.5 Number of levels for Decomposition

The original signals in figure 4-1 is decomposed into coefficients at different scale levels to detect abnormalities in each frequency ranges. The number of levels to decompose the sampled signal during the denoising process is not as important as the selection of threshold values. However, a decent decomposition level is found to be essential as too low a decomposition level would result in a poorly denoised signal with incorrect PD amplitudes. A decomposition level of 6 or 7 is determined to be sufficient for detection of PDs. As the number of decomposition level increases, it takes more computational time and memory and the end results do not improve much. Matlab software encounters “Out of Memory” problem for decomposition level of 8 and above when a sampled signal with 5 million sampled points in 20ms is analyzed.

Figure 4-19 shows the typical denoised results of the original surface PD distribution shown in figure 4-1b by changing levels from 2 to 12 even though the analysis is done by incrementing one level at a time. The number of pulses changes from 54 to 55 and the maximum peak changes from 6.8 V to 9.5 V for the denoised surface PD distribution. Improvement in PD pulse extraction as the number of level increases is not significant, but employing levels lower than 6 results in significantly lower maximum PD amplitudes which are a fraction of the original maximum PD amplitudes. That observation is evident by comparing the maximum PD heights obtained by using different levels (examples are shown in figure 4-19) with the original surface PD distribution (figure 4-1b). Thus decomposition levels lower than 6 are not selected for PD analysis. In addition, improved denoised signals are achieved as the number of decomposition levels increases. It is also observed that upon reaching level 6 and above, the number of extracted PD pulses is the same i.e. saturates and the maximum number and magnitude of PD peaks improve only slightly. The mentioned phenomena are also observed on the original corona and cavity PD distribution shown in figures 4-1a and 4-1c respectively with different decomposition levels. Thus, for application of DWT on PD detection, a decomposition level of 6 is sufficient to get reasonable results.

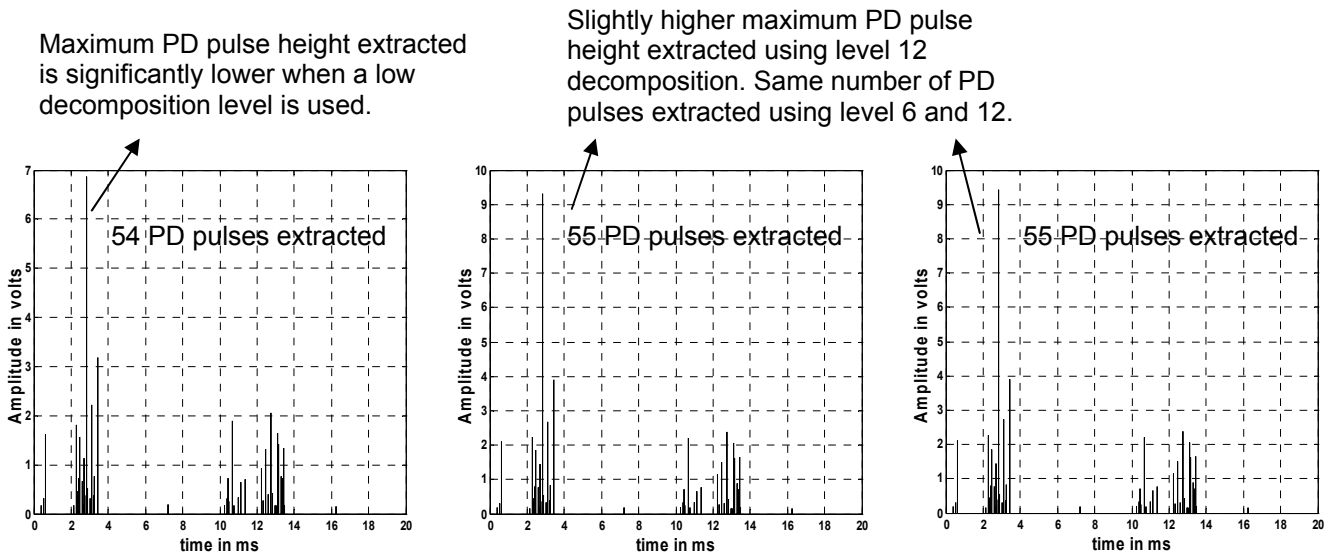

(a) 2 levels decomposition (b) 6 levels decomposition (c) 12 levels decomposition

Figure 4-19: Denoised surface PD pattern by changing the number of levels of decomposition

4.3.6 Selecting an appropriate threshold value

This step is found to be the most important step for the application of DWT in PD analysis because it directly affects the ability to obtain good denoised signals which are essential for PD analysis. The process of denoising may lower the original PD peak amplitude. However, with good selection of decomposition level and threshold values, denoised PD peaks can be made close to the original. With 6 decomposition levels, appropriate threshold value is applied to the detail coefficients at lower levels (i.e. 1, 2, and 3) as they contain information about the high frequency components of the original PD signal. Maximum possible threshold values are set for other higher levels so as to make them all to zero. The modified detail coefficients are used to inverse transform back to time domain to obtain the denoised signal. Figure 4-20 shows the use of Matlab wavelet toolbox [98,99] to set the maximum possible threshold value for d4 to d6

and pre-determined threshold value at levels 1, 2, and 3. The obtained denoised signal denotes the number and locations of PD occurrences in the original signal.

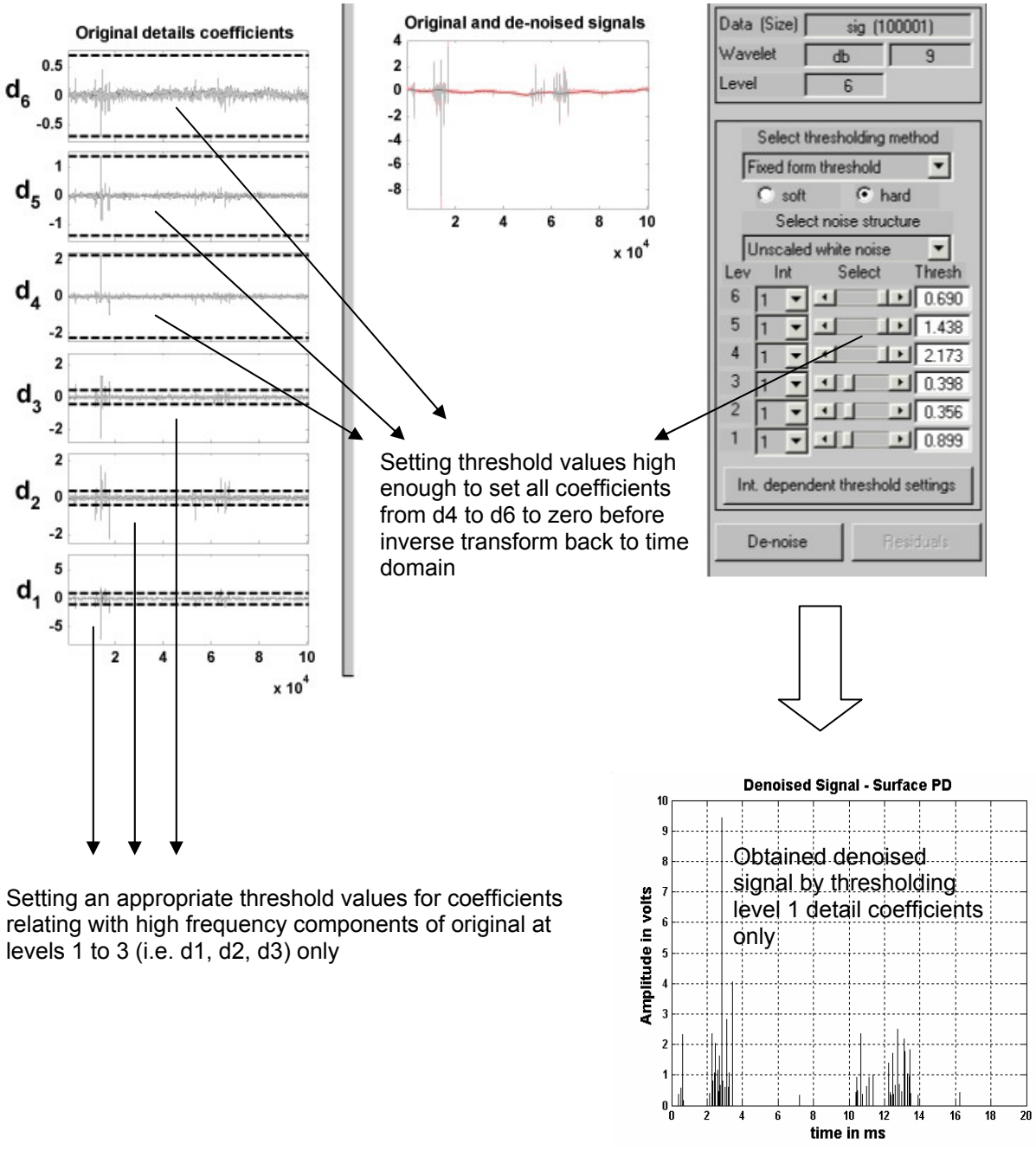

Figure 4-20: Screen to vary the threshold values for getting denoised signal

4.3.6.1 Methods to set the threshold value

The threshold value can either be set manually or calculated based on algorithms [100]. The objective of setting threshold value is to discard lower DWT coefficient values while retaining higher ones at lower levels (i.e. d1 & d2). DWT coefficients at higher decomposition are all set to zero (i.e. discarded). This is because PD events being high frequency pulses reside at lower levels of the DWT decomposition tree. It was noted that the PD pulses in the denoised signal (after thresholding and inverse transformed back to time domain) were attenuated. Therefore, they do not represent true PD amplitudes. True PD amplitudes can be obtained from the original time domain signal. Although attenuation factor is present, thresholding to obtain the denoised signal allow us to obtain the time locations of PD events and that is the main purpose. Two methods are investigated for the estimation of the threshold value to achieve good denoised results. They are:

1) Manual setting of the threshold value and

2) Any one of the four popular *reported and published* automatic threshold estimation methods [101]

4.3.6.2 Manual setting of the threshold value

Without relying on available threshold estimation methods, the threshold value can be set to be higher than the “envelope” (or maximum amplitude) of the coefficients associated with noise. Figure 4-21 which shows the surface PD distribution in 20ms illustrates an example of determining the value of the threshold based on the noise. Sampling rate of the signal containing surface PD

is 5 Mega-samples per second. Dominant frequencies within the frequency band (1.25 MHz to 2.5 MHz) of scale 1 of the decomposition tree of DWT exhibit high coefficient values (see figure 4-21(b)). From the zoomed view of the DWT coefficients at scale 1 shown as figure 4-21(c), the threshold value is set to 0.4 so as to chop off the lower coefficient values and retain the higher coefficient values associated with PD events. Figure 4-26 shows the denoised signal after executing soft and hard thresholding by using the desired threshold value. Similar procedure is applied to the detection of corona and cavity PDs.

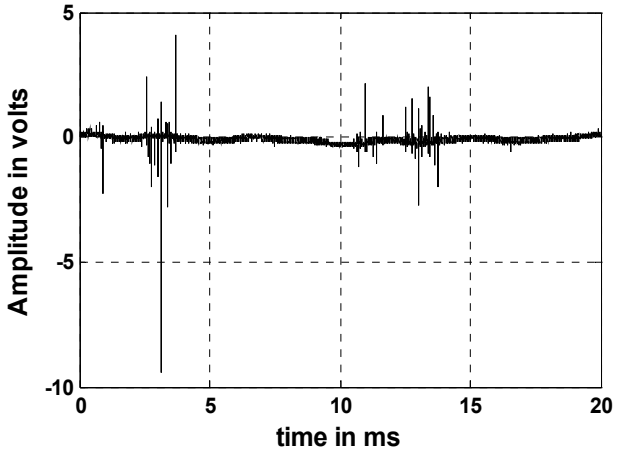

(a) Original time domain signal (surface PD)

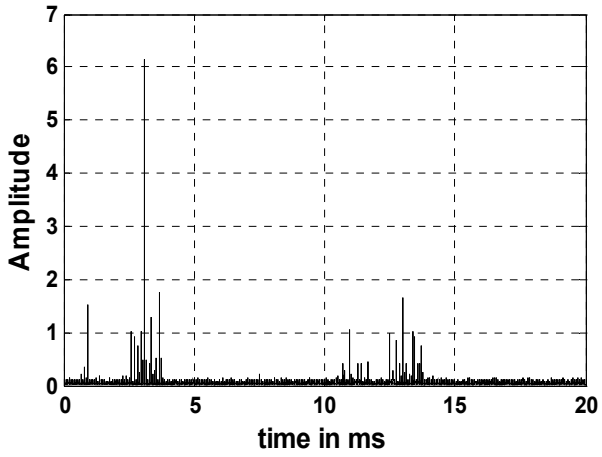

(b) DWT coefficients at scale 1

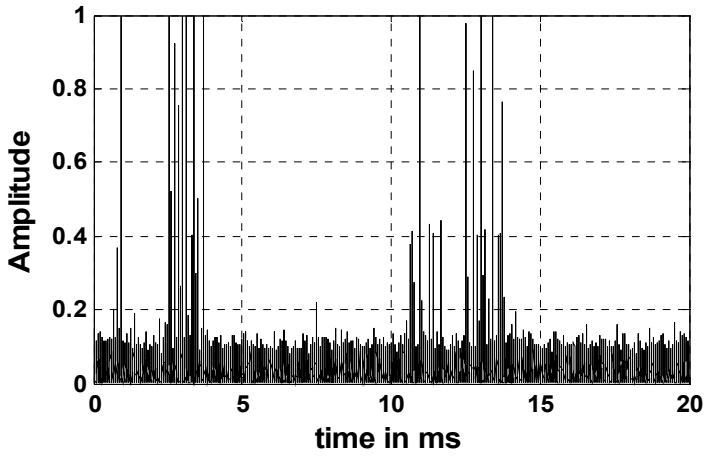

(c) Zoomed view of DWT coefficients at scale 1

Figure 4-21: Setting appropriate threshold values based on noise

Besides writing program codes to extract the detail coefficients at the lower scale level of a DWT decomposition tree, the Graphical User Interface (GUI) in the Matlab wavelet toolbox can be utilized to adjust manually a threshold value for the detail coefficients at scale 1 as shown in figure 4-22. The highest value of the lower coefficients at scale 1 is noted down and the threshold level is set slightly above that value. The rest of the coefficients at higher decomposition levels (i.e. d4 to d6) are all discarded by setting a high threshold value as shown in figure 4-20. The advantage of the manual method is that the end denoised signal is shown on the same GUI page immediately after a threshold value is applied. In this way, an appropriate threshold value can be determined.

Three scenarios are encountered when using the manual method to set a threshold value for detail coefficients. They are:

1) Setting a rather high threshold value

2) Setting a threshold value lower than noise coefficient values, and

3) Setting an appropriate threshold value

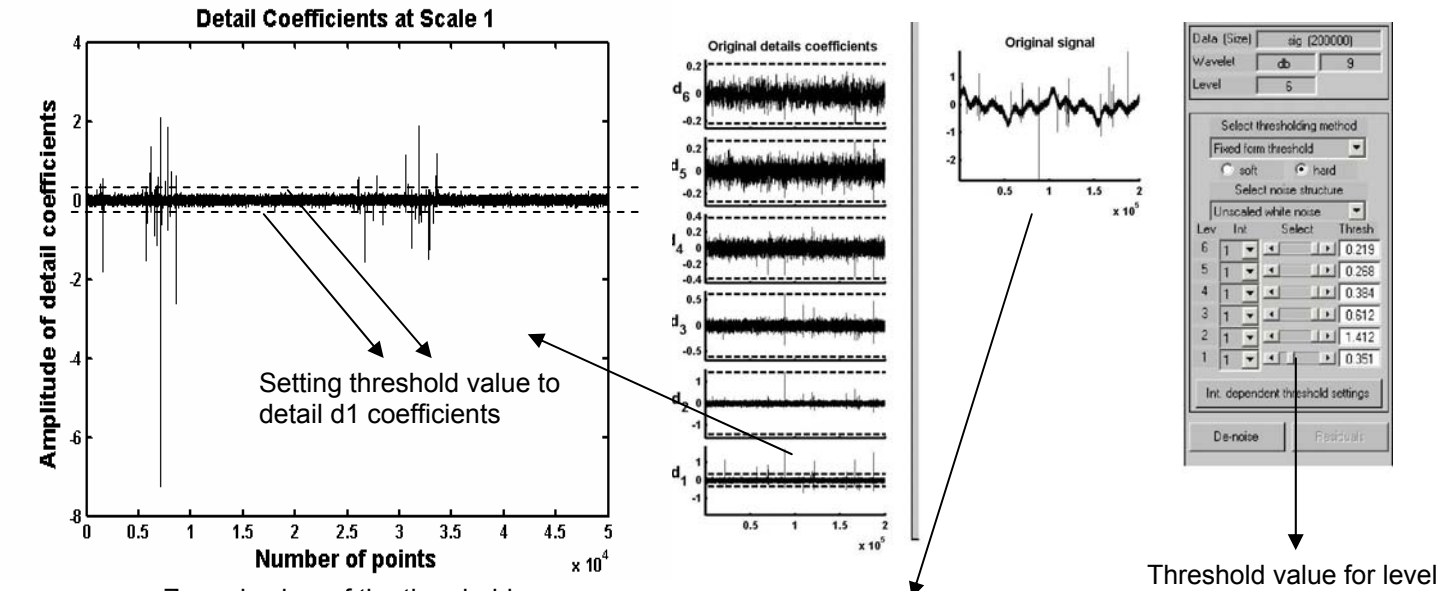

Zoom-in view of the threshold value manual adjustment

Effects of selecting different threshold values are updated here upon execution of the denoise command.

Threshold value for level 1 is shown here and adjusted by keying in a numerical value or sliding the magnitude bar. Coefficients at higher scale levels are discarded by setting maximum possible threshold values on them

Figure 4-22: Screen to vary the threshold values manually

Typical results on denoising of corona PD by varying the setting under three scenarios are shown in figure 4-23 below.

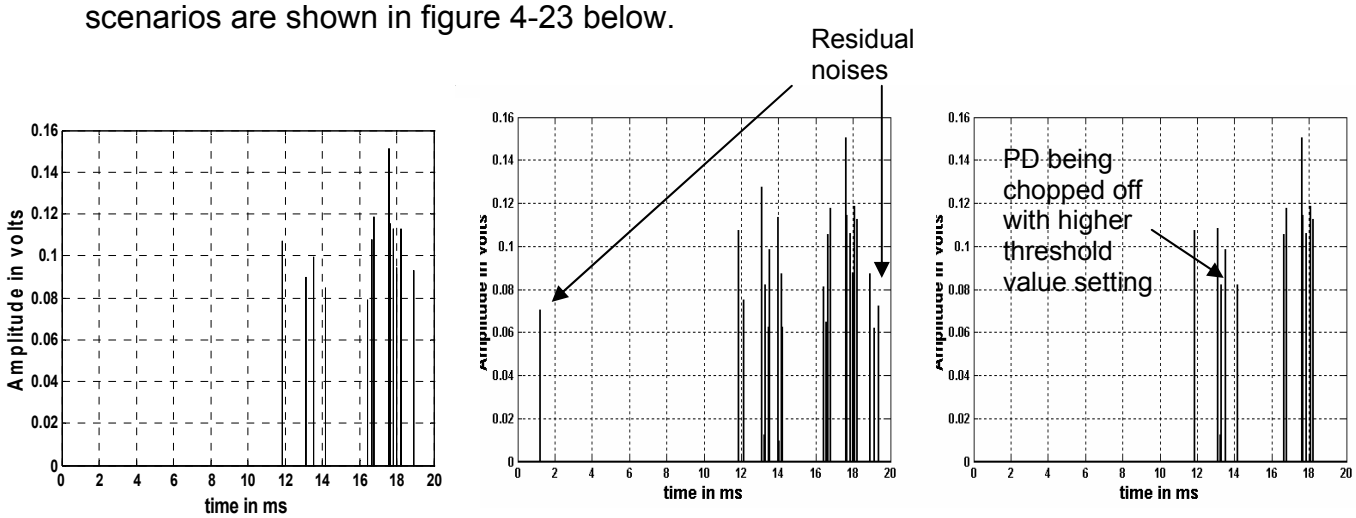

(a) Appropriate threshold value (b) Low threshold value (c) High threshold value

Figure 4-23: Effect of different threshold settings on denoised corona PD

More spikes are observed in the denoised signal when a low threshold value is set. The extra introduced residual noises can be identified by zooming and the typical shape can be identified as noise. With high threshold level, number of extracted PDs may decrease as only dominant PDs will alone be picked. Similar observation is made with surface and cavity discharges. Comparing the maximum PD pulse height (about 0.15 V) with the original corona distribution shown in figure 4-1a showed that obtained maximum PD peak is close to that of the original which is about 0.17 V.

Selecting a threshold value for wavelet coefficients automatically

In a software program dealing with several sets of data, it would be tedious and time consuming to set the threshold manually. Therefore, it is desirable to automate the selection of threshold value for the wavelet coefficients at lower scale level. Without using the four threshold estimation methods as depicted in section 4.3.6.3, a threshold value $\lambda = \sigma\sqrt{2 * \log n}$ of Donoho and Johnstone [102] was used. σ is the standard deviation of the wavelet coefficients at a chosen scale level and n being the size of the data. Figure 4-24 shows the calculated threshold value of 0.23 by using the formula. In this project, an automated threshold value is set to be slightly higher by rounding to the first digit as i.e. 0.3. In this way, PDs are extracted from the noisy data (see figures 4-23(a) and 4-26). The use of Donoho and Johnstone method to estimate the threshold value for the detail coefficients was found to have almost similar results (in terms of the number of PD pulses extracted) when compared to that of the manual method because the threshold value can be set at any value by using manual method based on lower coefficients associated with background noises.

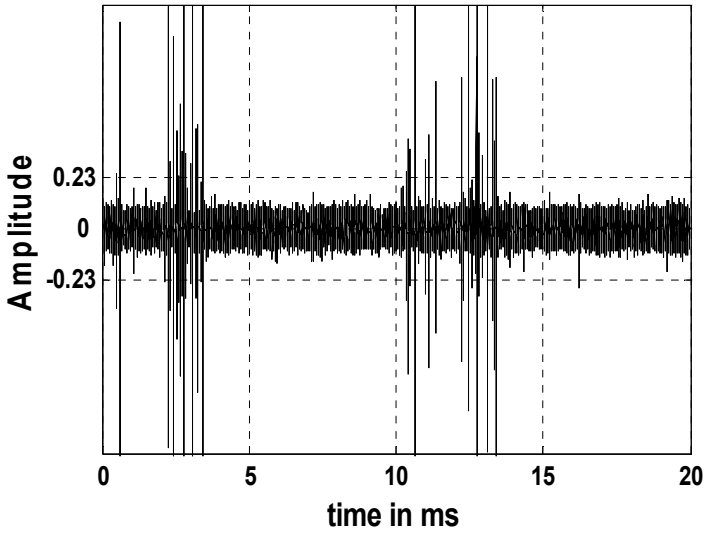

Zoomed view of DWT coefficients at scale 1

Figure 4-24: Setting appropriate threshold value automatically (Donoho and Johnstone)

4.3.6.3 Four threshold estimation methods

Four types of threshold estimation methods are proposed by Donoho et al [103]. They are:

1) Rigrsure – adaptive threshold selection using principle of **S**tein's **U**nbiased **R**isk **E**stimate (in short SURE)
2) Heursure – heuristic variant of the Rigrsure method
3) Sqtwolog – universal threshold
4) Minimaxi – minimax threshold

Each method estimates an optimal threshold value for the detail coefficients at each decomposition level based on their algorithms. In the manual method, only the coefficients of lower levels i.e. scales 1, 2, and 3 are set with a threshold value while the rest of the coefficients at higher levels are discarded by setting maximum possible threshold values. PDs are high frequency pulses residing in lower levels of a

decomposition tree. Therefore, the setting of optimal threshold values for higher levels by these four estimation methods is not necessary as information about PDs do not appear at those levels. Hence, these threshold estimation methods are not as flexible as the manual method. Figure 4-25 shows the denoised corona PD distribution of the original (see figure 4-1a) by using all the four threshold estimation methods to set threshold values for the detail coefficients of a 6 level decomposition.

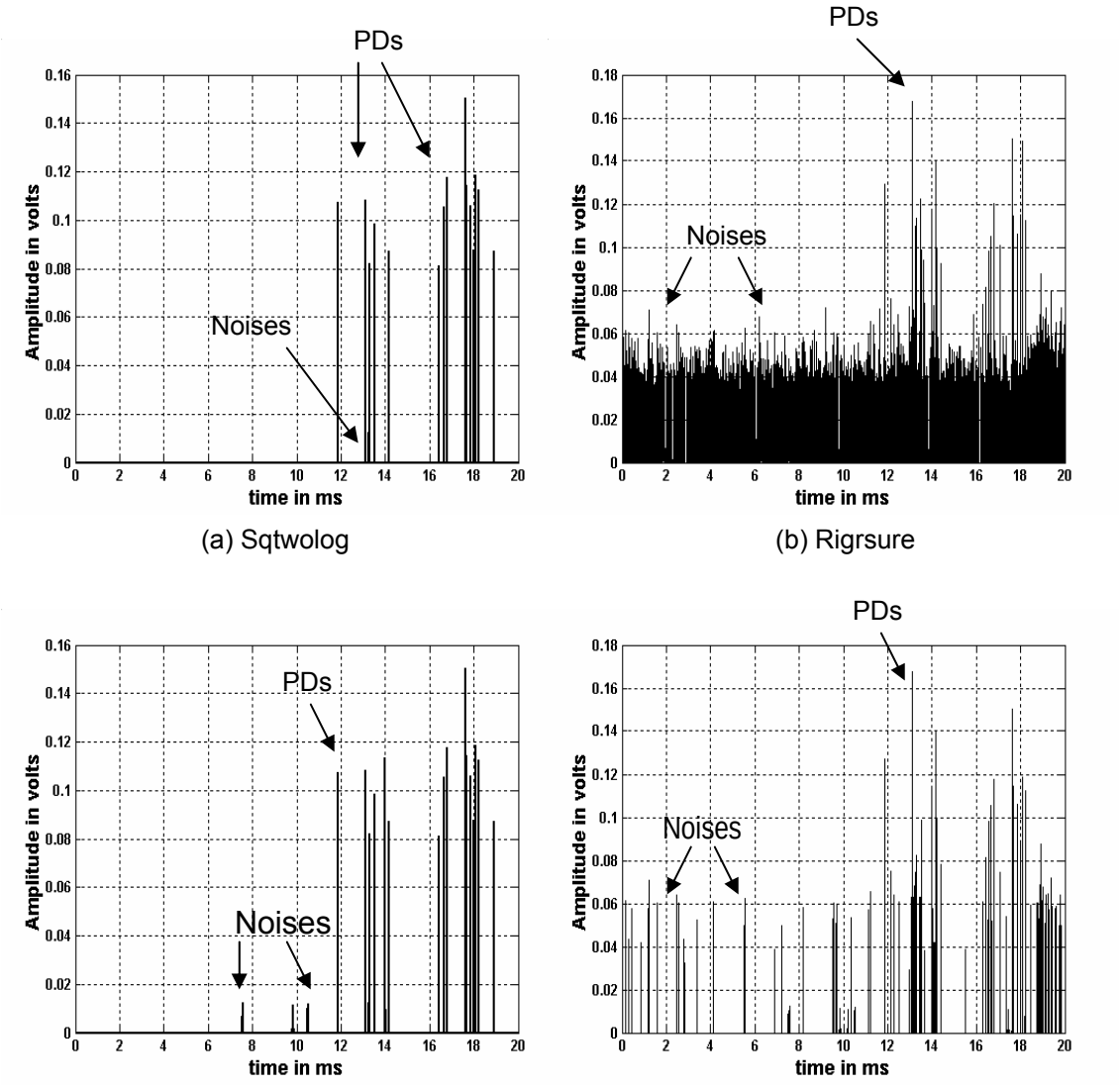

Figure 4-25: Effect of different threshold estimation methods on denoised corona PD in 20ms

From figure 4-25, it can be seen that the Sqtwolog threshold estimation method delivers better denoised results than the other three threshold estimation methods. The Sqtwolog method is found to eliminate most of the background noises as compared to the other three methods.

Comparing denoised results of the corona distribution (see figure 4-1) as shown in figures 4-23 (a) (which is obtained by applying the manual and Donoho & Johnstone method [102]) and 4-25 (obtained by the four existing threshold estimation methods), it was found that the above two methods (Donoho & Johnstone [102] and manual) are able to detect the true number of PD pulses as compared to that of the existing four threshold estimation methods simply because the latter contains residual noises. Similar observations are obtained for surface and cavity distributions. Table 4-1 show quantitatively the number of PD pulses extracted for the corona, surface and cavity discharge distributions as shown in figures 4-1 (a), (b), and (c) respectively by using all six methods. From the table and based on consistent statistical results, it is concluded that by using the manual and Donoho & Johnstone [102] methods correct number of PD pulses are extracted.

Therefore, in this work the threshold value is set manually based on coefficients of lower values which are associated with noises or obtained by using the calculated value by Donoho & Johnstone method [102] for the detail coefficients at lower scale levels of the DWT decomposition tree.

Table 4-1: Number of pulses extracted for the corona, surface and cavity discharge signals in 20 ms as shown in figure 4-1.

	Threshold value estimation methods					
	Manual	Donoho & Johnstone	Sqtwolog	Rigrsure	Heursure	Minimaxi
Corona	13 pulses (0.09)	13 pulses (0.0888 ~ round up to 0.09)	13 pulses (0.096)	> 1000 pulses (0.046)	13 pulses (0.093)	> 1000 pulses (0.069)
Surface	22 pulses (0.4)	25 pulses (0.3)	31 pulses (0.245)	> 1000 pulses (0.105)	> 1000 pulses (0.105)	49 pulses (0.175)
Cavity	4 pulses (0.3)	4 pulses (0.3)	4 pulses (0.242)	> 100 pulses (0.143)	4 pulses (0.235)	23 pulses (0.173)

Note: Estimated threshold value is given in the bracket

4.3.7 Hard Thresholding against Soft Thresholding

After the threshold value is determined, a thresholding method is used to perform the "chopping-off" the unwanted coefficients associated with the noises. Two types of thresholding methods are investigated. They are the Hard Thresholding and Soft Thresholding methods [104,105].

Hard Thresholding

$$D(Y, thr) \equiv \begin{matrix} Y & if \ |Y| > thr \\ 0 & if \ Otherwise \end{matrix} \longrightarrow \quad (4\text{-}3)$$

Where:

Y contains the detail coefficients of signal after performing DWT

thr is the threshold value

Operator D denotes the thresholding process.

From (4-3), detail coefficients that are lower than the threshold value are set to zero while coefficients above the threshold value remain at their own values.

Soft Thresholding

$$D(Y, thr) \equiv \begin{cases} sign(Y)(|Y| - thr) & if \ |Y| > thr \\ 0 & if \ Otherwise \end{cases} \longrightarrow \quad (4\text{-}4)$$

From (4-4), detail coefficients below the threshold value are similarly set to zero but coefficients above the threshold value do not retain their own values. They are decreased i.e. they are subtracted by the threshold value. It has been found statistically in this project that the soft thresholding technique output denoised signals of much lower amplitude values than that of hard thresholding due to the shrinking effect of the soft technique. Although the soft-thresholding method reduces the signal level in comparison with the hard-thresholding, literature has shown that the resulting denoised signal is smoother if the soft threshold filter is used [106]. However, for PD pulse-shape

approximation, the smoothing effect of the soft-thresholding technique is not significantly better than hard-thresholding. That argument is evident in figure 4-27.

Typical plots on surface PDs in 20ms as shown in figure 4-26 show that by applying the hard-thresholding method, more PD spikes are observed and they have the absolute amplitudes comparable to the absolute amplitude of original PDs. The soft thresholding method shrinks some of the lower PD spikes to an amplitude level near to zero and hence making them hard to detect by eye inspection. Similar observation is made with corona and cavity PDs. To achieve better identification of PDs, the hard thresholding method is selected during the denoising process of the original signals in this work.

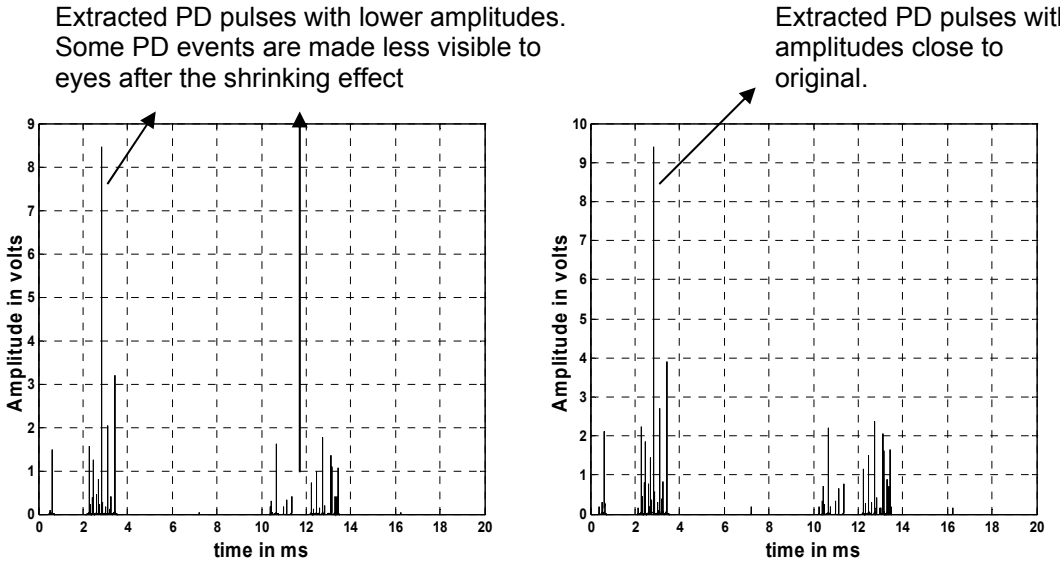

Soft Thresholding Hard Thresholding

Figure 4-26: Effect of hard and soft thresholding on denoised surface PD distribution

In addition, employing the Hard-thresholding does not result in poor PD pulse-shape approximation. Figures 4-27 (a), (b), and (c) show the approximations of each type of PD by soft and hard thresholding respectively. It can be seen that there is not much

difference in shape approximation of single PD pulse by both methods except for magnitude difference.

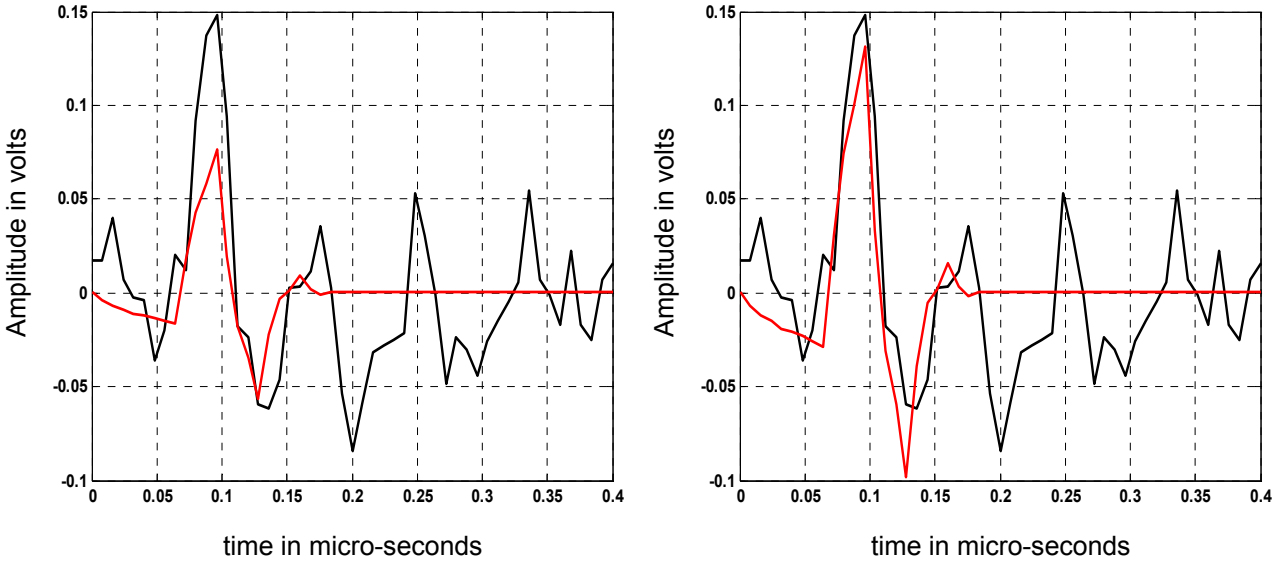

(a) Approximation of single corona PD pulse by WT
Left – Soft thresholding; Right – Hard thresholding

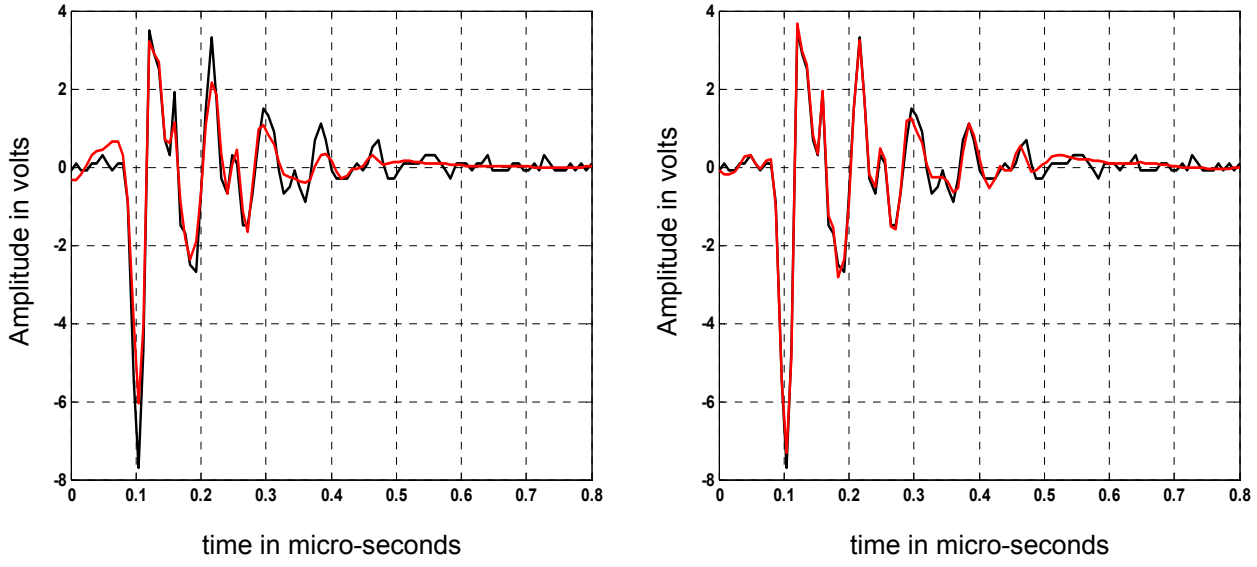

(b) Approximation of single surface PD pulse by WT
Left – Soft thresholding: Right – Hard thresholding

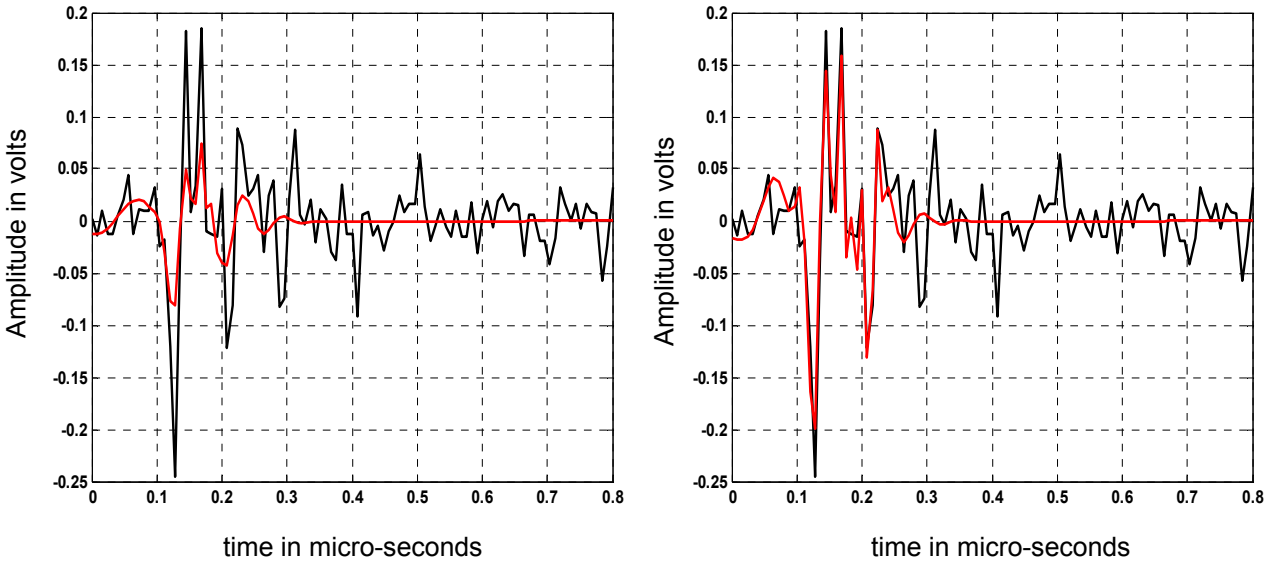

(c) Approximation of single cavity PD pulse by WT
Left – Soft thresholding; Right – Hard thresholding

Figure 4-27: Comparison of Soft thresholding against Hard thresholding on approximation of single PD pulses

4.3.8 Obtaining the denoised signal by extracting and reconstructing the detail coefficients

The detail signals constructed from the modified detail coefficients at lower scale levels are also found to be useful for PD detection. The denoised signal should retain closely the original PD amplitudes while the detail signal does not reflect true PD amplitudes. The objective of using the detail signal is to obtain a quick estimation of the severity in terms of number and Φ locations of the PD occurrences. The detail signals are high frequency representation of the original signal in time domain. Figure 4-28 illustrates the constructed detail signals at level 1 for the 20ms distributions of the three discharges shown in figure 4-1.

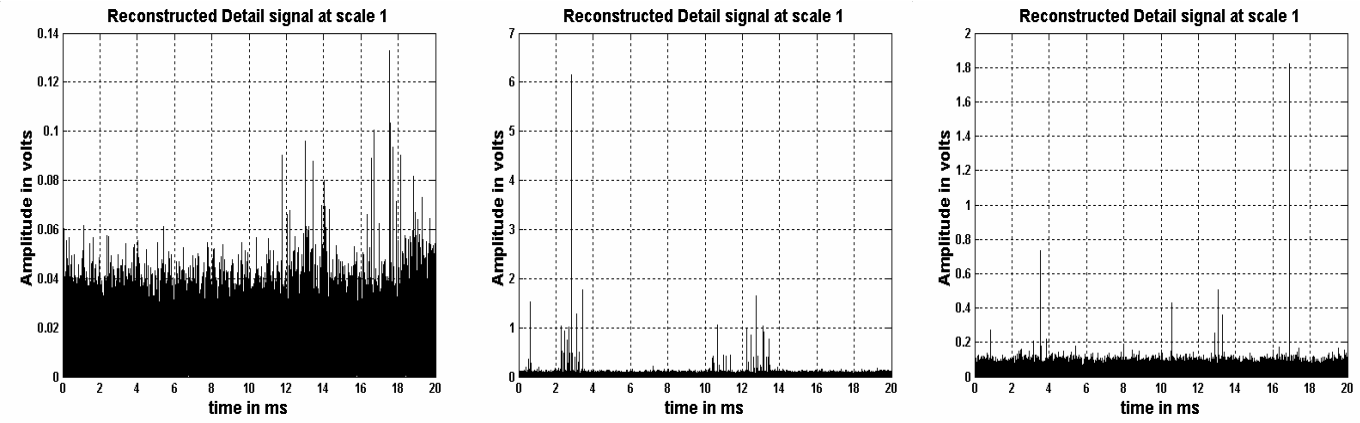

Detail signal d1 - corona PDs **Detail signal d1 - surface PDs** **Detail signal d1 - cavity PDs**

Figure 4-28: Reconstructed detail signals at scale 1

From the plots, the time location of PD occurrences is “blurred” by the background noises because the constructed detail signals are not denoised. However, the time location of the occurrence of PDs, and the severity of the PDs can be estimated.

4.3.9 Comparison of the two transform techniques – CWT and DWT

The objective of using the transform techniques is to identify the time locations of different PDs lying in a frequency band (time-frequency plots) for noise separation and PD type identification. A better transform is the one which can detect the correct number of PD pulses by indication of their presence with high coefficient values and ability to capture true time locations of PD occurrences.

CWT and DWT coefficients associated with PDs in 20ms

Figures 4-29 (a), (d) and (g) show the recorded corona, surface and cavity PD signals and noise with fabricated samples in 20ms period using the test setup shown in figure 3.1. Figures 4-29 (a), (b) and (c) show the corona PD distribution with the analysed CWT and DWT coefficients respectively. Similarly figures 4-29 (d), (e) and (f) show the results for surface PD and figures 4-29 (g), (h) and (i) show the results for cavity PD.

Both techniques used wavelet db9 with scale 1. From the plots, it can be observed that DWT represents PDs with higher coefficient values as compared to that of CWT which are desirable for thresholding and PD identification.

Different types of PD can be detected with distinct scale level using a high sampling rate like 250 Mega-Samples per second (5 million sampled points in 20 ms) as shown in section 6.2.4 of the thesis in page 6-15. With limited sampling rate of 5 Mega-Samples per second (100,000 sampled points in 20 ms), scale 1 is chosen because at this level all three types of PDs can be detected as the frequency range lies in a band of 1.25 MHz to 2.5 MHz with that sampling rate.

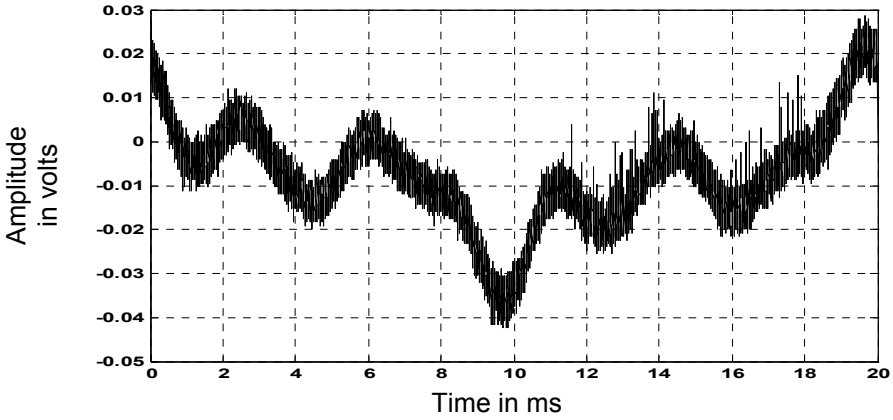

(a) Original time domain signal (corona PD)

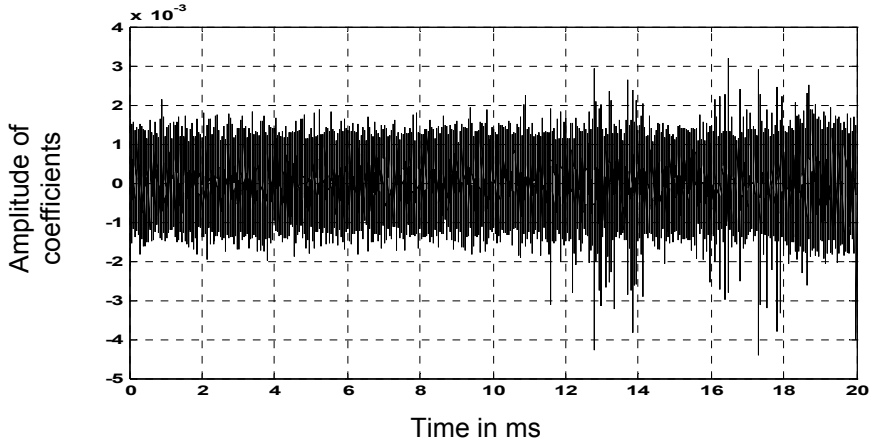

(b) CWT coefficients at scale 1 (corona PD)

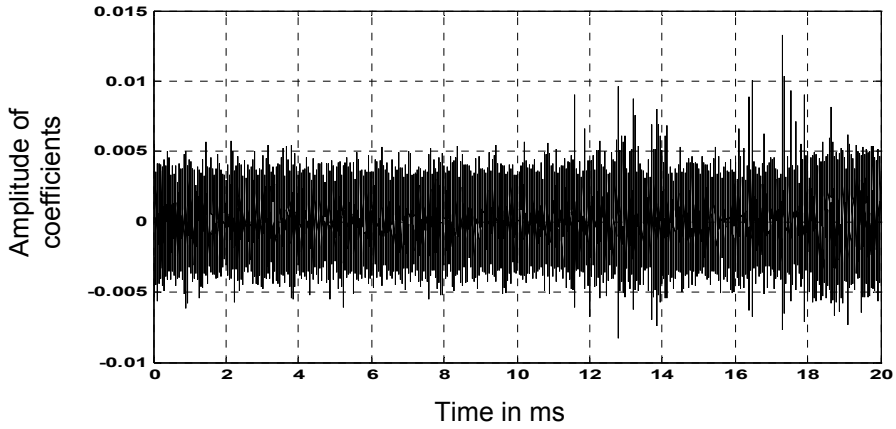

(c) DWT coefficients at scale 1 (corona PD)

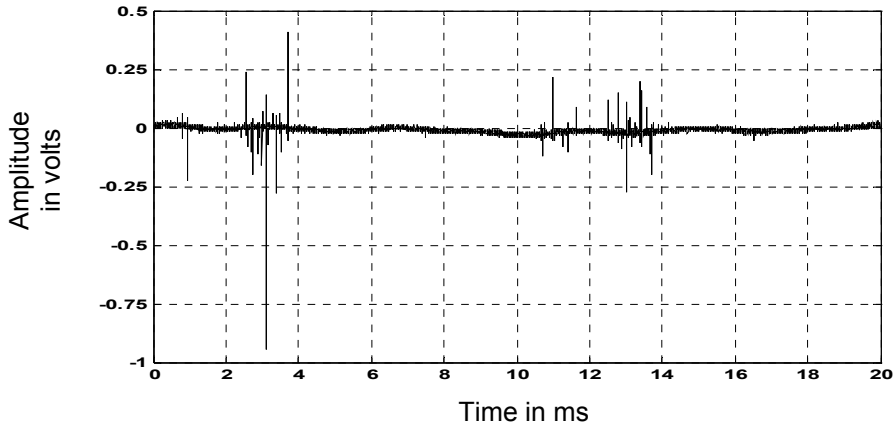

(d) Original time domain signal (surface PD)

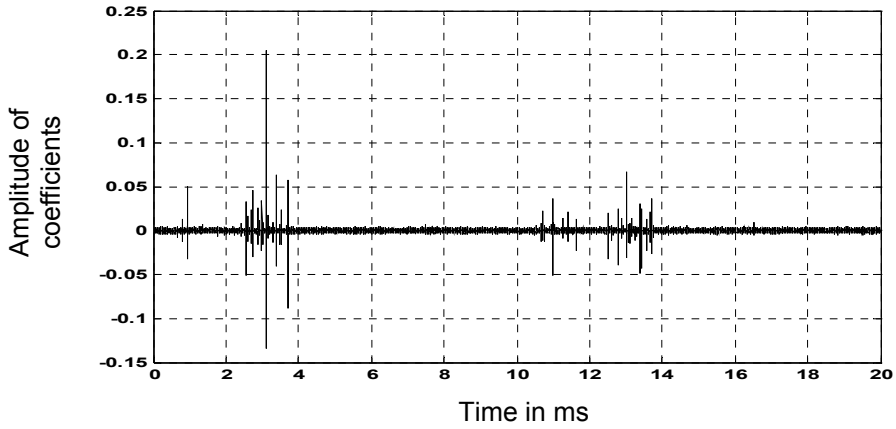

(e) CWT coefficients at scale 1 (surface PD)

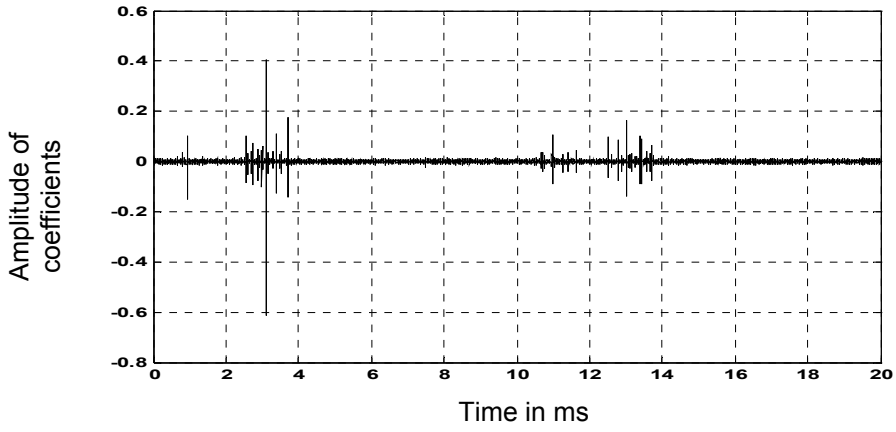

(f) DWT coefficients at scale 1 (surface PD)

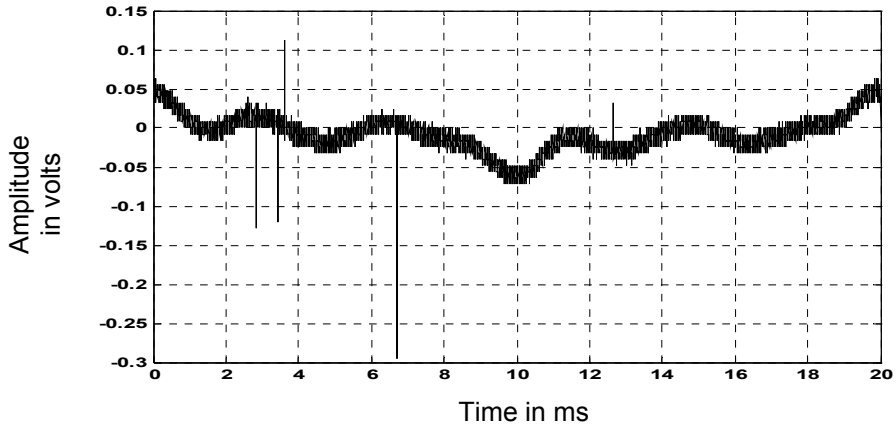

(g) Original time domain signal (cavity PD)

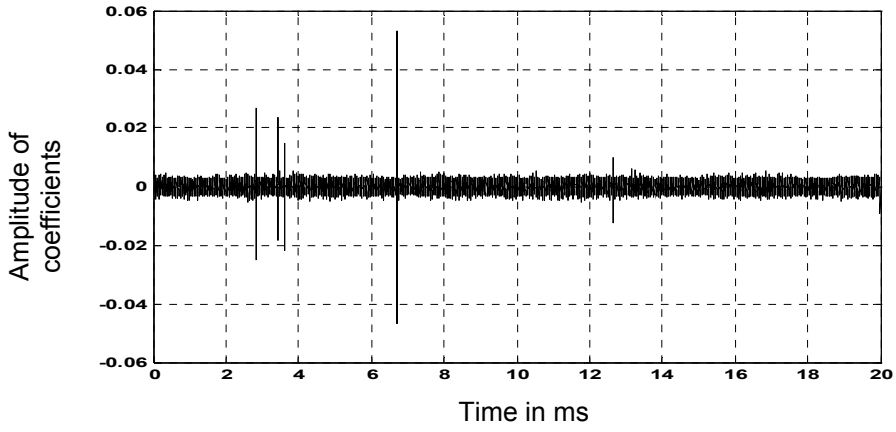

(h) CWT coefficients at scale 1 (cavity PD)

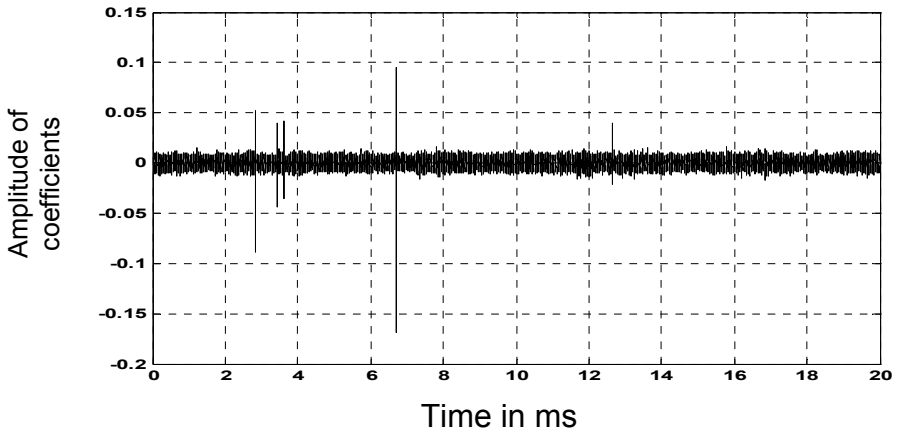

(i) DWT coefficients at scale 1 (cavity PD)

Fig 4-29: Variations of CWT and DWT coefficients associated with corona, surface and cavity PDs in 20ms

CWT and DWT coefficients associated with PDs in 1.6ms

Using a higher sampling rate of 1.25 Giga-samples per second, single PD pulse shape is more accurately captured. Then, both CWT and DWT are applied to detect the single pulse. Figures 4-30 (a), (b), and (c) presented below show the approximation of an extracted single corona PD by CWT and DWT coefficients at scale 2. Scale 2 with such high sampling rate is chosen because corona PD is detected by CWT and DWT only starting from that scale. Similarly figures 4-30 (d), (e), and (f) and (g), (h) and (i) show that of cavity PD distribution at scale 1 and surface PD distribution at scale 1 respectively because of the bandwidth of the detected single PD. It can be observed that dominant coefficients of DWT capture the time locations of all the three discharges using a common scale for comparison. Figure 4-31 shows a blown-up view of CWT and DWT coefficients variation with single corona, cavity and surface PD pulses. Distributions shown in red colour are approximations of the original signal by WT, whereas distributions shown in black colour are the original signal. It can be seen that

coefficients tag closely to the time locations of the original corona pulse as compared to that of CWT. Similar observations are obtained for variations of CWT and DWT coefficients with surface and cavity pulses. Accurate detection of the time locations of PDs is important for statistical analysis.

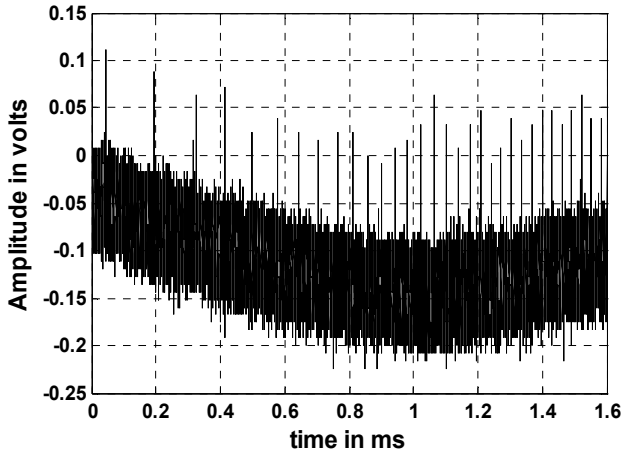

(a) Original time domain signal (corona PD)

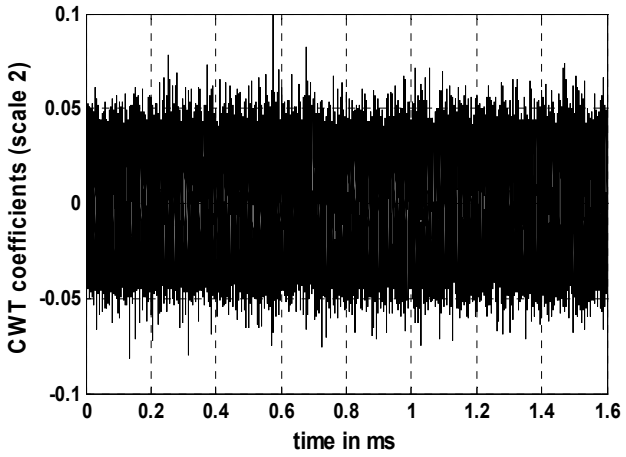

(b) Approximation of corona PD by CWT coefficients at scale 2

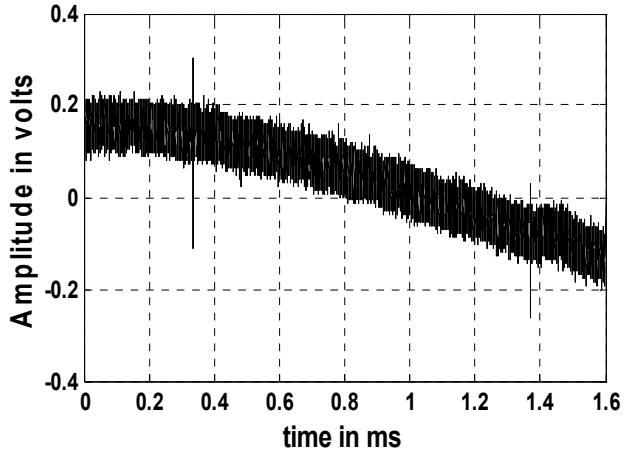

(d) Original time domain signal (cavity PD)

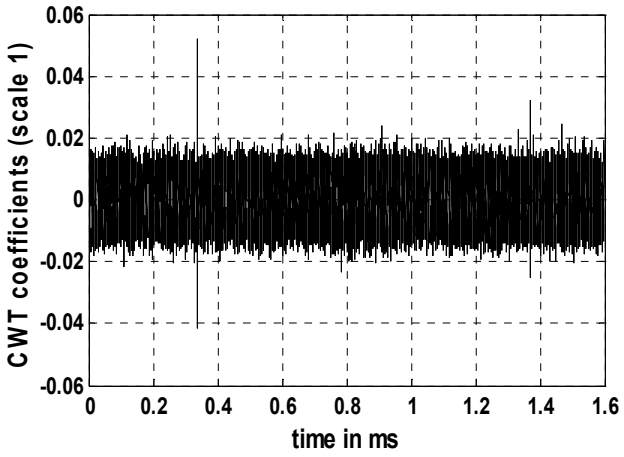

(e) Approximation of cavity PD by CWT coefficients at scale 1

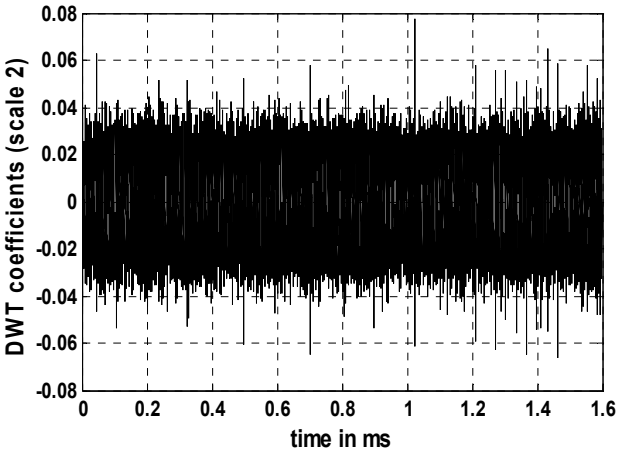

(c) Approximation of corona PD by DWT coefficients scale 2

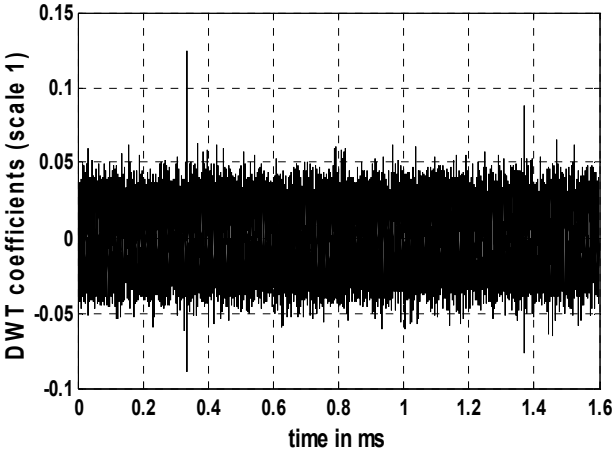

(f) Approximation of cavity PD by DWT coefficients at scale 1

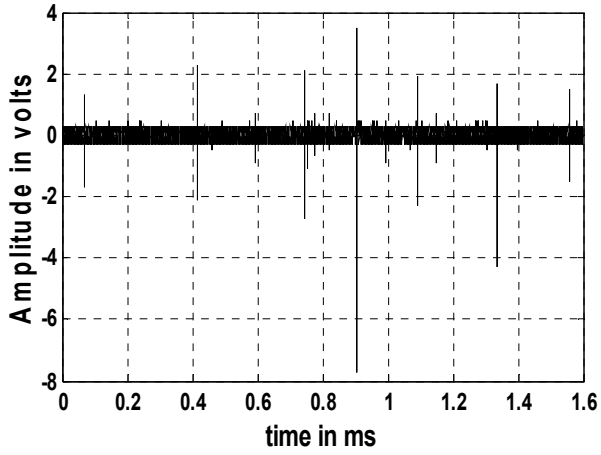

(g) Original time domain signal (surface PD)

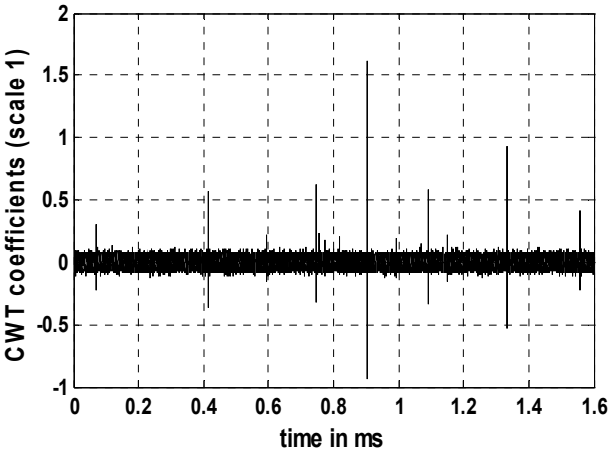

(h) Approximation of surface PD by CWT coefficients at scale 1

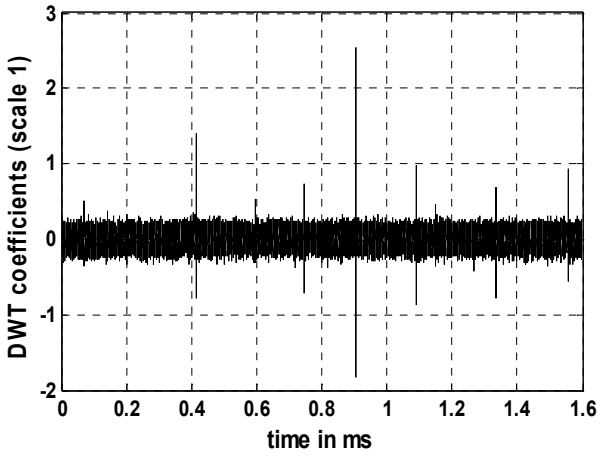

(i) Approximation of surface PD by DWT coefficients at scale 1

Fig 4-30: Variation of CWT and DWT coefficients associated with corona, surface and cavity distribution in 1.6ms

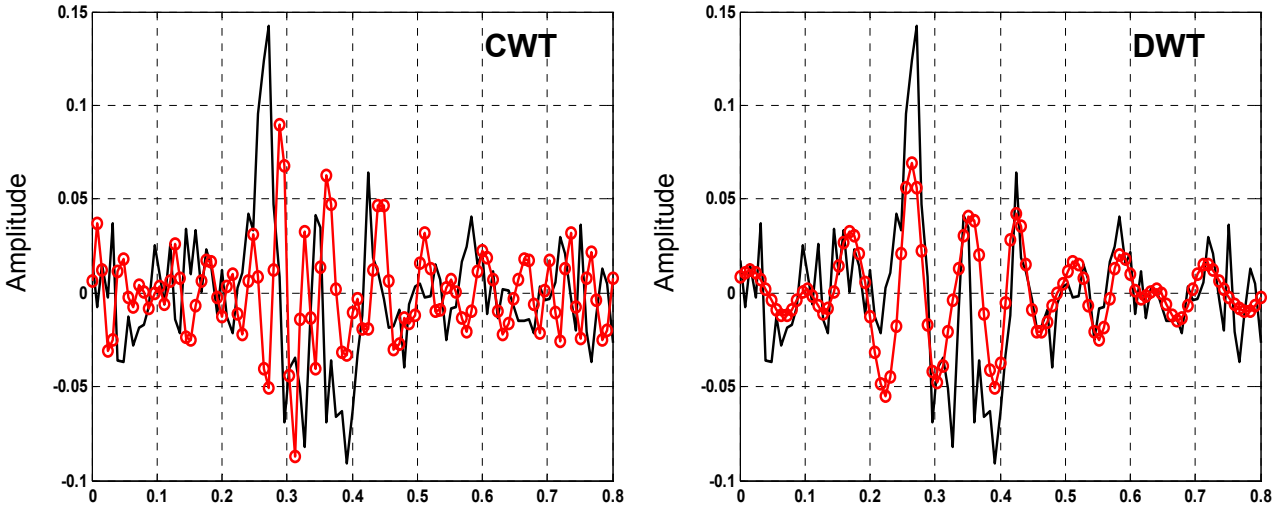

(a) Zoomed in view of the variation of CWT and DWT coefficients associated with single corona PD pulse at scale 4

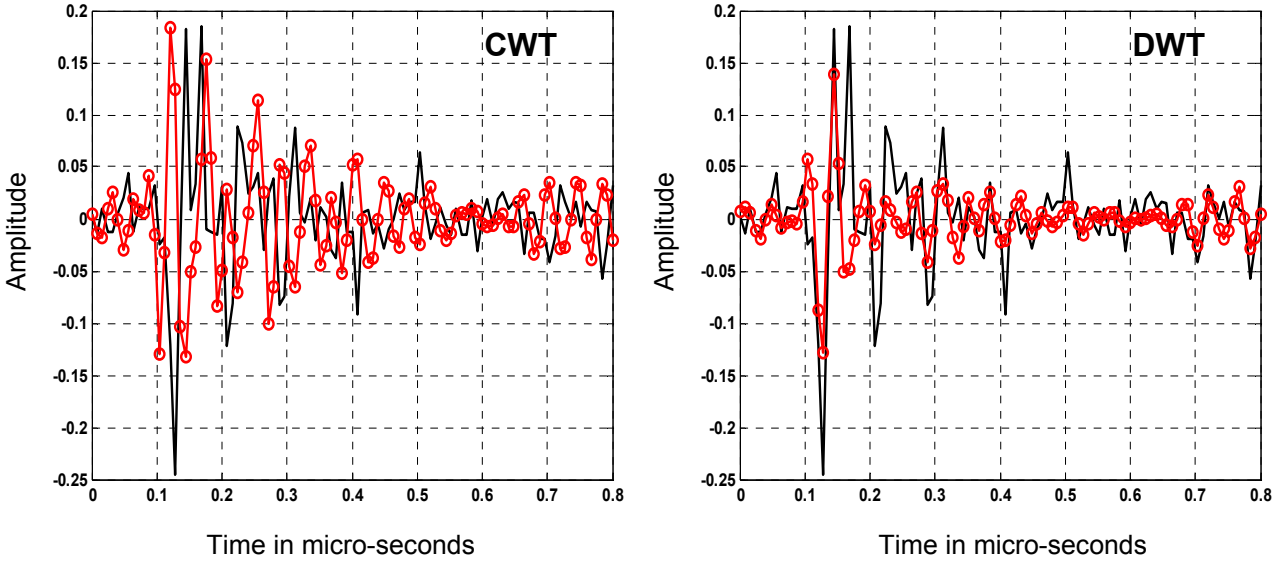

(b) Zoomed in view of the variation of CWT and DWT coefficients associated with single cavity PD pulse at scale 1

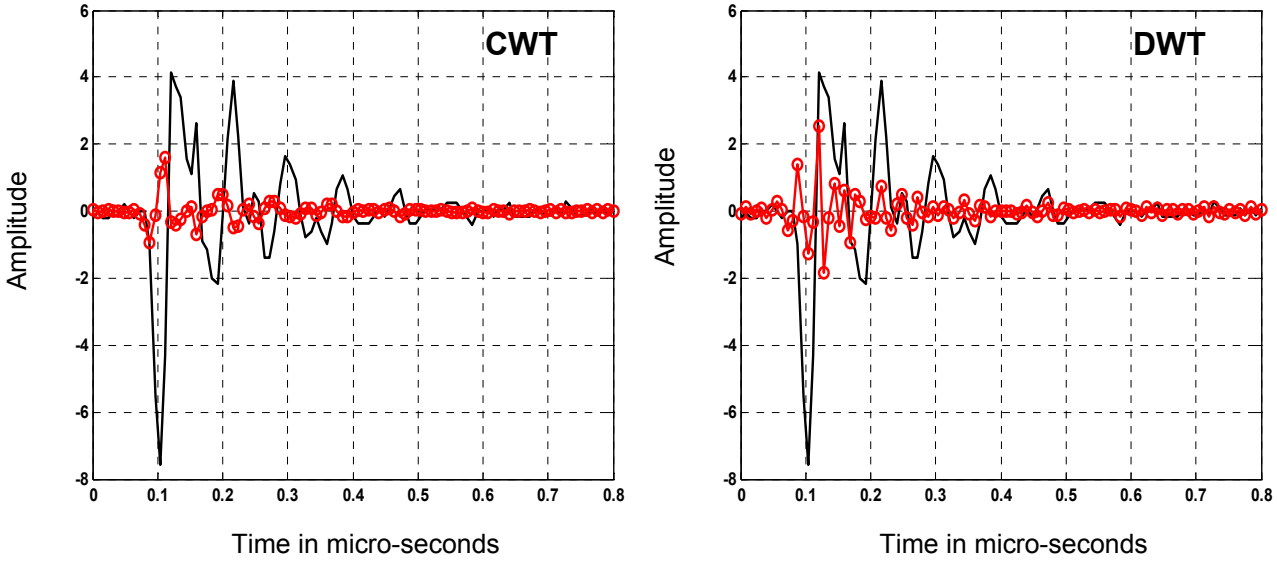

(c) Zoomed in view of the variation of CWT and DWT coefficients associated with single surface PD pulse at scale 1

Fig 4-31: Zoomed view of the variation of CWT and DWT coefficients associated with single corona, cavity & surface PD pulses at appropriate scale

Comparing the results obtained in periods of 20ms and 1.6ms by CWT and DWT, it is concluded that DWT is better than CWT in PD detection and approximation. Also, DWT being less computational intensive is chosen as the tool for PD detection and noise removal which are essential for statistical and single PD pulse analysis reported in chapters 5 and 6.

4.3.10 Identifying PDs from high frequency noises

One limitation of applying DWT for PD detection is found from the obtained denoised results. Figure 4-32 shows a case of high frequency noise picked up and approximated by DWT. A PD is seen to have much higher amplitude than high frequency noise and the background signal. In addition, the shape of the noise spike in the denoised signal is found to be different from that of the PD spike. Difference in shape and amplitude is used to identify true PDs from noise.

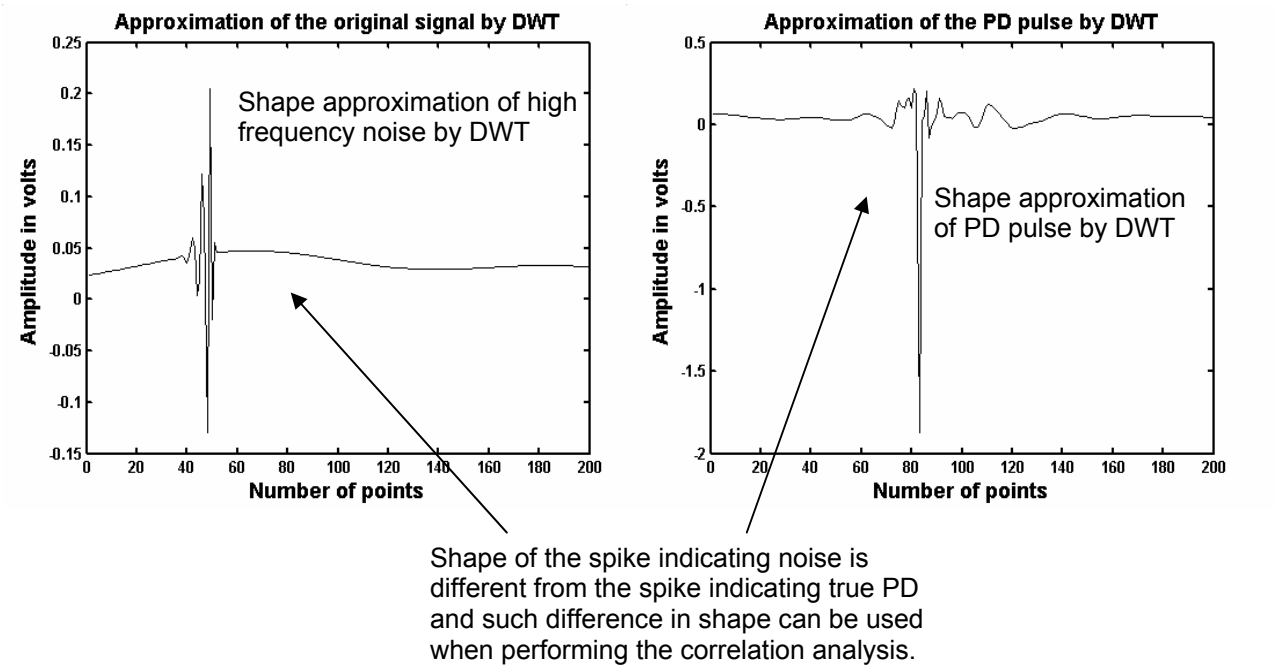

Figure 4-32: Shape approximation of PD and noise by DWT

The procedure can be as follows:

1) Firstly, the locations of “spikes” or “bursts” in the denoised signal are recorded down.

2) With the knowledge of the time location of the first spike in the denoised signal, the original signal at the same time location is zoomed and the shape of small portion of the original signal is extracted out.

3) The extracted portion of the original signal is related to PD or noise by

   a) Using the amplitude and shape difference between PD and high frequency noises and

   b) Correlating with known shape of each type of PD

4) Spikes which are found to be high frequency noises are discarded i.e. set to zero.

4.4 Summary

1) Both CWT and DWT are found to be useful in PD detection.

2) A highly localized wavelet like the Coif5, daubechies (db9) , Symlets, and Biorthogonal families of wavelets are effective in picking up PDs. Scaling of wavelets is important when CWT is applied to detect PDs. Different scale levels of a wavelet are used to identify corona PDs from surface and cavity PDs using CWT.

2) In CWT and DWT, the selection of a best fit wavelet is based on two methods described in sections 4.2.2.1, 4.2.2.2, 4.3.4.1 and 4.3.4.2, and proper wavelet scale, and the extracted PD should satisfy the following points.

a) Using the selected wavelet, the spikes in the denoised signal must be able to give good approximation of the shape of the single PD especially same pulse width as the original individual PD.

b) Using the selected wavelet, the spikes in the denoised signal must be able to retain the true amplitudes or comparable amplitudes of the PDs in the original signal.

c) In 20 ms, it should retain the number of PDs

d) It should get high coefficient values at the desired scale to apply thresholding properly.

3) DWT is found to have less computational time and less memory intensive than CWT. The detail signals at lower scale levels obtained by reconstructing the detail coefficients offer a useful way to estimate the occurrence and severity of PDs in measured signals.

4) Four main steps to denoise any signal containing PDs using DWT are:

a) The selection of a best fit wavelet (db9 and Coif5 in PD extraction are found to be the best).

b) The number of decomposition levels to be used (level 6 or 7 is found to be sufficient for PD applications)

c) The threshold value to be used (The manual method is found to be more flexible in estimating threshold value without loosing PD signals)

d) The thresholding method to be used (Hard thresholding is found to be better than soft thresholding method)

5) The “Shape and Amplitude comparison method” is found to be useful in identifying PDs from high frequency noises.

To conclude this chapter, it is planned to use DWT for further PD denoising and identification since it uses dyadic scales of the mother wavelet resulting in lower computational requirements. Unlike DWT, CWT employs continuous scales (i.e. 1, 2, 3, 4,….n) and thus is good for observing for minute changes in the coefficients when the scale is increased by an increment of 1. By using a sampling rate with a nyquist frequency higher than a pure PD (i.e. surface, cavity, or corona) and employing a continuous scale of 1 to 10 of the mother wavelet for CWT analysis, surface PDs were found to exhibit high derived CWT coefficients at a lower scale level than that of corona PDs (see section 4.2.3). Therefore, CWT will be used for identifying corona from surface PDs in a mixed-sources signal which will be presented in section 6.2.4

Chapter 5

Group and Single PDs Analysis

5.1 A brief overview

This chapter presents the computational analysis on single source PD signal recorded in the laboratory. Characteristics of PD are extracted by analyzing the statistical random occurrence of PD in 20 ms period known as *group PD analysis*, and by extracting with more number of sampled points and analyzing single PDs occurring in 1.6 ms period known as *single PD analysis*.

In group PD analysis, the statistical distribution of PD magnitude (q) with phase (ϕ) over several voltage cycles is analyzed for each type of PD and compared to the standard normal distribution. In single PD analysis, time domain characteristics of single PD peak magnitude, shape and pulse duration, and frequency domain characteristics like FFT content and its magnitude are extracted for each type of single PD.

The obtained results are used for the identification of the types of PD embedded in a mixed-sources signal (i.e. a signal which contains both corona and surface PDs, or any other combination of studied 3 PDs occurring simultaneously) reported in next chapter.

5.2 Group PD Analysis

PDs occur randomly across a voltage cycle. The statistical occurrence of PD in 20 voltage cycles is analysed to obtain the scientific features of PD. The

objective of group PD analysis is to investigate ϕ and q distribution of each type PDs occurrence in 20 cycles. Removal of background 50 Hz frequency noises is done by the DWT denoising technique prior to the group PD analysis. In ϕ distribution, the voltage cycle is chopped into 360 windows so that each ϕ window width is one degree. Within each window, the mean, and maximum magnitudes of PDs are calculated. This is repeatedly done for 20 voltage cycles. The calculated results are plotted against the corresponding ϕ of the voltage cycle. Similar to ϕ windows, q distribution in magnitude window is analysed. The magnitude axis is divided into 50 magnitude windows and the number of PDs (n) lying within each magnitude window is determined and plotted for grouped 20 voltage cycles. The following distributions are analysed:

a) q vs ϕ

b) q_{mean} vs ϕ

c) q_{max} vs ϕ

d) n vs ϕ

e) n vs q

f) Cumulative number of PDs vs q

(weibull parameters are determined from cumulative distribution plot)

g) Cluster analysis using Δq and $\Delta\phi$ distribution

5.3 Results of group PD Analysis

The 7 analyses indicated above may be grouped depending on the selected parameters.

5.3.1 Phase distribution of corona PD

It is well known [107,108] that corona PD occurs in negative half of 20 ms cycle. After denoising 20 of 20 ms data and phase referencing, the PD data is analyzed. Figure 5-1 shows the distribution of original q with ϕ, averaged q in the 1° window with ϕ, maximum q in the 1° window with ϕ, and number of PDs in the 1° window with ϕ.

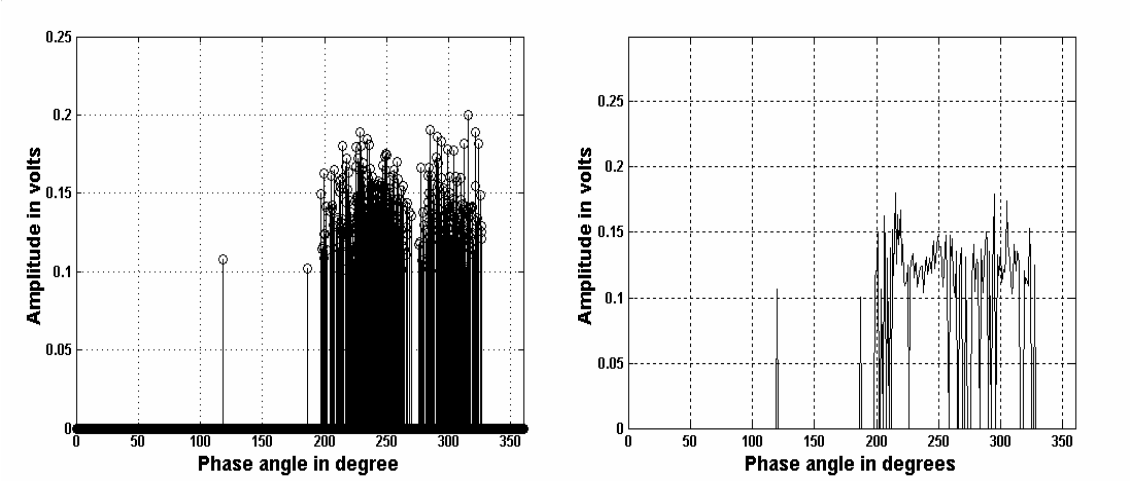

(a) Original q with ϕ

(b) Mean q in 1° window with ϕ

(c) Max q in 1° window with ϕ

(d) n in 1° window with ϕ

Figure 5-1: corona PD occurrences in 20 ms period at 5 kV

Corona PDs are seen to clutter mainly in the negative half of the voltage cycle and the separation between consecutive corona pulses is small. This unique behaviour can be explained from the fact that electrons being mobile and much lighter than positive ions gain kinetic energy rapidly from high electric field generated by HV [109]. In addition, the outside surface of the air molecule is made up of electrons and hence, high electric field cause electrons to break off from the air molecule leaving behind the positive ions. During the negative cycle of the AC voltage, corona causes the electrons to propagate away from needle and thus create more electrons through molecular collisions. Therefore, negative corona appears as numerous small pulses crowded in Φ from 200° to 330° as seen from the superimposed plots. The magnitudes of corona PDs are almost constant and low around 100mV to 170mV. Maximum number of occurring pulses is around 7 with Φ = 250°.

5.3.2 Phase distribution of surface PD

Similar to the analysis on corona PD, analysis on pure surface PD is done as shown in figure 5-2.

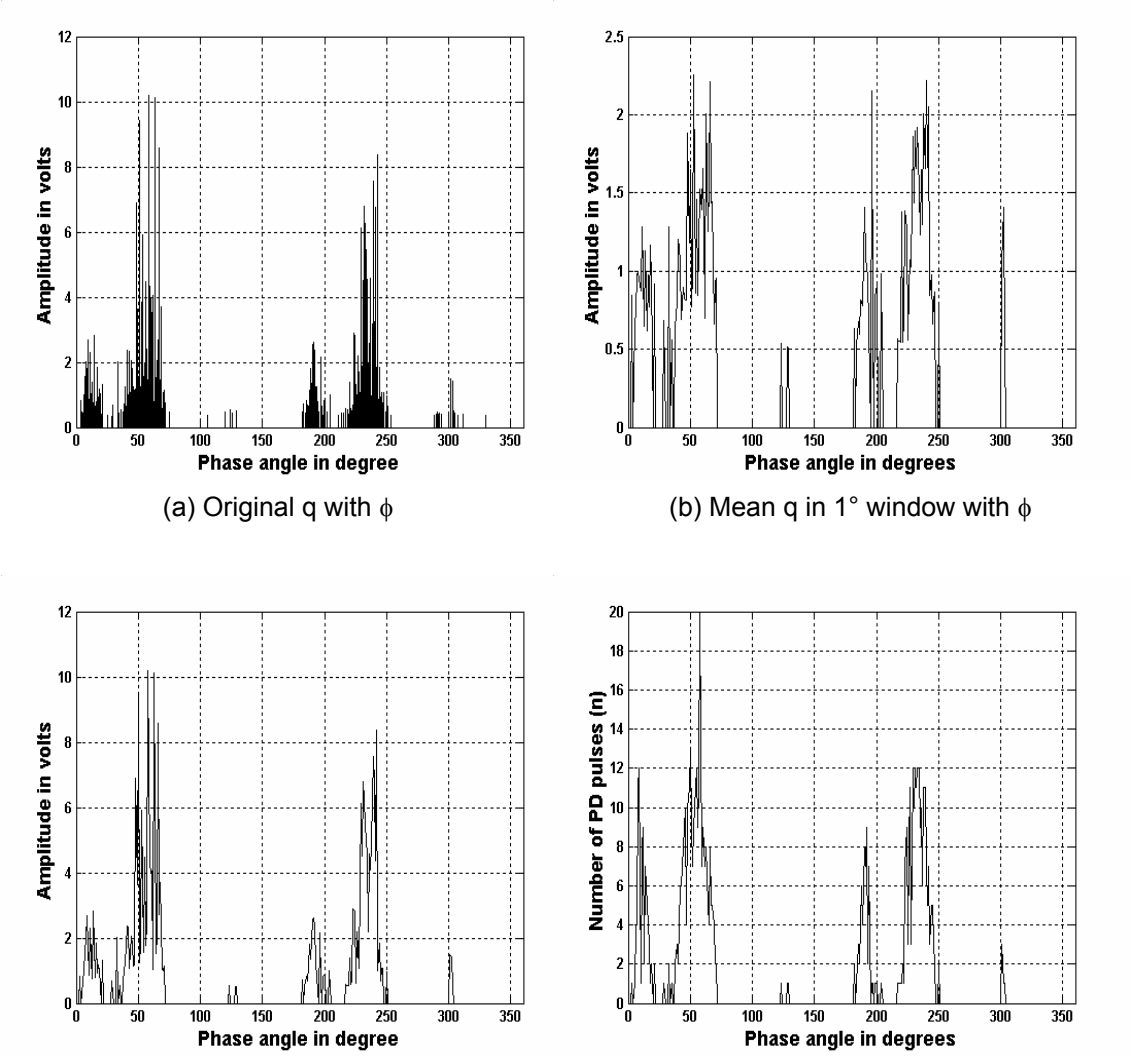

(a) Original q with ϕ

(b) Mean q in 1° window with ϕ

(c) Max. q in 1° window with ϕ

(d) n in 1° window with ϕ

Figure 5-2: surface PD occurrences in 20 ms period at 5 kV

Unlike corona discharges, surface PD pulses occur from 0° to 80° in positive half cycle with a peak magnitude of 10.5 V and from 180° to 260° in negative half cycle with a peak magnitude of 8.5V. Mean value of peak reduces to 2.3 V. Maximum number of occurring PDs are 20 in positive half cycle and 12 in negative half cycle. The peak magnitude of surface discharges is much higher than that of corona. The shape of the phase distribution in the positive half cycle is similar by visual inspection to that of the negative half cycle. However, these shapes do not follow the standard normal distribution.

5.3.3 Phase distribution of cavity PD

Figure 5-3 shows the cavity PD distribution at 9 kV. Cavity PDs are seen to occur in both positive and negative half of a voltage cycle like surface PD. However, the amplitudes of cavity PDs are lower than that of surface PDs but are seen higher than corona PDs. Unlike surface PD, the shape of the phase distribution in the positive half cycle is not similar to that of the negative half cycle for all the four distribution plots. In addition, the shape of the phase distribution in the positive half cycle for all four distribution plots is more similar to the standard normal distribution. PD occurs for longer period. During positive half cycle, it occurs from 10° to 80° while in negative half cycle, it occurs for longer period from 190° to 330°. The peak magnitude in both half cycles is around 5 V. The maximum number of PD is 11 occurring at ϕ = 50° and 13 occurring at ϕ = 240°.

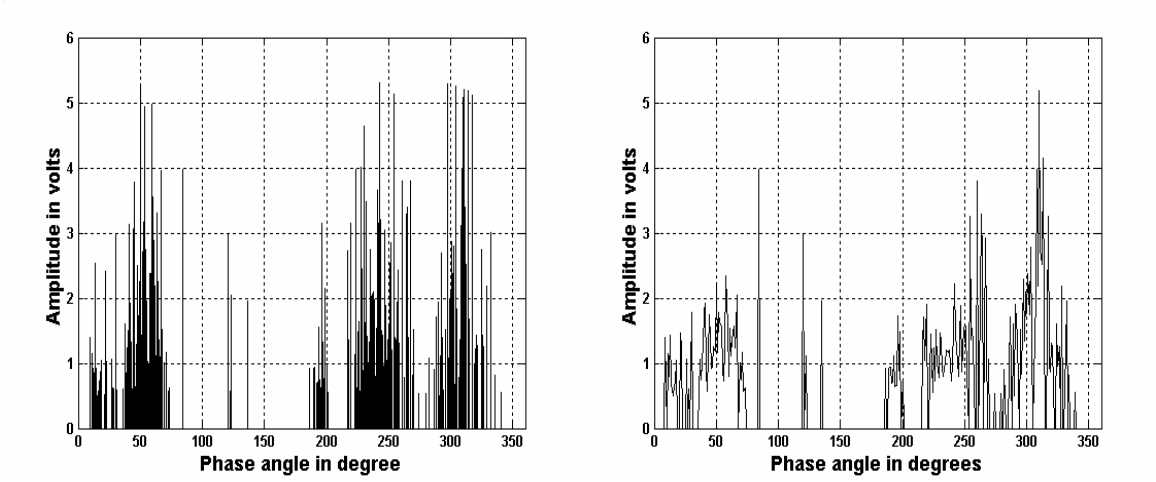

(a) Original q with ϕ

(b) Mean q in 1° window with ϕ

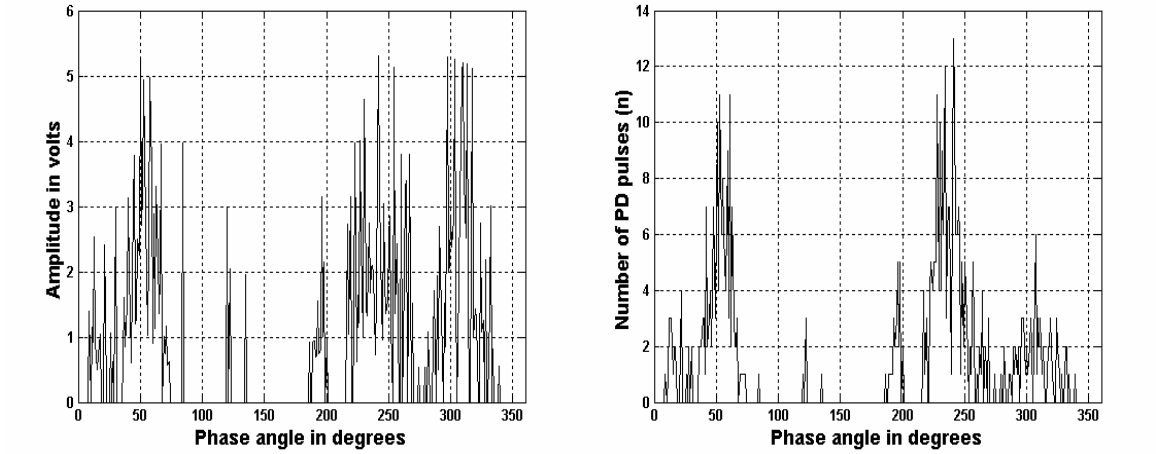

(c) Max. q in 1° window with ϕ

(d) n in 1° window with ϕ

Figure 5-3: Cavity PD occurrences in 20 ms period at 9 kV

5.3.4 Statistical operators to quantify PD distribution in 20 ms

The shape of the phase distribution in positive and negative half cycles of the PD occurrence may be quantified by using statistical operators like skewness, kurtosis and cross-correlation. These statistical quantities numerically describe the closeness of the shape to a standard normal distribution and are used for identifying the characteristics of each type of PD.

5.3.5 Results on Sk, Ku, and CC

For each type of PD distribution (q-Φ) in 20 ms shown in figures 5-1 to 5-3 , the statistical operators Sk, Ku and CC described in section 2.5 are determined in each half of ac cycle. The deviation of the phase distribution from the normal reveals the characteristics of each type of PD. Figure 5-4 shows the bar graph of the variation of Sk and Ku in both half cycles using mean, maximum and number distribution on corona PD.

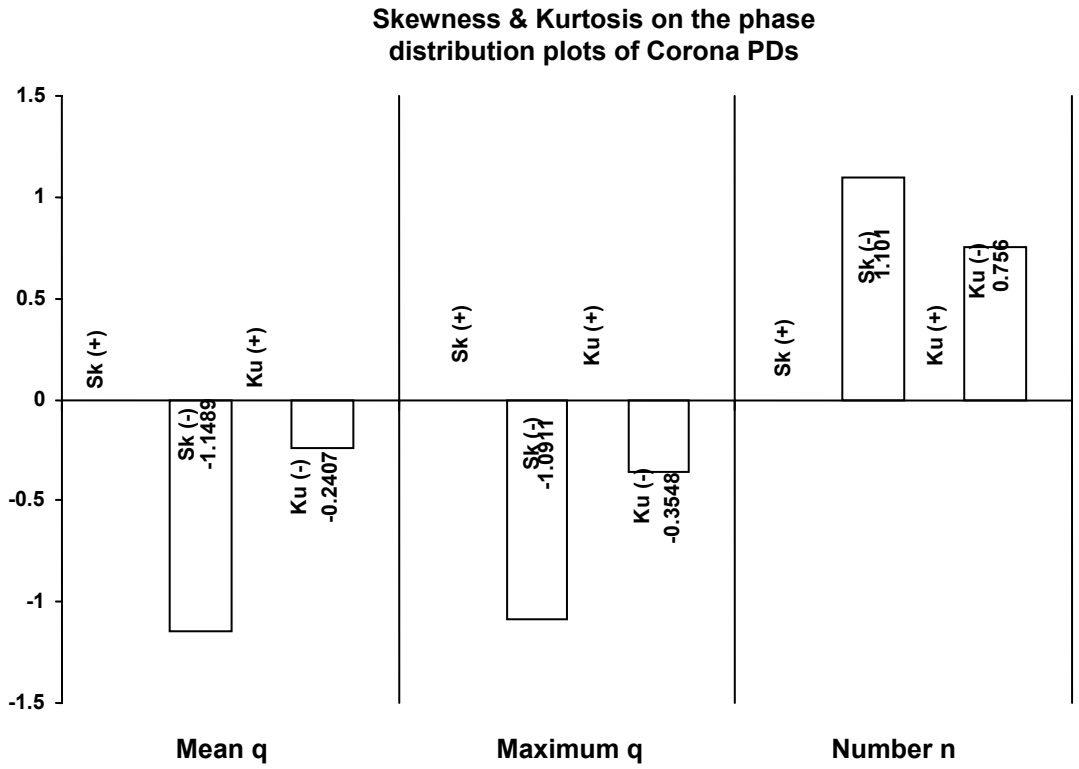

Figure 5-4: Variation in Sk and Ku using q-Φ and q-n data on corona PD

Corona PDs are found to exhibit dominant negative Sk and Ku for the mean and maximum distribution plots. That implies that the mean and maximum distributions are asymmetric to the right and flatter (less peaked) when compared to the shape of a standard normal distribution. In addition, corona PD has absolute Sk values greater than unity for all the phase distribution plots (mean, maximum, and number) implying more deviations away from a normal distribution. However, the Ku values for all three distribution plots are near to zero implying closeness to a normal. With number, it is always positive indicating asymmetry to left with sharp peak. Since corona occurs mostly in negative half cycle, there is no cross-correlation factor.

Similar analysis is made on surface PD distribution. Figure 5-5 shows the bar graph of the variation of Sk and Ku in both half cycles using mean, maximum and number distribution on surface PD. Surface PDs are observed to exhibit positive Ku in the positive half cycle and negative Ku in the negative half cycle for all the three phase distribution plots. This implies that the shape of PD distribution in the positive half cycle is sharper (more peaked at the centre) than a normal distribution while the shape in the negative half cycle is flatter than a normal distribution. For maximum and number plots, Sk is positive in both half cycles indicating asymmetry to the left. Computed CC for mean, maximum and number distribution between positive and negative half cycles are 0.47, 0.49 and 0.66 respectively indicating the existence of some correlation.

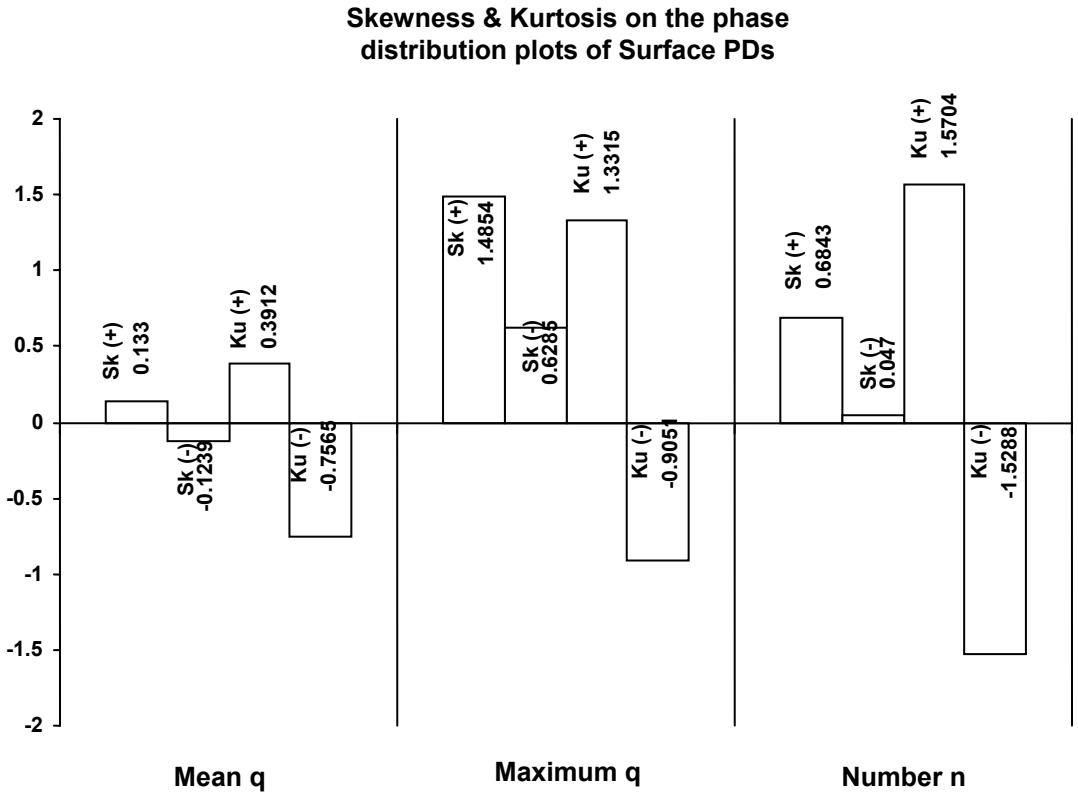

Figure 5-5: Variation in Sk and Ku using q-Φ and q-n data on surface PD

The analysis is extended to cavity PD distribution. Unlike surface and corona PDs, the shape of PD distribution of cavity PDs are the closest to a normal distribution as denoted by the low Sk and Ku values (see figure 5-6). In addition, cavity PD exhibits positive Sk for all its phase distribution plots (Mean, Maximum, and number). It implies that the phase distributions are spread more towards the right of the mean (asymmetric to the left). This is quite opposite to that of corona PDs. The shape of the phase distributions in the positive half cycle does not correlate well with the shape in the negative half cycle for all the three PD plots. Computed CC for mean, maximum and number distribution between positive and negative half cycles is 0.1, 0.1 and 0.13 respectively indicating the poor correlation.

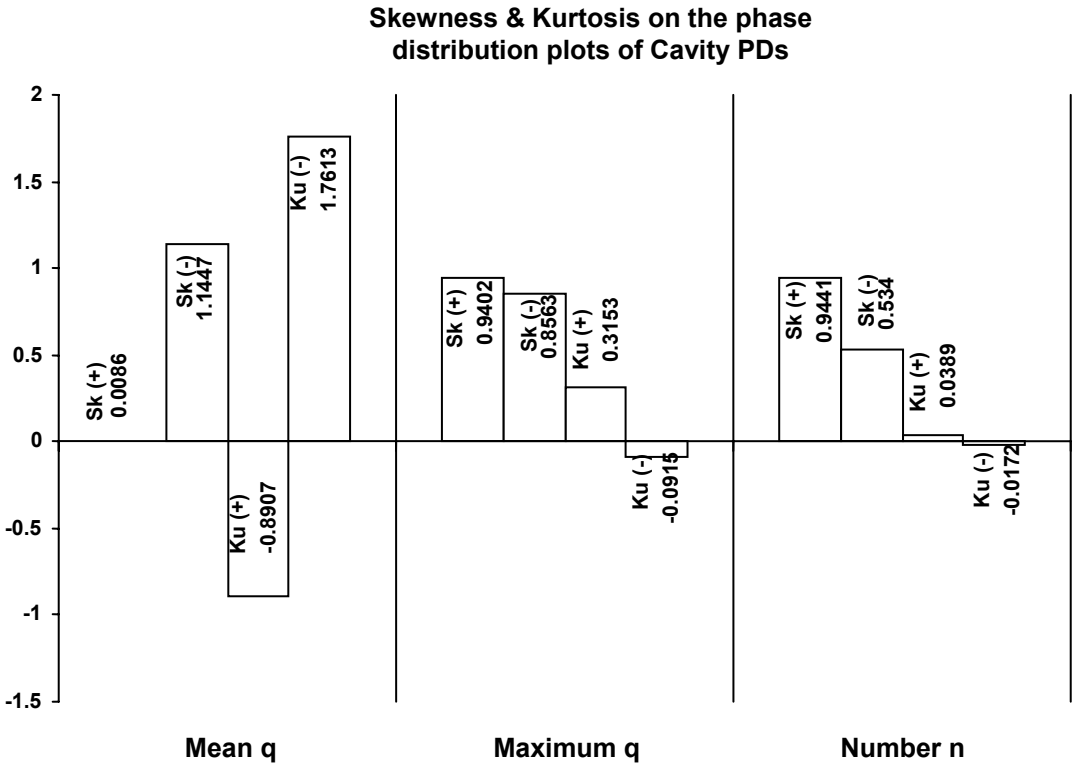

Figure 5-6: Variation in Sk and Ku using q-Φ and q-n data on cavity PD

5.3.6 Factors affecting statistical results

Several factors may result in different statistical results like different shapes of the phase distribution for each type of PD. For example, varying physical dimensions (i.e. dimensions of needle and cavity) and types of materials used, ambient temperature and humidity fluctuation, loading conditions, distortion in propagation path etc. But it may indicate a rough indication of the type of developing PD.

5.3.7 Variation of n with q

Next series of analysis is done to know the PD activity in terms its magnitude and the number of occurrence. Using the maximum magnitude as reference, the magnitude axis (in volts) is “chopped” into 50 magnitude windows. Number of PDs that fall into each magnitude window during positive and negative half cycles is determined and plotted as shown in figures 5-7a to 5-7e. A resolution higher than 50 can be used but the clarity is found to improve only slightly and it takes up more time and computational resources. Therefore, a resolution of 50 magnitude windows is used.

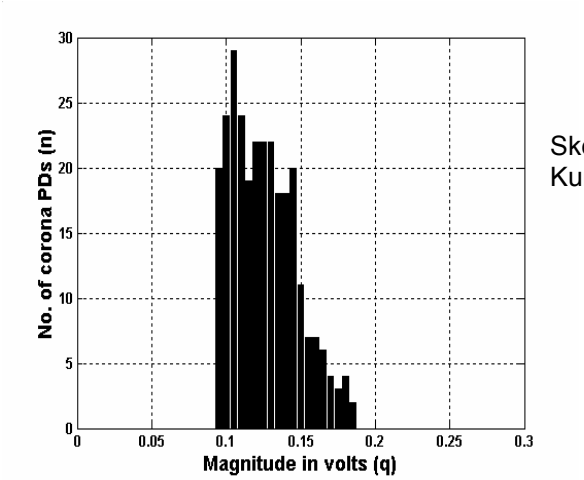

Figure 5-7a: q-n plot of corona PD at 5kV- negative half cycle

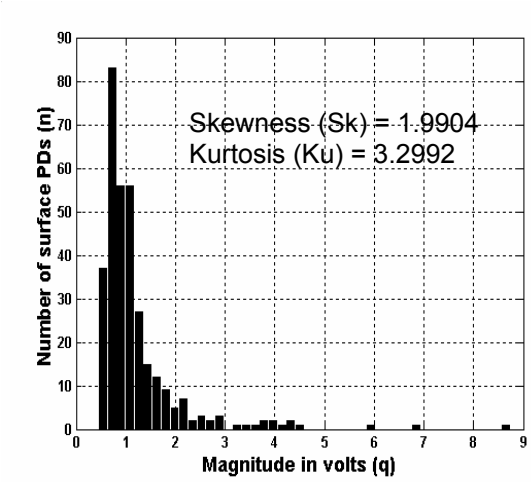

Figure 5-7b: q-n plot of surface PD

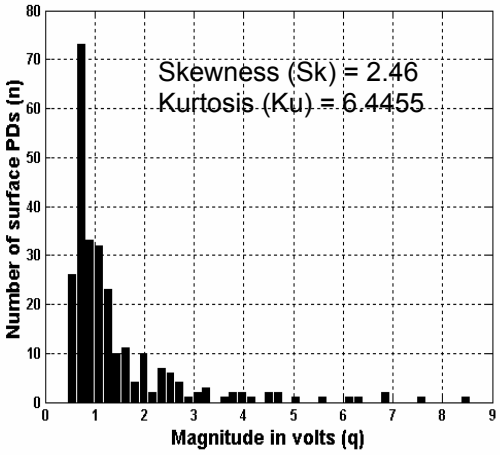

Figure 5-7c: q-n plot of surface PD at 5kV – negative half cycle

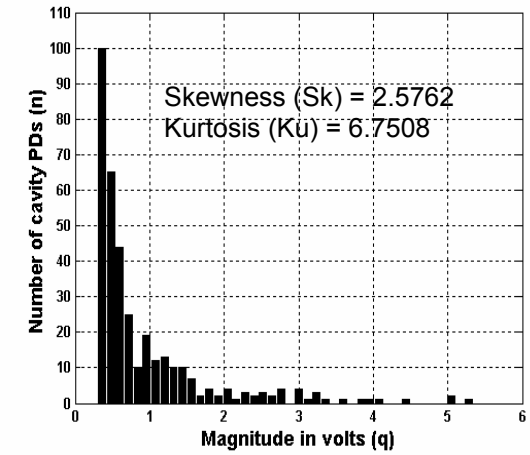

Figure 5-7d: q-n plot of cavity PD at 9kV – positive half cycle

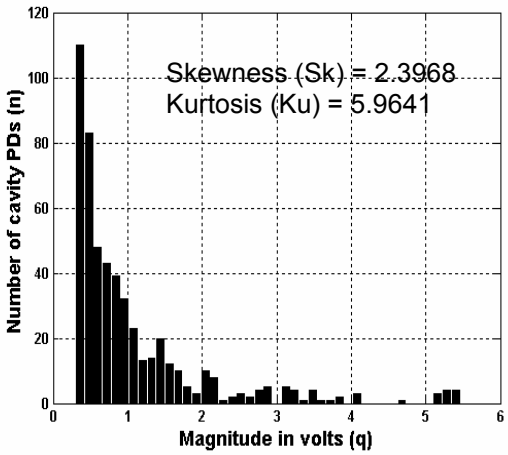

Figure 5-7e: q-n plot of cavity PD at 9kV – negative half cycle

Figure 5-7: Variation of n with q and statistical operators

As seen from figure 5-7, surface and cavity PDs are distributed with long tail in their magnitude ranges. Magnitude of surface PDs varies from 500mV to about 9000mV at an applied voltage of 5kV, cavity PDs range from 250mV to 5500mV using an applied voltage of 9kV and corona PDs cover a much lesser magnitude range from 90mV to 170mV at 5 kV. The calculated Sk and Ku values for corona, surface and cavity PDs are indicated in the figure. It is positive for surface and cavity PD distributions indicating asymmetric distribution to the left. For corona, value of Sk is negative and low in magnitude (very close to zero) indicating the small asymmetric distribution to the right and very close in shape to a normal as compared to that of surface and cavity PDs. On the other extreme, q-n distribution profiles of cavity PDs in both positive and negative half cycles exhibit the highest positive Sk values implying more deviation away from a normal distribution and having wide distribution spread to the right (i.e. long tailing to the right). Sk values for q-n distribution profiles of surface PDs are close to that of

cavity PDs indicating similar distribution pattern but to a slightly lesser extent. Therefore, it is possible to identify corona PDs from surface and cavity PDs in an unknown single source signal by knowing the Sk values of their q-n distribution profiles also.

Ku for corona PDs is negative and at minimum when compared to that of distribution profiles of surface and cavity PDs indicating q-n distribution profile is less peaked and has short tails. Its distribution profile is also deviated away from a normal distribution. Ku values for q-n distribution profiles of surface and cavity PDs in both positive and negative half cycles are positive indicating more peaked distribution and have some long tailing as compared to that of corona distribution. Ku values for surface and cavity distribution profiles are high indicating more peaks and long tailing in the nature of plots. Again, it is possible to identify corona PDs from surface and cavity PDs in an unknown single source signal by knowing the Ku values of their q-n distribution profiles.

It is found that the Sk and Ku values for corona q-n distribution profile in the negative half cycle are negative and significantly low in magnitude than that of the q-n distribution profiles of surface and cavity PDs (which exhibited positive and larger Sk and Ku values during negative half cycle). Hence, it is concluded that by knowing the magnitude and polarity of the Sk and Ku values for the q-n distribution profile of an unknown single-source signal, it may be possible to identify the presence of corona PD. Unfortunately, we cannot rely on the Sk and Ku quantities to identify surface from cavity PDs because they exhibited close range of those values.

5.4 Weibull distribution

5.4.1 Weibull fitting on q-cumulative n distribution profiles

Weibull distribution of q with cumulative n is used to identify and characterize the type of PD. The variation of cumulative number of PDs against the magnitude is fitted to a 2-parameter weibull distribution model discussed in section 2.3.1.3. The beta (β)-shape parameter and alpha (α)-scale parameter are determined from the weibull fitting. The β value is used for the identification of the type of PD present in a sampled signal because each type of PD exhibits a unique range of β values [110,111]. Figure 5-8 shows the typical weibull distribution with q and cumulative n for corona, and the fitted α is 132.5 and β is 10.72. Figure 5-9 shows the typical fitted α as 395 and β as 2.1 for surface PD while Figure 5-10 shows the typical fitted α as 533 and β as 2.9 for cavity PD.

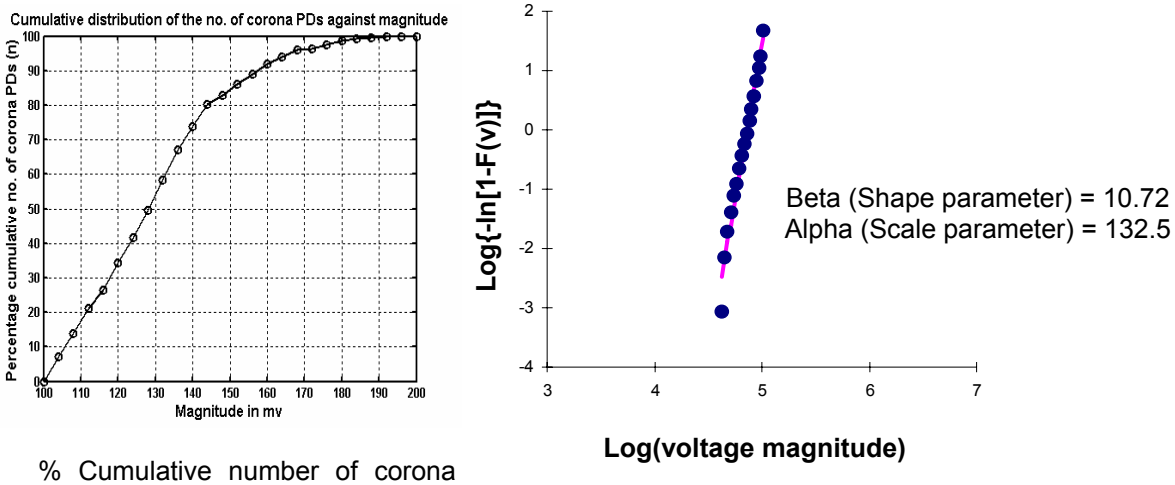

Figure 5-8: Weibull distribution with q-cumulative n on corona PD

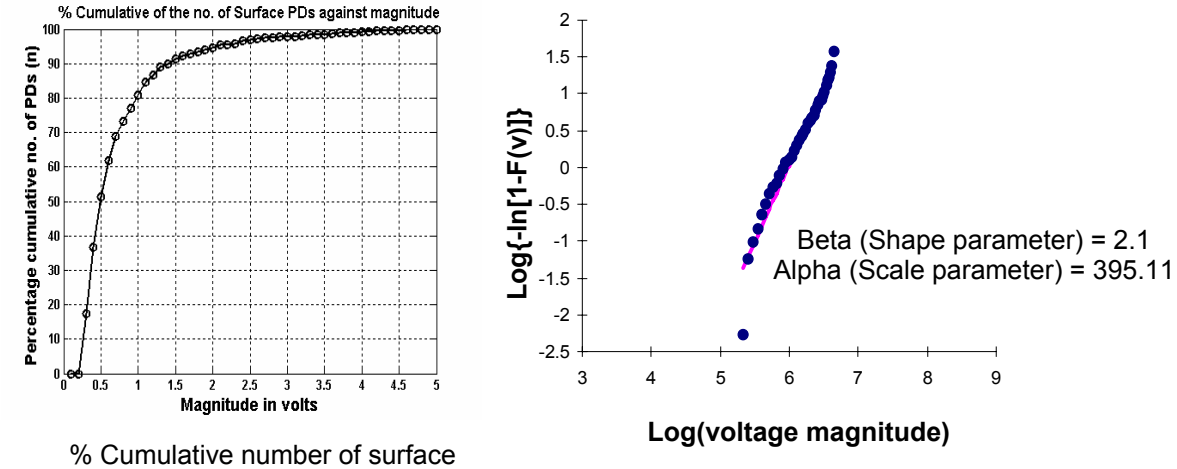

% Cumulative number of surface PDs against magnitude

Figure 5-9: Weibull distribution with q-cumulative n on surface PD

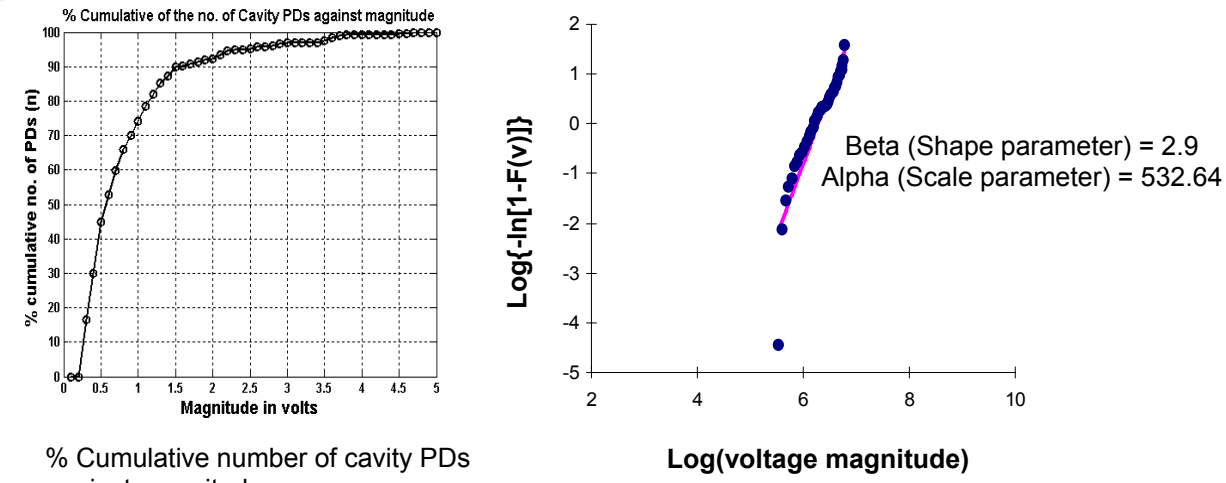

% Cumulative number of cavity PDs against magnitude

Figure 5-10: Weibull distribution with q-cumulative n on cavity PD

Weibull β value for corona PD is found to be much greater than that of surface and cavity PDs. The computed value for corona PD is consistently greater than 10 and indicating steeper Weibull slope. For surface PD, weibull β value is found to be the lowest in the range of 1.5 to 2.5 based on the data collected. For cavity PDs, weibull β value is not the lowest but is slightly greater than that of surface

PDs and found to lie in the range from 2.5 to 5 based on the processed data. The scale parameter α is estimated to be the highest for distribution profile of cavity PD distribution followed by surface with α = 395 and then corona with α =132.5. It closely agrees with the earlier work [112,113]. Goodness of straight line fitting in figures 5-8 to 5-10 indicates that the recorded PDs are from single or pure PD source. The estimated parameters are used for the identification of the type of PD source in future unknown PD occurrence.

5.4.2 Weibull fitting on Φ-cumulative n distribution profiles

Weibull fitting is also performed on the Φ-cumulative n distribution profile of each type of PD. The period (180 degree) of the positive and negative half cycles of an ac voltage cycle is chopped into 60 phase windows, and within each phase window, the percentage of cumulative number of PDs is calculated. This is done on 20 voltage cycles. The Φ-n distribution profile of each type of PD is shown in sections 5.3.1 to 5.3.3. Figures 5-11 to 5-15 show the weibull fittings on the Φ-cumulative n distribution profiles for the three types of PDs. The results of weibull fitting on Φ-cumulative n distribution profiles reveal identical outcome on the ranking of beta values for each type of PD i.e. the β of corona PD is maximum in value, followed by cavity and then surface PDs. Φ-cumulative n distribution profile of corona PDs exhibit weibull α and β values of 274.61 and 12.05 respectively. Cavity PDs exhibit α and β values of 50.175 and 2.086 respectively during positive half cycle and α and β values of 257.92 and 8.1 respectively during negative half cycle. Surface PDs exhibit the lowest α and β values of

43.86 and 1.47 during positive half cycle while showing α and β values of 246.92 and 7.65 during negative half cycle.

The weibull analysis with Φ and cumulative n is to be researched further as linear fit may not be adequate and the fitting gives different values during positive and negative half cycles giving more characterizing parameters.

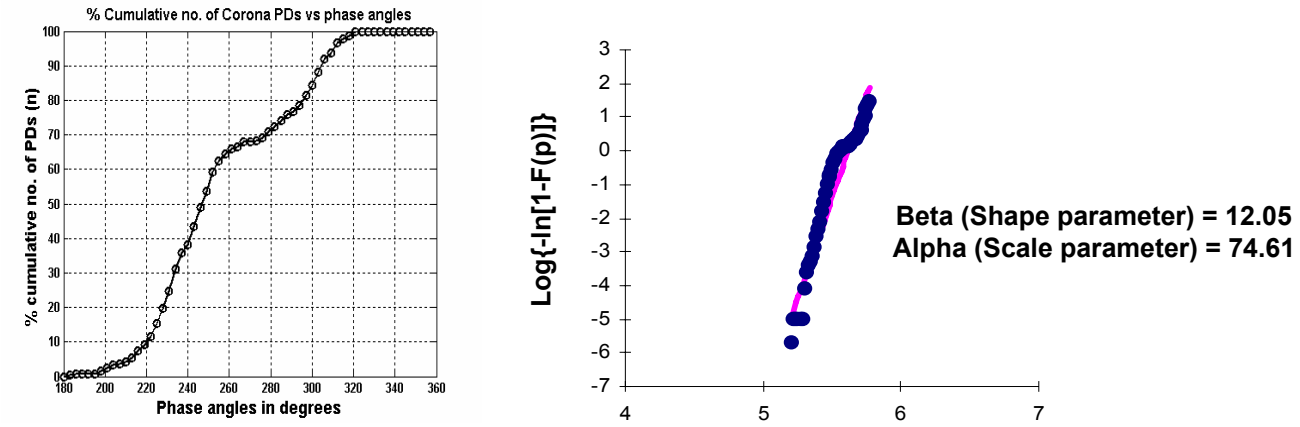

% Cumulative number of corona PDs against phase angles – negative half cycle

Figure 5-11: Weibull distribution with Φ-cumulative n on corona PDs – Negative half cycle

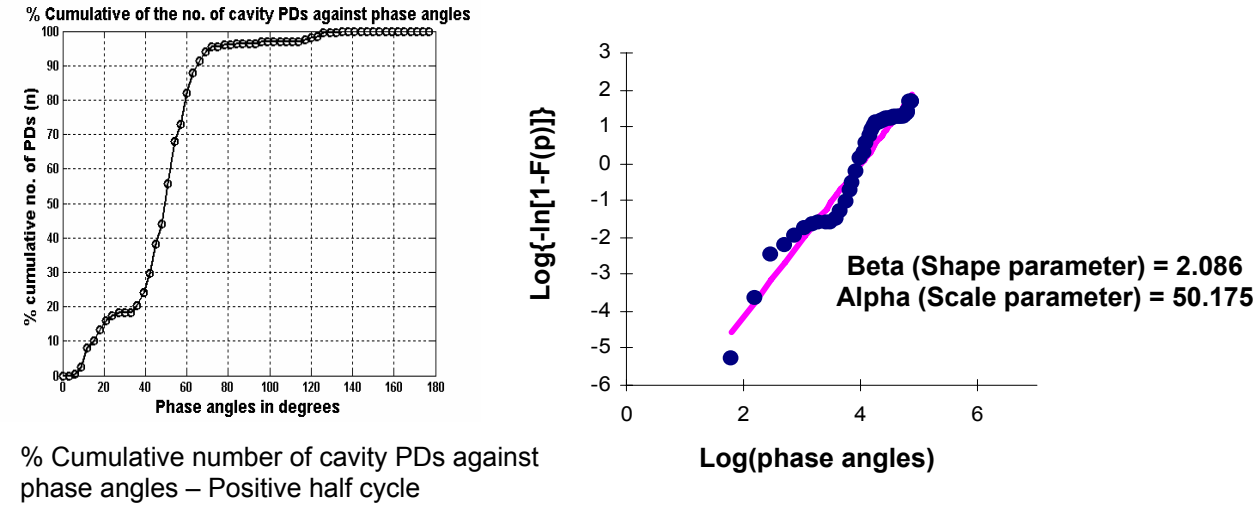

% Cumulative number of cavity PDs against phase angles – Positive half cycle

Figure 5-12: Weibull distribution with Φ-cumulative n on Cavity PDs – Positive half cycle

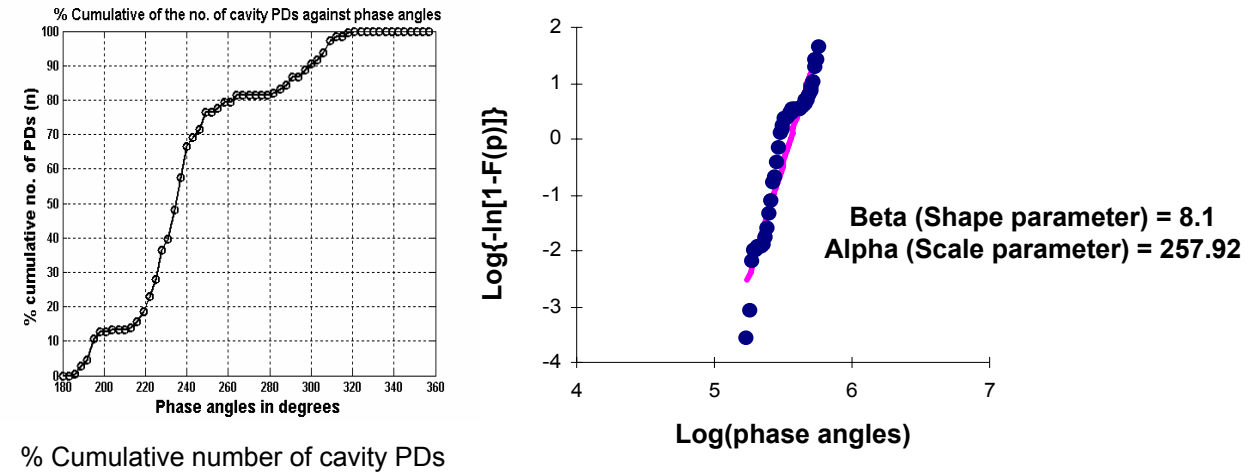

% Cumulative number of cavity PDs against phase angles – negative half cycle

Figure 5-13: Weibull distribution with Φ-cumulative n on Cavity PDs – Negative half cycle

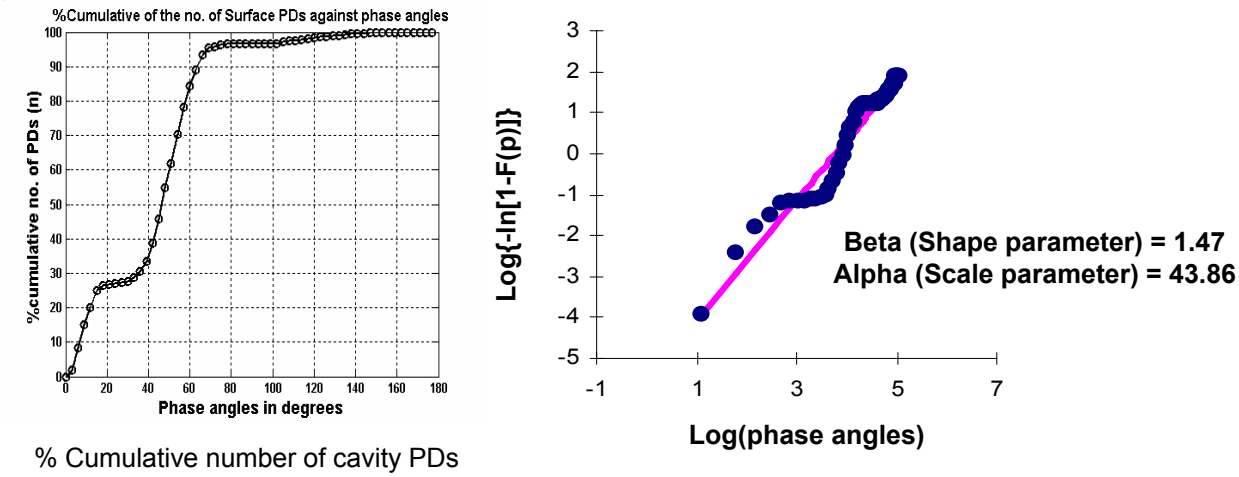

% Cumulative number of cavity PDs against phase angles – positive half cycle

Figure 5-14: Weibull distribution with Φ-cumulative n on Surface PDs – Positive half cycle

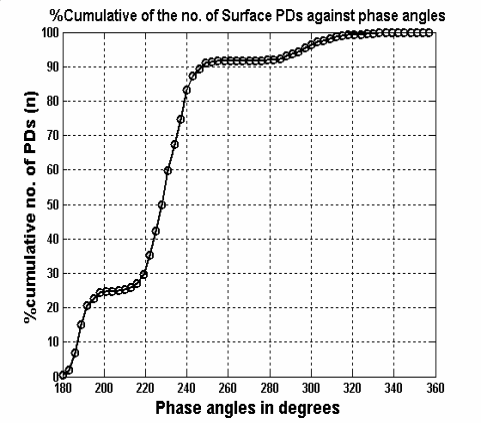

% Cumulative number of cavity PDs against phase angles – negative half cycle

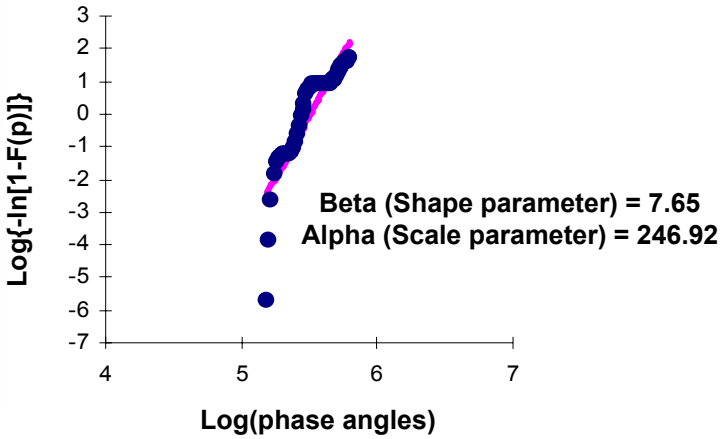

Figure 5-15: Weibull distribution with Φ-cumulative n on Surface PDs – Negative half cycle

5.5 Cluster analysis of PD

The calculated sequential amplitude and time changes (ΔV & Δt) between consecutive PD pulses within a voltage cycle, and repeated over 20 voltage cycles reveal how ΔV is statistically changing with corresponding change in Δt sequentially. Different cluster patterns for each type of PD are found. The diagram in figure 5-16 shows the scenario of getting ΔV and Δt. ΔV is the sequential change in the amplitudes of PD pulses and Δt is the corresponding sequential change in the time locations between consecutive PD pulses.

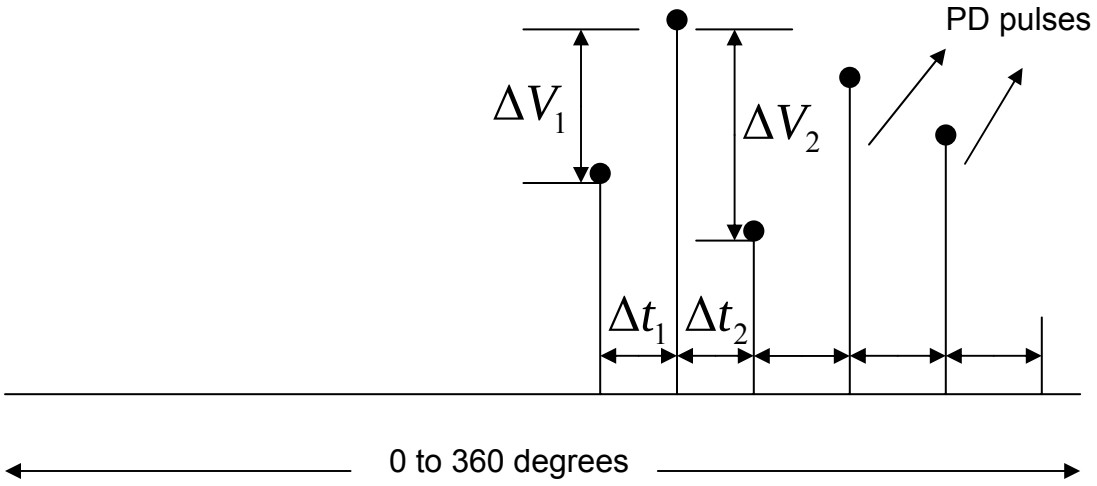

Figure 5-16: Extraction of ΔV and Δt occurrence of consecutive PDs

$$\Delta V = [\Delta V_1, \Delta V_2, \Delta V_3 .....]$$

$$\Delta t = [\Delta t_1, \Delta t_2, \Delta t_3 .....]$$

Four types of cluster distributions are calculated and plotted.

a) Variation of ΔV against Δt over 20 voltage cycles.

b) Variation of ΔVn against ΔVn-1 over 20 voltage cycles.

c) Variation of Δtn against Δtn-1 over 20 voltage cycles.

d) Variation of Δ(ΔV) against Δ(Δt) over 20 voltage cycles.

Characteristic cluster patterns for each type of PD are observed.

5.5.1 Variation of ΔV against Δt in 20 voltage cycles

Figure 5-17 shows the obtained result of computed ΔV against Δt in 20 voltage cycles for corona PDs. Corona pulses occurring in negative half cycle have very small ΔV and Δt spread of 0.08 V and 1.4 ms respectively.

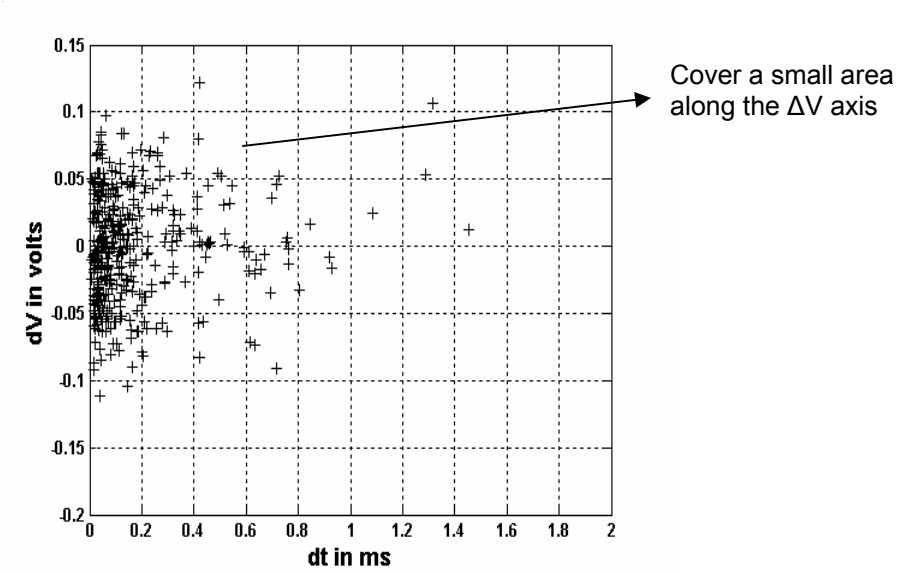

Figure 5-17: Variation of ΔV with Δt for corona PD at 5 kV (negative half cycle)

Figure 5-18 shows the obtained result of computed ΔV against Δt in 20 voltage cycles for surface PDs. Surface PD pulses occurring in positive and negative half cycles have very wide ΔV and Δt spread of 8 V and 3.8 ms respectively. 8 to 10 V wide and dense ΔV cluster decreases to 2 V in a Δt of 0.5 ms.

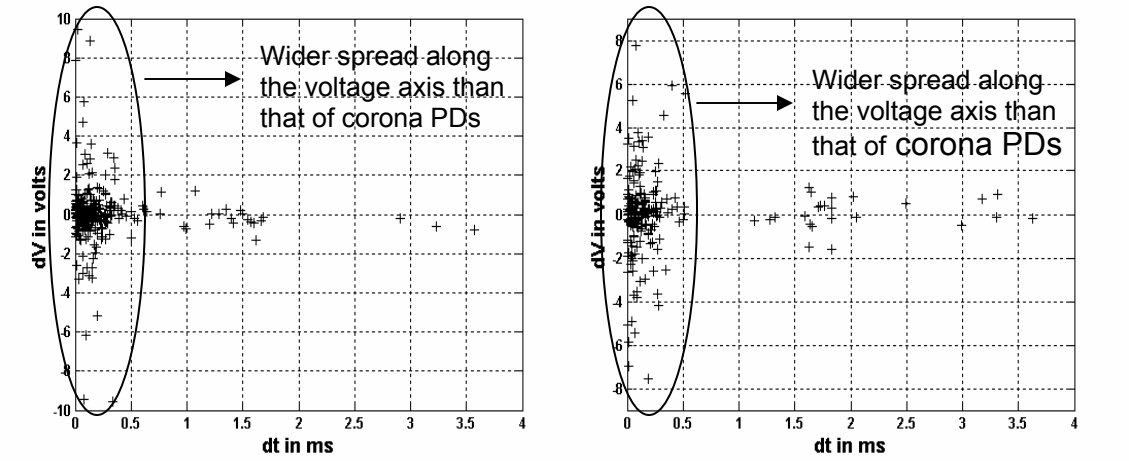

Plot of ΔV vs Δt (positive half cycle) surface PD (5kV)

(b) Plot of ΔV vs Δt (negative half cycle) surface PD (5kV)

Figure 5-18: Variation of ΔV with Δt for surface PD at 5 kV

Figure 5-19 shows the obtained result of computed ΔV against Δt in 20 voltage cycles for cavity PDs. Almost identical cluster patterns between positive and negative half cycles is noticed. It is more densed and scattered in negative half cycle compared to positive half cycle. Cavity PD pulses occurring in positive and negative half cycles have moderate ΔV spread of 5 V and Δt spread of 4ms which is comparable to that of surface PD distribution. In positive half cycle, 5 V range of ΔV decreases to 2 V range in Δt of 0.5 ms. In negative half cycle, 5 V range and ΔV decreases to 2 V range in Δt of 0.8 ms.

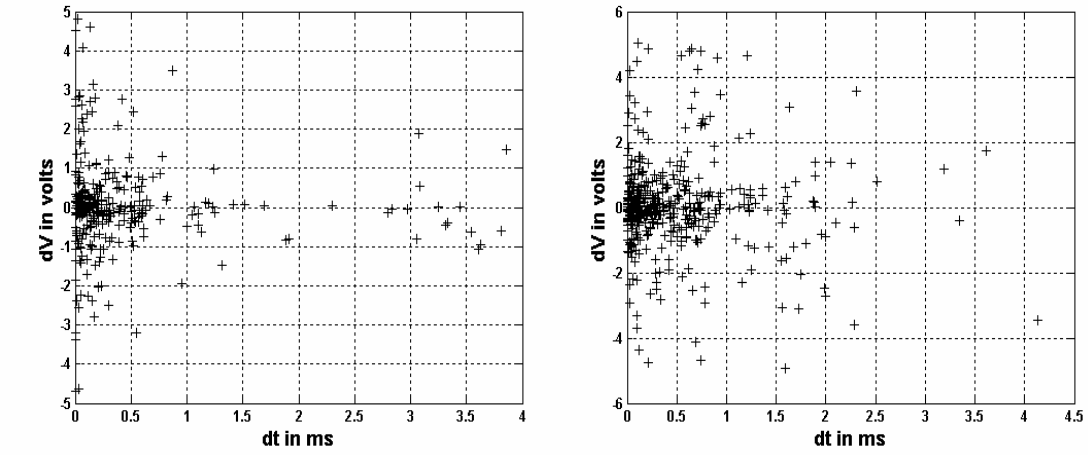

Plot of ΔV vs Δt (positive half cycle) cavity PD (9 kV)

Plot of ΔV vs Δt (negative half cycle) cavity PD (9 kV)

Figure 5-19: Variation of ΔV with Δt for cavity PD at 9 kV

5.5.2 Variation of ΔVn against ΔVn-1 in 20 voltage cycles

The difference in voltage amplitudes between consecutive n pulses is determined. A plot of ΔVn against ΔVn-1 reveals the characteristic pattern for each type of PD.

ΔVn = V(n+1) – V(n) and …… (5.1)

ΔVn-1 = V(n) – V(n-1)

Figure 5-20 shows the plot of ΔVn-1 against ΔVn for corona PD. Corona pulses tend to clutter around the origin with pulses spread quite uniformly in the four quadrants and covering small parameter range of 0.05 V. It suggests that scatter in corona discharge magnitude is uniform and minimum.

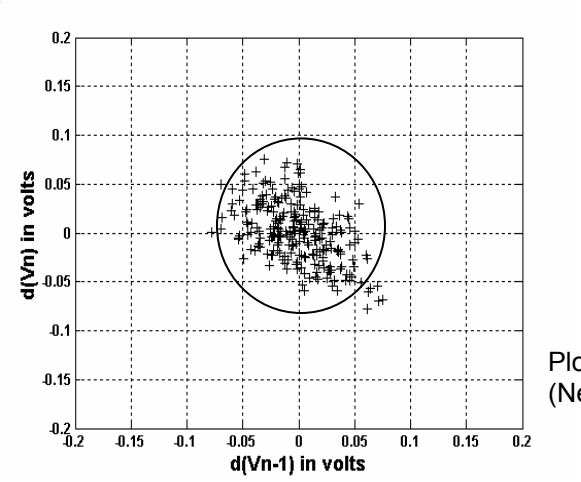

Plot of ΔVn vs ΔVn-1
(Negative half cycle)

Figure 5-20: Variation of ΔVn-1 with ΔVn for corona PD at 5 kV

Figure 5-21 shows the plot of ΔVn-1 against ΔVn for surface PD. Surface PD pulses appear to scatter more freely in the four quadrants during positive and negative half cycles than that of corona PDs. The scatter in surface discharge magnitude is significantly larger than that of corona PDs and appears to be less uniform. The distribution is more concentrated in the fourth quadrant up to 5 V and to a lesser degree in second quadrant. It appears that out of 3 consecutive pulses, the starting and ending PDs have less magnitude.

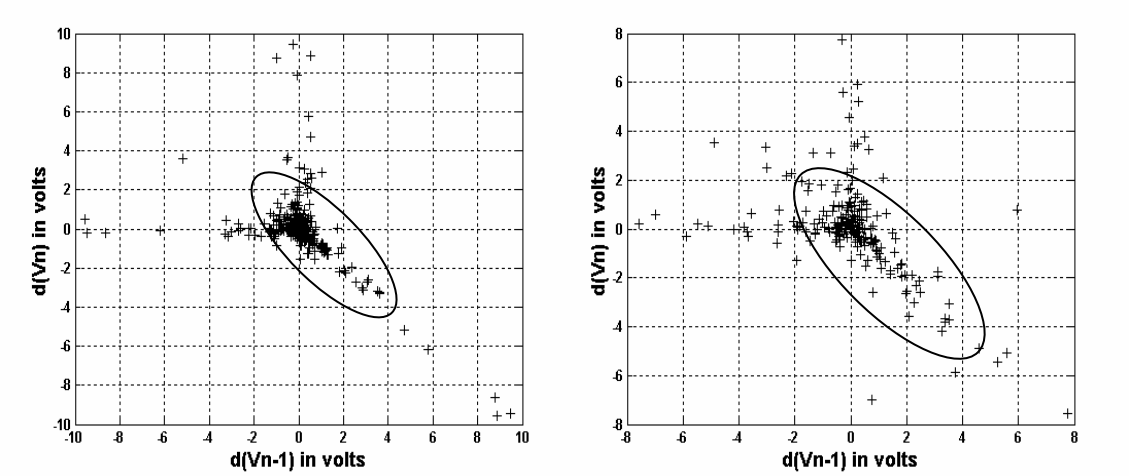

Plot of ΔVn vs ΔVn-1 (positive half cycle)

Plot of ΔVn vs ΔVn-1 (negative half cycle)

Figure 5-21: Variation of ΔVn with ΔVn-1 for surface PD at 5 kV

Figure 5-22 shows the plot of ΔVn-1 against ΔVn for cavity PD. It is quite similar to surface cluster patterns. Cavity pulses also appear to scatter more freely in the fourth and second quadrants during positive and negative half cycles than that of corona PDs. The scatter in cavity discharge magnitude is also significantly larger than that of corona PDs but to a lesser extent when compared to surface distribution. It also appears to be less uniform. The distribution is more concentrated in fourth quadrant up to 3 V and in second quadrant up to 2V.

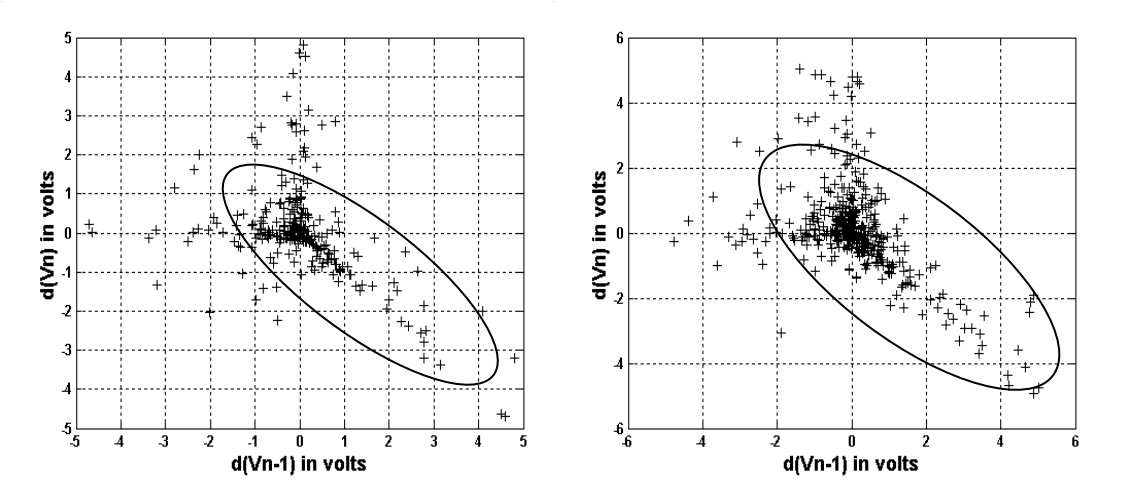

Plot of ΔVn vs ΔVn-1 (Positive half cycle)

Plot of ΔVn vs ΔVn-1 (negative half cycle)

Figure 5-22: Variation of ΔVn with ΔVn-1 for cavity PD at 9 kV

5.5.3 Variation of Δtn against Δtn-1 in 20 voltage cycles

Similar to ΔVn against ΔVn-1, the distribution due to differences between times of statistical occurrence of consecutive n PD pulses is investigated. Δtn and Δtn-1 are determined by (5.2). Plots of Δtn against Δtn-1 for each type of PD are shown in figures 5-23 to 5-25.

$\Delta tn = t(n+1) - t(n)$ and …… (5.2)

$\Delta tn-1 = t(n) - t(n-1)$

Cluster pattern derived from the plot of Δtn against Δtn-1 for corona PDs indicate that the sequential time separation between consecutive pulses is the lowest as compared to that of surface and cavity PDs. Time separation between consecutive corona pulses are seen to reside mostly within 1ms range in both axis. In addition, another minor distribution with a maximum Δtn and Δtn-1 spread of about 1.4ms is also observed. No significant difference in time separation between consecutive pulses is seen for surface and cavity PDs. They both have

more distributed ∆tn and ∆tn-1 spread as compared to that of corona PDs. Majority of the cluster lie in a time duration of 0.5 ms. The maximum spread of ∆tn for surface and cavity PDs is close to 4ms and as for ∆tn-1, it is less than 3ms. The first 2 consecutive pulses of 3 occur in short time. More scatter is noticed in negative cycle for cavity distribution. Surface distribution exhibits almost identical scatter during positive and negative half cycles.

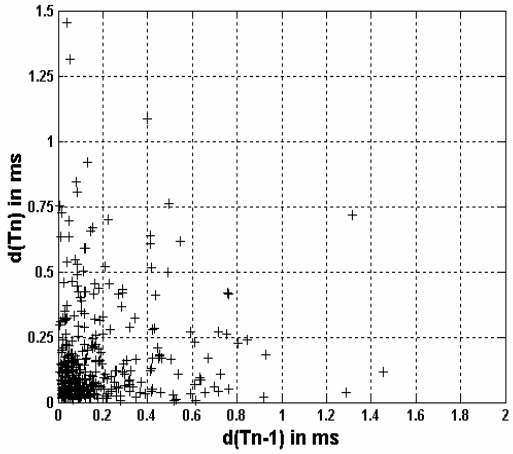

Figure 5-23: Plot of ∆tn vs ∆tn-1
for **corona at 5 KV**

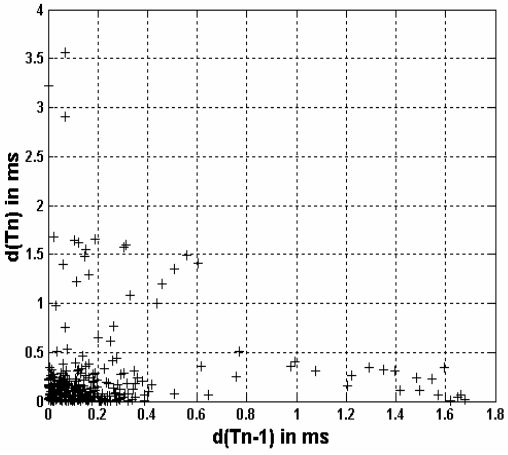

Figure 5-24(a): Plot of ∆tn vs ∆tn-1
(*Positive* half cycle - **surface**)

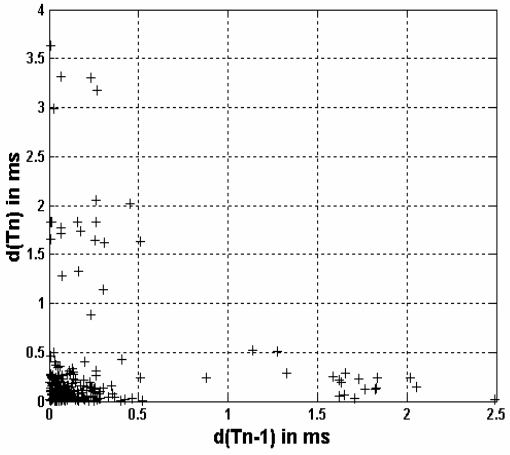

Figure 5-24(b): Plot of ∆tn vs ∆tn-1
(*Negative* half cycle - **surface**)

Figure 5-24 Variation of ∆tn with ∆tn-1 for surface PD at 5KV

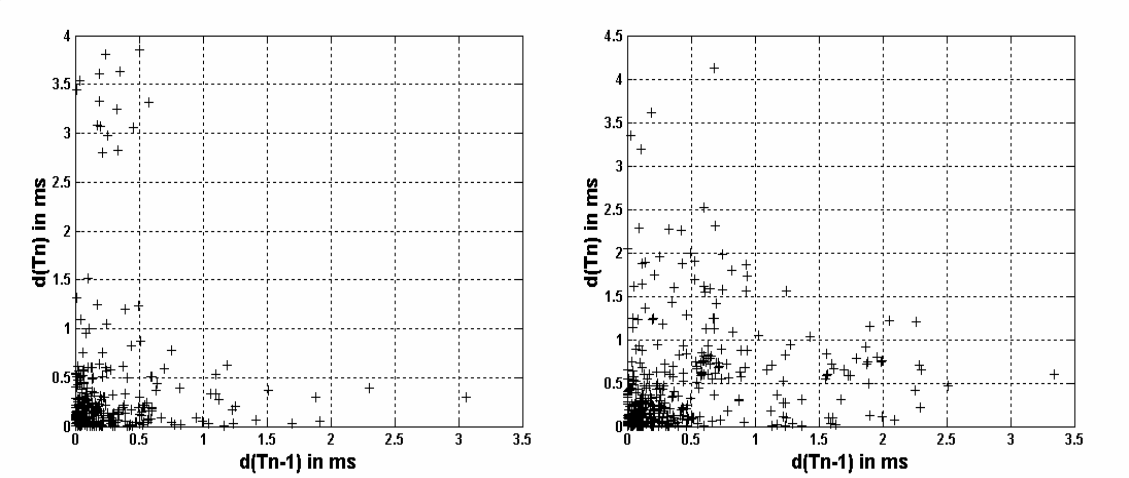

Figure 5-25(a): Plot of Δtn vs Δtn-1 (*Positive* half cycle - **cavity**)

Figure 5-25(b): Plot of Δtn vs Δtn-1 (*Negative* half cycle - **cavity**)

Figure 5-25 Variation of Δtn with Δtn-1 for cavity PD at 9 KV

5.5.4 Plot of Δ(ΔV) against Δ(Δt)

The resultant change in amplitude separation between derived consecutive n amplitude separations against the resultant change in time separation between derived consecutive n time separation (equation 5.3) also reveal the characteristics patterns of each type of PD.

Δ(ΔV) = ΔVn – ΔVn-1 and ---------- (5.3)

Δ(Δt) = Δtn – Δtn-1

Distribution of corona PD is found to be densely crowded near the origin while that of surface and cavity are spread more along both *Δ(ΔV) and Δ(Δt) axes.* Figure 5-26 shows *Δ(ΔV)* of corona pulses remain well within 0.1 Volts absolute and *Δ(Δt)* of the majority pulses remain in less than 1 ms absolute. Corona pulses clutter close to the origin in a round shape which is quite similar to the previous ΔVn-1 against ΔVn plot

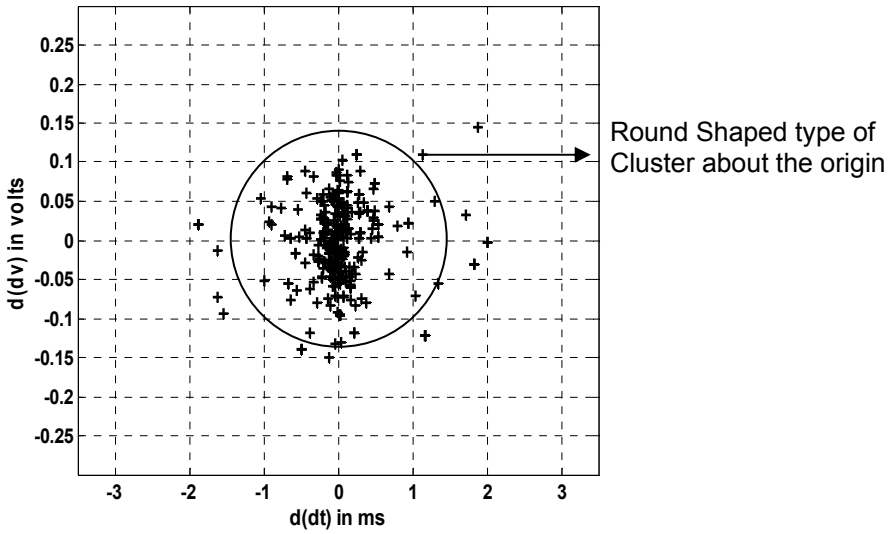

Figure 5-26: Variation of $\Delta(\Delta V)$ with $\Delta(\Delta t)$ for corona PD at 5 kV

Figure 5-27 shows the scattered wide distribution spread of surface PD pulses with $\Delta(\Delta V)$ extending to about 6 V and $\Delta(\Delta t)$ within 2 ms absolute. $\Delta(\Delta V)$ and $\Delta(\Delta t)$ scattered distribution of cavity PD pulses are quite similar that of surface PDs and is shown in figure 5-28. It can be seen that the $\Delta(\Delta V)$ extend to about 6 V and $\Delta(\Delta t)$ within 3 ms absolute. Therefore, the plots of $\Delta(\Delta V)$ and $\Delta(\Delta t)$ distribution of each type of PD can only be used to separate corona PDs from surface or cavity PDs. This method cannot be used to separate surface from cavity PDs since they have quite similar distribution quantitatively.

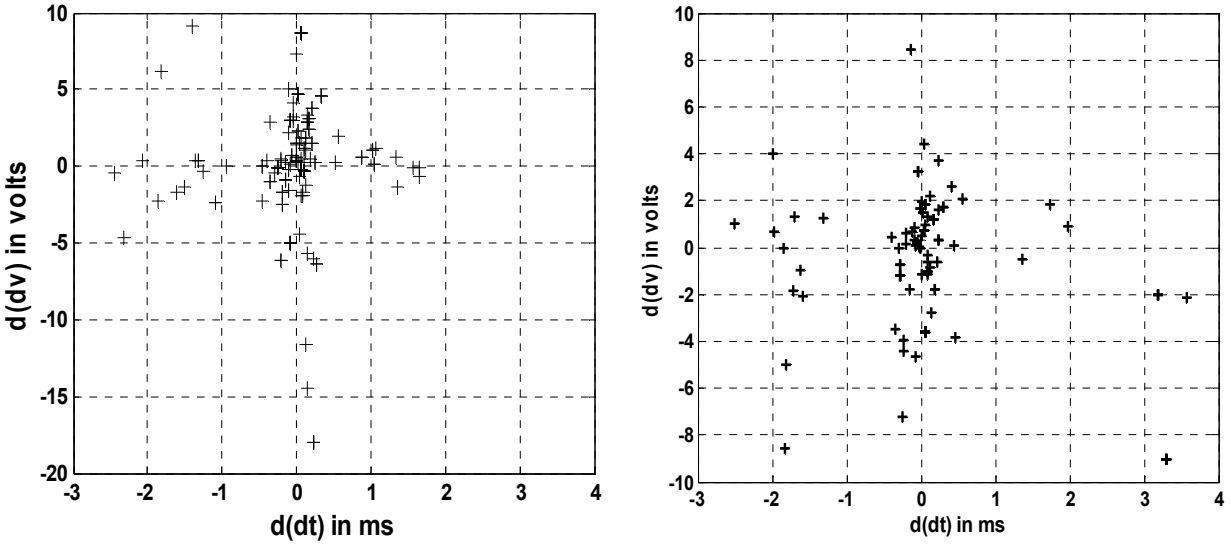

Plot of Δ(ΔV) vs Δ(Δt)
(Positive half cycle)

Plot of Δ(ΔV) vs Δ(Δt)
(Negative half cycle)

Figure 5-27: Variation Δ(ΔV) with Δ(Δt) for surface PD at 5 kV

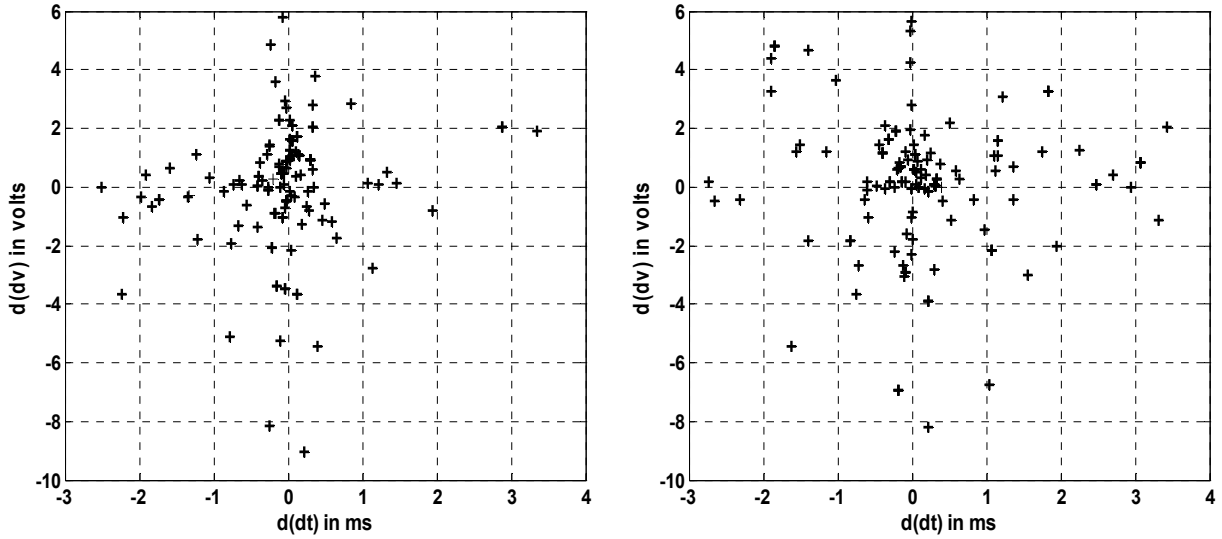

Plot of Δ(ΔV) vs Δ(Δt)
(positive half cycle)

Plot of Δ(ΔV) vs Δ(Δt)
(negative half cycle)

Figure 5-28: Variation of Δ(ΔV) with Δ(Δt) for cavity PD at 9 kV

Cluster analysis using ΔV with Δt, ΔVn with ΔVn-1, Δtn with Δtn-1 and Δ(ΔV) with Δ(Δt) clearly indicates the difference in cluster occurrence pattern of different types of PD. In general, cluster analysis can be used to identify corona PDs in an unknown single-source signal because corona exhibits consistently small voltage and time amplitude spreads in all the cluster plots i.e. corona distribution is always cluttered around the origin. However, cluster analysis may not be able to deduce occurrence of surface or cavity PDs in an unknown single-source signal if larger amplitude spreads of the four types of cluster plots are obtained, because cavity and surface PDs have close spread in those quantities. After characterizing the PD random occurrence in 20 ms period, the characterization of individual PD waveshape is taken up.

5.6 Individual PD pulse Analysis

The objective of individual pulse analysis is to determine the unique characteristics of each type of PD pulse individually. Four dominant characteristics of each type of PD pulse are of interest for classification. In time domain, the shape of each type of PD pulse, pulse width and peak magnitude are compared. In frequency domain, characteristic frequencies at which resonance occurs and the corresponding resonance voltage magnitudes are compared.

High sampling rate of the digital oscilloscope at 1.25 GSamples per second is used to capture the details of individual PD pulses. In this work, as described in chapter 3, 8 ns/sampling points is used. DWT is utilized to remove the background noises, and to determine the time location of PD. Then using the

time location of PD, the shape of each type of individual PD is extracted from the original recorded data.

5.6.1 Time domain characteristics of each type of single PD pulse

From 1.6ms data, single PD is extracted. Corona PD pulses are non-oscillatory and corona pulse decays to signal background level with a smooth tail. For corona PD, it appears like a double exponential waveshape with pulse width duration of about 1 μs as shown in figure 5-29. By increasing voltage, the peak magnitude of 0.44 V or shape does not change much. The polarity of the pulse is negative. There is some dc offset in the recording. The corona PD pulses were extracted from the original time domain signal by using the locations of them detected by WT and not WT approximations of the original corona PD pulses. The same PD pulse extraction method applies to the following surface and cavity PD pulses.

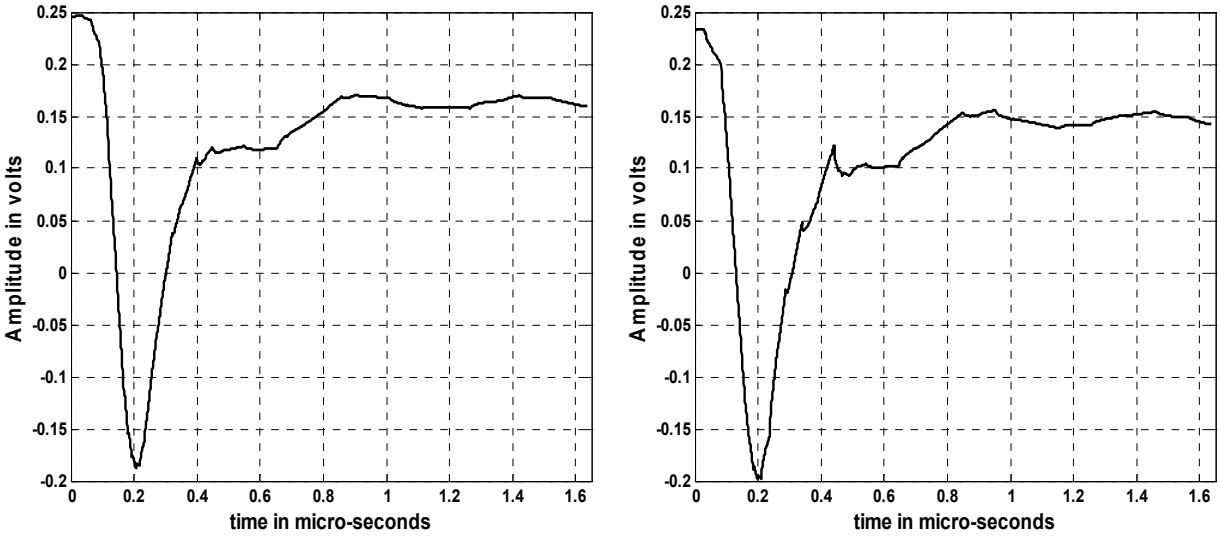

(a) at 10 kV (b) at 15 kV

Figure 5-29: Shape of corona PD by changing voltage

Surface PD pulse is oscillatory. It looks like a sharp pulse with fast decaying oscillation as shown in figure 5-30. By increasing voltage, the shape does not change. But the peak to peak magnitude increases at a fast rate from 0.75 V to 11 V for the applied HV change from 3 kV to 5 kV. The duration of the pulse increases from 200 ns to 300 ns. The polarity of the dominant peak is negative. There is some dc offset in the recording at 3 kV in figure 5-30(a).

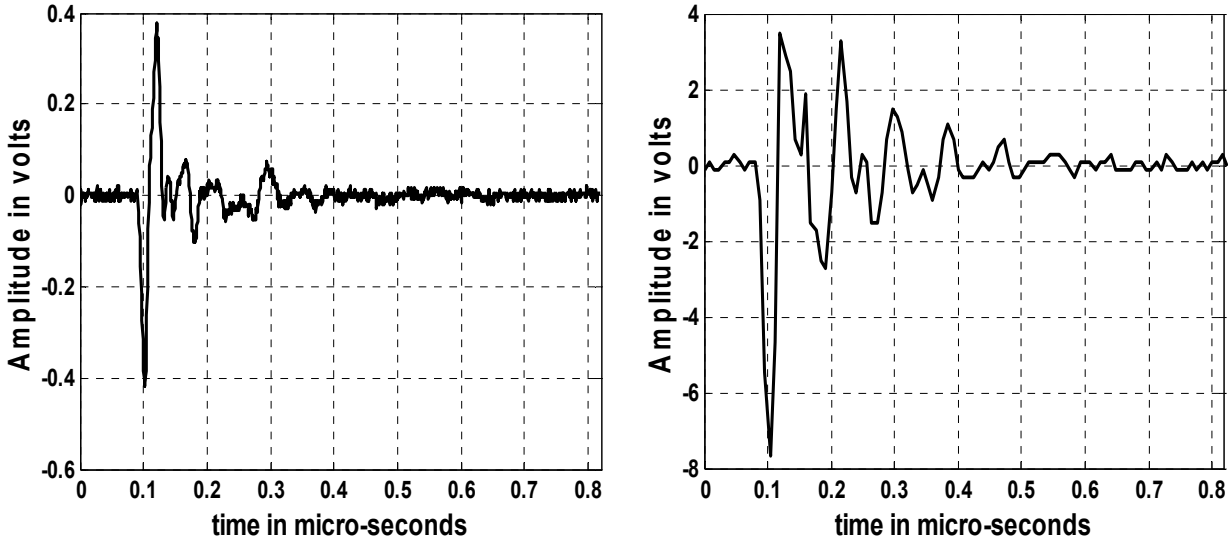

(a) at 3 kV (b) at 5 kV

Figure 5-30: Shape of surface PD by changing voltage

Cavity PD is also an oscillatory one. Cavity PD also looks like a sharp pulse with fast decaying oscillation as shown in figure 5-31. By marginally increasing voltage, the shape and peak to peak magnitude do not change much. The peak to peak magnitude is around 0.41 V. The duration of the pulse is around 200 ns. The polarity of the dominant peak is negative.

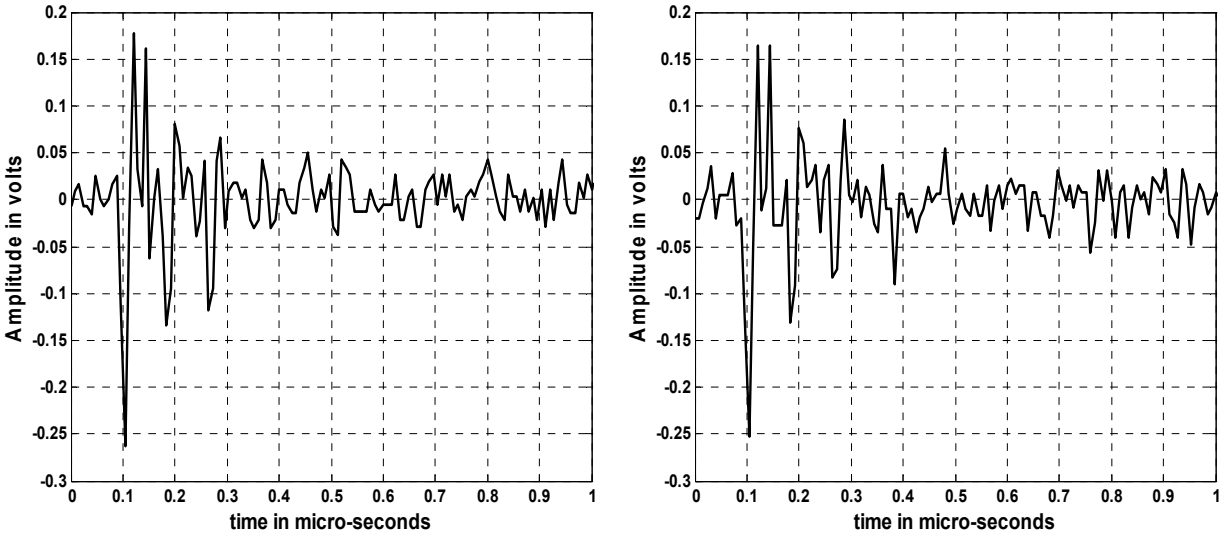

(a) at 9 kV (b) at 9.5 kV

Figure 5-31: Shape of cavity PD by changing voltage

From the above time domain observations, it is deduced that surface and cavity pulses may have higher frequency oscillatory components than that of corona pulses. Surface PD peak to peak magnitude is very sensitive to applied HV. For cavity PDs, the applied source is increased in modest step of 0.5 kV to observe for changes in amplitude and phase of the cavity PDs because the cavity models developed (see section 3.4.3) are prone to breakdown with sudden increase in applied voltage. Cavity PDs start to emerge at about 9 kV and become more in number at 9.5 kV. Upon reaching 11 kV, cavity PDs are seen to be severe and that voltage is deemed to be the maximum applied voltage before breakdown occurs. Once the cavity PD model breaks, it cannot be used anymore and a new one has to be developed again. Peak to peak PD signal for cavity PD does not vary much upon increased applied HV source as seen from the single pulses in figure 5-31.

5.6.2 Frequency domain characteristics of each type of single PD pulse

Each type of PD pulse is found to be well defined in shape and therefore FFT is performed on the single PD pulse to determine its frequency contents. A total of 512 sampled points are used for the FFT calculation of each type of PD pulse. For corona PD, the determined power spectral density decays exponentially with increase in frequency as shown in figure 5-32. Corona PD is found to have energy up to 5 MHz. By increasing voltage, low frequency spectral energy of corona PD increased marginally with decrease in high frequency spectral energy.

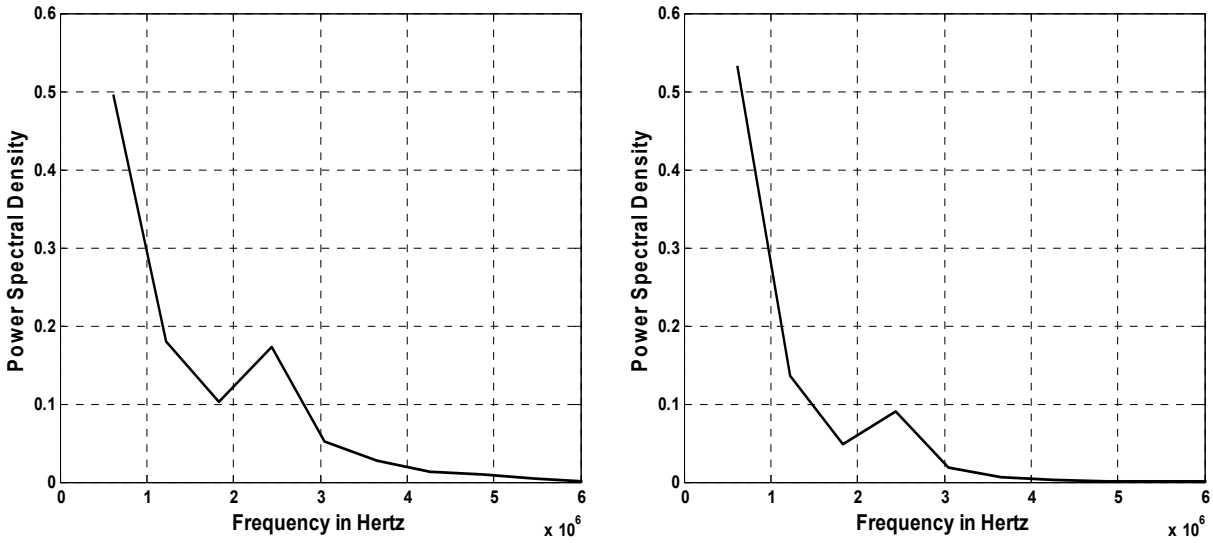

10 kV 15 kV

Figure 5-32: FFT content of single corona PD at 10 kV and 15 kV

Characteristic frequency peaks are obtained with surface single PD analysis shown in figure 5-33. Up to 35 MHz, it is found to carry the energy. At 3 kV, the determined characteristic frequencies are 12 MHz, 22 MHz, and 30.5 MHz with the relative PSD magnitudes of 1.4, 1.78, and 0.55 respectively. At 5 kV, relative PSD magnitude increases significantly (by 15 times). The calculated characteristic frequencies are 12 MHz, 22 MHz, 30.5 MHz with the relative PSD

magnitudes of 30, 13.5 and 4 respectively. It appears that the characteristic frequencies are the same with the increased energy on raising the voltage.

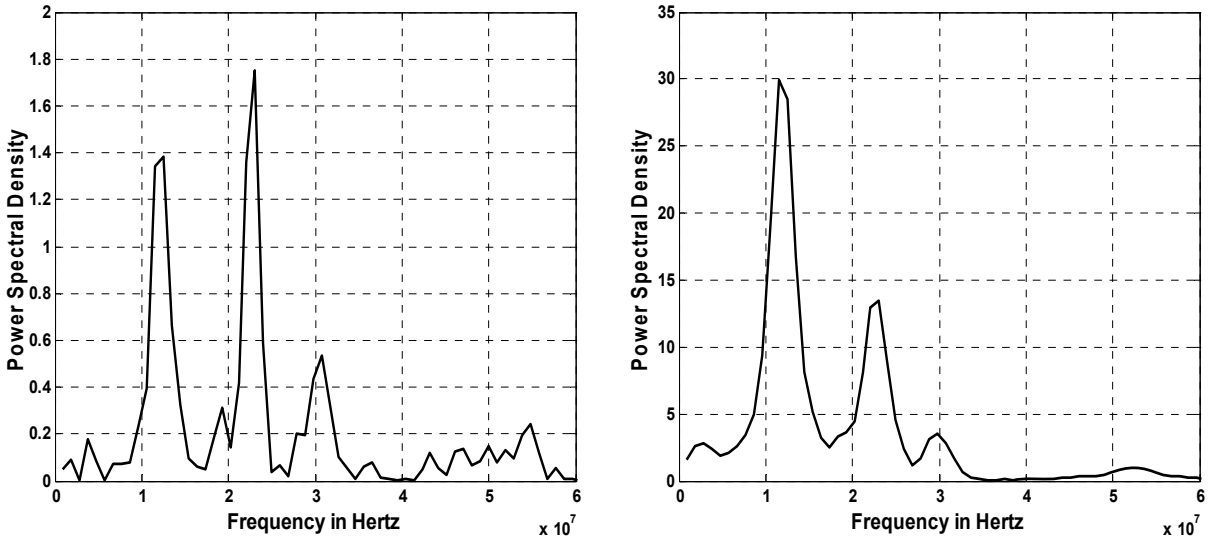

3 kV 5 kV

Figure 5-33: FFT content of single surface PD at 3 kV and 5 kV

Characteristic frequency peaks are obtained with cavity single PD analysis shown in figure 5-34. Up to 40 MHz, it is found to carry the energy. At 9 kV, the determined characteristic frequencies are 13 MHz, 25 MHz, and 35 MHz with the relative PSD magnitudes of 0.0097, 0.008, and 0.0072 respectively. At 9.5 kV, relative PSD magnitude increases marginally. The calculated characteristic frequencies are 12 MHz, 23 MHz, and 35 MHz with the relative PSD magnitudes of 0.011, 0.008, and 0.0178 respectively. It appears that the characteristic frequencies change slightly with the marginally increased energy on raising the voltage. The spectrum range of the peaks lied in a range of 4 to 40 MHz with energy significantly less than surface PD.

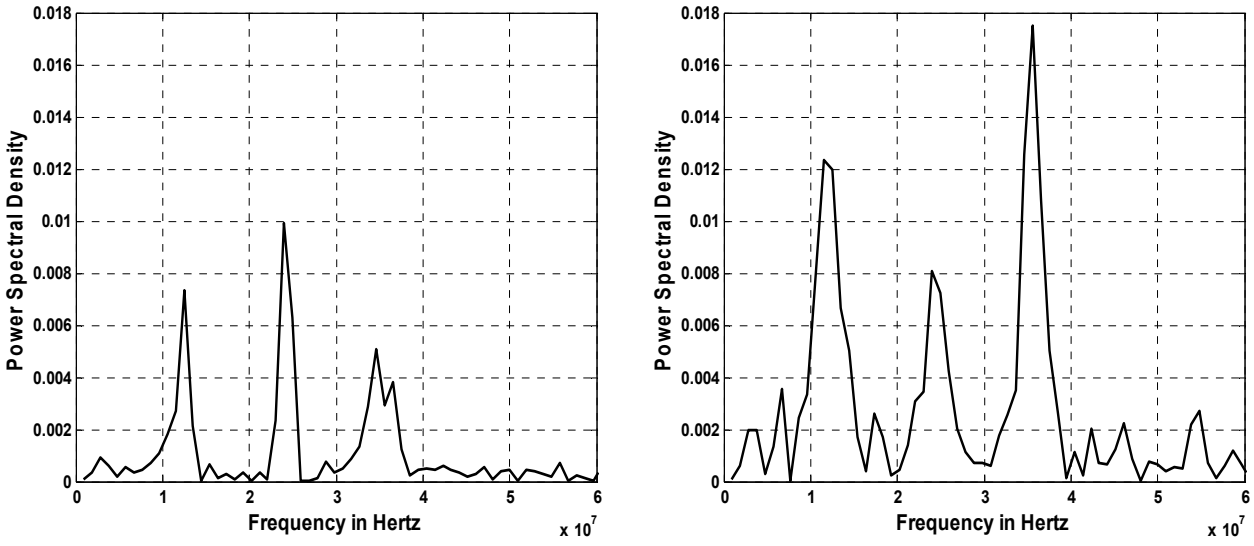

9 kV 9.5 kV

Figure 5-34: FFT content of single cavity PD at 9 kV and 9.5 kV

5.7 Summary of the characteristics of corona, surface and cavity PDs

Based on the analysis, a brief summary of the characteristics of each PD is presented below in Tables 5-1, 5-2, and 5-3 for corona, surface, cavity PDs respectively.

Table 5-1: Summary of the characteristics of corona PDs based on statistical and individual pulse analysis

Characteristics of corona PDs: T –Time domain; F- Frequency domain		
S/No	**Characteristics**	**Behaviour/Pattern observed**
1	Single PD pulse duration (T)	About 1us. Longest as compared to that of surface and cavity PDs.
2	Dominant frequency content (F)	Energy up to 5MHz. (lowest as compared to that of surface and cavity PDs).
3	PSD (F)	Stronger than cavity PDs but lower than that of surface PDs
4	Shape of single pulse (T)	Non-oscillatory. Decays with a rather exponential smooth “tail”.
5	Phase distribution (T)	Majority of PDs occur at negative half cycle
6	Magnitude distribution(T)	Lowest magnitude as compared to surface and cavity PDs and exhibits the narrowest magnitude distribution profile which ranges only from 90mv to about 170mv. Shape of distribution profile is closest to a normal distribution when compared with that of surface and cavity PD distributions.
7	Weibull β value (T)	Corona PDs are found to exhibit Weibull β (shape parameter) values close to 10. β values for q-cumulative-n, and Φ-cumulative-n distribution profiles of corona PDs are determined to be the highest as compared to that of cavity and surface PDs.
8	Cluster analysis (T)	Corona pulses occurring in negative half cycle have very small ΔV and Δt spread (i.e. cluttered around the origin) as seen so consistently in the four types of cluster plots.

Table 5-2: Summary of the characteristics of surface PDs based on statistical and individual PD pulse analysis.

Characteristics of surface PDs: T –Time domain; F- Frequency domain		
S/No	**Characteristics**	**Behaviour/Pattern observed**
1	Single PD pulse duration (T)	About 0.3us – slightly longer than cavity PDs but lower than that of corona PDs.
2	Dominant frequency content (F)	Energy up to 35MHz.
3	PSD(F)	Strongest as compared to that of corona and cavity PDs.
4	Shape of single pulse (T)	Oscillatory. Decays with a few oscillating spikes before dropping to signal background level.
5	Phase distribution (T)	Occurs in both positive and negative half cycles
6	Magnitude distribution (T)	Highest magnitude as compared to that of corona and cavity PDs, and exhibits the widest magnitude distribution profile which ranges from 500mV to 9000mV.
7	Weibull beta value (T)	β values for q-cumulative-n, and Φ-cumulative-n distribution profiles of surface PDs are determined to be the lowest as compared to that of corona and cavity PDs. Typical value ranges from 1.5 to less than 2.5 for q-cumulative-n distribution profile.
8	Cluster analysis (T)	Surface PD pulses occurring in positive and negative half cycles have wide ΔV and Δt spread.

Table 5-3: Summary of the characteristics of cavity PDs based on statistical and individual pulse analysis.

Characteristics of cavity PDs: T –Time domain; F- Frequency domain		
S/No	**Characteristics**	**Behaviour/Pattern observed**
1	Single PD pulse duration (T)	About 0.2us – Shortest as compared to that of surface and corona PDs.
2	Dominant frequency content (F)	Energy up to 40MHz.
3	PSD (F)	Weakest as compared to that of corona and surface PDs.
4	Shape of single pulse (T)	Oscillatory. Decays with a few oscillating spikes before dropping to signal background level.
5	Phase distribution (T)	Occurs in both positive and negative half cycles.
6	Magnitude distribution (T)	Magnitude of cavity PDs lies between that of surface and corona. It spans a relatively large magnitude distribution profile which ranges from 250mV to about 5500mV.
7	Weibull beta value (T)	β for q-cumulative-n, and Φ-cumulative-n distribution profiles of cavity PDs are determined to be lower than that of corona but higher than that of surface PDs. Typical values range from 2.5 to less than 5 for q-cumulative-n distribution profile.
8	Cluster analysis (T) (ΔV vs Δt)	Cavity PD pulses occurring in positive and negative half cycles has moderate ΔV and Δt spread, sometimes comparable to that of surface cluster distributions. Appear to be scattered most freely in all the four quadrants as compared to that of corona and surface distributions. Scatter is also seen to be more during negative half cycle.

The difference in characteristics of each type of PD (as shown in Tables 5-1 to 5-3) can be used as a reference guide for the identification of the type of unknown PDs in a practical environment. Many factors like physical parameters of PD samples, sensitivity of the measuring transducers, measuring environment conditions, noises and distortions, etc. may affect the end results. Hence the statistical and individual pulse analysis method described in this report cannot have similar results in every unknown case. However by using these methods, individuals can develop his knowledge base of PD characteristics based on his PD test with the known tested objects unique to his own measuring environmental conditions. The important step is that the sampled signal must be

denoised and phase referenced (using DWT or high-pass filtering technique) in order to detect and extract PDs prior to statistical and individual pulse analysis.

Chapter 6

Identification of the types of PD in mixed-sources signal

After studying the identification techniques on pure type of PD, the laboratory study is extended to the identification of real practical situation of mixed PD sources signal. This chapter presents the analysis, and the identified types of PD in mixed-PD-sources signal generated in the laboratory and measured data on an operating 2 MVA/22 kV rated dry transformer. The generated mixed-sources signal contains the known surface and corona PDs generated as per the layout described in chapter 3. The types of PD in the operating transformer are not known. The five used analyzing tests for the identification process are as follows:

a) PD distribution profiles in ϕ-q, n-q and Δt-ΔV plots

b) Correlation Method

c) FFT content of extracted individual PD pulses

d) Intensity level of the CWT coefficients from lower to higher scale levels

e) Mixed- Weibull parameters

The selected five tests were performed in sequential manner with the following objectives. The first test aims to find the typical statistical PD pattern in the unknown mixed-sources signal. It may identify qualitatively how many types of PDs occurring in the signal by observing PD amplitude (q), phase (Φ) and number (n) distributions, and the time (Δt) and amplitude (ΔV) separation between consecutive PD pulses. If pure corona is the only prominent PD in the

measured signal, then the first test can identify it straightaway because corona exhibits unique statistical patterns when compared to that of surface and cavity (see sections 5.3.1, 5.3.7, and 5.5.1). The first test can only suggest an initial qualitative guess of single corona PD present from random occurrence of PDs in 20 ms period. If two or more types of PD are present, the first test is able to reveal two or more statistical patterns but cannot confirm the exact type of PDs (i.e. surface, corona, or cavity) and the remaining four tests are employed. The second time domain test - correlation method groups similar PD pulses by auto-correlation calculation. For correlating with the unknown PDs, the extracted PD pulses or the data base pulses are used. A correlation level above 0.7 is used to group one type. The correlation method is able to group the exact number of different types of PD. Correlating the extracted unknown PD pulses with the pulse shapes in the database often results in low value and thus most of the time this approach cannot be used for PD identification. Identified pure PD pulse-shape from laboratory data for correlation study may be distorted in field data due to distortions caused by measurement, propagation and other environment interferences. Using the second test, it is possible to identify the number of PD groups. The third frequency domain test on single PDs (PSD of extracted PD pulses) aims to find the dominant frequency contents of the identified PD groups by the second test. The evaluated frequency spectrum and the dominant strength of PSD and the corresponding frequency are then compared with typical frequency ranges of pure surface, corona, and cavity PDs. In this way, the types of PDs may be identified. The fourth test with wavelet transform using CWT

analysis has been proven to identify surface and corona PDs in mixed-sources signal. The CWT works by observing the amplitudes of the CWT coefficients from lower to higher scales of the mother wavelet. It is based on a high sampling rate which has nyquist frequency higher than the dominant frequencies of a pure PD. This test again provides the results for additional consideration during the PD identification process. The fifth test - Weibull analysis works on the PD number (n) distribution of the signal. The number of significant different gradients of the q-cumulative n distribution profile denotes the number of types of PDs. This test has also been found to be useful in PD identification. Using the above five tests, the types of PD in an unknown signal can be very closely identified.

6.1 Generated mixed-sources signal at the laboratory

Surface and corona PDs are generated simultaneously at around 10 kV and the recorded PD distribution in 20 ms period is shown in figure 6-1. It shows the presence of dominant surface PDs in both half cycles, small magnitude corona PDs crowded in negative half of cycle, 50 Hz and its harmonics with some dc offset. PSD of the recorded signal shows the dominant frequency bands at around 5MHz, 10MHz, 30MHz, 38MHz, 50MHz, 60MHz, 80MHz, 100MHz, and extending up to about 110 MHz based on a high sampling rate of 0.25 Giga-Samples per second. In section 5.6.2, it was seen that corona PDs occurred at lower frequency band around 5 MHz as compared to that of surface PDs. Surface PDs were observed to lie in high frequency band around 30MHz to 40MHz. The frequency spectrum of the entire mixed-sources distribution shown

in figure 6-1 with similar dominant frequency bands suggests the possibility of existence of two known types of PDs.

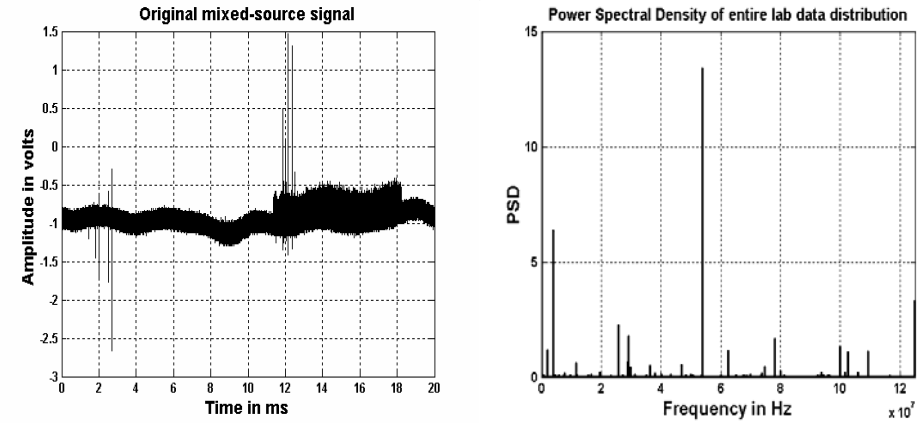

Figure 6-1: Generated mixed sources signal and PSD content of signal

6.2 Identification of the types of PD in mixed-sources signal generated at laboratory

The types of PD buried in recorded signal can be identified by performing the described independent tests. The analysed results are reported in this chapter. Before processing the data, the signal is denoised using the methods described in chapter 4.

6.2.1 Analysis of PD distribution using ϕ-q, q-n, and Δt-ΔV plots

The objective of this test is to observe for similar PD clusters using different plots. Denoised signal is made unipolar and the distribution of PD occurrence with Φ is plotted in figure 6-2. It shows the maximum PD amplitude close to 2.4 volts.

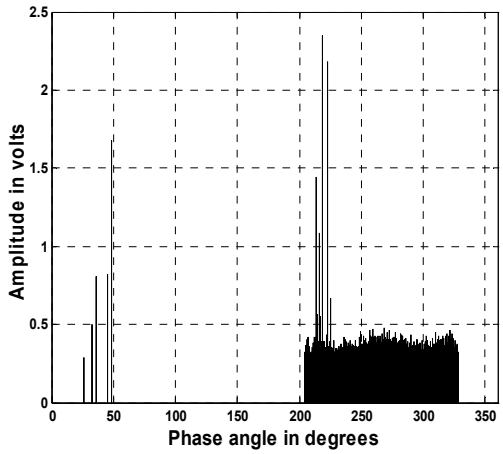

Figure 6-2: Denoised absolute q variation with Φ

Upon visual inspection of the denoised signal, it can be seen clearly that there are at least two clusters of distinct PDs occurring in the measured signal. A small number of distributed spikes of higher amplitudes are seen in the positive and negative half cycles while a large number of crowded spikes of lower amplitudes occur mainly in the negative half cycle. The consecutive high magnitude spikes are seen to be visually phase spaced at finite phase angle apart from each other while the low magnitude spikes are cluttered in the negative half cycle.

In sections 5.3.2 and 5.5.1, it is shown that surface PDs occur with high amplitude than that of corona PDs and the phase angle between consecutive surface PDs is more than that of corona. The visual method is able to infer logically the existence of two known different types of PD created in the laboratory.

A plot of the q-n distribution for the positive and negative cycles shows that number of PD occurrence is more in the negative half cycle compared to positive half cycle and q is spread in the magnitude range of 0.2 V to 2.5 V.

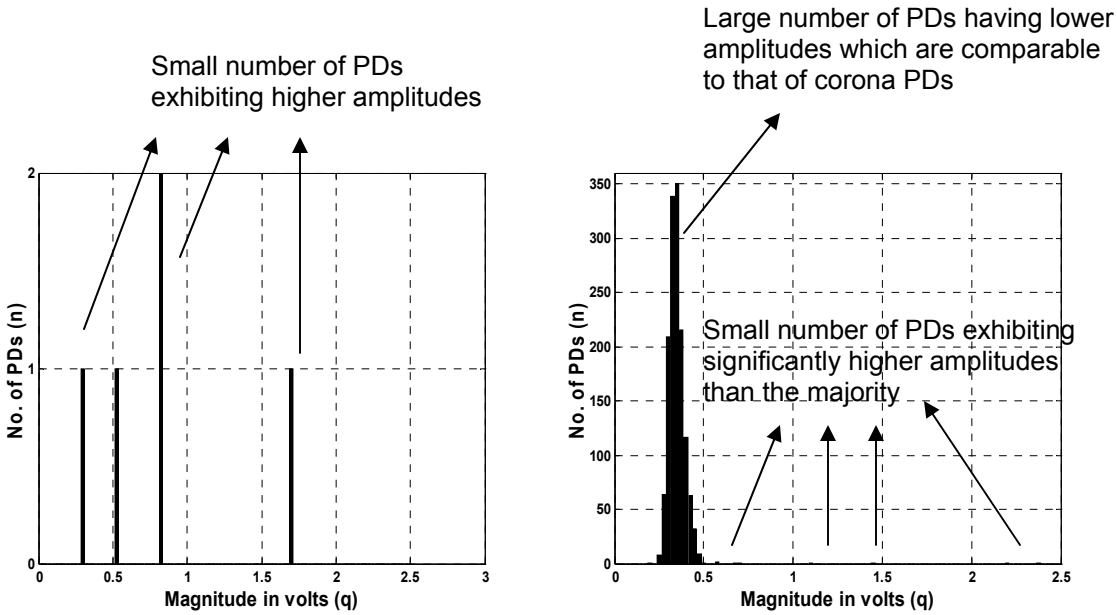

(a) q-n distribution (Positive half cycle) (b) q-n distribution (Negative half cycle)

Figure 6-3: q-n distribution profiles of generated mixed-sources signal during positive and negative half cycles

The presence of large number of pulses in the finite q range of 0.25V to 0.45V of the negative half cycle indicates the presence of corona PD. Small number of high magnitude pulses may be due to surface PDs. In section 5.5.1, the Δt-ΔV distribution profile of each type of pure PD revealed characteristic cluster patterns. With mixed-source signals, the plot of Δt-ΔV (dt-dV) distribution in figure 6-4 shows different clusters of PD distribution. Here, the plot of the Δt-ΔV distribution during positive and negative half cycles for the generated multi-sources signal (containing known corona and surface PDs) reveals two different cluster distributions. In the positive half cycle, points are limited. Δt varies from 0.18ms to 0.5ms while ΔV varies from 0.002V to 0.088V. Larger Δt pulses may be due to surface PDs. In the negative half cycle, Δt varies from 0 ms to 0.2ms while ΔV varies from 0 to ± 0.02V. ΔV variation in the range of ±0.02 V may be

due to corona pulse. Also, more number of PD occurrences in the negative half cycle and low ΔV are indicators of corona discharge. On the other hand, small number of PDs occurring in both cycles and wide ΔV and Δt are the characteristics of surface PD.

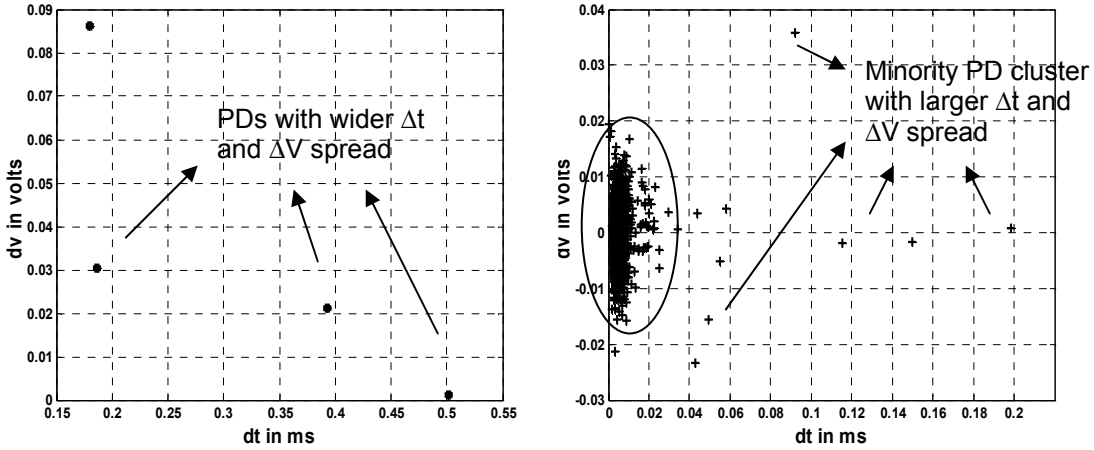

(a) Δt-ΔV (positive half cycle) (b) Δt-ΔV (negative half cycle)

Figure 6-4: Δt-ΔV distribution profiles of laboratory mixed-sources signal during positive and negative half cycles

The above distributions indicate the presence of two or more types of PD in a qualitative manner.

6.2.2 Analysis by Correlation Method

This analysis is done on each single PD present in the recorded signal. For identification, the shape of pure single PD reported in section 5.6.1 is used. Figure 6-5(a) shows the typical shape of a pure surface PD while figure 6-5(b) shows that of corona PD.

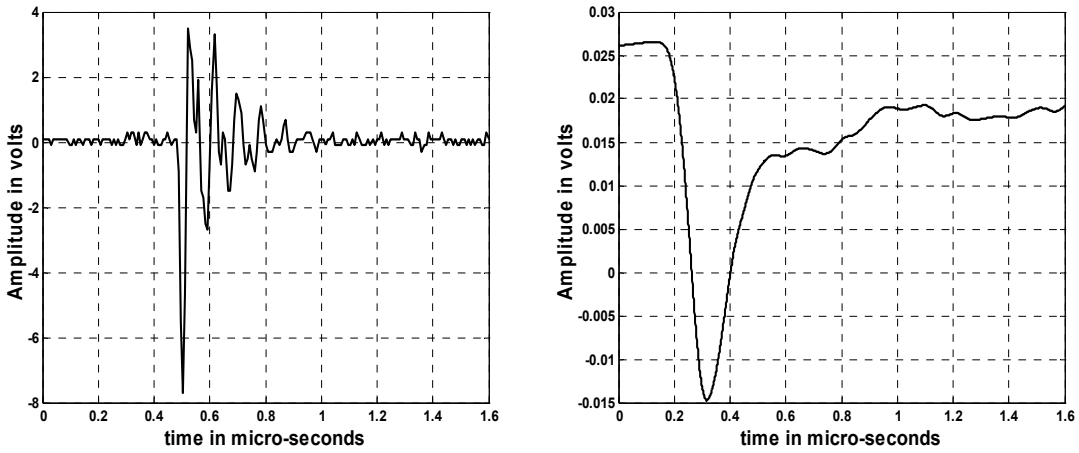

(a) surface PD at 5 kV (b) corona PD at 5 kV

Figure 6-5: Extracted shapes of single pure PD

The correlation analysis on 20ms data is carried out sequentially by following the steps indicated below:

1) 20ms data is denoised using DWT.

2) From the denoised signal, the first single pulse with the detailed sampling points is extracted and correlated with the selected second pulse. By time shifting, the maximum correlation factor between the first and second pulse is determined.

3) Next, the same correlation process is repeated between the first and third PD pulse of the denoised signal. The correlation is continued until the last pulse is correlated with the first pulse.

4) Pulses with the correlation factor equal to and greater than 0.7 are grouped together with the first pulse and are characterized as one type of PD. The 0.7 factor was chosen because pulses which correlate with a factor of 0.7 or higher were statistically found to have closer similarity.

Other correlation factors can be set. For example, if one desires very close similarity between single pulses in comparison to be considered as a group, then higher correlation factor like 0.8 can be set as a cut-off point. In this work, it is found that 0.7 factor is adequate to group the PD pulses with known PD sources. After removing that group of pulses, the rest of the PD pulses with the correlation factors less than 0.7 is correlated with each other again for similarity. By this way, the PD pulses can be grouped into different types of PD.

5) Next, these groups of similar PD pulses are to be compared for similarity with the pre-measured pure PD shapes reported in section 5.6.1. In this way, the type of PD in any unknown signal can be identified.

The above four steps are applied on the data reported in figure 6-1. The existence of two groups of PD pulses is found. The typical shapes of the two groups of PD pulse extracted from the mixed-sources signal are shown in figures 6-6(a) and 6-6(b) respectively.

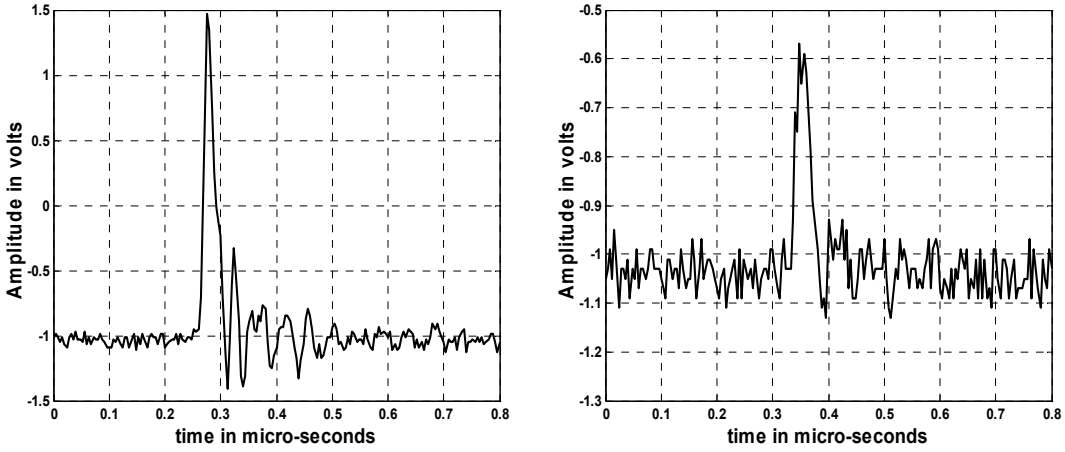

(a) Extracted group 1 PD pulse (b) Extracted group 2 PD pulse

Figure 6-6: Extracted shapes of group 1 and group 2 single PD pulse in mixed-sources signal

Figure 6-7(a) shows the correlation results using the extracted group 1 PD pulse as reference while figure 6-7(b) shows the correlation results using group 2 PD pulse as reference. Looking at the correlation results, it is deduced that there are two types of PD occurring in the mixed-sources signal. Correlating the extracted groups 1 and 2 PD pulses with pure surface and corona PD single pulse, they are identified as surface and corona PDs respectively.

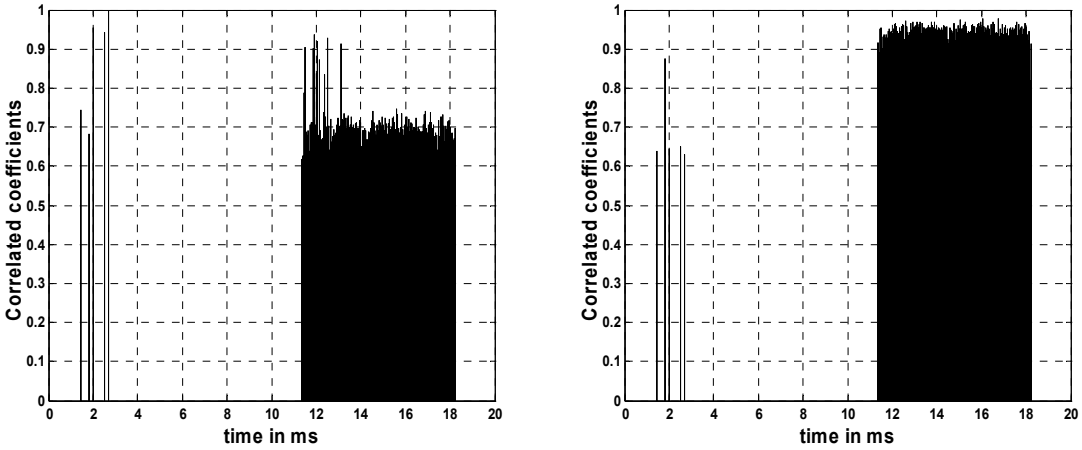

(a) Using group 1 PD pulse as reference (b) Using group 2 PD pulse as reference

Figure 6-7: Evaluated correlation factors for laboratory generated mixed-sources signal

By knowing the locations of maximum correlation factor, the denoised signal in figure 6-7 is divided into two separate groups as shown in figure 6-8.

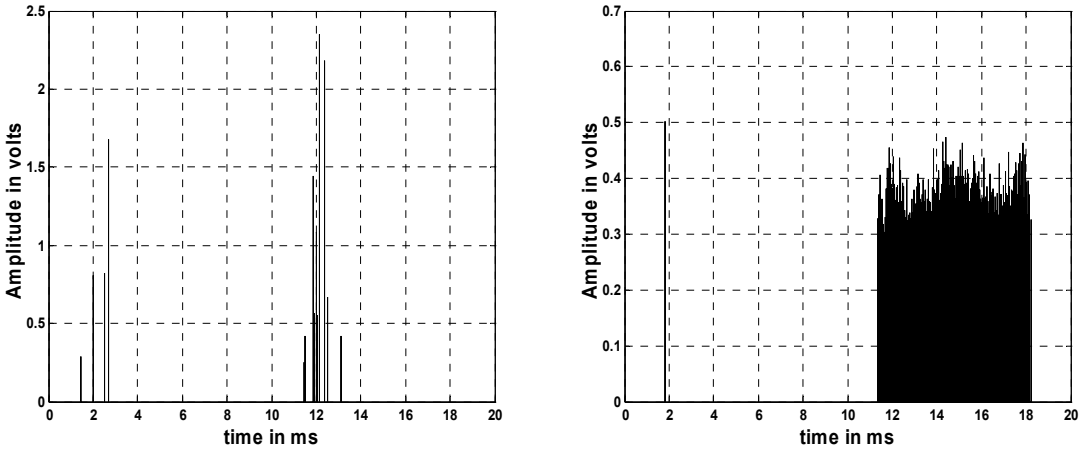

(a) Extracted group 1 PD after correlation

(b) Extracted group 2 PD after correlation

Figure 6-8: Extracted types of PD in the mixed PD sources signal using correlation results

Two groups of PD are identified. Group 1 PDs on the average appears to exhibit higher amplitudes and wide time separation between consecutive pulses and it also occurs during positive and negative half cycles. PD spikes in group 2 are seen to exhibit lower amplitudes and short time separation between consecutive pulses and they occur mainly in the negative half cycle. In an actual field environment, pre-determined shape of each type of PD is difficult to get. PD original waveshape can vary depending on the type of PD fault, and can be distorted due to propagation from origin to the monitoring node and sensor responses. In addition, the field environmental high frequency noises can corrupt the measured signal making it even harder for us to identify the type of PD. It is found that the correlation method is able to identify the types of PD in a measured signal. Further improvement is to be done to suit the practical environment with many unknown PD sources and the modulated noise pulses. The correlation analysis shows the presence of corona and surface PDs in the laboratory mixed- PD sources data.

6.2.3 Analysis by Power Spectral Density Calculation

After the correlation analysis, PSD of the two types of extracted PD pulses is calculated as each PD is well-defined in shape with at least 256 sampled points using a recording sampling rate of 0.25 Giga-Samples per second. Figure 6-9 shows the determined PSD of the extracted groups 1 and 2 PD pulses.

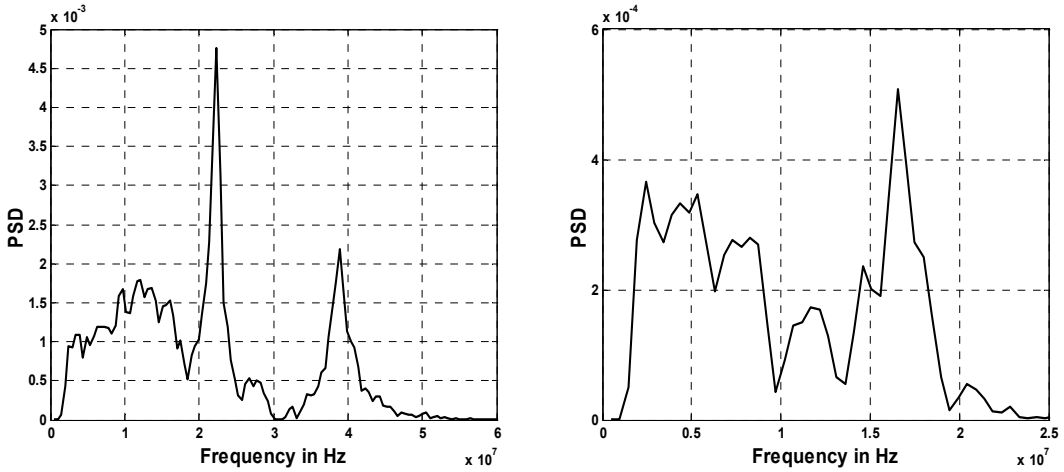

(a) PSD of group 1 PD pulse

(b) PSD of group 2 PD pulse

Figure 6-9: PSD of extracted groups 1 and 2 PD pulses

Group 1 PD pulse exhibits higher PSD strength (about 10 times higher) as compared to that of group 2 PD pulse. In addition, dominant frequency contents of group 1 PD pulse are around 10MHz, 22MHz and close to 40MHz, while that of group 2 PD pulse lies at lower ranges i.e. around 2MHz to 16MHz. Frequency contents and PSD of these pulses are compared to the derived typical frequency ranges of each type of pure PDs discussed in section 5.6.2. Figure 6-9(a) results match the pure surface PD while figure 6-9(b) results match the pure corona. The frequency plots for both groups of single PD pulses are seen to have broad

frequency spread which can be improved by using more sampled points for the FFT calculations.

6.2.4 Analysis by the Continuous Wavelet Transform

CWT is a more quantitative analysis method to identify the presence of different types of PDs. Mother wavelets db2, db4, db6, db9, db15, db20, coif5, sym4, sym8 and bior6.8 are used to determine the correlation coefficients by varying the frequency scaling up to 10. The relation of wavelet scaling factor to the frequency was shown in chapter 2. Nyquist frequency is determined using the sampling rate. It is selected to a higher frequency band than that of measured corona and surface PD pulses (derived in section 5.6.2). Then, CWT is found to be useful in separating surface PD from corona. Based on the results reported in sections 6.2.1 to 6.2.4, sampling rate of 0.25 Giga-Samples per second corresponds to a nyquist frequency of 125 MHz. Figure 6.10 shows the various scales of the db9 wavelet and the corresponding proportional frequencies in percentage of the nyquist frequency (i.e. 125 MHz). From the graph, scales 1.5 and 5 of the db9 wavelet correspond to 117.5 MHz and 35 MHz respectively. The lower scales can detect high frequency content of mixed PD signal.

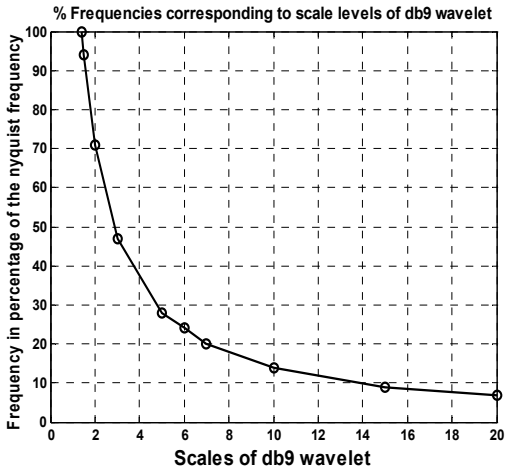

Laboratory data
Sampling rate used: 250 Mega-samples per second
Nyquist frequency: 125 MHz

Industrial data
Sampling rate used: 50 Mega-samples per second
Nyquist frequency: 25 MHz

Figure 6-10: Frequency in percentage of the nyquist frequency against scale levels of db9

CWT is performed on the original 20ms distribution (see figure 6-1) and figure 6-11 shows the CWT analysis on the entire mixed-sources distribution using mother wavelet db9. Two other wavelets coif5 and sym8 were tested and similar results were obtained. The typical results at scales 1.5, 5 and 10 are shown. It is evident that group 2 PD pulses of figure 6-8 (b) appear as high CWT coefficients only after scale 10 i.e. from 17.5 MHz to lower frequencies using db9 (Refer figure 6-10). Comparing that observation with the frequency content of extracted group 2 PD (See figure 6.9b) and the dominant frequency content of a pure corona PD in section 5.6.2, group 2 PD can be identified as corona. All the tested wavelets identify corona PD beyond scale 10. The presence of high CWT coefficients at scale levels 5 and 1.5 (i.e. 35 MHz and 117.5 MHz respectively using figure 6-10) indicates the possibility of occurrence of surface PDs and not corona PD. The time location of high amplitude CWT coefficient indicates the Φ occurrence of that particular type of PD.

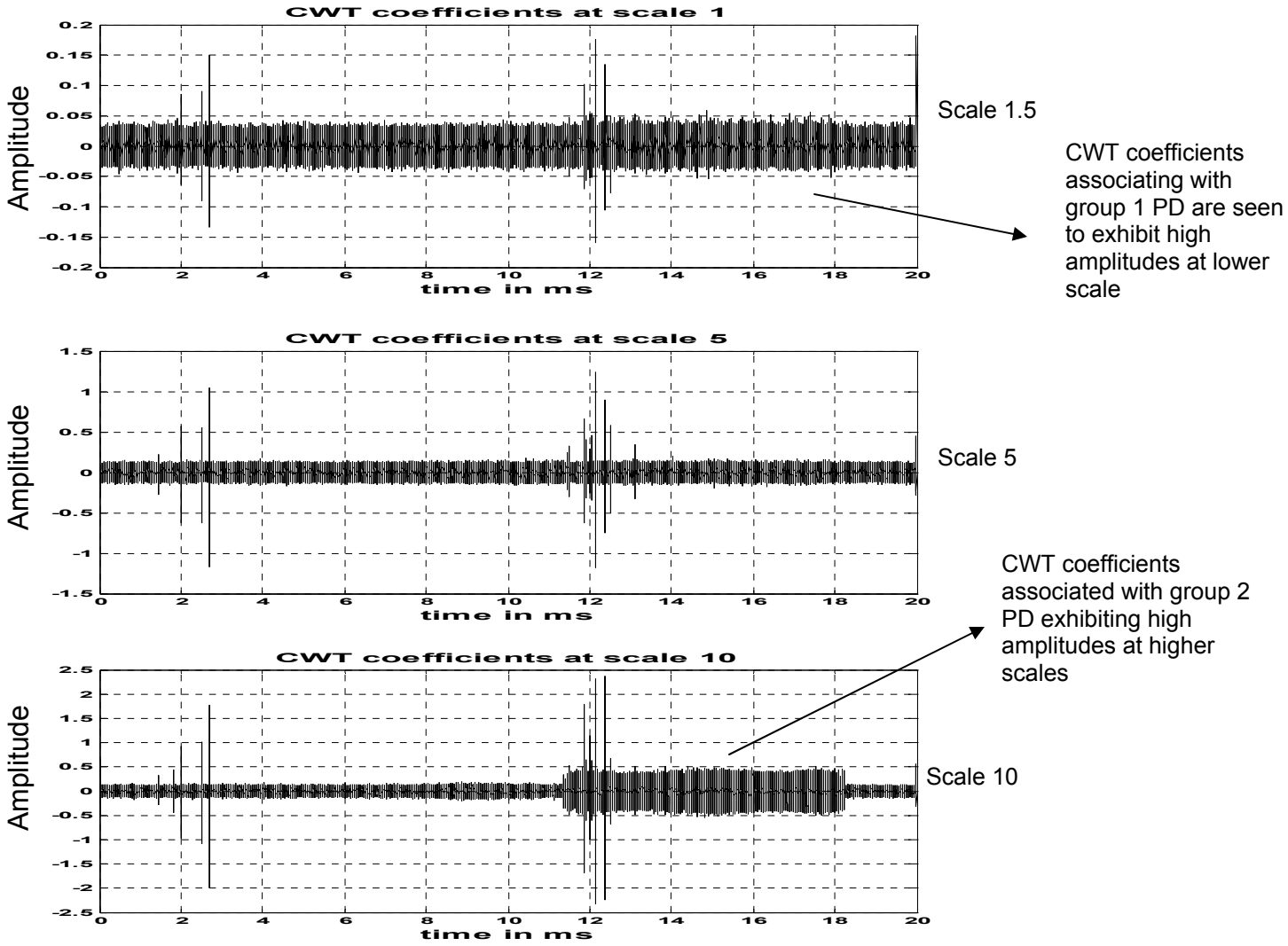

Figure 6-11: CWT analysis on laboratory generated mixed-source PD distribution in 20ms duration using db9

Therefore, based on the CWT coefficient distributions for the entire 20ms duration on laboratory generated mixed-sources signal, high coefficient amplitudes within scales of 1.5 to 5 indicate the phase/time occurrence of surface PDs [114]. Similarly, high coefficient values within scales of 5 to 10 indicate the occurrences of corona and surface PDs. Using the detected high coefficients associated with surface PDs from any one of the scales from 1.5 to 5, time locations of the occurrence of surface PD can be identified. Then by elimination

technique, time locations of corona PDs can be identified with high coefficient results at scale 10.

6.2.5 Analysis by Mixed-Weibull fitting

In section 5.4.1, the weibull fitting is applied to the plots of cumulative number of PDs against q and the result shows that the different types of pure PD exhibit different ranges of weibull β (shape parameter) values. A two-parameter weibull fitting which offers only one β is used for pure single-source signal. In this mixed sources signal, there are two types of PD present in the collected signals. α_1 , β_1, α_2 and β_2 are needed to identify them. After applying the mixed-weibull fitting on the mixed-souces signal shown in figure 6-1, the two calculated β values are compared to the calculated β values in section 5.4.1 for each type of PD. In this way, the types of PD in the mixed-sources signal can be determined based on comparison.

Figure 6-12(a) shows the variation of the number of PDs against the magnitude windows in a mixed-sources signal shown in figure 6-1. A large number of PDs can be seen occurring in the range from 250mV to about 450mV. There is also a small percentage of the total number of PDs occurring in the magnitude range from 450mV to about 2500mV which hardly can be seen by visual inspection in figure 6-12(a). Figures 6-12(b) and 6-12(c) show the zoomed view of the magnitude distribution plots in two ranges. The maximum number of PDs in small magnitude range from 250 mV to 450 mV goes up to 340 and the shape distribution appears close to a normal distribution. About 95% of the total number of PD pulses lies in this distribution. The second distribution lies in the magnitude

range from 450 mV to 2.5 V and the maximum number of PDs in that range goes up to 12. It follows an exponentially decaying distribution for increased magnitude and about 5% of the total number of PD pulses resides in this amplitude range.

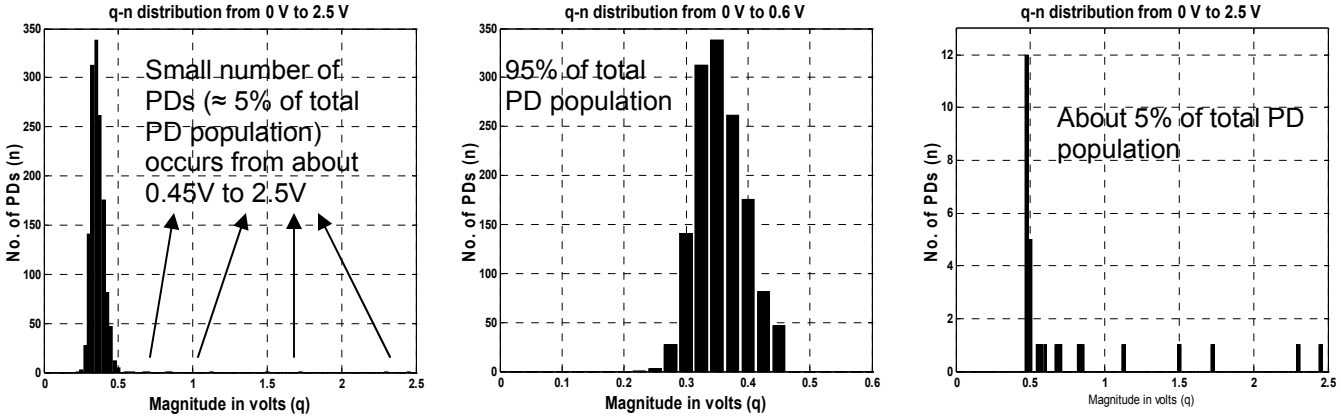

(a) Distribution from 0 to 2.5V

(b) Zoomed view from 0.25 V to 0.45 V

(c) Zoomed view from 0.45 V to 2.5 V

Figure 6-12: q-n plots of laboratory generated mixed sources signal

Figure 6-13 shows the percentage cumulative number of PDs (n) against magnitude. Two different gradients are seen. The abrupt change in gradient of slope occurs at around 95 percent of the total PD population which agrees well with the amplitude distribution.

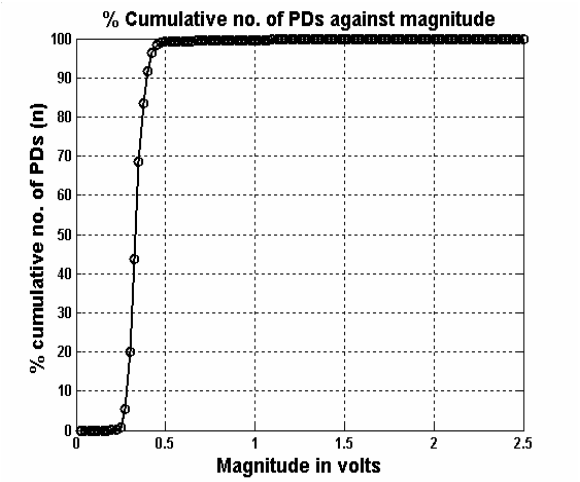

Figure 6-13: q - %cumulative n plots of laboratory generated mixed-sources signal

Hence, two groups of PD populations are found. The first group of population lying up to 0.45 V is chosen to contain up to 95 percent of the total PD population while second group of population beyond 0.45 V contains the remaining 5 percent.

Figure 6-14 shows the q- cumulative n plots of two separated populations. Different gradients can be observed from the cumulative plots signifying the presence of two different types of PD distribution.

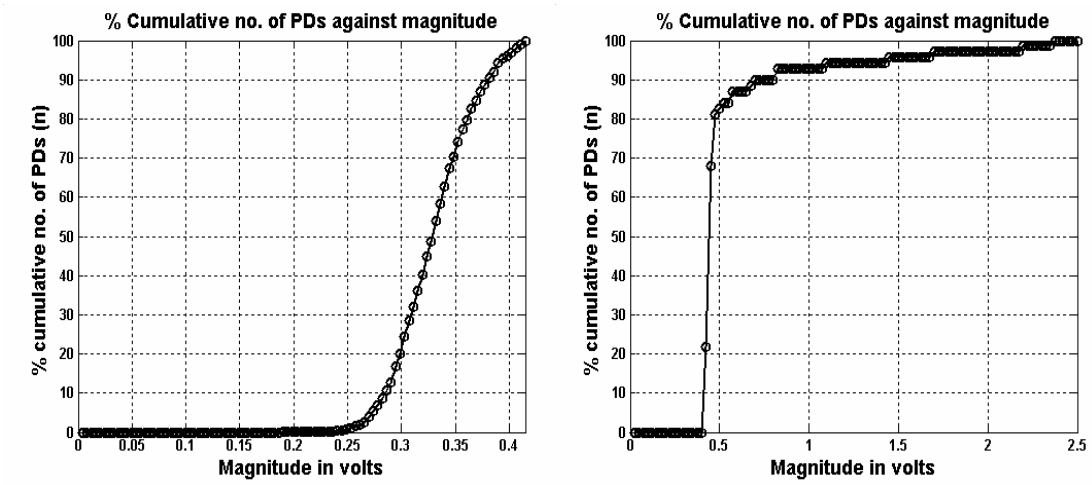

(a) from 0.25 V to 0.45 V (b) from 0.45 V to 2.5 V

Figure 6-14: q-cumulative-n plots of groups 1 and 2 PD population

Two parameter weibull fitting is made on the population-1 lying in the range from 0.25 V to 0.45 V and the population-2 lying in the range from 0.45 V to 2.5 V. The closely fitted α and β values for population-1 in figure 6-15(a) are 0.35 and 12.63 and for population-2 in figure 6-15(b) are 0.25 and 0.643 respectively.

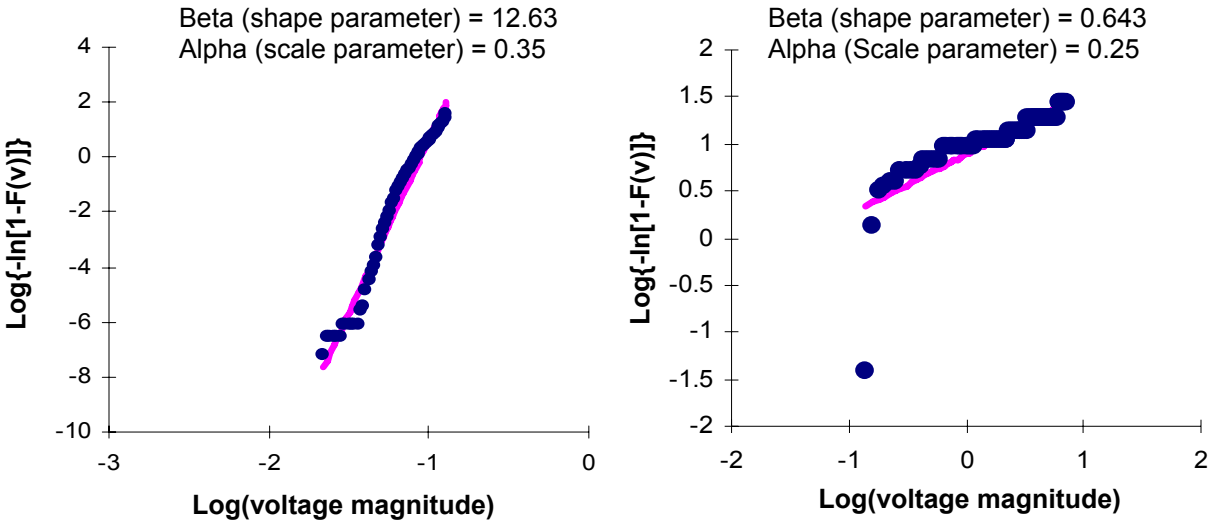

(a) Weibull fitting **from 0.25 V to 0.45 V**

(b) Weibull fitting **from 0.45 V to 2.5 V**

Figure 6-15: Two parameters Weibull fitting on q-cumulative-n distribution of laboratory generated mixed sources PD

With population-1, β of 12.63 is obtained. Likewise for the population-2, β of 0.643 is obtained. The obtained β values for the two groups of population are compared to the range of β values for each type of pure PD found earlier in section 5.4.1. The comparison reveals that β value of more than 10 (i.e. 12.63) is due to corona PD distribution and β value of 0.643 is due to surface PD distribution. Since the original mixed-sources signal is known, the prediction by weibull analysis is verified for PD types identification.

6.3 Conclusion on the selected five PD identification tests

The results obtained by each test provide useful information about the types of PD embedded in the measured signal. The results are compared with the obtained group and individual characteristics of each type of pure PD (see chapter 5). In this way, the types of PD embedded in the signal can be identified based on closest similarity in characteristics. From the analysis, it can be seen that all the five tests are able to identify surface and corona PDs in the laboratory generated mixed-sources signal with qualitative and quantitative features.

6.4 Identification of the types of PD in an operating 2 MVA rated industrial transformer

In order to verify the usefulness of the five PD identification tests for unknown mixed-sources signal, an attempt is made to analyse the data from an operating 2 MVA rated transformer. Figure 6-16(a) shows a typical set of recorded data collected from an operating 2MVA/22 kV/415 V rated 3Φ dry type transformer using sampling rate of 5 Mega-Samples per second. Figure 6-16(b) shows the PSD of the entire recorded data of 20ms with 100200 sample points. Figures 6-16(c) and 6-16(d) show the recorded 2ms distribution of 50 Mega-Samples per second and its corresponding PSD distribution respectively.

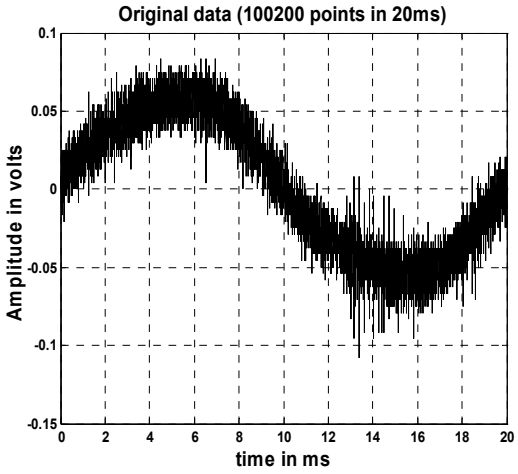

(a) Measured 20ms distribution from an operating 2 MVA transformer

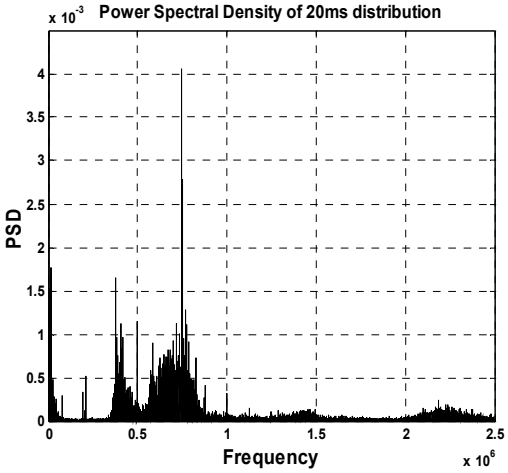

(b) PSD of LHS 20ms data distribution

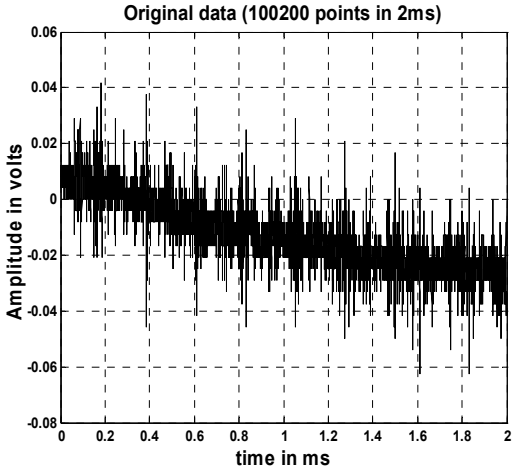

(c) Measured 2ms distribution from an operating 2 MVA transformer

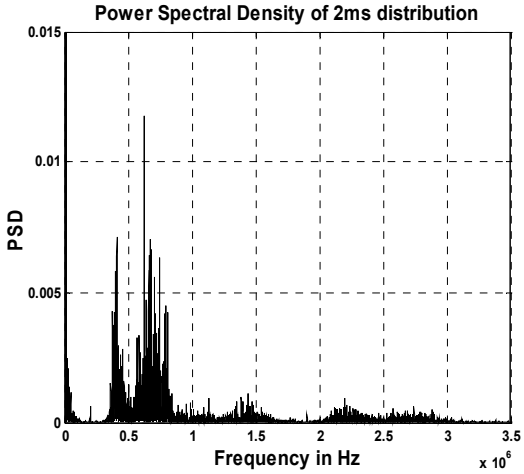

(d) PSD of LHS 2ms data distribution

Figure 6-16: Measured time and calculated frequency domain responses of industrial data in 20ms and 2ms duration

PSD analysis for both 20ms and 2ms distributions suggest the existence of dominant frequency spectrum lying in the range from 0.4 MHz to 0.8 MHz. The denoised mixed-sources signal shown in figure 6-17 shows maximum peak to peak voltage amplitude of about 100mV based on the 20ms distribution while the denoised signal in figure 6-18 shows a maximum peak to peak of about 85mV based on 2ms distribution. The amplitudes of each extracted PD pulses in the

20ms and 2ms distribution mostly appear to lie in close time ranges. Another observation is that the extracted pulses seem to be evenly time-spaced apart and occur mainly in the negative half cycle. Such observations indicate a possibility of just one type of PD occurring. It may be corona PD because corona occurs mainly in negative half cycle. (See earlier analysis of pure corona in sections 5.3.7 and 5.6.2).

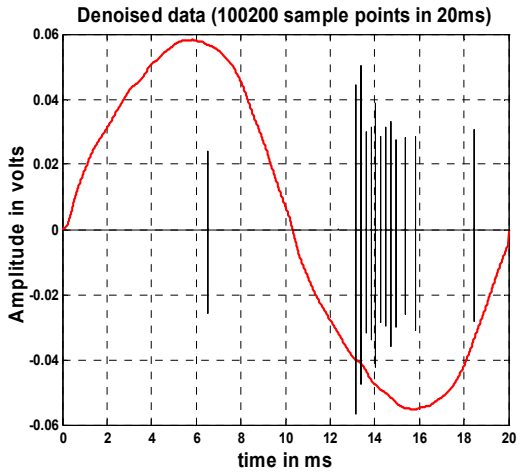

Figure 6-17: Denoised 20ms distribution of industrial data

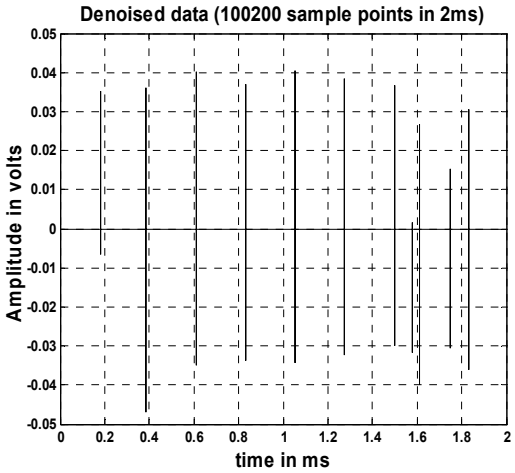

Figure 6-18: Denoised 2ms distribution of industrial data

6.4.1 Analysis of PD distribution using ϕ-q, q-n, and Δt-ΔV plots

For group PD analysis, the 20ms data is used. After denoising and phase referencing, the ϕ-q distribution of PD pulses in a single 20 ms cycle and consecutive 9 cycles of 20 ms duration (superposed) are plotted as shown in figures 6-19a and 6-19b respectively.

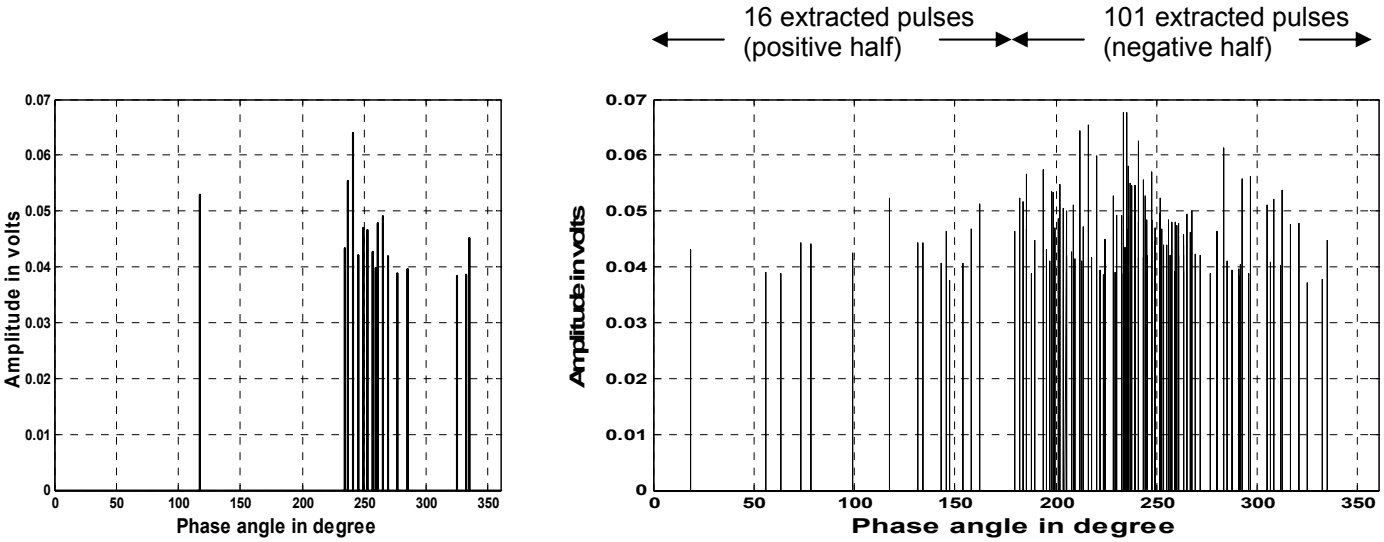

(a) Single cycle of 20ms duration

(b) 9 cycles of 20ms duration

Figure 6-19 Denoised Φ-q distribution of industrial data

By visual inspection of the Φ-q distribution plots over single and 9 cycles of 20ms duration, magnitudes of PD pulse fall well below 70 mV and are observed to occur mainly in negative half cycles. Qualitatively, it is inferred that only one type of PD is present in the measured signal.

Figure 6-20 shows the separate plots of the q-n distribution profiles for the positive and negative half cycles over 9 cycles data. More number of PD pulses (i.e. 101 extracted pulses) reside in the negative half cycle with amplitude range of 38 mV to 68 mV while only a small number of PD pulses (i.e. 16 extracted pulses) occur in the positive half cycle with amplitudes extending from 38 mV to about 52 mV. The q-n distribution profile agrees with the visual inspection of the Φ-q distribution which signifies the occurrence of one type of PD event.

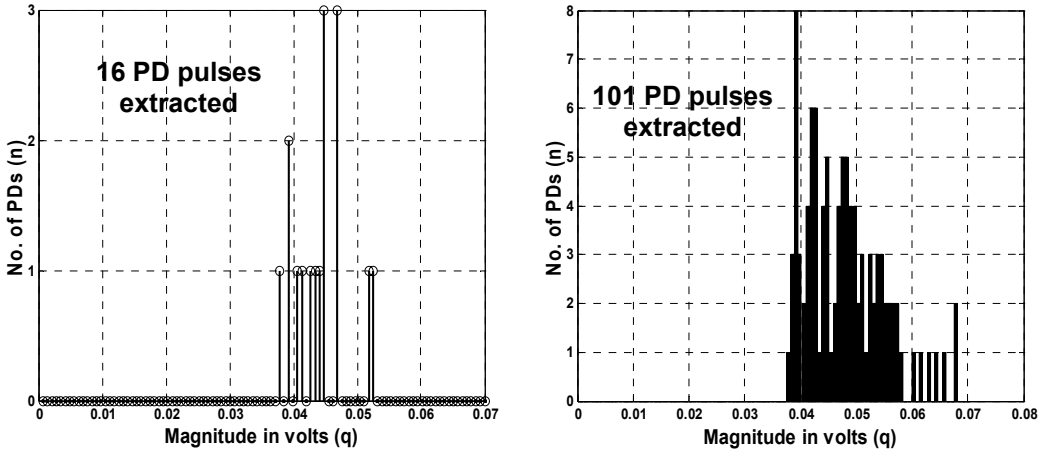

(a) positive half cycle (b) negative half cycle

Figure 6-20: q-n distribution profiles of mixed-source industrial data during positive and negative half cycles

To identify further with another pattern, the Δt-ΔV distribution profile is evaluated. Figures 6-21a and 6-21b show the Δt-ΔV (dt-dV) distribution profiles during the positive and negative half cycles respectively.

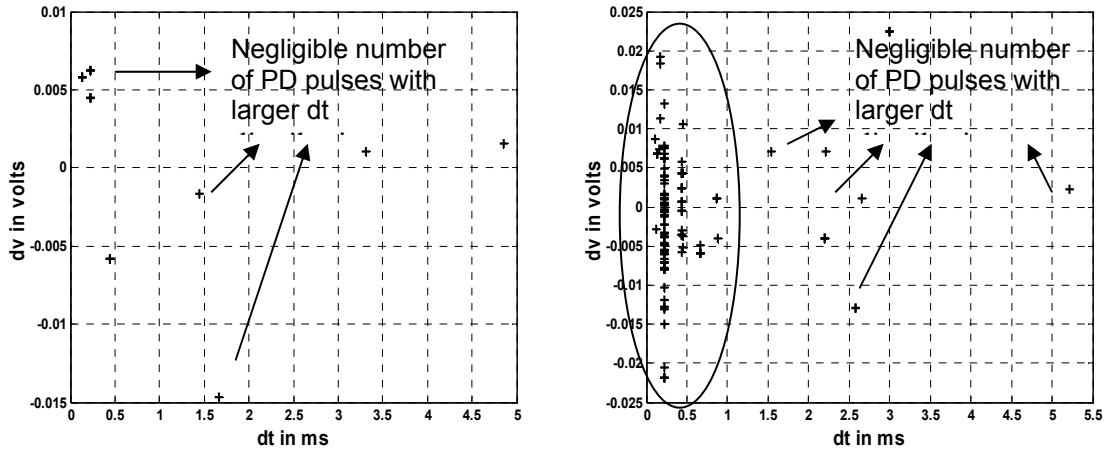

(a) positive half cycle (b) negative half cycle

Figure 6-21: Δt-ΔV (dt-dV) distribution profiles of mixed-source industrial data during positive & negative half cycles

By inspection of the Δt-ΔV distribution profiles, a significant number of PDs (LHS cluster) “crowded” with very small Δt spread and exhibited an average ΔV spread of about 5 mV in the negative half cycle. Because only a very small number of PDs reside in the positive half cycle, therefore the cluster pattern cannot be deduced. By inspection, during the positive half cycle, the PDs exhibit wider spread in Δt with an average ΔV spread of about 5.5 mV. While in negative half cycle, the crowded cluster occurs around Δt of 0.5 ms. Other scattered distribution occurs up to 5.5 ms in both half cycles. Such cluster pattern observed during the negative half cycle is typical of corona PDs (see section 5.5.1) while the scattered pattern may be due to some minor developing surface PD.

Further analysis is needed to confirm the exact type of PD occurring in the data at this instant. The results obtained from Φ-q, q-n, and Δt-ΔV distribution profiles confirm the definite existence of corona PD.

6.4.2 Analysis by Correlation Method

After the initial guess of corona PD embedded in the industrial transformer measurements based on earlier analysis, the correlation method is used to confirm the exact number of different types of PD occurring and also to identify the types of PD using shapes of each type of pure single PD pulses found in section 5.6.1.

The group analysis uses data with 20ms time duration. For the correlation analysis, high sampling rate (i.e. 50 Mega-Samples per second) is used to capture single PD pulse-shapes with enough sampled points. The original 2ms distribution (see figure 6-16c) is denoised by using DWT and thereafter the

correlation method is used to group similar PD pulses occurring in 2ms in the denoised version of the original. Only one group of PD pulses is found after the correlation analysis indicating occurrence of one type of PD. Figures 6-22 shows the shape of single PD pulse extracted from the original. The PD pulse is seen to have several oscillations before attenuating to background signal level. This could be due to distortions of the PD pulses by measurement and environmental factors.

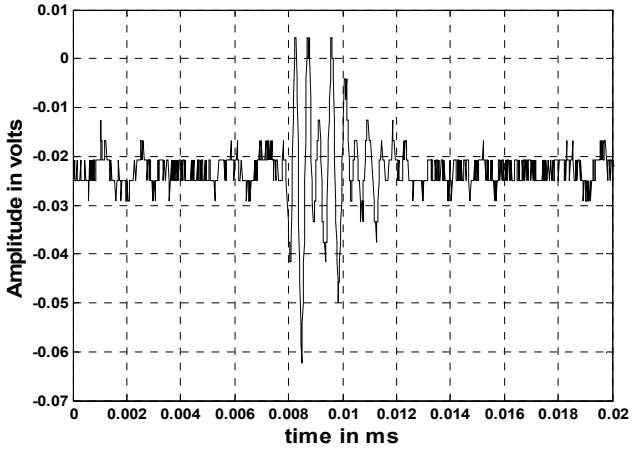

Figure 6-22: Extracted single PD pulse
from industrial data after correlation analysis

Similar correlation analysis is done with 20ms data sampled at 5 Mega-samples per second. Using the first detected single PD pulse extracted from the denoised signal of 20 ms as the reference, auto-correlation is performed on the denoised signal over single and 9 cycles of 20 ms duration. Figures 6-23a and 6-23b show the correlated coefficients for single and 9 cycles of 20ms duration respectively. It can be seen that almost all PDs have a correlation factor greater than 0.7 suggesting the existence of only one type of PD present in the original signal.

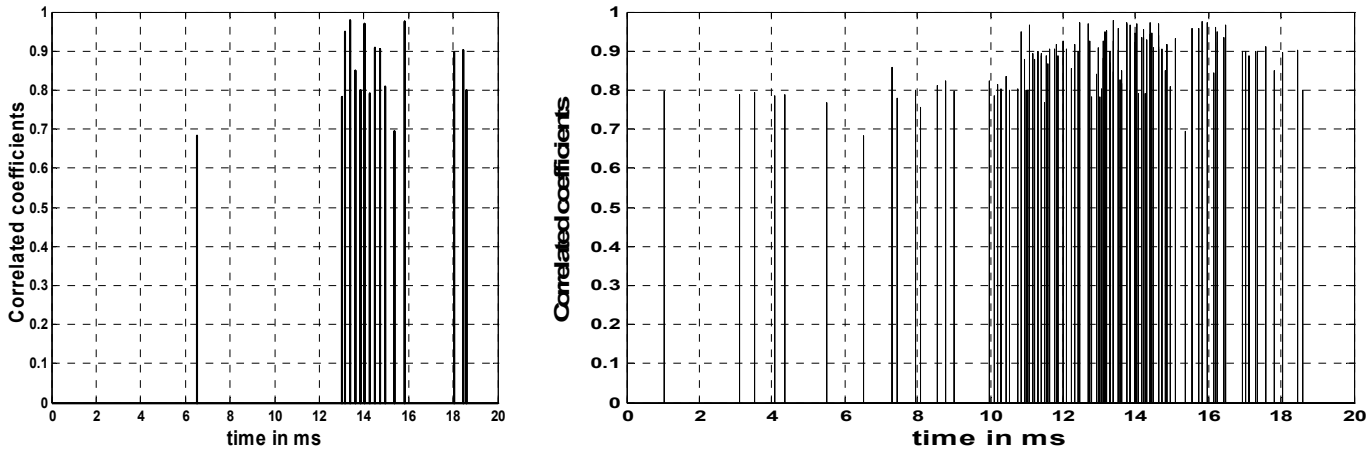

(a) Single cycle of 20ms duration

(b) 9 cycles of 20ms duration

Figure 6-23: Correlated coefficients using the extracted single PD pulse as reference in 20ms

In order to determine the nature of the extracted PD pulses (i.e. surface, corona, or cavity PD), the extracted PD pulse shown in figure 6-22 is correlated with the derived surface, corona and cavity PD pulses in the database. However, low correlation coefficient (i.e. CC < 0.7) values are obtained. Poor correlated results between the extracted PD pulse and the derived PD shape from laboratory database suggest that there may be introduced distortions in the extracted PD pulses of the industrial data due to propagation and used transient earth voltage probe sensor. Furthermore, it also indicates that universal PD pulse-shape for each type of PD does not exist for correlation study.

6.4.3 Analysis by Power Spectral Density Calculation

The extracted PD pulse is seen to be well-defined in shape and FFT is performed on them. Figure 6-24 above shows the PSD of the extracted single PD pulse shown in figure 6-22. The single PD pulse has dominant frequency contents at 1.5 MHz and 2.2 MHz (which is similar to the frequency contents of a pure

corona PD pulse shown in sections 5.6.2 and 6.2.3). In addition, magnitude of PSD of the PD pulse is seen to be small which is also a typical characteristic of corona (see section 5.6.2). The frequency plot appears to be more “precise or less spread” when compared to the more “broadly spread” frequency plot of a laboratory generated PD pulse (see figures 6-9a and 6-9b). This could be due to the tuning effect induced by the inductance and capacitance along the propagation path (i.e. from PD site to measured tank surface).

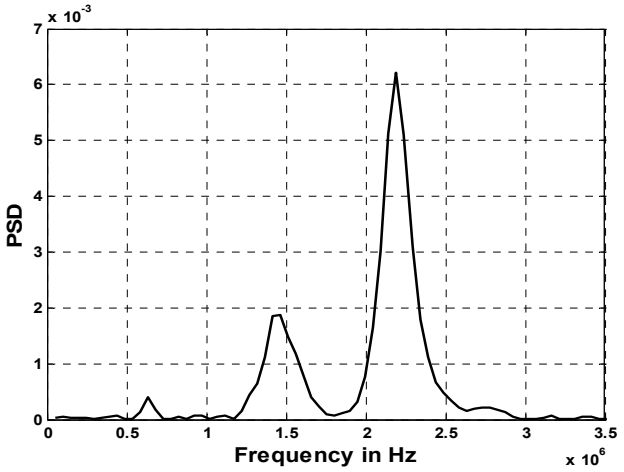

Figure 6-24: Power Spectral Density of extracted single PD

6.4.4 Analysis by Continuous Wavelet Transform

The PD distribution analysis is able to confirm that there are two types of PD. The CWT analysis is used to identify the type of PD pulse. Figure 6-25 shows the CWT results of 2ms distribution with 100200 sample points using mother wavelet db9. The sampling rate used is 50 Mega Samples per second with a nyquist frequency of 25 MHz. The scales used for CWT analysis is 1.5, 5, and 10. Using the derived scale to frequency conversion shown in figure 6-10, scales 1.5, 5 and 10 correspond to 23.5 MHz, 7 MHz, and 3.5 MHz respectively. It can be seen

that coefficients associated with burst of PD spikes in the original (see figure 6-16c) are much higher than the background coefficients, and are only evident or more pronounced in scale 10. Scale levels 1.5 and 5 which correspond to higher frequencies 23.5 MHz and 7 MHz (using figure 6-10) respectively reveal no significant high amplitude of CWT coefficients. Since a pure corona PD pulse has energy up to 5 MHz (derived in section 5.6.2), the presence of high CWT coefficients in scale 10 (which correspond to 3.5 MHz) after the transform indicate a high possibility of occurrence of corona in the original. Other wavelets like Coif5, db4, and Sym8 were also tested and similar observations on the obtained coefficients were obtained indicating consistent results. The observations here agree well with the results of CWT analysis on laboratory generated mixed-sources data which contains surface and corona PDs. In figure 6-25, the locations of higher CWT coefficients are verified to be true PD and not high frequency noises by zooming into those locations and analyzing their amplitude and shapes in comparison with background signal. No analysis is done on 20 ms data as the data is not sampled at the required Nyquist frequency range.

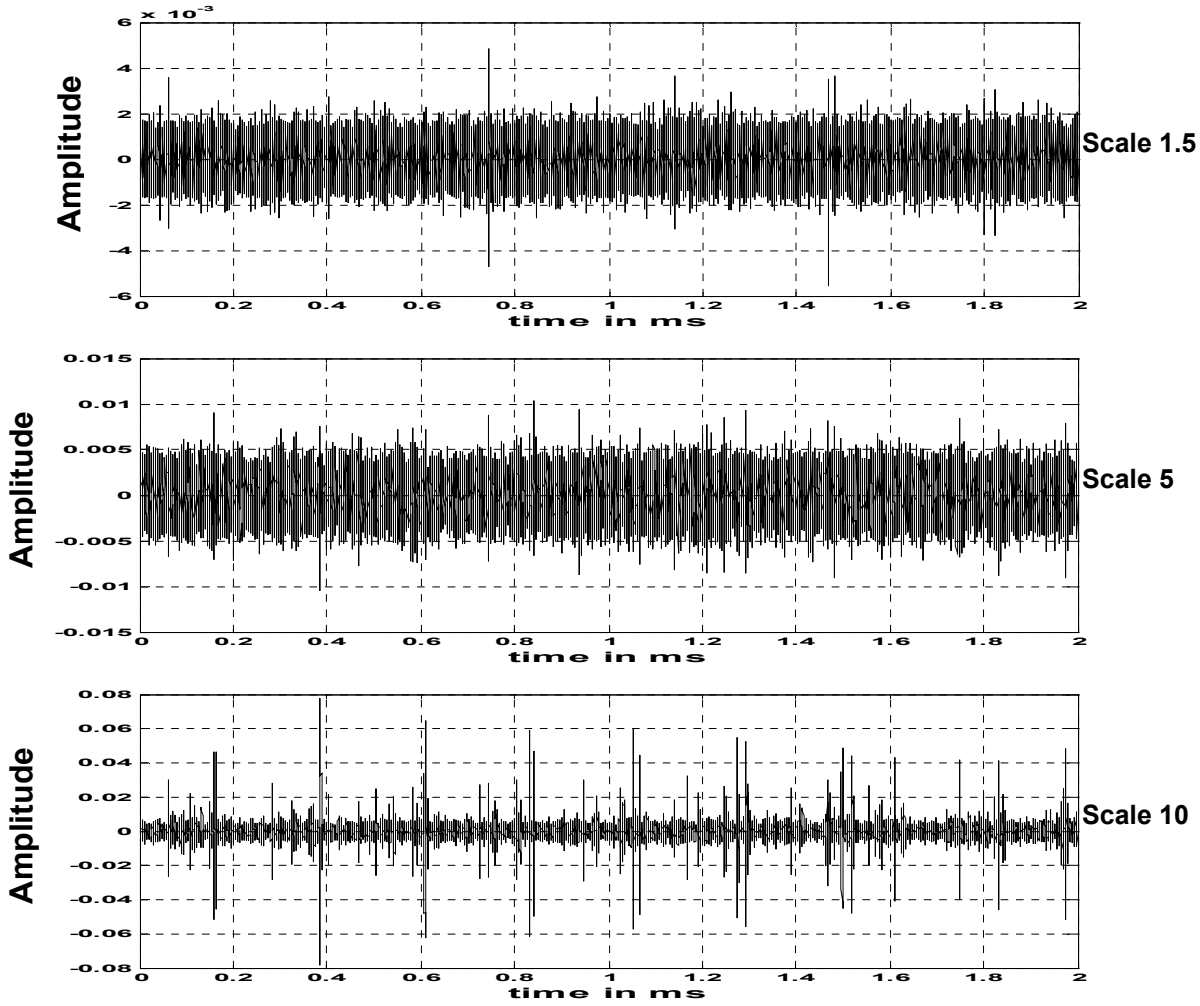

Figure 6-25: CWT analysis of industrial data
of 2ms duration using mother wavelet db9

6.4.5 Analysis by Mixed Weibull fitting

In order to seek yet another confirmation on the exact types of PD embedded in the industrial data, the mixed-weibull fitting test is performed on the collected data over 10 voltage cycles. Figure 6-26 shows the variation of cumulative n distribution over 10 voltage cycles with measured q.

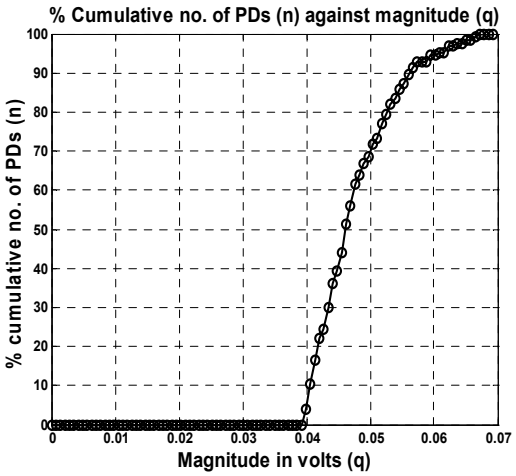

Figure 6-26: q-cumulative-n distribution of industrial data of 20ms duration (10 data sets)

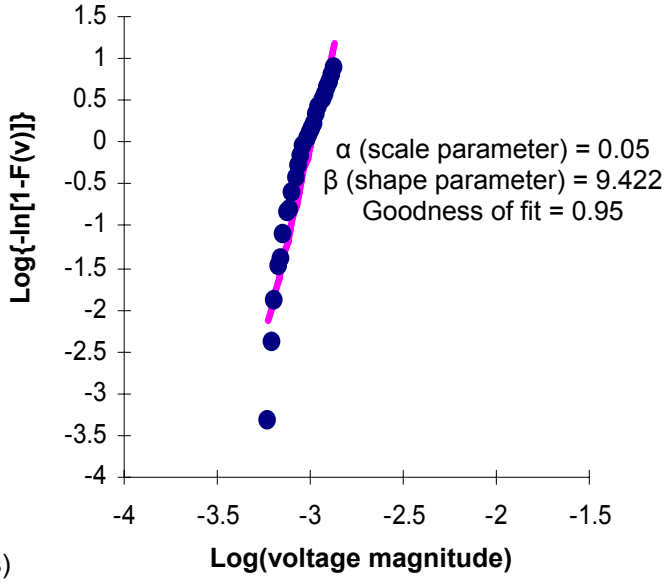

Figure 6-27: Weibull analysis on PD population

No significant gradient change is observed indicating that only one type of PD is inherent in the original data. Figure 6-27 shows the weibull fitting on the LHS distribution of PD population. The fitted α and β for the PD population are found to be 0.05 and 9.422 respectively. Good linearity fit value of 0.95 suggests the presence of single PD. Since a β (shape parameter) value of 9.422 is obtained from the weibull fitting, the type of PD is determined to be corona based on the β value found earlier for single pure corona PD (see section 5.4.1).

6.5 Conclusion on the selected five PD identification tests on industrial data

After obtaining the results by using the five identification tests, it is quite certain that corona PD is present in the original data based on (i) the Φ-q distribution profile (i.e. occurring mainly in negative half cycle), as well as the q-n distribution profile which indicated small amplitude range of 38 mV to 68 mV, and small Δt and ΔV spreads during the negative half cycle, (ii) high correlation factors in

figure 6-23, (iii) the dominant FFT contents (1.5MHz and 2.2MHz) of the single extracted PD pulse, (iv) significantly high coefficient values in CWT results at high scale level of 10 which corresponds to 3.5 MHz range, and (v) a β value of 9.422 after weibull fitting. Δt and ΔV spreads and weibull distribution suggest that there may be the presence of minor surface discharge. Hence it is concluded that the selected five analyzing methods can be easily applied on any industrial data to identify the types of PD provided the data are sampled beyond the nyquist frequency range. The shape of extracted single PD pulse is seen to exhibit much more oscillations and not quite similar to a laboratory generated PD pulse-shape. This could be due to the introduced distortions due to propagation path and used transient earth voltage probe sensor and other physical factors.

6.6 Summary

The five identification tests listed in this chapter are tested and found to be useful to identify the types of PD in mixed sources PD signal measured at the laboratory and an industrial 2 MVA operating transformer. The five identification tests are performed in sequential manner because the results of each test can be used as inputs to the next test. The five tests are performed on pure single-source signals to gain essential knowledge about the typical behaviours and patterns (both statistical and individual PD pulse analysis) prior to analysis on unknown single and multi-sources signals. The observations obtained from each tests are compared to earlier findings reported in chapter 5. The five identification tests are useful methodologies but its accuracy on identifying the types of PD embedded in an unknown data relies heavily on the database which contains characteristics

of each type of pure PD. Thus, a strong database about PD statistical and individual pulse patterns is very essential for accurate PD identification. Practical working experience in PD measurements and detection will aid the identification process.

One major problem encountered while performing the second test (correlation analysis) on various data is that PD pulse-shapes are found not to be universal especially in industrial measurement due to several factors like distortions, physical factors, noises, etc. PD pulse-shapes may be quite different for different harsh measuring environments. PD pulse-shapes generated in laboratory are seen to be with less oscillation and reproducible as distortions are minimum.

Finally, further research work may be necessary to verify the usefulness of the five identification tests on predicting other types of PDs like oil discharges, electrical and water trees or even multi-sources signal which contain all three common types of PD (i.e. surface, corona, and cavity) or modulated PD signals.

Chapter 7

Discussion, Conclusion, and Recommendations

7.1 Discussion

This research study explored the existing signal processing techniques and developed new techniques to identify the types of PD existing in operating electrical apparatus.

Literature study reported in chapter 2 discovers the most common types of PD to be identified are corona, surface and cavity PDs. It identified that wavelet transforms – DWT and CWT could be used for PD analysis. But no detailed study is reported relating the various factors in identifying PD. Regarding the statistical operators, no conclusive decisions were identified.

To get reliable PD data with corona, surface and cavity PDs, laboratory studies are carried out with the developed test objects reported in chapter 3.

PD detection using wavelet transform and laboratory data are done in chapter 4 and its various needed critical factors are determined.

In CWT, best fit wavelets are identified as db9 and coif5 using correlation method and newly developed squared coefficient method. Using scale levels above 5, corona PDs with low frequency component are identified while surface and cavity PDs are identified at low scales below 2 indicating the presence of high frequency component. The scale is a function of sampling rate and the tested sampling rate is chosen so that the nyquist frequency is higher than a typical PD.

In DWT also, best fit wavelets are identified as db9 and coif5 using the above two methods. The best fit wavelet is identified in matching the individual PD waveshape and in getting maximum detail coefficient. A decomposition level at 7 is determined to be sufficient for detection of PDs at a sampling interval of 0.25ns per point. It is found that the manual and Donoho & Johnstone methods [102] of setting the threshold value and hard thresholding methods are the best ways to get the original PD. Known Laboratory data is analysed for PD occurrence in 20ms known as group PD analysis and for the details on individual PD known as individual PD analysis. In group PD analysis, phase distributions using q, q_{mean}, $q_{\max}$, and n are qualitatively studied. It is found that these distributions are sensitive to the size of the window taken for calculation. For quantitative comparison, the calculated statistical operators sk, ku and cc for corona, surface, and cavity PDs Φ-q distributions are shown in figures 5-4, 5-5, and 5-6 respectively. For q-n distribution, it is shown in figure 5-7.

Weibull distribution on q and cumulative n yields the results which are close to the reported literature. New weibull analysis using Φ and cumulative n yields additional characterizing parameters in section 5.4.2.

Cluster analysis of the statistical occurrence of PDs are made using ΔV-Δt plot, $\Delta V_n - \Delta V_{n-1}$ plot, $\Delta t_n - \Delta t_{n-1}$ plot, and Δ(ΔV)-Δ(Δt) plot. The scatter range and shape of crowded clusters vary with the type of PD.

With the individual PD data having at least 128 sampled points, the time and frequency domain characteristics of single PD are extracted in section 5.6. In time domain, the shape of corona PD is exponentially decaying one with less

amplitude and other two are found to be oscillatory with large peak to peak amplitude. Corona PD is less sensitive to increase in voltage and surface PD is very sensitive to increase in voltage. FFT content is found upto 5MHz for corona with exponentially decreasing response. Surface and cavity PDs have characteristic resonance peaks spread upto 35 MHz and 40 MHz respectively.

An attempt is made to identify the types of PD in mixed sources signal recorded in the laboratory and operating transformer using the selected techniques reported in chapters 4 and 5. Very conclusive results are obtained if we analyse the signal sequentially by these five methods – Φ-q, n-q, and ΔV-Δt distribution in group PD analysis can identify the presence of corona PD. Correlation study can group the existing types of PD. Power spectral density calculation can indicate the frequency resonance peaks with its magnitude to characterize the type of PD in the respective group of PDs.

CWT analysis with scale level and sampling rate identifies the locations of each type of PD. Mixed weibull analysis shape parameter of the respective population identify the type of PD. Using the above, laboratory mixed sources signal is found to have corona and surface PDs. Industrial mixed sources signal is found to have dominant corona PD with very minor surface PD occurrences. Also, it is realized that for correlation study, we cannot use an universal single PD shape matching the type of PD.

7.2 Conclusion

In this research work, the main objectives planned in chapter 1 are completed to the requirement. The developed wavelet techniques with optimized

control parameters and scale levels can denoise, identify the time location of PD and recover the shape of PD without distortion.

The selected five tests can be performed on any unknown PD data in sequential manner with the objectives of estimating the severity level of PD and identifying the types of PD without any previous history.

The first group PD analysis was based on PD amplitude (q) distribution with phase (Φ) which is the recommended method by different international standards [115], [116], [117]. It will identify qualitatively the types of PDs occurring. The severity of PD level can be identified with distribution of number (n) of occurrences with a range of q. The merits of this analysis are that it does not need any history and the type of sensor used. The drawback of this method is that it presents the features in a qualitative way. To improve that statistical operators are introduced but it will be affected by the size of selected window. If two or more types of PD were present, the first test was able to reveal two or more statistical patterns but cannot confirm the exact type of PDs (i.e. surface, corona, or cavity) because the distribution patterns of cavity and surface discharges are quite similar although surface discharges exhibit higher amplitudes than that of cavity.

In the second analysis, the time interval (Δt) and amplitude difference (ΔV) between consecutive random occurring PD pulses in 20 ms were studied as the physics of ionization differ with each type of PD. This cluster analysis again provided features in a qualitative way and type of PD can be estimated in a very general way. With multi PD sources, clusters can be observed.

In the third analysis, single PD analysis was taken up. After extracting single PDs, similarity between pulses was determined by auto-correlation calculation. Similar types of PDs were grouped if they correlated to a level of 0.7. This way, the groups of PD existing in the system can be identified. But it cannot diagnose the type of PD because it is found that there cannot be an universal waveshape of single PD for a type of PD used in correlation analysis. Also, it requires a high sampling rate as the detailed shape of single PD had to be analysed. It can group the noise pulses. By determining the time and frequency domain features of the grouped single PDs and comparing with known laboratory data on pure corona, surface and cavity discharges, that group PD can be related to that type of discharge. This method is one of the best methods for classification.

The fourth analysis uses wavelet transform. The CWT works by observing the amplitudes of the CWT coefficients from lower to higher scales of the mother wavelet. Using CWT analysis, surface and corona PDs in mixed-sources signal were identified. The drawback of this technique is that it needs data at a high sampling rate which has nyquist frequency higher than the dominant frequencies of the desired PD and it is computational intensive. This method can identify PD occurrence buried in high noise level. By comparing the scale of its occurrence, the type of PD can be identified. This is another promising method for PD identification and classification.

The last fifth analysis used Weibull method by using q-n distribution. The number of significant different gradients of the q-cumulative n distribution profile

denoted the number of types of PDs. This analysis depended on the size of selected window for q and n distribution and the mathematical fitting methods to determine population size, shape and slope parameters.

To summarize the research work, three types of pure PD signals were characterized in time and frequency domain analysis and five PD diagnosing methods were developed to estimate PD severity and identify the type of PD qualitatively and quantitatively. The developed methods were tested to identify the types of PD buried in generated mixed sources signal in laboratory and in operating 2 MVA/ 22 kV rated dry type transformer.

7.3 Recommendations for further research

1) The usefulness of the developed signal processing techniques in identifying PDs of the following types may be explored.

- Identification of 3 or more types of PD embedded in multi-sources signal.
- Identification of similar types of PD by changing the geometry
    i. corona PD with various needles of different sharpness, gap length in different insulations.
    ii. cavity PD with different sized and shaped cavities located in different positions.
    iii. Surface PD with different conducting and non-conducting track lengths with different electrodes.
    iv. Identification of treeing in solid insulation and water treeing phenomenon.

2) Validity of the signal processing techniques using signals from different sensors of different frequency responses and housed at different locations may be researched.

3) PD location techniques using responses from multi-sensors may be developed.

References:

Chapter 1

[1] G.C. Stone, “Advancements during the Past Quarter Century in On-line Monitoring of Motor and Generator Winding Insulation”, IEEE Transactions on Dielectrics and Electrical Insulation, Vol.9, No.5, pp746-751, Oct 2002.

[2] Y. Tian, P.L. Lewin, A.E. Davies, S.G. Swingler, S.J. Sutton, and G.M. Hathaway, “Comparison of On-line Partial Discharge Detection Methods for HV Cable Joints”, IEEE Transactions on Dielectrics and Electrical Insulation, Vol.9, No.4, pp604-615, Aug 2002.

[3] H.J. van Breen, E. Gulski, J.J. Smit, H.F.A. Verhaart, W. de Leeuw, and M. Krieg-Wezelenburg, “Standardization of On-line VHF PD Measurements on Turbo Generators, IEEE Transactions on Dielectrics and Electrical Insulation, Vol.9, No.1, pp140-149, Feb 2002.

[4] Zhu H., Green V., Sasic M., and Halliburton S, Increased sensitivity of capacitor couplers for in-service PD measurement in rotating machines, IEEE Trans. On Energy Conversion, Vol.14-4, pp.1184-1192, 1999.

[5] A. Contin, A. Cavallini, G.C. Montanari, G. Pasini, and F. Puletti, “Digital Detection and Fuzzy Classification of Partial Discharge Signals”, IEEE Transactions on Dielectrics and Electrical Insulation, Vol.9, No.3, pp335-348, Jun 2002.

[6] Fruth B and Niemeyer L, The importance of statistical characteristics of partial discharge data, IEEE Transaction on Dielectrics and Electrical Insulation, Vol.27-1, pp.60-69, 1992.

[7] Nakao K, Kondo T, Suzuoki Y and Mizutani T, Φ-q-n patterns and current shapes of partial discharges in void, Proc. of International Symp. on Electrical Insulating Materials, pp. 665-668, 1998.

[8] R. Candela, G. Mirelli, R. Schifani, "PD Recognition by means of Statistical and Fractal parameters and a Neural Network, IEEE Transaction on Dielectrics and Electrical Insulation, Vol.7, No.1, pp87-94, Feb 2000.

[9] Greg Stone, "Importance of bandwidth in PD measurement in operating motors and generators", IEEE Transaction on Dielectrics and Electrical Insulation, Vol.7, No.1, pp6-11, Feb 2000.

[10] Akiyoshi Tatematsu, Shoji Hamada, Tadasu Takuma, and Hiroshi Morii, "A study on the accuracy of Surface Charge measurement", IEEE Transaction on Dielectrics and Electrical Insulation, Vol.9, No.3, pp406-415, Jun 2002.

[11] Pietro Romano, "Influence on PD parameters due to Voltage conducted disturbances", IEEE Transaction on Dielectrics and Electrical Insulation, Vol.11, No.1, pp160-165, Feb 2004.

[12] H. Borsi, "A PD measuring and evaluation system based on digital signal processing", IEEE Transaction on Dielectrics and Electrical Insulation, Vol.7, No.1, pp21-29, Feb 2000.

[13] H.-G. Kranz, "Fundamentals in computer aided PD processing, PD pattern recognition and automated diagnosis in GIS, IEEE Transaction on Dielectrics and Electrical Insulation, Vol.7, No.1, pp12-20, Feb 2000.

[14] A. Cavallini, A. Contin, Gian Carlo Montanari, and F. Puletti, “Advanced PD Inference in On-Field measurements. Part 1: Noise rejection“,IEEE Transaction on Dielectrics and Electrical Insulation, Vol.10, No.2, pp216-224, April 2003.

[15] Chien Hsing Lee, Yaw Juen Wang, Wen Liang Huang, “A Literature Survey of Wavelets in Power Engineering Applications”, Proc. Natl. Sci. Counc. ROC(A), Vol. 24, No. 4, 2000. pp. 249-258.

[16] Ma X, Zhou C, and Kemp I J, “Investigations into the use of wavelet theory for partial discharge pulse extraction in electrically noisy environments”, 8th International Conf. on Dielectric Materials, Measurements and Applications, IEE Conf. Publ. No. 473, pp.123-126, 2000.

[17] X. Ma, C. Zhou, I. J. Kemp, “A Feasibility Study into the use of Wavelet Transform in Partial Discharge Analysis”, Proceedings of 35th Universities’ Power Engineering Conference (UPEC2000), Belfast, UK, pp6-8, September 2000.

[18] Yusheng Quan, Ning Gao, Guanjun Zhang, and Zhang Yan, “Wavelet Transform applying in Partial Discharge Measurement”, Conference Record of the 1998 IEEE International Symposium on Electrical Insulation, June 7-10, pp428-431, 1998.

[19] X.D.Ma, C.Zhou and I.J.Kemp, “Interpretation of Wavelet Analysis and its application in Partial Discharge Detection”, IEEE Transactions on Dielectrics and Electrical Insulation, Vol. 9, No.3, pp446-457, Jun 2002.

[20] Lalitha E.M and Satish L, “Wavelet analysis for classification of multi-source PD patterns”, IEEE Transaction on Dielectrics and Electrical Insulation, Vol.7, No.1, pp.40-47, 2000.

[21] L. Satish, and B. Nazneen, “Wavelet-based denoising of Partial Discharge signals buried in excessive noise and interference”, Vol.10, No.2, pp354-367, April 2003.

[22] S. Senthil Kumar, Y. P. Nerkar, M. N. Narayanachar, and R. S. Nema, “Effect of Detector and Analyzer Settings on Partial Discharge Measurement and Representation”, IEEE Transactions on Dielectrics and Electrical Insulation, Vol. 11, No. 4, pp568-576, August 2004.

Chapter 2

[23] I. Shim, J.J. Saraghan, and W.H. Siew, “Digital Signal Processing applied to the detection of Partial Discharge: an overview”, IEEE Electrical Insulation magazine, Vol.16, No.3, pp6-12, May/June 2000.

[24] Lamela-Rivera H.; Macià-Sanahuja C.; García-Souto J.A., “Detection and wavelet analysis of partial discharges using an optical fibre interferometric sensor for high-power transformers”, Journal of Optics A: Pure and Applied Optics, vol. 5, no. 1, pp. 66-72, 2003.

[25] X.D.Ma, C.Zhou and I.J.Kemp, “DSP Based Partial Discharge Characterisation by Wavelet Analysis”, IEEE 19th International Symposium on Discharges and Electrical Insulation in Vacuum, Xi’an, pp780-783, 2000.

[26] Yoh Yasuda, Jun Matsuura, Takehisa Hara, Chen Min, Ken ichiro Hirotsu, and Siegeki Isojima, “Application of FWT (Fast Wavelet Transform) for auto-detection system of Partial Discharge in power cables”, High Voltage Engineering Symposium, Conference Publication No.467, IEE, pp5.301.P5-5.304.P5, 22-27 Aug 1999.

[27] R Altenburger, C Heitz and J Timmer, “Analysis of phase-resolved partial discharge patterns of voids based on a stochastic process approach”, Journal of Physics D: Applied Physics, Vol. 35, pp1149.1163, 2002.

[28] Contin A, Gulski E, Cacciari M and Montanari G C, Applications of the weibull function to partial discharge data coming from different sources topologies, Annual report on conference on Electrical Insulation and Dielectric Phenomena, pp.335-338, 1995.

[29] A. Contin, G.C. Montanari, and C. Ferraro, “PD source recognition by Weibull Processing of pulse height distributions”, IEEE Transaction on Dielectrics and Electrical Insulation, Vol.7, No.1, pp48-58, Feb 2000.

[30] Y. Yamano, and M. Okada, “Reduction of PD in a void by additives of azobenzoic compound in HDPE insulating material”, IEEE Transaction on Dielectrics and Electrical Insulation, Vol.8, No.6, pp889-896, Dec 2001.

[31] Florkowska, and B. Wlodek, R, “Pulse height analysis of partial discharges in air”, IEEE Transaction on Dielectrics and Electrical Insulation, Vol. 28, No.6, pp932-940, Dec 1993.

[32] Van Brunt, R.J, Cernyar, E.W, and von Glahn, P, “Importance of unraveling memory propagation effects in interpreting data on partial discharge statistics”, IEEE Transaction on Dielectrics and Electrical Insulation, Vol. 28, No.6, pp905-916, Dec 1993.

[33] G.C. Montanari, “Aging and life models for insulation systems based on PD detection”, IEEE Transaction on Dielectrics and Electrical Insulation, Vol.2, No.4, pp667-670, Aug 1995.

[34] H. Debruyne, and O. Lesaint, “About the significance of PD measurements in liquids”, IEEE Transaction on Dielectrics and Electrical Insulation, Vol.10, No.3, pp385-392, June 2003.

[35] Er-ning Li, and J.M.K. MacAlpine, “Negative Corona in air using a point/cup electrode system”, IEEE Transaction on Dielectrics and Electrical Insulation, Vol.7, No.6, pp752-757, Dec 2000.

[36] A. Cavallini, M. Conti, A. Contin, and G.C. Montanari, “Advanced PD inference in On-Field measurements. Part 2: Identification of defects in solid insulation system”, IEEE Transaction on Dielectrics and Electrical Insulation, Vol.10, No.3, pp528-538, Jun 2003.

[37] C. Mayoux, and C. Laurent, “Contribution of Partial Discharges to electrical breakdown of solid insulating materials”, IEEE Transaction on Dielectrics and Electrical Insulation, Vol.2, No.4, pp641-652, Aug 1995.

[38] Edward Gulski, “Digital analysis of Partial discharges”, IEEE Transaction on Dielectrics and Electrical Insulation, Vol.2, No.5, pp822-837, Oct 1995.

[39] Lutz Niemeyer, “A generalized approach to Partial discharge modeling”, IEEE Transaction on Dielectrics and Electrical Insulation, Vol.2, No.4, pp510-528, Aug 1995.

[40] P. von Glahn, and R.J. Van Brunt, “Continuous recording and stochastic analysis of PD”, IEEE Transaction on Dielectrics and Electrical Insulation, Vol.2, No.4, pp590-601, Aug 1995.

[41] K. Chrzan, and J.M. Andino, “Electrical strength of air containing Ozone Nitric Oxides produced by intensive Partial Discharges”, IEEE Transaction on Dielectrics and Electrical Insulation, Vol.8, No.4, pp607-611, Aug 2001

[42] T. Yamada, T. Ishida, N. Hayakawa, and H. Okubo, “Partial Discharge and breakdown mechanisms in ultra-dilute SF6/N2 gas mixtures”, IEEE Transaction on Dielectrics and Electrical Insulation, Vol.8, No.1, pp137-142, Feb 2001.

[43] I.A. Metwally, “Factors affecting Corona on twin-point gaps under dc and ac HV”, IEEE Transaction on Dielectrics and Electrical Insulation, Vol.3, No.4, pp544-553, Aug 1996.

[44] Zhifang Du, P.K. Willett, and M.S. Mashikian, “Performance limits of PD location based on time-domain reflectometry”, IEEE Transaction on Dielectrics and Electrical Insulation, Vol.4, No.2, pp182-188, April 1997.

[45] V.M. Moreno, R.S. Gorur, and A. Kroese, “Impact of Corona on the long-term performance of nonceramic insulators”, IEEE Transaction on Dielectrics and Electrical Insulation, Vol.10, No.1, pp80-95, Feb 2003.

[46] Huang Wei-Gang, and Wang Xiao-Ping, “Corona Q-V characteristics under Uniploar-damped oscillating impulses”, IEEE Transaction on Dielectrics and Electrical Insulation, Vol.4, No.6, pp758-762, Dec 1997.

[47] Gabe Paoletti, and Alex Golubev, “Partial Discharge Theory and applications to electrical equipment”, Western Mining electrical Association, http://www.wmea.net/.

[48] G.C. Stone, T.E. Goodeve, H.G. Sedding, and W. McDermid, “Unusual PD pulse phase distributions in operating rotating machines”, IEEE Transaction on Dielectrics and Electrical Insulation, Vol.2, No.4, pp567-577, Aug 1995.

[49] J. Densley, T. Kalicki, and Z. Nadolny, “Characteristics of PD pulses in electrical trees and interfaces in extended cables”, IEEE Transaction on Dielectrics and Electrical Insulation, Vol.8, No.1, pp-48-57, Feb 2001.

[50] R. Vogelsang, B. Fruth, T. Farr, K. Frohlich, “Detection of electrical tree propagation by partial discharge measurements”, European Transactions on Electrical Power, ETEP, 15, pp. 1-14, (DOI: 10.1002/etep.60), John Wiley & Sons, Ltd, 2005.

[51] Kai Gao, Kexiong Tan, Fuqi Li, and Chengqi Wu, “PD pattern recognition for stator bar models with six kinds of characteristic vectors using BP network”, IEEE Transaction on Dielectrics and Electrical Insulation, Vol.9, No.3, pp381-389, Jun 2002.

[52] N.H. Ahmed, and N.N. Srinivas, “On-line Partial Discharge detection in cables”, IEEE Transaction on Dielectrics and Electrical Insulation, Vol.5, No.2, pp181-188, April 1998.

[53] Yoh Yasuda, Jun Matsuura, Takehisa Hara, Chen Min, Ken’ichiro Hirotsu, and Siegeki Isojima, “Application of FWT (Fast Wavelet Transform) for auto-detection system of Partial Discharge in power cables”, IEE High Voltage Engineering Symposium, Conference Publication No. 467, pp22-27, Aug 1999.

[54] P. Purkait, and S. Chakravorti, “Pattern Classification of Impulse faults in Transformers by wavelet analysis”, IEEE Transaction on Dielectrics and Electrical Insulation, Vol.9, No.4, pp555-561, Aug 2002.

[55] U. Kopf, and K. Feser, “Rejection of narrow-band noise and repetitive pulses in on-site PD measurements”, IEEE Transaction on Dielectrics and Electrical Insulation, Vol.12, No.6, pp1180-1191, Dec 1995.

[56] Masatake Kawada, Zen-Ichiro Kawasaki, Kenji Matsu-ura, “Time-frequency analysis of E-M signals from a Partial Discharge occurring in GIS using Wavelet Transform”, Conference Record of the 1998 IEEE International Symposium on Electrical Insulation, Arlington, Virginia, USA, pp57-60, 7-10 Jun 1998.

[57] C. S. Burrus and T. W. Parks, DFT/FFT and Convolution Algorithms, New York: John Wiley and Sons, Inc., 1985.

[58] Simon Haykin, “Commumication Systems”, Published by John Wiley & Sons, Inc, 1978.

[59] Martin Vetterli and Jelena Kovacevic, “Wavelets and Subband Coding”, Published by Prentice Hall, 1995.

[60] D.M. Monro, B.E. Bassil & G.J. Dickson, “Orthonormal wavelets with balanced uncertainty”, Proceedings IEEE International Confrerence on Image Processing ICIP, Vol. 2, pp. 581-584, 1996.

[61] X. Ma, C. Zhou, I. J. Kemp, “Wavelets for the Analysis and Compression of Partial Discharge Data”, Proceedings of 2001 Conference on Electrical Insulation and Dielectric Phenomena (CEIDP2001), Kitchener, Ontario, Canada, 14-17 October 2001.

[62] Raghuveer M. Rao & Ajit S. Bopardikar, **“**Wavelet Transforms: Introduction to Theory and Applications”, Addison-Wesley, 1998.

[63] Matlab Wavelet toolbox documentation, The Mathworks Inc, Website: http://www.mathworks.com/access/helpdesk/help/toolbox/wavelet.

[64] Ridsdill-Smith, T.A, “Wavelet design of time-varying filters”, IEEE 5th International Symposium on Signal Processing and its Applications, pp599-602, 1999.

[65] Chien-Hsing Lee, Yaw-Juen Wang, and Wen-Liang Huang, “A Literature Survey of Wavelets in Power Engineering applications”, Proc. Natl. Sci. Counc.ROC(A), Vol. 24, No. 4, pp. 249-258, 2000.

[66] Karen L. Butler-Purry, and Mustafa Bagriyanik, “Characterization of Transients in Transformers Using Discrete Wavelet Transforms”, IEEE Transaction on Power Systems, Vol.18, No.2, pp648-656, May 2003.

[67] Boczar, T, and Zmarzly, D, “Application of wavelet analysis to acoustic emission pulses generated by partial discharges”, IEEE Transaction on Dielectrics and Electrical Insulation, Vol.11, No.3, pp433-449, Jun 2004.

[68] Xiao-Ping Zhang, Li-Sheng Tian, and Ying-Ning Peng, “From the Wavelet Series to the Discrete Wavelet Transform - the Initialization”, IEEE Transactions On Signal Processing, Vol. 44, No. 1, pp129-133, Jan 1996.

[69] Mallat, S. G, “A Theory for Multi-resolution signal decomposition: The Wavelet Representation”, IEEE Transactions on Pattern Analysis and Machine Intelligence, Vol. 11, No. 7, pp674-693, 1989.

[70] Kreuger. F.H, Gulski, E, and Krivda. A, “Classification of partial discharges”, IEEE Transaction on Dielectrics and Electrical Insulation, Vol.28, No.6, pp917-931, Dec 1993.

[71] Karen L. Butler-Purry, and Mustafa Bagriyanik, “Identifying Transformer Incipient Events for Maintaining Distribution System Reliability”, Proceedings of the 36th Hawaii International Conference on System Sciences, pp1-8, 2003.

[72] Paulo Gon, calv_es, and Richard G. Baraniuk, “Time-Frequency /Time-Scale Signal Analysis”, IEEE Signal Processing Letters, pp1-9, 05, April 1995.

[73] R. J. Dickenson and Z. Ghassemlooy, “A feature extraction and pattern recognition receiver employing Wavelet Analysis and Artificial Intelligence for signal detection in diffuse optical wireless communications”, IEEE Wireless Communication, pp64-72, 2003.

[74] Francis Quek and Yingen Xiong, “Oscillatory gestures and discourse”, IEEE International Conference on Multimedia & Expo (ICME2003), Baltimore, Maryland, pp181-184, July 6-9, 2003.

[75] Kranz, H.-G, and Krump, R, “Partial discharge diagnosis using statistical optimization on a PC-based system”, IEEE Transaction on Dielectrics and Electrical Insulation, Vol.27, No.1, pp93-98, Feb 1992.

[76] Kranz, H.-G, “Diagnosis of partial discharge signals using neural networks and minimum distance classification”, IEEE Transaction on Dielectrics and Electrical Insulation, Vol.28, No.6, pp1016-1024, Dec 1993.

[77] Van Brunt, R.J. Cernyar, E.W. von Glahn, P, “Importance of unraveling memory propagation effects in interpreting data on partial discharge statistics”, IEEE Transaction on Dielectrics and Electrical Insulation, Vol.28, No.6, pp905-916, Dec 1993.

[78] Gulski, E, “Computer-aided measurement of partial discharges in HV equipment”, IEEE Transaction on Dielectrics and Electrical Insulation, Vol.28, No.6, pp969-983, Dec 1993.

[79] I.A.D Giriantari, and T.R Blackburn, "Condition Monitoring of Contaminated composite insulators using partial discharge analysis", AUPEC2002, Melbourne, 29 Sept - 2Oct 2002.

[80] Ulf Grenander and Anuj Srivastava, “Probability Models for Clutter in Natural Images”, IEEE Transaction on Pattern Analysis and Machine Intelligence, Vol. 23, No. 4, pp424-429, April 2001.

[81] George K. Karagiannidis, Dimitris A. Zogas, and Stavros A. Kotsopoulos, "Statistical Properties of the EGC Output SNR Over Correlated Nakagami-m Fading Channels", IEEE Transactions on wireless communications, Vol. 3, No. 5, pp164-1769, Sep 2004.

[82] Yicheng Wang, "New methods for measuring statistical distributions of Partial Discharge pulse**s",** Journal of Research of the National Institute of Standards and Technology, Volume 102, Number 5, pp569-576, September–October 1997.

1.2 [83] Rainer Patsch and Farhad Berton, "Pulse Sequence Analysis – a diagnostic tool based on the physics behind partial discharges", Journal of Physics D: Applied Physics, Vol.35, No.1, pp25-32, 2002.

[84] G.C.Montanari, M.Cacciari, and A.Contin, "Use of a Mixed-Weibull Distribution for the identification of PD phenomena", IEEE Transactions on Dielectrics and Electrical Insulation vol. 2 No.4, pp628-629, Aug 1995.

[85] R. Schifani, R. Candela, "A new algorithm for Mixed Weibull analysis of Partial Discharge amplitude distributions", IEEE Transactions on Dielectrics and Electrical Insulation vol. 6 No.2, pp242-249, April 1999.

[86] Y Tian, P L Lewin, J S Wilkinson, S J Sutton and S G Swingler, "Continuous On-line Monitoring of Partial Discharges in High Voltage Cables", Conference Record of the 2004 IEEE International Symposium on Electrical Insulation, pp454-457, 19-22 September 2004.

[87] Contin, A.; Contessotto, G.; Montanari, G.C.; Cacciari, M., Comparing different stochastic models for the identification and separation of concurrent partial discharge phenomena, Dielectric Materials, Measurements and Applications, 2000. Eighth International Conference on (IEE Conf. Publ. No. 473), pp374 -379, 2000.

[88] Contin, A.; Montanari, G.C.; Conti, M.; Cacciari, M, "An invariant diagnostic marker for the identification of partial discharge sources in electrical apparatus", Solid Dielectrics, 2001. ICSD '01. Proceedings of the 2001 IEEE 7th International Conference on, pp287-290, 2001.

Chapter 4

[89] Stephane Mallat, "A Wavelet Tour of Signal Processing (Wavelet Analysis & Its Applications)**",** Second Edition, Academic Press, 1999.

1.3 [90] Wei Wang and Don H. Johnson, "Computing Linear Transforms of Symbolic signals", IEEE Transactions on Signal Processing, Vol. 50, No. 3, pp628-634, Mar 2002.

[91] Sardy, S, "Minimax threshold for denoising complex signals with Waveshrink", IEEE Transactions on Signal Processing, Vol. 48, No.4, pp1023-1028, April 2000.

[92] Imola K. Fodor and Chandrika Kamath, "Denoising through wavelet shrinkage: an empirical study", Journal of Electronic Imaging, Vol. 12, Issue 1, pp151-160, Jan 2003.

[93] Shou-Yan Wang, Xuguang Liu, John Yianni, Tipu Z. Aziz, and John F. Stein, "Extracting burst and tonic components from surface electromyograms in dystonia using adaptive wavelet shrinkage", Journal of Neuroscience Methods, Vol.139, pp177–184, 2004.

[94] Julio Cesar Soares de Oliveira Lyrio, Luis Tenorio, and Yaoguo Li, "Efficient automatic denoising of gravity gradiometry data", Journal of Geophysics, Vol. 69, No.3, pp772-782, May-June 2004.

[95] A.P. Bradley, and W.J. Wilson, "On wavelet analysis of auditory evoked potentials", Journal of Clinical Neurophysiology, Vol.115, pp1114–1128, 2004.

[96] Pierre Vandergheynst, and Jean-François Gobbers, "Directional Dyadic Wavelet Transforms: Design and Algorithms", IEEE Transaction on Image-Processing, Vol.11, No.4, pp363-372, April 2002.

[97] Jelena Kovacevic, and Wim Sweldens. "Wavelet families of increasing order in arbitrary dimensions', IEEE Transaction on Image-Processing, Vol.9, No.3, pp480-496, March 2000.

[98] Nickolas Adler, Paul Costa, Andrew V. Dowd, Anne Mascarin, and Don Orofino, "Eliminate Signal Noise With Discrete Wavelet Transformation", Electronic Design Online Magazine, ID No. 4695, Web site address: http://www.elecdesign.com/Articles/Print.cfm/ArticleID=4695, 5 Sep 2000.

[99] MathWorks, Matlab wavelet toolbox, Web site address: http://www.mathworks.com/products/wavelet/.

[100] Levent Sendur and Ivan W. Selesnick, “Bivariate Shrinkage With Local Variance Estimation”, IEEE Signal Processing Letters, Vol. 9, No. 12, pp438-441, Dec 2002.

[101] Zhang Ji-dong, Zheng Bao-yu, and Fu Hong-liang, “A novel constant modulus array for multiuser detection”, Journal of Zhejiang University Science, 6A(1), pp38-42, 2005.

[102] Donoho, D. L. and Johnstone, I. M “Ideal spatial adaptation by wavelet shrinkage”, Biometrika 81 425 455. Z, 1994.

[103] Donoho, D.L. (1995), "De-noising by soft-thresholding”, IEEE Transaction on Information Theory, Vol. 41, No.3, pp. 613-627, 1995.

[104] M. Lang, H. Guo, J. E. Odegard, C. S. Burrus, and R. O. Wells, “Noise Reduction Using an Undecimated Discrete Wavelet Transform”, IEEE Signal Processing Letters, Vol.3, No.1, pp10-12, Jan 1996.

[105] S. Grace Chang, Bin Yu, and Martin Vetterli, “Wavelet Thresholding for Multiple Noisy Image Copies”, IEEE Transactions on Image Processing, Vol. 9, No. 9, Sept 2000.

[106] S. Gupta, R. C. Chauhan, and S. C. Sexana, “Wavelet-based statistical approach for speckle reduction in medical ultrasound images”, Medical & Biological Engineering & Computing 2004, Vol. 42, pp189-192, 2004.

Chapter 5

[107] D J Swaffield, P L Lewin, Y Tian, G Chen and S G Swingler, "Characterisation of Partial Discharge Behaviour in Liquid Nitrogen", Conference Record of the 2004 IEEE International Symposium on Electrical Insulation, Indianapolis, IN USA, pp19-22 Sept 2004.

[108] Zhang, C.H. MacAlpine, and J.M.K, "A phase-related investigation of AC corona in air", IEEE Transactions on Dielectrics and Electrical Insulation, Vol.10, No.2, pp312-319, April 2003.

[109] Andreas Schutze, James Y. Jeong, Steven E. Babayan, Jaeyoung Park, Gary S. Selwyn, and Robert F. Hicks, "The Atmospheric-Pressure Plasma Jet: A Review and Comparison to Other Plasma Sources", IEEE Transactions on Plasma Science, Vol. 26, No. 6, pp1685-1694, Dec 1998.

[110] Contin, A. Cacciari, M. Montanari, and G.C, "Estimation of Weibull distribution parameters for partial discharge inference", IEEE 1994 Annual Report., Conference on Electrical Insulation and Dielectric Phenomena, pp71-78, 1994.

[111] Chia P.Y, and Liew A.C, "Defect classification based on Weibull statistic of partial discharge height distribution with wavelet preprocessing", Proceedings of PowerCon 2000. International Conference on Power System Technology, Vol.2, pp1035-1040, 2000.

[112] Yu Ming, S. Birlasekaran, and Soo Siak Chye, "Characterization of Partial Discharge Signals from operating 300MVA generator", AUPEC2002, Monash University Clayton, Victoria, 3800, Australia.

[113] Montanari, G.C. Mazzanti, G. Cacciari, M. Fothergill, and J.C, "Optimum estimators for the Weibull distribution from censored test data. Progressively-censored tests [breakdown statistics]", IEEE Transactions on Dielectrics and Electrical Insulation, Vol.5, No.2, pp157-164, April 1998.

Chapter 6

[114] Karen L. Butler-Purry, and Mustafa Bagriyanik, "Identifying Transformer Incipient Events for Maintaining Distribution System Reliability", Proceedings of the 36th Hawaii International Conference on System Sciences, 2003.

Chapter 7

[115] IEC Standard. IEC 60270 – Third Edition, High-voltage test techniques – Partial Discharge Measurements, 2000-12.

[116] IEEE Standard C57.124 – IEEE Recommended Practice for the detection of partial discharge and the measurement of apparent discharge in dry-type transformers, 1991.

[117] IEEE Standard 1434 – Trial-use Guide to the measurement of Partial Discharge in Rotating Machinery, 2000.